INVESTIGATING THE MECHANISMS UNDERLYING MYOCARDIAL REGENERATION IN THE MEXICAN CAVEFISH



William Thomas Stockdale

Wolfson College, University of Oxford

Department of Physiology, Anatomy and Genetics

Supervised by

Prof Mathilda Mommersteeg & Prof Paul Riley

A thesis submitted for the degree of Doctor of Philosophy

2021

Abstract

Following myocardial infarction (MI), the adult human heart is unable to regenerate and replace the lost cardiac muscle with new functioning cardiomyocytes. Instead, it forms a permanent non-contractile scar that impairs cardiac function, which may later result in heart failure. In contrast, the adult zebrafish and neonatal mouse heart possess an innate ability to regenerate their heart after injury, with studies revealing myocardial proliferation in the border zone next to the injury site as a key driver to the regenerative process.

The *Astyanax mexicanus* is a unique cardiac regeneration fish model that enables the comparison of adult regeneration with human-like scarring all within the same species. In this model, the *Astyanax* surface fish regenerate their heart after injury, while their Pachón cave-dwelling counterparts cannot, and similar to humans, form a permanent scar. These opposing regenerative capacities coincide with contrasting myocardial proliferation profiles, which are characterised by initiation of cardiomyocyte proliferation in both Pachón and surface fish, but no observable cardiomyocyte expansion in Pachón.

To determine the capability of the *Astyanax* model to detect novel genes in regeneration and decipher the mechanisms behind these contrasting myocardial regeneration capacities, comparative bulk and single cell transcriptomics were employed. Bulk transcriptome analysis identified upregulation of *lrrc10*, a novel gene to regeneration, in the surface fish compared to Pachón heart. CRISPR mediated knockout of *lrrc10* in zebrafish impaired heart regeneration, with *lrrc10*$^{-/-}$ zebrafish displaying a Pachón-like phenotype, confirming the ability of the *Astyanax* model to detect novel genes.

Targeted analysis of the cardiomyocytes using single cell transcriptomics revealed myocardial heterogeneity in *Astyanax* hearts, with a transcriptionally distinct myocardial border zone after injury. This highly proliferative border zone generally possessed characteristics consistent with reduced maturity, dedifferentiation, cell proliferation and metabolic reprogramming in both surface fish and Pachón. However, differential expression of cell cycle genes between surface fish and Pachón border zone cardiomyocytes alongside cardiomyocyte DNA quantification suggested cell cycle arrest and polyploidisation in Pachón proliferating cardiomyocytes at the expense of meaningful cardiomyocyte expansion. The finding of polyploidisation in Pachón coincided with lack of upregulation of glucose uptake and glycolytic genes as observed in the surface fish myocardial border zone. In contrast, evidence suggested increased fatty acid uptake/utilisation and metabolic inflexibility after injury in the Pachón heart – all characteristics consistent with the diabetic heart. However, the *insra* P211L mutation, which is responsible for insulin resistance in Pachón, does not have a negative impact on cardiac regeneration.

The *Astyanax* is a model capable of enhancing our understanding of regeneration and identification of the above metabolic differences provides the initial strides into establishing the metabolic fingerprint required for successful cardiomyocyte proliferation during cardiac regeneration.

Acknowledgments

First and foremost, I want to thank Tilly Mommersteeg for giving me this opportunity and your continuous support from my RA position and all the way through my DPhil. It has been a pleasure to work under your supervision and I could not have imagined a more interesting project. I've truly had a great experience, from presenting in Japan to exploring the caves in Mexico. I will always be in your debt – Thank you.

I want to also extend my gratitude to my co supervisor, Paul Riley, who backed me for this DPhil right from the start. It has been a privilege to work with you and I have learnt a lot from your experience.

I want to thank all Mommersteeg, Riley and Smart group members both past and present for all their contributions and advice during my project. It has been an absolute pleasure to work with you all. A special acknowledgement needs to be made to Andia, Helen and Irina - the best of friends.

Outside the lab, my most heartfelt thanks go to my partner, Aini. You have been an amazing and supportive partner during the ups and downs of my DPhil and particularly during the last few months. I cannot thank you enough for that. Now is your time to rest because I will cook dinner for you and do all the cleaning!

To my family and particularly my parents, Jenny and Paul, who have always been there for me and encouraged me throughout my life. Without your endless support, I would not be here.

You all have truly inspired me to continue my career in research.

Table of contents

Chapter 1 Introduction **13**
1.1 The lasting damage of myocardial infarction **13**
1.2 Heart Regeneration across the animal kingdom **15**
1.3 Mechanisms of heart regeneration **18**
1.3.1 Cardiomyocyte proliferation 18
1.3.2 Coronary revascularisation 22
1.3.3 The scar and the extracellular matrix 23
1.3.4 Activation of the Epicardium & Endocardium 26
1.3.5 A balanced immune response 29
1.4 The *Astyanax mexicanus* – A potential new model for regeneration **33**
1.4.1 Limitations of current models of regeneration 33
1.4.2 What is the *Astyanax mexicanus*? 34
1.4.3 Heart regeneration in the *Astyanax mexicanus* 35
1.5 DPhil project aims **38**
Chapter 2 Materials & Methods **40**
2.1 Animal husbandry **40**
2.2 Cryoinjury **40**
2.3 BrdU exposure **41**
2.4 Heart processing - fixing and paraffin embedding **41**
2.5 AFOG **41**
2.6 RNAscope on tissue sections **42**
2.7 Immunohistochemistry (IHC) on tissue sections **43**
2.8 Proliferation counts **44**
2.9 Wound size measurement **44**
2.10 quantitative PCR (qPCR) **45**
2.10.1 RNA extraction and cDNA preparation 45
2.10.2 qPCR 45
2.11 CRISPR mediated generation of zebrafish mutants **46**
2.11.1 sgRNA and ssODN design and construction 46
2.11.2 Mutant generation & Genotyping 48
2.12 Bulk RNAseq **49**
2.12.1 RNA extraction and RNA sequencing preparation 49
2.12.2 Data analysis 49
2.13 Single cell RNAseq **50**
2.13.1 Heart dissociation 50

2.13.2 Single cell RNAseq data analysis 51
2.14 Polyploid analysis 54
2.14.1 Heart dissociation 54
2.14.2 IHC 55
2.14.3 DNA content measurement – Cell profiler 56
2.15 Metabolomics 57
2.15.1 Metabolite extraction 57
2.15.2 Liquid chromatography–mass spectrometry (LC–MS) 58
2.14.3 Data Analysis 60
2.16 Statistical Analysis 61
Chapter 3 *Astyanax mexicanus* identifies genes key for cardiac regeneration 62
3.1 Introduction 62
3.1.1 Background to candidate genes *fmoda*, *tmem198a*, *gpc5b*, and *lrrc10* 64
3.1.2 Aim 66
3.2 Results 67
3.2.1 Analysis of the differential expression kinetics in response to wounding in the *Astyanax* 67
3.2.2 *tmem198a*, *gpc5b* and *fmoda* knockout has no effect on regeneration capacity in zebrafish 70
3.2.3 lrrc10 Is required for heart regeneration in zebrafish 77
3.3 Discussion 84
3.3.1 Differential kinetics in a wide range of genes and the identification *lrrc10* 84
3.3.2 Normal regeneration in *Tmem198a*, *gpc5b*, *fmoda* knockouts 88
3.3.3 Pachón-like phenotype in zebrafish *lrrc10* mutants 90
3.3.4 Limitations 92
3.3.5 Conclusions 93
Chapter 4 Single-cell transcriptomics to explore the molecular mechanisms underlying the cardiomyocyte profile after injury 94
4.1 Introduction 94
4.1.1 Myocardial proliferation in the *Astyanax* 95
4.1.2 Single cell RNAseq 97
4.1.3 Aim 99
4.2 Results 100
4.2.1 Identification of trabecular, cortical, primordial and border zone cardiomyocytes 100
4.2.2 Primordial and border zone cardiomyocytes have reduced maturity 107
4.2.3 Cardiomyocyte border zone clusters display characteristics consistent with dedifferentiation/migration and phases of the cell cycle 109
4.2.4 Cardiomyocyte subtype composition after injury 113
4.2.5 No increased apoptotic signature between Pachón and Surface fish cardiomyocytes 116

4.2.6 Cell cycle transcriptional differences at 7dpi between Pachón and Surface fish 118
4.2.7 Ploidy analysis of *Astyanax* cycling cardiomyocytes after injury 121
4.2.8 Differences in metabolic gene expression between Pachón and Surface fish border zone cardiomyocytes 125
4.3 Discussion 128
4.3.1 Cardiomyocyte heterogeneity in the *Astyanax* heart 128
4.3.2 *Astyanax* border zone cardiomyocytes have similar characteristics with the zebrafish border zone 130
4.3.3 Potential cell cycle arrest in Pachón cycling cardiomyocytes – ploidy 132
4.3.4 Metabolic differences between surface fish and Pachón underlie the contrasting proliferation profiles in the order zone 136
4.3.5 Limitations 137
4.3.6 Conclusion 139
Chapter 5 Metabolic differences between Pachón and surface fish cardiomyocytes after injury 140
5.1 Introduction 140
5.1.1 Metabolism in the *Astyanax* 140
5.1.2 Metabolism during myocardial regeneration 141
5.1.3 Aim 143
5.2 Results 144
5.2.1 Glucose uptake and glycolysis are increased in the surface fish border zone versus the Pachón 144
5.2.2 Increased gluconeogenesis in Pachón 151
5.2.3 Key fatty acid transporter, *cd36*, localises to proliferating cardiomyocytes in Pachón 153
5.2.4 Metabolomics indicates metabolic inflexibility in the Pachón heart after injury 156
5.2.5 Pachón insulin receptor mutation does not negatively impact on regeneration in zebrafish 163
5.3 Discussion 166
5.3.1 Differences in glycolysis, particularly *glut1a*, could underlie cardiomyocytes proliferation profile in Pachón 166
5.3.2 Increased Fatty acid metabolism but reduced TCA cycle in the Pachón heart 168
5.3.3 Is the lack of cardiomyocyte expansion in the Pachón a consequence of its diabetic phenotype? 170
5.3.4 Limitations 172
5.3.5 Conclusion 173
Chapter 6 General Discussion 175
6.1 Main findings 175
6.1.1 Lrrc10 is required for heart regeneration 177
6.1.2 *Astyanax* myocardial border zone displays characteristics consistent with reduced maturity, dedifferentiation, cell proliferation and metabolic reprogramming 178

6.1.3 Evidence of cell cycle arrest and polyploidisation of Pachón proliferating cardiomyocytes 180
6.1.4 Increased fatty acid uptake and utilisation but reduced oxidative metabolism in Pachón border zone 183
6.2.5 Increased glucose uptake and glycolytic reprogramming in the surface fish myocardial border zone 185
6.1.5 Diabetic characteristics in the Pachón heart, but cavefish *insra* P211L mutation, does not have a negative impact cardiac regeneration. 188
6.2 Study translational prospective 191
6.3 Future work 194
6.4 Concluding remarks 198
Appendix 200
Contributions 200
Publications 200
References 202

List of Figures

Figure 1.1 Permanent scar formation after injury in the Pachón Cavefish. 36
Figure 1.2 Myocardial proliferation differences between Pachón cavefish and surface fish after injury..... 37
Figure 3.1 Transcriptomic analysis of *Astyanax* hearts after injury. 64
Figure 3.2 141 genes with differential kinetics after injury in the *Astyanax* – identifying *lrrc10*. 69
Figure 3.3 Differential expression of candidate genes, *tmem19a*, *gpc5b* and *fmoda*. 71
Figure 3.4 CRISPR-cas9 knockout strategy in zebrafish for candidate genes, *tmem19a*, *gpc5b*, *fmoda* and *lrrc10*. 72
Figure 3.5 Normal regeneration in *tmem19a-/-* zebrafish. 74
Figure 3.6 Normal regeneration in *gpc5b-/-* zebrafish. 75
Figure 3.7 Normal regeneration in *fmoda-/-* zebrafish. 76
Figure 3.8 Increased *lrrc10* expression at myocardial border zone in surface fish and zebrafish but not in Pachón. 79
Figure 3.9 *lrrc10* is required for heart regeneration in the regenerating zebrafish..... 82
Figure 4.1 No difference in myocardial apoptosis in either Pachón or surface fish. 96
Figure 4.2 scRNAseq analysis on *Astyanax* cardiomyocytes before and after injury. 102
Figure 4.3 *Astyanax* cardiomyocyte subtype annotation. 103
Figure 4.4 Markers of trabecular, cortical, primordial and border zone cardiomyocytes. 106
Figure 4.5 *Astyanax* cardiomyocyte maturation estimation by Cytotrace and cellular entropy. 108
Figure 4.6 Specific border zone clusters display dedifferentiating/migration characteristics and features of the cell cycle. 112
Figure 4.7 Cardiomyocyte cluster composition after injury. 115
Figure 4.8 Similar apoptotic gene signature between Pachón and surface fish cardiomyocytes after injury..... 117
Figure 4.9 Differential expression of cell cycle genes between Pachón and Surface fish in the proliferating cluster - cluster 5 120
Figure 4.10 Potential arrest of Pachón cycling cardiomyocytes in the S phase. 124
Figure 4.11 Transcriptional differences of metabolic genes between surface fish and Pachón border zone cardiomyocytes. 127
Figure 5.1 Increased *glut1a* expression in surface fish but minimal expression of glucose transporters in Pachón. 147

Figure 5.2 Increased expression of glycolysis genes in surface fish versus Pachón cavefish at the wound border. 150
Figure 5.3 Pachón cavefish have increased expression of *fbp2*, a key enzyme in gluconeogenesis.. 152
Figure 5.4 Upregulation of *cd36*, a fatty acid transporter, in the proliferating cardiomyocytes in Pachón. 155
Figure 5.5 Metabolomics reveals a metabolic inflexibility in Pachón hearts after injury. 158
Figure 5.6 Metabolomics analysis shows increased abundance of TCA cycle metabolites in surface fish. 160
Figure 5.7 Metabolomics analysis shows increased abundance of lipid metabolites in Pachón versus surface fish. 162
Figure 5.8 Zebrafish with the Pachón insulin receptor mutation have enhanced regeneration. 165
Figure 6.1 Summary of main findings and possible mechanisms highlighted in the study 199

List of tables

Table 2.1 List of primary antibodies used 44
Table 2.2 *Astyanax* specific primers used for qPCR 46
Table 2.3 sgRNAs used for CRISPR mediated knockout in zebrafish 48
Table 2.4 ssODNs used in zebrafish knockout 48
Table 2.5 Genotyping primers for zebrafish knockouts 49
Table 2.6 scRNAseq: Digestion buffer for heart dissociation 51
Table 2.7 Polyploid analysis: Stopping buffer for heart dissociation 55
Table 2.8 Polyploid analysis: Dissection buffer for heart dissociation 55

List of Abbreviations

AFOG	Acid Fuchsin Orange G
AGE	Advanced glycation end product
BMP	Bone morphogenetic protein
bp	Base pair
BrdU	Bromodeoxyuridine
CHD	Coronary heart disease
CM	Cardiomyocyte
CNV	Copy number variation
CVD	Cardiovascular disease
DAMP	Damage-associated molecular pattern
DCM	Dilated cardiomyopathy
DDR	DNA-damage response
dpa	Days post amputation
dpi	Days post injury
ECM	Extracellular matrix
EMT	Epithelial-to-mesenchymal transition
EPDC	Epicardium-derived cell
FDR	False discovery rate
FGF	Fibroblast growth factor
GLUT	Glucose transporter
GO	Gene ontology
GSEA	Gene set enrichment analysis
HA	Hyaluronic acid
HH	Hedgehog
hPSC-CM	Human pluripotent stem cell-derived cardiomyocyte

IHC	Immunohistochemistry
LAD	Left anterior descending
MI	Myocardial infarction
mRNA	Messenger RNA
miRNA	microRNA
MMP	Matrix metalloproteinase
PALS	Pathway activity level score
PCA	Principal component analysis
PDGF	Platelet-derived growth factor
qPCR	Quantitative polymerase chain reaction
RA	Retinoic acid
ROS	Reactive oxygen species
SEM	Standard error of mean
scRNAseq	Single cell RNA sequencing
sgRNA	Single guide RNA
ssODN	Single stranded oligonucleotide
TCA	Tricarboxylic acid
TEM	Transmission electron microscopy
TLR	Toll-like receptor
UMAP	Uniform Manifold Approximation and Projection
WT	Wild type

Chapter 1
Introduction

1.1 The lasting damage of myocardial infarction

Cardiovascular disease (CVD) is a large umbrella term that includes conditions affecting both the heart and vascular system. It has long been one of the leading causes of death both in the UK and worldwide, with the majority of these fatalities caused by coronary heart disease (CHD) (*1-3*). CHD largely manifests as an acute injury to the heart that is caused by blockage of the coronary blood supply, a process known as myocardial infarction (MI) or more commonly known as a heart attack (*3*). Great strides forward in risk-factor management, as well as advanced therapies for coronary revascularisation have significantly improved survival after MI(*4, 5*). However, the lasting myocardial damage from non-lethal MI has contributed to the increased incidence of end stage heart failure – a pathological state where the heart is unable to pump blood to support the requirements of the body (*4, 5*).

During MI, the blockage in a coronary artery starves cells, particularly the cardiomyocytes, of both oxygen and nutrients causing them to die. This activates an immune response, which culminates in activation of fibroblasts to myofibroblasts and deposition of a permanent non-contractile collagen scar. Critically, the lost cardiomyocytes are not replaced and the permanent scar causes complications, particularly affecting the contractile function of the heart leading to ventricular dysfunction (*6*). Ventricular dysfunction is further driven by an adaptive physiological response to injury, which is initially compensatory, but maladaptive in

the long term due to its continued activation. As a result, ventricular dilation, scar thinning, interstitial fibrosis and additional cardiomyocyte death can occur. Ultimately, this can lead to recurring MI and or even the progression into heart failure (*6*).

Currently, therapies are limited to simply delaying the progression of heart failure after the initial injury and do not deal with the central issue - the loss of functional myocardium (*7, 8*). As such, it would be highly desirable to replace the dead cells with new, endogenous cardiac muscle. This concept to reconstitute the heart after MI with new cardiomyocytes – effectively regenerating the heart – is a tantalizing prospect, which could combat heart failure.

1.2 Heart Regeneration across the animal kingdom

The process of organ regeneration has long been observed across the animal kingdom, occurring in multiple different organs, even in the human in the context of the liver (*9*). But what about the heart?

Cardiac regeneration was first suggested in amphibians, but it was not until the seminal paper by Poss and colleagues almost 20 years ago, that natural heart regeneration was conclusively reported in an organism (*10, 11*). Here they showed complete and natural regeneration after apical resection of the heart in the zebrafish (*Danio rerio*), a teleost fish native to south Asia (*9, 11*). Resection of the heart involves surgically cutting ~20% of the heart apex, which results in a scar largely composed of fibrin. The authors found that proliferating cardiomyocytes replaced the lost myocardium, and that the fibrin scar is fully resolved within ~2 months of injury(*11*). Since the publication of this study, further injury models for the zebrafish have been established, which include genetic ablation of cardiomyocytes (*12*), hypoxia/reoxygenation (*13*) and cryoinjury (*14-16*) – all of which the zebrafish regenerate from with cardiomyocyte proliferation. In particular, cryoinjury utilizes a cryoprobe to cauterize the heart, generating an injury involving necrotic and apoptotic cell death with the subsequent formation of a collagen scar, which takes longer to resolve than the fibrin scar after resection (*14-16*). Therefore, cryoinjury better mimics the cell death and collagen scar induced by MI in humans, and as such has become the preferred injury model in the zebrafish. The regenerative ability is not just limited to the heart in these fish but also extends to multiple organs including the fins (*17*), the spinal cord (*18*), the retina (*19*) and the kidney (*20*). Zebrafish is quite clearly a species with huge regenerative potential.

The discovery of this impressive cardiac regenerative ability in zebrafish has led to the subsequent investigation of heart regeneration in a variety of teleost fish. These include the giant zebrafish (*D. aequipinnatus*) (*21*), the goldfish (*C. auratus*) (*22*) and the killifish (*N. furzeri*) (*23*). However, the regenerative capacity of the heart is not completely conserved in the teleost lineage as the medaka (*O. latipes*) does not regenerate its heart and forms a permanent fibrotic scar after injury(*24*). Heart regeneration has also been found in other vertebrates, including the newt (*Notophthalmus viridescens*) and the axolotl (*Ambystoma mexicanum*), both urodele amphibians (*9*).

Heart regeneration is extensive across vertebrates, but is there a possibility for mammals to regenerate their heart? In a standout study, Porrello *et al*. showed that the developing neonatal mouse (*Mus musculus*) can also regenerate its heart (*25*). Here, they found resection of the ventricular apex on 1-day-old mice resulted in complete cardiac regeneration within ~21 days. Significantly, this regenerative potential was present for a limited time and was lost by 7 days after birth – also known as the "regenerative window". The regenerative response was characterized by cardiomyocyte proliferation with fibrosis, which was later resolved with minimal hypertrophy (*25*). After this initial study, the regenerative response in the neonatal mouse was also reported using several other injury models including ligation of the left anterior descending coronary artery (LAD ligation), an injury model more mimicking MI (*26, 27*). More recently, the larger neonatal porcine heart was also described to regenerate after LAD ligation within the small-time window immediately following birth – similar to the mouse (*28*). In addition to neonatal stages, this mammalian cardiac regenerative potential also appears to occur during foetal development (*29*). This is supported by raised cardiomyocyte

proliferation rates and no obvious adult cardiac functional deficit as a result of embryonic mouse heart cardiomyocyte ablation (*29*).

It appears that mammals are capable of undergoing regeneration at foetal and neonatal stages of development, but this potential rapidly declines after birth, drawing correlations between developmental mechanisms and regenerative capacity. However, questions remain how much of regeneration in the post-natal setting is down to the ongoing growth response that is prevalent at this stage. Nonetheless, the impressive finding of neonatal regeneration in the mammalian heart has suggested that regeneration is not a programme totally lost to mammals over the course of evolution and therein lies the potential to unlock it.

One of the major questions is whether this post-natal regenerative window seen in the pig and mouse is conserved in humans. Interestingly, a number of clinical case studies have provided preliminary evidence of regenerative repair in humans (*30, 31*). One such study reported severe myocardial infarction due to coronary artery occlusion in a new-born infant. Massive cardiac damage developed, but within a number of weeks functional cardiac recovery was observed, ending with normal cardiac function in the long-term (*30*). Additionally, case studies have reported that infants with congenital heart disease develop little to no scarring following corrective surgery (*31*). Overall these case studies seem to support the prospect of human heart regeneration in early life.

The identification of heart regeneration in both the zebrafish and the neonatal mouse has ignited the field of heart regeneration leading to an array of studies attempting to understand the innate mechanisms underlying the regenerative process. It is the hope that insights into the cellular and molecular mechanisms from these animal models will lead to therapies that can induce human heart repair.

1.3 Mechanisms of heart regeneration

Cardiac regeneration is a complex multifactorial process, requiring a delicate interplay between many major cell types. A balanced immune response, neovascularization, activation of the epicardium and endocardium, the composition of the extracellular matrix (ECM) with scar resolution, and of course cardiomyocyte replacement via proliferation are all factors implicated in the regenerative process. Use of animal models such as the zebrafish and neonatal mouse have enabled insights into the mechanisms underlying these processes.

1.3.1 Cardiomyocyte proliferation

The primary functional component lost after MI is the cardiomyocyte, and replacement of these cells is undeniably key for effective repair. To achieve this, animal models capable of natural heart regeneration undergo significant spontaneous cardiomyocyte proliferation after injury, an observation that is remarkably consistent across all these models, including the regenerating zebrafish and neonatal mouse (*11, 25, 32*). After injury, cardiomyocyte proliferation increases globally but mostly in the region adjacent to the wound border, which is normally referred to as the border zone (*14, 15, 25, 33, 34*). Significantly, this proliferation in the zebrafish and neonatal mouse occurs from pre-existing cardiomyocytes rather than a stem or progenitor cell population (*25, 33-35*). In order to proliferate, cardiomyocytes undergo 'dedifferentiation', which is a state defined by cell-to-cell separation with loss of mature cardiomyocyte characteristics such as disassembly of sarcomere and Z-disc structures (*33, 36, 37*). Following this dedifferentiated state, cardiomyocytes proliferate and then redifferentiate to enable the daughter cells to regain cardiomyocyte contractile properties and establish normal cardiac function (*33, 34*). In an essential step, the proliferating cardiomyocytes also migrate and repopulate the wound by the support from other

tissues/cell types and signalling from Cxcl12/Cxcr4 (C-X-C motif chemokine ligand 12/receptor 4) (*38, 39*).

This robust and effective proliferation of pre-existing cardiomyocytes in the regenerating zebrafish and neonatal mouse is in contrast to the adult mammalian heart. Historically, it was believed adult mammalian hearts were completely incapable of cardiomyocyte renewal. However, impressive carbon dating and stable isotope labelling studies revealed a measurable, albeit small, turnover of cardiomyocytes in the hearts of both humans and mice during the course of aging (*40, 41*). Moreover, several studies have reported increased cardiomyocyte cycling in the myocardial border zone in the adult mouse after MI, but again this turnover was relatively low (*41, 42*). Despite the apparent capacity for renewal in the adult mammalian heart, MI fails to activate robust and effective cardiomyocyte proliferation to counteract the substantial cell loss caused by cardiac injury. Why is this and what are the mechanisms that control proliferation?

After injury, the border zone cardiomyocytes come into contact with a range of ligands from surrounding cell types, initiating a multitude of signalling pathways in order to regulate proliferation. Many of the emerging ligands and signalling pathways are well known from their role in cardiac development leading to the term, reactivation of the foetal gene program, and the idea of its necessity in stimulating cardiomyocyte proliferation. Some of the main implicated ligands and pathways include, Nrg1-ERBB signalling (*43, 44*), the Hippo-Yap pathway (*45, 46*), bone morphogenetic protein (BMP) signalling (*37*), hedgehog (HH) pathway (*47, 48*), insulin-like growth factor 1 (IGF1) signalling (*49, 50*) as well as signalling from fibroblast growth factors (FGFs) (*51, 52*) and platelet-derived growth factors (*49, 53, 54*). All of which have key roles in cardiomyocyte proliferation during development and have now

been implicated in regeneration. Further to the idea that a foetal gene program promotes proliferation and regeneration, a number of downstream transcription factors with key roles during development have been reported with regards to proliferation after injury. This includes Gata4, PITX2, Hand2 and Tbx20, which are all transcription factors that are essential to cardiomyocyte proliferation in either the zebrafish or neonatal mouse during regeneration (*34, 51, 55-57*). Conversely, there are negative roles of the transcription factors MEIS1 (Meis homeobox 1) and Runx1 (RUNX family transcription factor 1), which respectively, induce post-natal cardiomyocyte cell cycle arrest in the mouse or restrict cardiomyocyte proliferation in the zebrafish (*58, 59*). Cardiomyocyte proliferation is also influenced by post-transcriptional regulation in the form of microRNAs (miRNAs). Multiple miRNAs have been characterised during regeneration and these can have both positive and negative effects depending on the specific miRNA (*27, 60-62*).

In response to these signalling pathways, particularly Nrg1-ERBB signalling, proliferating cardiomyocytes at the border zone in zebrafish undergo a metabolic reprogramming, specifically upregulating anaerobic glycolysis (*63, 64*). In both the zebrafish and neonatal mouse, this capacity for anaerobic glycolysis is essential for cardiomyocyte proliferation during heart regeneration (*63, 64*). In particular, pyruvate dehydrogenase kinase activity and the function of the glycolysis enzyme, Pkma2 (Pyruvate kinase M1/2), are key factors in cardiomyocyte dedifferentiation and proliferation during regeneration in zebrafish (*64*).

Aside from Nrg1-ERBB, this metabolic reprogramming underlying cardiomyocyte proliferation has also been correlated with the environmental conditions regenerative models live in – namely the low atmospheric oxygen (hypoxic) levels (*63, 65*). In the murine heart, a temporal shift to oxidative metabolism, as a result from transitioning from hypoxic conditions to high

oxygen availability after birth, is associated with increased oxidative stress via the production of reactive oxygen species (ROS) and in turn cardiomyocyte cell cycle arrest (*65*). Indeed, either ROS scavenging or induction of hypoxia is capable of inducing cardiomyocyte proliferation in mice (*65, 66*), while induction of hypoxia can enhance cardiomyocyte proliferation in zebrafish (*67*). Ultimately, reducing oxidative stress by maintaining a low oxidative state is a prerequisite for cardiomyocyte proliferation. Notably, reduced oxidative metabolism forms another component of the metabolic reprogramming that occurs in the zebrafish myocardial border zone, where mitochondrial oxidative metabolism is downregulated (*63*). This finding is in common with the neonatal mouse, where an immature cardiomyocyte population transcriptionally downregulates oxidative metabolism as they proliferate after injury (*68*).

The finding of low-level turnover of cardiomyocytes in the mammalian heart throughout life offers the intriguing potential of inducing proliferation of pre-existing cardiomyocytes after MI in the adult human heart. However, the limited turnover mostly results in polyploidisation and multinucleation with minimal formation of new diploid, mononucleated cardiomyocytes (*41*). This highlights one of the notable differences between the zebrafish and neonatal mouse hearts with the adult mammalian heart – their ploidy status. Both the regenerating zebrafish and neonatal mouse hearts are formed mostly of mononucleated diploid (two chromosome sets) cardiomyocytes, while adult mammalian cardiomyocytes are mostly tetraploid (four chromosome sets), or also known as polyploid (*69*). In the adult mouse, cardiomyocytes are typically composed of two diploid nuclei (binucleated), and in adult human heart, cardiomyocytes mostly contain a single tetraploid nucleus. In support of the correlation of diploid cardiomyocytes and regenerative potential, a greater abundance of diploid

cardiomyocytes in different strains of adult mice leads to increased functional recovery following MI (*70*). Also, genetically induced polyploidy in zebrafish cardiomyocytes inhibits myocardial proliferation and regeneration (*71*). In combination, this evidence points to ploidy as an important determining factor in cardiomyocyte proliferative potential.

As alluded to above, heart regeneration is an interconnected multifactorial process. As such, the ability of the heart to proliferate cardiomyocytes after injury is also dependant on the action of other tissue/cell types. The effect of these other factors not only on proliferation but also on heart regeneration in general is described below.

1.3.2 Coronary revascularisation

After MI, timely revascularisation in the adult mammalian heart can improve cardiac function. As such, it is perhaps unsurprising that coronary revascularisation of the wound is essential for cardiac regeneration in the zebrafish and neonatal mouse. In terms of regeneration, revascularisation has been best explored in the zebrafish.

The zebrafish mounts a fast and strong revascularisation response to reperfuse the wound and support regeneration of the lost tissue. Here, the coronary vessels sprout into the wound ~15hrs post injury and then form a coronary plexus by ~2 days post injury (*72*). Currently, it is not completely clear what the source of these regenerating coronary vessels is, but evidence strongly suggests pre-existing coronary vessels are the primary source rather than sprouting of endocardial cells (*39*). The revascularisation is supported by a number of proangiogenic factors from several cell types, particularly, the activated endocardium and epicardium (*73, 74*). In the neonatal mouse, revascularisation occurs by the migration of arterial endothelial cells, which reassemble into collateral arteries (*75, 76*).

In the regenerating heart, both Fgf (*77, 78*) and Pdgf (*49, 54*) signalling play a central role promoting neovascularization. More recently, Marín-Juez *et al*. reported that regenerating coronaries sprout intra-ventricularly towards the activated endocardium, which is driven in part by proangiogenic Vegfa signalling (*39*). *vegfaa* (vascular endothelial growth factor aa) is expressed in the activated endocardium early after injury coinciding with the fast revascularisation response and in its absence, fast neovascularisation and cardiomyocyte proliferation did not occur - impairing regeneration overall (*39, 72*). In addition to the intra-ventricular sprouting, the authors also reported superficial sprouting of coronaries from the activated epicardium, which is regulated in part by epicardial Cxcl12/Cxcr4 signalling. The specific epicardial expression of *cxcl12b*, a ligand for the Cxcr4a receptor, appears to be regulated by the hypoxic conditions of the wound and the key hypoxia effector Hif1a (*39*). In evidence of the importance of superficial revascularisation in cardiac regeneration, genetic and chemical inhibition of the Cxcr4a receptor, blocks superficial coronary revascularisation and impairs regeneration (*39, 79*). Ultimately, revascularisation is key to providing a supporting scaffold for cardiomyocyte repopulation of the injury (*39*).

1.3.3 The scar and the extracellular matrix

Scarring is a necessary factor in the response to cardiac injury, occurring in all model organisms, both regenerative and non-regenerative models (*32*). The non-contractile scar tissue is rapidly laid down after cardiac injury to replace the dead cardiomyocytes, which in the short term is vital to stabilising the injury site and preventing rupture of the ventricle. However, in the longer term, the inability to resolve the scar results in the pathological remodelling and heart failure seen in humans (*80*). Thus, a balance is required between a scar that stabilises the injury, but that can be resolved in the long term.

The scar formed after injury is composed of ECM proteins, which dynamically change throughout the scarring process. The ECM scar formation starts early on after MI, with inflammation causing formation of a transient fibrin-based ECM (*81*). During this transient state, proliferation and trans-differentiation of several potential cell types – cardiac resident fibroblasts and epicardial cells – gives rise to myofibroblasts in both non-regenerating scar-based repair models and regenerating models (*82-84*). In the context of regeneration, myofibroblasts are believed to be the main contributor to the scar but contributions from macrophages, epicardial cells and endocardial cells have also been observed, namely in the form of collagens and fibronectin (*58, 85-87*). This is similar to the adult mammalian heart, where contribution occurs mainly from myofibroblasts but also some contribution from epicardial cells and macrophages (*82, 86, 88*). However, whilst the collagen-based scar matures and persists in the adult mammalian heart, the scar in zebrafish is gradually degraded over time. Interestingly, zebrafish fibroblasts inactivate and down regulate ECM production over time, in a key step that is required for scar regression (*87*).

Originally thought to be an inert structural scaffold, it has now become apparent the ECM has a more sophisticated role, influencing cell proliferation, migration, growth factor presentation and particularly intercellular signalling (*81, 89*). Therefore, the ECM composition in the scar has a more complex role during regeneration other than simply being a scaffold stabilising the injury area. Indeed, differences in ECM composition have been correlated to regeneration. This was immediately demonstrated with the different injury models in zebrafish, where the collagen-inducing cryoinjury model delays regeneration versus the resection model, which induces a fibrin dominated scar (*11, 14, 15*). Furthermore, both the regenerating zebrafish and neonatal mouse ECM composition after injury is significantly

different from the non-regenerative adult mouse heart (*90*). In evidence of the ECMs ability to regulate heart regeneration, decellularized zebrafish cardiac ECM made from normal or healing hearts can induce cardiomyocyte proliferation and heart regeneration in the adult mouse via Nrg-ERBB signalling (*90*).

Candidate approaches and unbiased screens are beginning to reveal specific components of the ECM that are key to successful regeneration. This includes Agrin, a component of the neonatal ECM, which has been demonstrated to be important for regeneration in the neonatal mouse heart. Significantly, administration of Agrin to the adult mouse heart after injury is capable of inducing regeneration and cardiomyocyte proliferation via the Hippo-Yap pathway (*91*). In addition, fibronectin, a major component of the ECM, is deposited by the epicardium after injury and is required for cardiomyocyte mobilization and in turn efficient heart regeneration in the zebrafish (*85*). Lastly, the fibroblast-derived factor, Periostin, was shown to be key to neonatal heart regeneration (*92*) and its administration in pigs after MI resulted in improved cardiac function - although this was at the expense of increased fibrosis (*93*).

The molecular pathways that coordinate the ideal scarring process for regeneration are still largely unexplored and poorly understood. Nonetheless roles of Smad3-dependent TGFβ signalling and Ccn2a (communication network factor 2a) have been implicated in ECM deposition and resolution during regeneration (*94, 95*). In zebrafish, *tgfβ* (transforming growth factor beta) and its receptor, *alk5β (tgfr1β)*, are expressed in cells of the injury area and the border zone cardiomyocytes. Inhibition of TGFβ signalling inhibited regeneration in the zebrafish, causing a range of phenotypes including, inhibition of cardiomyocyte proliferation and migration, suppression of Tenascin C (a cell migration factor) and inhibition

of collagen deposition in the scar. These phenotypes suggest TGFβ signalling coordinates deposition of ECM components that are crucial for scar-based repair and cardiomyocyte-based regeneration (*95*). More recently, matricellular factor Ccn2a has been demonstrated to positively modulate the natural regenerative response of the zebrafish heart. The authors of the study propose Ccn2a achieves this by enhancing expression of pro-regenerative ECM genes by inhibiting the chemokine receptor gene *cxcr3.1* (chemokine (C-X-C motif) receptor 3, tandem duplicate 1) through a mechanism involving the already implicated TGFβ signalling pathway. This pathway regulates cardiomyocyte proliferation and the migration of cardiomyocytes into the damaged tissue (*94*). Lastly, what causes the resolution of the scar is one of the least explored areas, but it has been suggested collagenolytic activity from matrix metalloproteinases (MMPs) could be responsible (*96, 97*).

Overall, the scar is not a passive element during regeneration, and as the field has begun to establish, the scar and its ECM components are vital in regulating the regenerative response. Indeed, as found in a number of studies, simply limiting the fibrotic response during the early phases after injury results in failed regeneration (*85, 87*). As such, it appears limiting fibrosis is not the answer, but manipulation of the ECM components towards a pro-regenerative scar is needed.

1.3.4 Activation of the Epicardium & Endocardium

The epicardium is a mesothelial cell sheet that covers the surface of the heart, while the endocardium forms the inner luminal surface of the heart. Endocardial cells are one of the largest cellular components of the adult heart, if not the largest, with proportions estimated at similar levels to cardiomyocytes or higher (*98*). During regeneration, the endocardium possesses a set of functions that largely are different to the endothelial cells of the coronary

vessels. In regenerating species both the endocardium and epicardium become activated relatively early after injury, providing mechanical and paracrine support to guide regeneration of the other cardiac tissues (*74, 99*).

After injury, the epicardium induces the expression of genes that mark the developing embryonic epicardium, in the case of zebrafish this includes *raldh2*, *tbx18*, and *wt1 (12, 15, 16, 78, 100, 101)*. At this point epicardial cells begin to proliferate, undergo epithelial-to-mesenchymal transition (EMT) and migrate into the injury site, leading to the generation of epicardium-derived cells (EPDCs) and an epicardial cap (*15, 54, 78*). This activation of the epicardium occurs early after injury, 1-2 days in zebrafish, and across the entire epicardial layer of the heart, but becomes confined to the injured area by 7 days after injury (*15, 16, 84*). This organ wide activation of developmental genes in the epicardium upon injury is consistent in the regenerating neonatal mouse, with *Raldh2* and *Wt1* becoming activated (*25, 102*). During regeneration, epicardial EMT and EPDC mobilisation is driven by a cascade of downstream signals induced by FGF and PDGF ligands secreted from cardiomyocytes and thrombocytes (*54, 78*). In addition, epicardial EMT during zebrafish heart regeneration is dependent on hyaluronic acid (HA) and its receptor hyaluronan-mediated motility receptor (Hmmr) (*103*).

Upon its activation, the epicardium/EPDCs become an important source of paracrine signals that regulate cardiomyocyte proliferation/migration and revascularisation during regeneration (*38, 39, 48, 95, 100, 104*). In addition, as the migrating EPDCs invade the injured myocardium they give rise to both myofibroblasts that are essential for scar formation and supporting perivascular cells, which stimulate cardiomyocyte proliferation by secreting additional paracrine factors, such as Nrg1 during regeneration (*44, 84*). Moreover, the

epicardial cells play an important role in establishing an extracellular environment that supports heart regeneration by strongly expressing the key ECM components, *fibronectin*, *periostin* and specific collagens (*84, 85, 105*). From this repertoire of supporting roles, it is unsurprising that ablation of the epicardium itself, inhibiting reactivation or even blocking its ability to undergo EMT, results in defective heart regeneration (*54, 78, 103, 106*).

The activity of the endocardial cells during regeneration has been best described in zebrafish. At 3 days after injury, the activated endocardial cells adjacent to the wound undergo genetic expression changes and morphological changes that are consistent with migration and expansion (*107*). At this point endocardial proliferation peaks - just prior to the 7-day proliferative peak for cardiomyocytes. These cells are then reported to spread into the wound and mature into a cohesive sheet of the newly formed endocardium. Endocardial *serpine1* expression is upregulated after injury and is implicated in endocardial proliferation (*107*). Additionally, the endocardium adjacent to the wound begins to express high levels of smooth muscle and collagen genes, hallmarks of myofibroblasts, whilst retaining endocardial characteristics (*58*). The endocardium after injury appears to function analogously to myofibroblasts and directly contributes to the scar, with this function in part, dependent on *runx1*. Significantly, *runx1* knockout results in loss of this subset of endocardial cells and significant reduction in collagen and fibrin in the wound (*58*). Could the presence of a more transient cell population that contributes to scar formation in fish, reflect deposition of a less stable and degradable scar compared to the mammalian situation?

Similar to the epicardium, the activated endocardial cells adjacent to the wound act as a signalling centre for heart regeneration. Many of these signalling pathways stimulated in the endocardium are shared between epicardium, such as Notch signalling (*107, 108*), IGF

signalling (*48, 50*), retinoic acid (RA) signalling (*100*) and BMP signalling (*37*). However, specific endocardial Notch signalling promotes cardiomyocyte proliferation during regeneration via antagonism of the Wnt pathway (*109*). As mentioned above, Vegfa signalling from the endocardium regulated intra-ventricular revascularisation of the zebrafish heart after injury (*39*).

The endocardium and epicardium during regeneration have a high degree of similarity in their response to injury, which results in both playing a major supporting role during regeneration. Ultimately, their activity helps to promote cardiomyocyte proliferation and migration with revascularisation, while creating an extracellular environment that supports regeneration.

1.3.5 A balanced immune response

After MI, the massive cell death triggers an immune response, which can be divided temporally into two phases; the early inflammatory phase and the subsequent reparative phase (*110*). These phases involve components of both the innate and adaptive immune systems. This inflammatory process after cardiac injury occurs in both regenerative and non-regenerative models but with noticeable differences which underpin resolution of the scar and tissue renewal versus scar persistence (*110*).

The immune response after MI kicks off by the presence of damage-associated molecular patterns (DAMPs). DAMPs are components from dead cells that trigger Toll-like receptors (TLRs), which are expressed on cardiomyocytes and cardiac-resident immune cells (*111*). Their activation is important for secreting growth factors and proinflammatory cytokines for the large-scale recruitment of neutrophils and monocytes, which characterises the early inflammatory phase (*110*). The potential of TLRs in regeneration is demonstrated by

administration of agonists for TLR2 and TLR4 in zebrafish and the neonatal mouse. This preconditions cardiomyocytes for cell cycle re-entry, which enhances proliferation and regeneration in zebrafish (*112*), as well as induces cardiomyocyte proliferation in the neonatal mouse heart (*113*). Additionally, DAMPs are capable of activating the complement system, which aids the clearance of damaged cells and the inflammatory process. The complement receptor, C5aR1 (complement 5a receptor 1), is highly expressed in cardiomyocytes and endothelial cells after injury in regenerative models. Importantly, complement via C5aR1 significantly contributes to cardiomyocyte proliferation, and promotes regeneration (*114*).

Neutrophils dominate the infarcted area early on after injury, in both the adult mouse and the regenerating zebrafish. In this early phase, neutrophils clear dead and dying cells by phagocytosis, as well as secrete inflammatory cytokines, proteases and MMPs (*111*). These degrade the provisional ECM, accelerate leukocyte influx and amplify inflammation. As the early response progresses, neutrophils are eventually removed from the infarct by phagocytosis from monocyte-derived macrophages (*111*). As such, prolonged and excessive neutrophil activity is typically associated with an unresolved inflammatory response, which has been suggested to affect scar-based repair and natural regeneration (*115, 116*). Indeed, the nonregenerative medaka has delayed neutrophil clearance versus the zebrafish, while delayed macrophage recruitment by pre-depletion in zebrafish leads to neutrophil retention, which ran alongside an unresolved scar (*115*).

In the adult mammalian heart, the recruited monocytes begin to differentiate into macrophages and take on a proinflammatory phenotype – also termed as Ly6C^{hi} or ‘M1’ (*112-114*). Together with the neutrophils, Ly6C^{hi} monocytes/macrophages participate in the phagocytosis of dead and dying cells and release MMPs, proteases and inflammatory

cytokines that further fuel inflammation by increasing immune cell recruitment (*110*). As the immune response moves into the reparative phase, monocytes/macrophages transition into a reparative phenotype (Ly6C^{low}or 'M2') (*117-119*). These Ly6C^{low} monocytes/macrophages become major coordinators of scar-based repair by directly contributing to the scar themselves, whilst releasing factors that promote fibroblast activation to form a scar, angiogenesis and attenuate inflammation (*86, 111*). Much of the work with regards to the immune response in regeneration has been around the action of macrophages and their polarising phenotypes.

Ultimately, macrophages are essential for heart regeneration (*115, 120, 121*). This is demonstrated in the non-regenerating medaka, which has reduced and delayed macrophage recruitment after injury in comparison to zebrafish. Importantly, recovering macrophage kinetics by stimulating TLRs in medaka promoted neovascularization, neutrophil clearance, cardiomyocyte proliferation and scar resolution (*115*). Additionally, depletion of macrophages in both zebrafish and the neonatal mouse results in compromised heart regeneration (*115, 120, 121*). However, inhibiting infiltration of monocytes has been correlated with improved outcomes in adult mice (*122*). These deleterious and beneficial observations of macrophages after injury are likely down to differences relating to the polarising macrophage phenotypes.

In contrast to the adult mammalian heart, the regenerative neonatal mouse heart expands embryonic-derived resident macrophages in response to injury, which dominate the injury area over recruited Ly6C^{hi} monocytes/macrophages (*123*). These embryonic macrophages are more similar to anti-inflammatory 'M2' macrophages and therefore generate minimal inflammation and promote angiogenesis with cardiomyocyte proliferation to mediate

regeneration (*120, 123*). Similar to the adult mammalian heart, polarising macrophage subsets have been observed in zebrafish, which are characterised as a *tnfα+* and *tnfα−* subsets (*124*). However, in contrast these end up promoting scar resolution. Work by Bevan *et al*. showed *tnfα+* macrophages promote scar deposition during the early phases after cryoinjury (*124*). They also demonstrate a rapid switch to anti-inflammatory *tnfα−* macrophages with increased expression of Osteopontin is vital for the quick attenuation of the inflammatory response and complete scar resolution in regeneration.

The inflammatory response after injury is complex and a double-edged sword. Inflammation is a requirement for heart regeneration (*77, 115, 120, 123*) and even acute inflammation can precondition the heart for enhanced regeneration (*112, 113*). On the other hand, inflammation can extend tissue damage after MI in adult mice, while reducing inflammation can reduce infarct size (*125-127*). Ultimately, balance of the inflammatory response, particularly the macrophage phenotype, is key for scar resolution and complete heart regeneration.

1.4 The *Astyanax mexicanus* – A potential new model for regeneration

1.4.1 Limitations of current models of regeneration

To date, heart regeneration has been observed in a range of fish, amphibian and mammalian models in response to a variety of injury methods. By using these models of regeneration, significant strides forward have been made in discovering signals that govern successful regeneration. However, as good as these models have been, they are not without their limitations. Many studies using these models typically use candidate gene approaches, which rely on priori hypotheses – investigating highly relevant genes and signalling pathways that are already predicted to influence regeneration. However, this approach is biased towards the identification of well-known, and well characterised genes and molecular mechanisms (*128*). With the onset of powerful -omics techniques, unbiased comparisons between models of regeneration have mitigated the disadvantages of candidate gene studies to a degree. Comparisons have been made between regenerative and nonregenerative models, between two regenerating models, as well as comparisons with other regenerating organs (*128*). All of which have proved to be an unbiased way of determining novel genes and mechanisms that regulate regeneration. Unfortunately, background variations such as developmental differences, interspecies differences and organ specific differences make it difficult to tease out mechanisms specific to heart regeneration from these background variations (*128*).

The *Astyanax mexicanus*, also referred to as the Mexican cavefish, is a new comparative model for heart regeneration that significantly overcomes many of the above problems and has the potential to enhance our understanding of heart regeneration (*129*).

1.4.2 What is the *Astyanax mexicanus*?

The *Astyanax mexicanus* is a close relative of zebrafish and is a single species consisting of two separate populations, an eyed surface fish population and an eyeless cavefish population. These two populations arose <20 000 years ago when surface fish living in rivers, in Northern Mexico, became separated into caves after flooding events, and subsequently evolved into many distinct cavefish populations (*130-132*).

During their evolution in the caves, cavefish have evolved a host of physiological and behavioural traits in order to contend with the many environmental pressures in the cave that are in contrast to life in the rivers. Some of the main hallmarks of the cave environment include perpetual darkness, reduced food availability, reduced biodiversity, and limited fluctuations in daily environmental cues. One of the most notable changes is the loss of their eyes (*133, 134*) and pigment (*135, 136*), both redundant characteristics in the absence of light. While conversely, they developed improved lateral line systems (*137, 138*), enhanced olfactory senses (*139*) and highly sensitive taste buds (*140*), which enabled navigation and sensing food within the caves. With the absence of light and reduced fluctuations in daily environmental cues, such as temperature and food availability, cavefish have evolved altered circadian rhythms (*141, 142*). These are observed as widespread reduction of rhythmic gene expression and changes to the timing of the activation/repression of the core clock (*142*). This dysregulation of the core clock is closely entwined with the sleep-wake cycle in cavefish, which exhibit reduced levels of sleep (*142, 143*). Due to the reduced nutrient levels within the cave, cavefish have adapted both their metabolism and behaviours to maximise energy uptake and reduce energy expenditure (*144-149*). Namely, cavefish are starvation resistant, have a reduced metabolic rate and developed an increased appetite through a mutation in

the melanocortin 4 receptor (MC4R) of the leptin/melanocortin pathway (*145*). These changes are also accompanied with insulin resistance, resulting in increased weight and hyperglycaemia but without the adverse effects (*144*). Interestingly, many of the adaptations in cavefish are believed to be in part, driven by the need to save energy.

As a research model, the value of the *Astyanax* lies in its ability to compare differing traits within the same species. This unique aspect of the *Astyanax* has led it to be proposed as a model for conditions affecting humans, such as understanding retinal degeneration and insulin resistance (*144, 150*). Here, the *Astyanax* is presented as a new and unique fish model to investigate cardiac regeneration.

1.4.3 Heart regeneration in the *Astyanax mexicanus*

The *Astyanax* is part of the highly regenerative teleost lineage. As such we have recently explored heart regeneration capacity within the *Astyanax* and found it sits uniquely in terms of cardiac regenerative potential of its morphotypes - namely the surface fish and cavefish from the Pachón cave. Following ventricular resection of the heart, both surface fish and Pachón cavefish laid down an extensive collagen scar - similar to the cryoinjury model in zebrafish (Fig 1.1C, D). Impressively, the surface fish was completely able to resolve this scar and regenerate its heart (Fig 1.1E, F). While significantly, the Pachón could not and formed a permanent fibrotic scar, much like the adult human heart (Fig 1.1F, G) (*129*). The opposing scarring and regenerative response were also recapitulated using the cryoinjury model (data not shown).

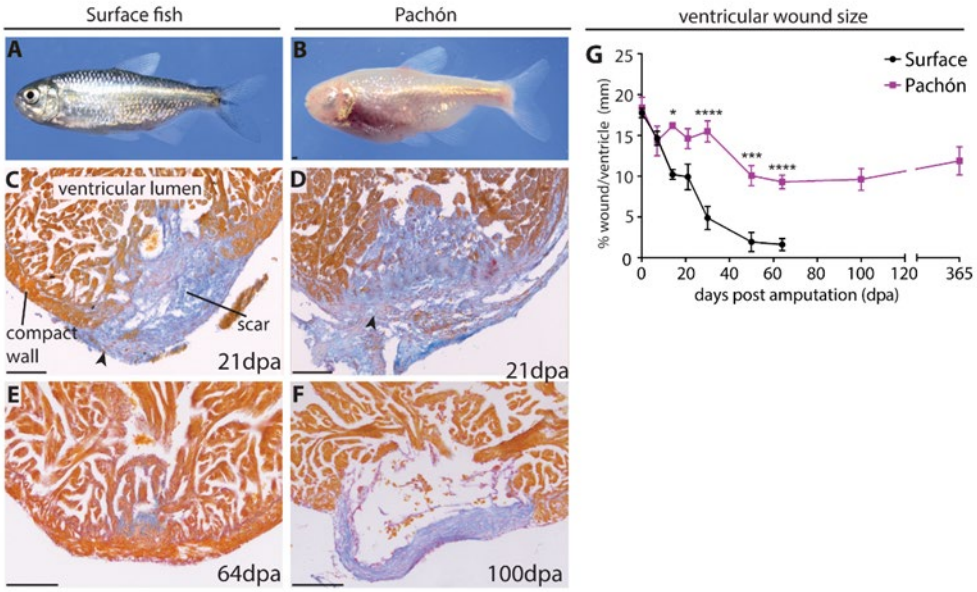


Figure 1.1 Permanent scar formation after injury in the Pachón Cavefish.
(A) *Adult surface fish.* ***(B)*** *Adult Pachón Cavefish.* ***(C–F)*** *AFOG staining of the ventricle at 21, 64- and 100-days post injury (dpi). The blue staining (arrow heads) shows that both fish form a collagen scar after injury, which disappears in the surface fish, but persists in the Pachón.* ***(G)*** *Timeline showing the reducing wound size in the surface fish but persisting wound in the Pachón, which lasts beyond a year. n ≥ 3 per population per time point, Two-way ANOVA with Sidak multiple comparisons test. All data shown as mean +/- SEM. p<0.05 (*), p<0.001 (***), p<0.0001 (****). Figure adapted from (Stockdale et al, 2018) (129).*

To help to understand what underlies this difference in regeneration between the surface fish and Pachón, levels of myocardial proliferation, a key driver behind cardiac regeneration, were investigated. Surprisingly, both the regenerating surface fish and non-regenerating Pachón cavefish are capable of initiating cardiomyocyte proliferation to similar levels, with proliferation peaking one week after injury (Fig 1.2A). However, whilst tracking the cell cycle of these proliferating cardiomyocytes over time it was found the Pachón fish cardiomyocytes did not complete the cell cycle and thus fail to replace the lost cardiomyocytes after injury (Fig 1.2B). The fate of proliferating cardiomyocytes in Pachón fish is currently unknown (*129*).

Ultimately, the *Astyanax* model enables the comparison of natural adult heart regeneration with permanent scarring within one species, mitigating confounding background variations such as interspecies differences.

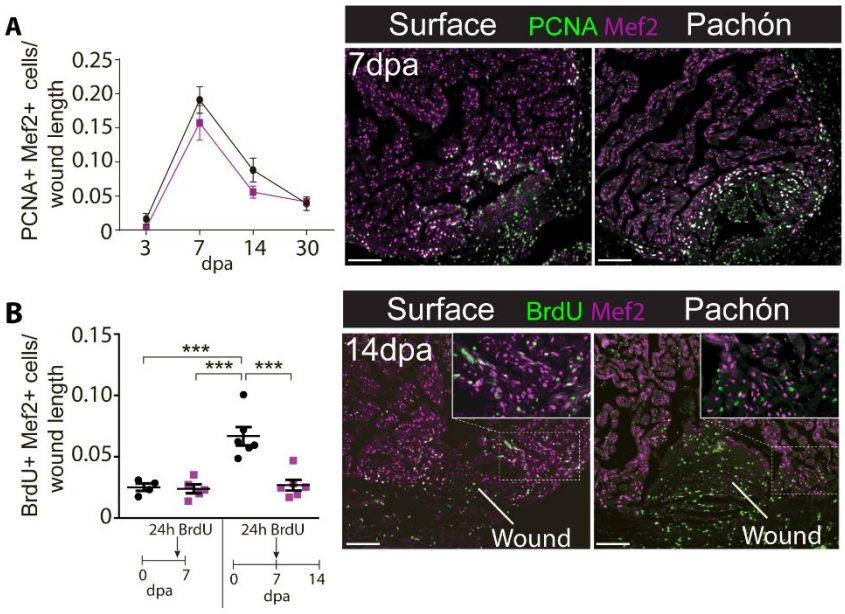


Figure 1.2 Myocardial proliferation differences between Pachón cavefish and surface fish after injury.

(A) *No significant difference in the number of PCNA/Mef2-positive cells surrounding the wound in Pachón compared to surface fish hearts. Proliferation peaks at 7dpi.* ***(B)*** *No difference in the number of BrdU-positive cells at 7 dpi (BrdU administration at 6dpi with heart isolation at 7dpi). However, BrdU pulse chase (24 hr BrdU exposure at 7 dpi with isolation at 14 dpi) shows reduced labelling in the Pachón compared to the surface fish at 14 dpi. Similar number of cells labelled in Pachón at 7 and 14 dpi. One-way ANOVA. All data shown as mean +/- SEM. p<0.001 (***). Figure adapted from (Stockdale et al, 2018) (129)*

1.5 DPhil project aims

As previously described, the differing regenerative capacities of surface fish and Pachón cavefish offer the unique opportunity to compare regeneration and scarring within the same species. These opposing regenerative capacities coincide with contrasting cardiomyocyte proliferation profiles, which are characterised by initiation of cardiomyocyte proliferation in both Pachón and surface fish, but no observable cardiomyocyte expansion in Pachón. As such, this a likely contributor to the lack of regeneration in the Pachón.

However, yet to be determined is whether comparison of surface fish and Pachón hearts can enhance our understanding of heart regeneration by detecting novel candidate genes. Moreover, the fate of the proliferating cardiomyocytes in Pachón is currently unknown, and the genetic mechanisms that are behind the contrasting proliferation profiles and regeneration capacities in *Astyanax* are also not known. These are open questions that are attempted to be answered in this work.

Preliminary data suggests there is no increased myocardial apoptosis that could account for the reduced myocardial expansion in Pachón. To establish a hypothesis that could account for the reduced cardiomyocyte expansion, this work draws on an observation that occurs in the adult mammalian heart - polyploidisation. The small amount of cardiomyocyte proliferation that occurs after MI in the adult mammalian heart typically results in polyploid cardiomyocytes (*41, 151*). As such, in the absence of cardiomyocyte death, and based on the adult mammalian response to MI, this work hypothesises that cycling cardiomyocytes in Pachón are becoming polyploid. In addition, cardiomyocyte proliferation and polyploidy has been linked to metabolism, which cavefish have significantly altered in adaption to cave life. Moreover, preliminary bulk RNAseq analysis revealed transcriptional differences relating the

metabolism. Therefore, this work also hypothesises that metabolic differences underlie the defective proliferation of Pachón cardiomyocytes.

Hypothesis:

Comparing the cardiac injury response in *Astyanax mexicanus* surface fish and cavefish will identify novel genes and mechanisms underlying heart regeneration

In light of this, the aims of this work are twofold:

- Firstly, this work sets out to use the advantages of the *Astyanax* with comparative bulk transcriptomics to unbiasedly detect novel genes that are generally key to cardiac regeneration and to functionally investigate their role in regeneration. Thereby validating the ability of the *Astyanax* as a model to enhance our understanding of natural regeneration.
- The second aim of the work is more targeted and specifically focuses on cardiomyocyte proliferation. Here, the work aims to investigate the fate of the impaired proliferating cardiomyocytes seen in the Pachón heart and determine the mechanisms that underlie this profile using singe cell transcriptomics.

Chapter 2
Materials & Methods

2.1 Animal husbandry

All experimental procedures were carried out in accordance with the UK Animals (Scientific Procedures) Act 1986 under the project licence 30/3258 and the subsequent project licence PP3939965. *Astyanax mexicanus* embryos and fish were kept on a 14-hour light and 10-hour dark photoperiod at 21-25°C . Fortnightly, *Astyanax* tank temperature was raised from 21°C to 25°C to induce spawning. Zebrafish were kept at 28°C on a 12/12-hour light/dark cycle.

2.2 Cryoinjury

Cryoinjury was performed as previously described (*15*). Briefly, fish were anaesthetised in 500mg/L MS222 (Sigma, E10521) prior to cardiac injury and a small was incision was made in the thorax and the pericardium. Apex of the ventricle was exposed by gently squeezing the abdomen and any moisture was removed from the ventricle surface with sterile tissue paper. The dry ventricle was injured by a copper probe cooled in liquid nitrogen and placed on the ventricle until thawed. Following surgery, fish were returned to water and stimulated to breathe by pipetting water over the gills. Hearts were isolated at the indicated time points and processed for RNA isolation, metabolite extraction or fixed in 4% PFA (Santa Cruz, sc-281692). Aseptic technique was performed throughout procedure.

2.3 BrdU exposure

For BrdU pulse chase, fish were exposed to 10mM 5-bromo-2'-deoxyuridine (BrdU, Alfa Aesar, H27260) in tank water at 6 days post injury for 24 hours. After 24 hours, fish were removed from BrdU and placed in fresh fish water. Hearts were isolated at 14 days post injury.

2.4 Heart processing - fixing and paraffin embedding

Following isolation, hearts were placed in 4% PFA (Santa Cruz, sc-281692) with gentle agitation overnight. After fixation hearts were washed twice with PBS before dehydrating across an ethanol series. This series consisted of sequential 1-hour incubations with 70%, 80, 90% and 96% ethanol before finishing with two 1-hour washes with 100% ethanol. All incubations performed with gentle agitation at room temperature. After the ethanol series hearts were incubated in butanol overnight. After butanol incubation, hearts were washed three times in melted paraffin (Paraplast Plus, Sigma, P3683) at ~65°C for 2 hours to ensure replacement of butanol and penetration of paraffin into the tissue. The hearts were then transferred to a cassette filled with paraffin and left to set. The mounted hearts set in the paraffin were sectioned on a microtome to either 7 µm or 10 µm thickness.

2.5 AFOG

Paraffin sections were first mounted on SuperFrost slides (VWR) and dried overnight at 37°C. Following this, sections were then deparaffinized with two 5 min xylene washes. Next, tissue sections were rehydrated in an ethanol series, which included two ~1 minute washes in 100% ethanol, followed by ~1-minute washes in 96%, 90%, 80% 70%, ethanol before placed into distilled water. Rehydrated tissue sections were then post fixed in Bouins fixative (Sigma, HT10132) for 2 hours at 60°C, before cooling to room temperature. The sections were then

washed in distilled water until the yellow colour was not visible (~20mins) and placed in 1% Phosphomolybdic acid (Alfa Aesar, 56166) for 5 mins with gentle agitation. The sections were briefly washed with distilled water before staining with AFOG (Acid Fuchsin Orange-G) for 5 mins. Following staining, sections were very briefly washed in distilled water and very quickly dehydrated through an ethanol series (70%, 80, 90%, 96%, 2x100%) before going two final washes in in xylene. Lastly, coverslips were mounted onto the slides using DPX mounting medium (Sigma, 44581). AFOG was imaged with Nikon Digital Sight stereo microscope (SMZ1500, Nikon).

2.6 RNAscope on tissue sections

Paraffin sections were first mounted on SuperFrost slides (VWR) and dried overnight at 37°C. These were then incubated for 1 hour at 60°C and then deparaffinized with two 5 min xylene washes before two washes in 100% ethanol. Sections were then left to air dry, which was followed by treatment with 3% hydrogen peroxide for 10 min at room temperature. Next, sections were boiled (98-102°C) with RNAscope target retrieval for 15 min, which was followed by incubation with RNAscope protease III at 40°C for 12 min. Following protease treatment, sections were incubated with probes for 2 hours at 40°C. To detect the hybridization signal, RNAscope Multiplex Fluorescent Detection Reagents v2 (ACD, 323100) utilizing the TSA Plus Cyanine 3 or Cyanine 5 fluorophore (Perkin Elmer, NEL744001KT) were applied according to the manufacturer's instructions. RNAscope was imaged on an Olympus FluoView3000 confocal microscope.

For antibody labelling after RNAscope, the Immunohistochemistry was continued from the TNB blocking step described below.

2.7 Immunohistochemistry (IHC) on tissue sections

Paraffin sections were first mounted on Superfrost slides (VWR) and dried overnight at 37°C. Following this, sections were then deparaffinized with two 5 min xylene washes. Next, tissue sections were rehydrated in an ethanol series, which included two ~1-minute washes in 100% ethanol, followed by ~1-minute sequential washes in 96%, 90%, 80% 70% ethanol before placed into 1xPBS. Next, sections underwent antigen retrieval, which consisted of boiling the sections in a pressure cooker filled with 1x Antigen Unmasking solution (Vector Laboratories, H-3300) for 4 mins. Tissue sections were then placed in 1xPBS and drawn around with an ImmEdge pen (Vector Laboratories) to create a hydrophobic border. Sections were then blocked with TNB blocking solution (0.5% TSA Blocking reagent (PerkinElmer, FP1012), 0.15M NaCl, 0.1M TRIS-HCl, pH 7.5) for 30 mins at room temperature to prevent non-specific binding of antibodies. Following blocking, sections were then incubated with primary antibodies diluted in TNB overnight in a humidity chamber. The following day, slides were washed 2x 5 mins with PBS-T (1xPBS 0.1% Tween80) and sections were incubated for 2 hours with corresponding secondary antibodies diluted in TNB (1:200). Simultaneously nuclei were counterstained with DAPI before final 2x 5-minute washes with PBS-T. Cover slips were mounted using ProLong Gold Antifade Reagent (Invitrogen, P36930). Images were processed in ImageJ to generate colour combinations. IHC was imaged on an Olympus FluoView3000 confocal microscope.

Table 2.1 List of primary antibodies used

Antibody	Company	Catalogue No.	Species	Dilution
Mef2c	Biorbyt	orb256682	Rabbit	1:100
PCNA	Dako	M0879	Mouse	1:200
BrdU	Progen	03-61015	Mouse	1:200
MF20	DSHB	AB_2147781	Mouse	1:200
MF20 – cy3 conjugated*	eBioscience	14-6503-82	Mouse	1:100

*Used in section 2.13

2.8 Proliferation counts

Cardiomyocyte proliferation indexes were determined by counting the number of BrdU/Mef2c or PCNA/Mef2c double positive cardiomyocytes in the myocardial border zone. BrdU and PCNA are nuclear proliferation markers (S phase) and Mef2c is a nuclear cardiomyocyte marker. These counts were then divided by the wound length in order to normalize for wound size variations. Wound length was determined by measuring on ImageJ. Indexes were determined for at least three sections per heart. Proliferation indexes for all sections within each heart are averaged (mean) to provide the overall cardiomyocyte proliferation index per heart.

2.9 Wound size measurement

For assessment of regenerative capacity, serial paraffin sections of the entire ventricle were mounted and analysed after AFOG staining. Using ImageJ, the area of the ventricle and scar was measured for each section. The scar area and ventricle area were then totalled across all the sections. The total scar area was divided by the total ventricle area followed by multiplying by 100 in order to determine the percentage of scar to ventricle.

2.10 quantitative PCR (qPCR)

2.10.1 RNA extraction and cDNA preparation

After isolation, all ventricles were immediately stored separately in 500 µl of RNAlater (QIAGEN) until further processing. RNA was isolated from a single ventricle per sample, with 3 samples for both surface fish and Pachón. RNA was extracted from the ventricles using the RNeasy Mini Plus kit (QIAGEN, 74134) according to manufactures instructions. Following RNA extraction, RNA was used with the QuantiTect Whole Transcriptome kit (QIAGEN, 207043), to both produce and amplify cDNA.

2.10.2 qPCR

Quantitative PCR (qPCR) was performed using the previously generated cDNA with the ViiA7 QPCR system (Applied Biosystems, Life Technologies) and Fast SYBR Green Master Mix (Life technologies, 4385612). Reactions were made to contain 1x Fast SYBR Green Master Mix, 150 – 400 nM of each primer set and 5 µL of cDNA (1:1000 dilution of amplified stock) for a final reaction volume of 25 µL. The reactions for genes of interest were performed simultaneously with the housekeeping genes, *rpl13a* and *18s*. Reactions were run in technical triplicates using optically clear fast 96-well plates (Applied Biosystems, Life Technologies, 4346907) and each qPCR run was repeated twice. Thermocycling parameters for each qPCR run consisted of a holding step for 20 s at 95°C, followed by 40 cycles of 95°C for 1 s and 60°C for 20 s. To ensure a single specific product a melt curve step was performed at 95°C for 15 s, 60°C for 1 minute, followed by 95°C for 15 s at the end of the amplification stage. A single specific melting peak was consistent with a single product. The relative expression of each gene was determined after normalization to the mean of the housekeeping genes, *rpl13a* and *18s* and using the

−ΔΔCT method (*152*). The relative expression of each gene was calculated relative to the surface fish expression. Primer sequences and concentrations are below.

Table 2.2 *Astyanax* specific primers used for qPCR

Gene	Forward primer sequence (5'-3')	Reverse primer sequence (5'-3')	Concentration
snai1b	GCGCTAAAGATGCACATCCG	GTGAGGACAGGAGAACGGAC	200 nM
xpo1a	CAGGAGGCATTTTGTTCAGGTG	CGCCAATCATATAACCCACTGC	200 nM
ckba	CTTCCCAACGTGAGCAAACA	TGAGAACCCCAGACGGTCA	200 nM
sfrp2	AAGACGACAGTGAGATGGTGG	CGCCGTTCAGCTTGTATATGG	200 nM
pitx2	GCAGTGTGGACGAATCTGAC	TAAACTGGGCACCAAAGCCG	200 nM
bcat1	GCGTGAAGGAGATGTTCGGT	CTAGAGACGAGTGGGGGACA	200 nM
fbp2	CAGGCTATGCTCTCTATGGC	ACGTTTCTGTCGGTAAGGATGA	200 nM
loxl2b	ACAGACACGACATCGACTGC	AGACTCAGCCACCTCGTAGT	200 nM
ncam1a	CCAATGAGACCACTCCCCTT	CTTTGCTCTCGTTGCCGTTT	200 nM
itgam	TGCTGAAGGAGATCATCGGC	TCAGGGGTCTCTCCATCAGG	200 nM
lrrc10	TCCCAACCTGAAAACCCTACAT	AGCTCATCCAACCTGACCAAC	200 nM
cav1	CAACGAGAGAGACCCACGAC	AGCTCATCCAACCTGACCAAC	200 nM
glut1a	AGTGACCTATCCTGTGTATGCT	GCCCAACAAGGTGCAGTGAT	200 nM
glut4a	CATGCTAGGACTGGCTGGAAT	TGGTCCCACCTCAAAGAACC	200 nM
rpl13a (Housekeeping)	TCTGGAGGACTGTAAGAGGTATGC	AGACGCACAATCTTGAGAGCAG	400 nM
18s (Housekeeping)	CGGAGGTTCGAAGACGATCA	GGAACCCAAAGACTCGTGGT	150 nM

2.11 CRISPR mediated generation of zebrafish mutants

2.11.1 sgRNA and ssODN design and construction

sgRNAs for *lrrc10*, *fmoda*, *tmem198a* and *gpc5b* knock out in zebrafish were designed and generated as a service from Dr. Joey Riepsaame (Genome Engineering Oxford, Sir William Dunn School of Pathology, University of Oxford).

Two sgRNAs were designed per gene and were selected using the sgRNA design tools, CCtop and CRISPOR (*153, 154*). The sgRNAs were made by utilizing a previously published *in vitro* transcription oligo-based method (*155*). In brief, sgRNAs were generated by using oligonucleotides containing the T7 promoter sequence, the sgRNA target site and a

complementary region. This complementary region was annealed to a constant oligonucleotide, which encodes the trans-activating CRISPR RNA (tracrRNA). The resulting oligo overhangs were then extended using T4 DNA polymerase (NEB, M0203L) followed by QIAquick purification (QIAGEN, 28104) to generate a double stranded DNA product. This was used as a template to generate the sgRNAs by *in vitro* transcription. *In vitro* transcription was performed by using the MEGAshortscript T7 Transcription Kit (Ambion, AM1354), which was followed by DNase treatment and precipitation with ammonium acetate/ethanol. This sgRNA method was also previously described in Stockdale et al (*129*).

Gene specific oligo:

5'-TAATACGACTCACTATAGG-N20-GTTTTAGAGCTAGAAATAGCAAG-3' (-N20- is the sgRNA target sequence)

Constant oligo:

5'AAAAGCACCGACTCGGTGCCACTTTTTCAAGTTGATAACGGACTAGCCTTATTTTAACTTGCTATTT CTAGCTCTAAAAC-3'.

A ssODN (single stranded oligonucleotide) was utilized to patch DNA strands together after cutting with cas9 and the sgRNAs. The ssODN possessed homologous arms complementary to the sequence either side of the cut site and contained a small sequence that would potentially insert a stop codon between the two cuts sites. The ssODNs were synthesized by IDT. sgRNA and ssODN sequences below.

Table 2.3 sgRNAs used for CRISPR mediated knockout in zebrafish

Gene	sgRNA 1 (5'-3')	sgRNA 2 (5'-3')
lrrc10	GGTTTAGGTATCCGAAAGCAGG	TTCCAGTCGCCCGAGCTCGGCGG
fmoda	TGTCGCAGTACATAGCGATTGGG	AAGCATAACCCATACAAGATTGG
gpc5b	TATGAAATAGCTGTTCGTGGAGG	GAGAGTAGCATGACTCACCACGG
tmem198a	CGCACAATGTGCCAATTCCCAGG	TGTGTCAGTTATGCAACCGAAGG

*PAMs (protospacer adjacent motif) underlined

Table 2.4 ssODNs used in zebrafish knockout

Gene	ssODN sequence (5'-3')
lrrc10	gcgcagctcTTCCAGTCGCCCGAGCTaGAATTCTTCGGATACCTAAACCAAGTCTTGATG
fmoda	GATTCTCATGAAGCATAACCCATACAAGAATTCagATTGGGAAAGTTGGAGGACAGTCGC
gpc5b	CTATGAATCAGAGAGTAGCATGACTCAGAATTCCGAACAGCTATTTCATAGTCATCTTAG
tmem198a	CGTACTGTATCTCAAATGACCTTCGGAATTCacCCCAGGccgatgcccacactggcctcc

2.11.2 Mutant generation & Genotyping

Prior to microinjection into zebrafish embryos, an injection mixture was made to contain 800 ng/µl cas9 protein (Cas9 nuclease 3NLS protein, IDT, 1081058), 80 ng/µl each sgRNA, 1 µM ssODN and 300 mM KCl. This mixture was incubated at 37°C for 5 min before microinjecting 1 nl of the mixture into the one cell stage of the zebrafish embryo.

Genotyping was performed by fin clipping zebrafish embryos at 3dpf as previously described (*156*). DNA was extracted from fin clips in 96 well plates (Applied Biosystems, 4316813) and mutant alleles were identified by using PCR amplification. Both DNA extraction and PCR amplification were performed using the REDExtract-N-Amp Tissue PCR Kit (Sigma, XNAT) according to manufacturer's instructions. Genotyping primer sequences and concentrations below. Lastly, fish were bred to F2 generation to generate homozygous knockouts of *lrrc10*, *fmoda*, *gpc5b*, *tmem198a*.

Table 2.5 Genotyping primers for zebrafish knockouts

Gene	Forward primer sequence (5'-3')	Reverse primer sequence (5'-3')	Amplicon size (bp)
lrrc10	GTAACGTGTTTCCTGATGCCA	CTGACAAATGCGATTGCGGT	Wt = 833, Mut = 232
fmoda	GCTTGGAGGCCAGTTAGATCA	TTGGGAGCCAACTTGCCAAT	Wt = 613, Mut = 493
gpc5b	CGCCCTGACTGCTAAAATTGG	TGCACAGACTACGATTGGTCG	Wt = 1239, Mut = 461
tmem198a	AGGCTGTAATGTTCCTCACGG	CCGTTTCTTTTGCACTTACCGA	Wt = 816, Mut = 351

2.12 Bulk RNAseq

RNA extraction, sequencing and data analysis was performed by Prof Mathilda Mommersteeg, University of Oxford and Dr Madeleine E. Lemieux, Bioinfo, Canada. Details of methods employed are described in Stockdale *et al (129)*.

2.12.1 RNA extraction and RNA sequencing preparation

Isolated ventricles were directly stored in 500µl RNAlater (QIAGEN) until further processing. Three ventricles were pooled per sample, with three different samples per timepoint for both surface fish and Pachón. Ventricles were placed in RLT buffer and 10 matrix beads before being lysed using the FastPrep FP120 tissue lyser. Next, RNA was extracted from the samples using the RNeasy Mini Plus kit (QIAGEN), which were then spiked in with ERCC RNA Spike-In Control Mixes (2µl of 1:100, Ambion). Samples were then prepared for RNA sequencing using the ScriptSeq v2 RNA-Seq Library Preparation Kit (Epicenter) and sequenced using the Illumina HiSeq 2000 (2x100bp paired-end protocol; Exeter Sequencing Service).

2.12.2 Data analysis

In brief, reads that had passed quality control from FastQC (v0.11.3) were first aligned to the *Astyanax* genome (AstMex02) by using STAR in single-pass mode (*157*). Unaligned reads were

aligned to the ERCC spike-in sequences with BWA (*158*). Transcripts were then filtered to remove transcripts that had low number of reads across the samples. EdgeR was then used to carry out normalization and dispersion estimates according to the edgeR documentation (*159*). RPKM values in the figures were generated using rpkm function of edgeR. edgeR was also used for pairwise comparisons and DESeq2 was used for the time series differential expression - the 141 gene cohort with differential kinetics (*160*).

2.13 Single cell RNAseq

2.13.1 Heart dissociation

Heart dissociation was performed by Helen Potts.

Surface fish and Pachón hearts were isolated on ice at 1dpi, 3dpi, 7dpi and 14dpi after cryoinjury, with uninjured and sham controls. Three hearts were isolated and pooled during dissociation for each of the above groups – creating 12 separate samples. While in ice cold 1xPBS, ventricles were separated from the bulbous arteriosus and atrium, before being cut into small pieces. The pieces of ventricles were then transferred into an Eppendorf with 500 µL of digestion buffer and digested at 32°C on an Eppendorf thermomixer at 800 rpm. Every 15 mins, undigested tissue was left to settle and the supernatant was transferred to a fresh tube on ice. The digestion in the separated supernatant was neutralized by adding sheep serum to create a final 1% sheep serum concentration. Simultaneously, undigested tissue was replenished with fresh digestion buffer and digested again at 32°C on an Eppendorf thermomixer at 800 rpm for 15 mins. This series of digestion and supernatant removal/neutralisation was repeated until fully digested (~1-2 hrs). Following digestion, cells were filtered through 100µm filter and then centrifuged at 300 g for 5 min at 4°C. Supernatant

was removed and the cell pellet was resuspended in 1xPBS before counting the number of cells and observing viability. Following the cell count, cells were centrifuged at 300 g for 5 min at 4°C before resuspension in DMEM plus 10% fetal bovine serum (FBS). Digestion buffer below

Table 2.6 scRNAseq: Digestion buffer for heart dissociation

Reagent	Company
1xPBS	Gibco, 18912014
30mM Taurine	Sigma, T8691
5.5mM Glucose	Sigma, G7528
10mM 2,3-Butanedione Monoxime	Sigma, B0753
10mM HEPES	Sigma, H3393
12.5uM CaCl2	Sigma, C4901
5mg/mL Collagenase II	Gibco, 17101-015
5mg/mL Collagenase IV	Gibco, 17104-019
30mg DNAse I	Roche, 11284932001

Cells were suspended at 2000 cells/µL for loading onto 10X Chromium Chip B and cell capture. Single Cell RNAseq libraries were generated using 10X Chromium Next GEM Single Cell 3' v3.1 kit and sequenced using the Illumina NextSeq 500 Sequencing System.

2.13.2 Single cell RNAseq data analysis

The CellRanger pipeline was utilized to process chromium single cell RNAseq data. Firstly, CellRanger mkfastq was used to demultiplex raw base call files generated by the sequencing into FASTQ files. Next, CellRanger count was used on the FASTQ files to perform alignment to the genome, filtering, barcode counting and UMI counting. This produced the filtered feature-barcode matrices for downstream analysis. The reads from the FASTQ files were aligned to

the *Astyanax mexicanus* v2.0 genome assembly. The above processing through the CellRanger was completed by Dr Madeleine E. Lemieux, Bioinfo, Canada.

Downstream analysis was performed using the R programming language and R studio. Firstly, the Seurat R package (*161*) (Ver 4.0.4) was used to generate a Seurat object from the output of the CellRanger pipeline, whilst filtering out genes that are only expressed in fewer than 2 cells. Next, low quality cells were removed based on several QC metrics, which included removing cells based on the total number of genes expressed in each cell and the total number of counts (UMI) per cell. This was performed using the "quickPerCellQC" function of the scuttle package (*162*), which unbiasedly determined cells that have QC metrics with more than 3 MADs (median absolute deviation) from the median. This function was applied to each sample individually, and all cells with a QC metric beyond 3 MADs were deemed poor quality and removed from the analysis.

After cell QC, each of the following steps was performed in Seurat (*161*). Cells were normalized to account for sequencing depth variations by using Seurat's global-scaling normalization method - the "LogNormalize" function. After normalization, 3000 highly variable features were calculated for each sample and highly variable features that were repeatably variable across samples were selected for anchor identification and sample Integration. Sample integration was performed to correct for technical differences between datasets (batch effects) and integrate similar cell types/subtypes across the samples for comparative analysis between sample datasets. Seurat integration generates an integrated matrix, which was then scaled before running a principal component analysis (PCA). Using 40 principal components (PCs) as input, UMAP (Uniform Manifold Approximation and Projection) plot was generated to visualize the integrated datasets. Again, using 40 PCs as input, Seurat's

graph-based clustering approach was used to cluster cells with similar transcriptional profiles together. At this point Seurat's cell cycle scoring metric was implemented to provide both a cell cycle score and assign a cell cycle phase to each cell.

For targeted analysis of cardiomyocytes, cells expressing high levels of known cardiomyocyte markers were annotated as cardiomyocytes and selected from uninjured, 3dpi, 7dpi and 14dpi samples for reprocessing using the same steps above. Common highly variable genes across samples were calculated, which was followed by anchor selection and integration. On the resulting integrated matrix, scaling and PCA was performed. From the PCA, 15PCs were used to generate the UMAP plot and cluster the annotated cardiomyocytes.

Markers for each cardiomyocyte cluster were determined using Seurat's "FindAllMarkers" function with the "MAST" differential expression test (*163*). This function compares each cluster with all remaining other clusters. Differential expression between Pachón and surface fish cardiomyocytes in selected clusters and timepoints after injury, was also performed using the "MAST" differential expression test (*163*) as part of Seurat's "FindMarkers" function. Statistically significant genes from above, were used in Metascape to identify enriched gene ontology clusters (*164*). During Metascape enrichment, the differentially expressed *Astyanax* genes were converted to zebrafish orthologs and analyzed as zebrafish genes.

To predict differentiation/maturation state of the cardiomyocytes both the Cytotrace package and the cardiomyocyte entropy scoring metric were implemented (*165, 166*). For Cytotrace, the raw counts were used as input, while the cardiomyocyte entropy metric utilized the normalized counts as input. In addition, genes from the programmed cell death (GO:0012501) GO term was used as input with the UCell package to generate an apoptotic gene signature score (*167*).

For heatmap generation, all normalized genes were scaled and each cluster was subsampled to 100 cells before using Seurat's heatmap function. Lastly, Dittoseq was used to generate all further plots (Violin plots, dotplots and etc) (*168*).

2.14 Polyploid analysis

Polyploid analysis was based on a previously established protocol but with adaptions (*71*).

2.14.1 Heart dissociation

To generate single cell suspensions, hearts from BrdU exposed *Astyanax* were isolated at 14dpi after cryoinjury into ice-cold 1xPBS. Next, the atrium and the bulbous arteriosus were removed before bisecting the ventricle in two. Tissue was then washed twice in ice cold dissection buffer and incubated in a solution containing 0.2% trypsin, 0.8 mM EDTA (Gibco, 25200-056) supplemented with 20 mM glucose (G7528, Sigma) and 10 mM 2,3-butanedione monoxime (BDM, Sigma, B0753) at 4°C with gentle agitation. Following trypsin incubation, ventricles were washed three times in dissection buffer supplemented with 10 mM BDM and transferred to a 24-well culture plate, where ventricles were digested in Accumax (SCR006, EMD Millipore) supplemented with 20 mM glucose and 10 mM BDM (digestion buffer) for 15 min at room temperature under mild agitation. After 15 min, the digestion buffer was removed and added to an equal volume of stopping buffer containing 10% FBS to neutralize the digestion. Simultaneously, undigested tissue fragments were transferred to a new well with fresh digestion buffer and gently pipetted up and down before incubating under mild agitation at room temperature. This was repeated until the tissue fragments had fully digested. After digestion, dissociated cells were pelleted by centrifugation at 400 g for 5 min before being resuspended in 2% PFA for 30 mins on ice (Santa Cruz, sc-281692). Following

fixation, cells were again centrifuged at 400 g for 5 min and resuspended in 1xPBS. Cells were spread on Superfrost Plus slides (1255015, ThermoFisher Scientific) and air dried overnight.

Table 2.7 Polyploid analysis: Stopping buffer for heart dissociation

Reagent	Company
1xPBS	Gibco, 18912014
30mM Taurine	Sigma, T8691
5.5mM Glucose	Sigma, G7528
10mM 2,3-Butanedione Monoxime	Sigma, B0753
10mM HEPES	Sigma, H3393
12.5uM CaCl2	Sigma, C4901
10% FBS	Sigma, TMS-013

Table 2.8 Polyploid analysis: Dissection buffer for heart dissociation

Reagent	Company
1xPBS	Gibco, 18912014
0.3% bovine serum albumin (BSA)	Sigma, A3059
20 mM glucose	G7528, Sigma

2.14.2 IHC

Cell spreads were first washed with distilled water and rehydrated for 5 mins in 1xPBS. Next, slides were boiled at 95°C in 1x Antigen Unmasking solution for 15 mins and then washed in 1xPBS. Cell spreads were then permeabilized in 0.1% PBS-Triton for 10 mins at room temperature. Following permeabilization, cell spreads were washed twice in 1xPBS and blocked using TNB blocking solution (0.5% TSA Blocking reagent (PerkinElmer), 0.15 M NaCl, 0.1 M TRIS-HCl, pH 7.5) for 30 mins at room temperature. Cell spreads were incubated with mouse anti-BrdU primary antibody (progen, 03-61015) diluted in TNB at 1:200 overnight. The next day, cell spreads were washed in 1xPBS and then incubated for 2 hours with, anti-mouse AlexaFluor 488 secondary antibody (Invitrogen) diluted in TNB (1:200). Following incubation,

cell spreads were washed in 1xPBS and incubated with mouse anti-MF20 antibody (eBioscience, 14-6503-82) that was conjugated to CY3 fluorophore using a fluorophore conjugation Kit (abcam ab188287). Cells were incubated for 4 hours with the conjugated antibody diluted in TNB (1:100) combined with 14.3 µM DAPI (Sigma, D9542). After washing in 1xPBS, cover slips were mounted using ProLong Gold Antifade Reagent (Thermo) and imaged with Nikon Digital Sight stereo microscope (SMZ1500, Nikon).

2.14.3 DNA content measurement – Cell profiler

DNA content was determined using a pipeline made in Cell profiler, which was applied to each field of view (*169*). In brief, images firstly underwent illumination correction to correct for any inconsistent illumination across the image. Next, using the "IdentifyPrimaryObjects" module, nuclei were thresholded based on the DAPI signal and selected as the primary objects. This was followed by using the "IdentifySecondaryObjects" module to identify and select cardiomyocytes based on the MF20 signal (cytoplasmic cardiomyocyte marker). The "IdentifySecondaryObjects" module was set to threshold on MF20 signal (cardiomyocyte marker) by propagating from identified nuclei. Next, cardiomyocyte and non-cardiomyocyte nuclei, were identified by using the "MaskObjects" module, which masked identified nuclei (primary objects) by the cytoplasmic MF20 signal (secondary objects). Lastly, Using the "MeasureObjectIntensity" module the integrated intensity of the DAPI signal was measured in every identified nucleus and exported for further analysis.

To normalize intensity measurements between images, the below calculation was performed on each nucleus:

$$DNA\ content = \frac{Integrated\ Intensity\ of\ nucleus}{Median\ Integrated\ Intensity\ of\ all\ nuclei\ in\ image} x2$$

Ultimately, the resulting value represents the DNA content of a given cell.

DNA content measurements of all cardiomyocyte nuclei across every heart analyzed (both surface fish and Pachón) were used to generate a frequency histogram using a bin size of 0.1n in GraphPad Prism 9. Based on the histogram peaks of surface fish cardiomyocytes, the phase or ploidy state was estimated for each surface and Pachón cardiomyocyte. The ploidy/phase cutoffs are below and were applied to both surface fish and Pachón cardiomyocytes:

1.2n – 2.8n = diploid or G0/G1 phase

2.8n – 3.6n = aneuploidy or S phase

3.6n – 5n = tetraploid or G2M

For each Pachón and surface fish heart, the proportion of cardiomyocytes in each phase was determined.

2.15 Metabolomics

2.15.1 Metabolite extraction

Pachón and surface fish cryoinjured hearts were isolated at 7dpi with uninjured control hearts for metabolite extraction and metabolomics. Metabolites were extracted from three individual ventricles per group.

After heart isolation, the ventricles were separated from the bulbous arteriosus and atrium, before being immediately weighed. Ventricles were then placed in <4°C extraction solution (Chloroform/Methanol/Water at 1:3:1 ratio). To maintain consistency of metabolite concentration across samples, the extraction solution volume was adjusted proportionally to

the mass of each ventricle. A single cavefish ventricle in 200 µl of extraction solution was used as a base line for adapting the volume of extraction solution. Ventricles were then homogenized using a motorized mortar and pestle (Argos Technologies) for 5 mins on ice, before being vortexed at 4°C on an Eppendorf thermomixer for 1 hour and at 1200 rpm. Next, samples were centrifuged at 13 000 g for 3 mins at 4°C, which was followed by removing and keeping the supernatant containing the extracted metabolites. Prior to storage a small 10 µl aliquot was taken from each sample and pooled together, which was used as a quality control sample in the LC-MS procedure. Additionally, a blank sample containing only extraction solution was made for removal of contaminants during the data analysis stage. All samples were stored at -80°C until LC-MS analysis.

2.15.2 Liquid chromatography–mass spectrometry (LC–MS)

LC-MS was performed as a service from Erin Manson as part of Glasgow polyomics.

Hydrophilic interaction liquid chromatography (HILIC) was carried out on a Dionex UltiMate 3000 RSLC system (Thermo Fisher Scientific, Hemel Hempstead, UK) using a ZIC-pHILIC column (150 mm × 4.6 mm, 5 µm column, Merck Sequant).

The column was maintained at 40°C and samples were eluted with a linear gradient (20 mM ammonium carbonate in water, A and acetonitrile, B) over 26 min at a flow rate of 0.3 ml/min as follows:

Time/mins	%A	%B
0	20	80
15	80	20
15	95	5
17	95	5
17	20	80
24	20	80

The injection volume was 10 µl and samples were maintained at 5°C prior to injection. For the MS analysis, a Thermo Orbitrap Fusion (Thermo Fisher Scientific) was operated in polarity switching mode and the MS settings were as follows:

- Resolution 120,000,
- AGC 2e5,
- m/z range 70–1000,
- sheath gas 40,
- Auxiliary gas 5,
- sweep gas 1,
- Probe temperature 150°C and
- Capillary temperature 325°C.

For positive mode ionisation: source voltage +4.3 kV. For negative mode ionisation: source voltage -3.2 kV. S-Lens RF level 60%. Fragmentation was performed with the following parameters:

- Collision energy: 60%
- Stepped collision energy: 35%
- Isolation window: 2
- Dynamic exclusion after 1 time
- Exclusion duration: 6 seconds
- Exclude isotopes: true
- Minimum intensity: 50000

The instrument was calibrated to standard operating parameters prior to sample run. To enhance calibration stability, lock-mass correction was also applied to each analytical run shown below.

Positive Mode Lock masses:

Number of Lock Masses: 1

Lock Mass #1 (m/z): 144.9821

Negative Mode Lock masses:

Number of Lock Masses: 1

Lock Mass #1 (m/z): 135.971

2.14.3 Data Analysis

Data analysis was performed as a service from Dr Gavin Backburn as a part of Glasgow polyomics.

In brief, Instrument .raw files were converted to positive and negative ionization mode mzXML files. These files were then analyzed using IDEOM (*170*), mzMatchISO (*171*) and PiMP with the FrAnK fragmentation data analysis software (Glasgow polyomics in house software) (*172*). The analytical process performed by PiMP is described within Scheltema et al (*173*).

PCA graph was generated in MetaboAnalyst 4.0 based on generalized log (glog)-transformed data obtained in IDEOM. In addition, significantly different metabolite pathways between Pachón and surface fish 7dpi hearts were identified using the PALS (Pathway Activity Level Scoring) (*174*).

2.16 Statistical Analysis

All differential expression from the single cell RNAseq was performed using the MAST differential expression test (*163*), which calculated adjusted P-values using Bonferroni correction.

The analytical process through PiMP for the metabolomics performed pairwise comparisons, producing P-values that were corrected using the Benjimini Hochberg correction (Adjusted P-values) (*172, 173*).

All other statistical analyses were performed in GraphPad Prism 9 software and the statistical test used in each circumstance is shown in the figure legend. A p-value of less than or equal to 0.05 was considered statistically significant.

Chapter 3
Astyanax mexicanus identifies genes key for cardiac regeneration

3.1 Introduction

The differing regenerative capacities between the surface fish and Pachón cavefish morphotypes make the *Astyanax* a unique intraspecies comparative model, and potentially, a powerful tool to identify novel mechanisms and genes behind cardiac regeneration. But what are the mechanisms that are behind this difference in regeneration and how to begin determining these mechanisms and genes – novel or otherwise?

Fortunately, similar to comparative strategies employed in other models, the *Astyanax* lends itself to powerful comparative transcriptomics but without compromising interspecies differences. Bulk RNAseq of whole ventricles from Pachón and surface fish at multiple timepoints after injury was performed to understand the mechanisms that underlie this difference in regeneration and scarring (Fig 3.1A) (*129*). This transcriptomic analysis revealed strong differences relating to the immune response at 3 days after injury followed by significant differences involving the extracellular matrix and the metabolism – all areas for further investigation (Fig 3.1B, C).

Interestingly, it also revealed a cohort of 141 genes with strong differential kinetics between the surface fish and Pachón over all time points (*129*). This cohort of genes experiencing differential kinetics is of particular significance, as it represents genes that are temporally

regulated in response to injury, whilst being differentially expressed between Pachón and surface fish. In effect these are injury responsive genes, which respond differently between fish, and as such, are likely to have a role in regeneration or scar-based wound healing. A small number of the genes from this cohort have been previously reported to have a role in regeneration. However, many of these genes have no previously reported role in cardiac regeneration. It is this cohort of genes, with their potential novel role in regeneration that are the focus of this chapter.

In this chapter, several of these potential novel genes were selected as candidates to explore their role in regeneration. These included *tmem198a, fmoda*, *gpc5b*. However, the chapter ultimately explores one particular gene more closely, Leucine-rich Repeat Containing protein 10, *lrrc10*.

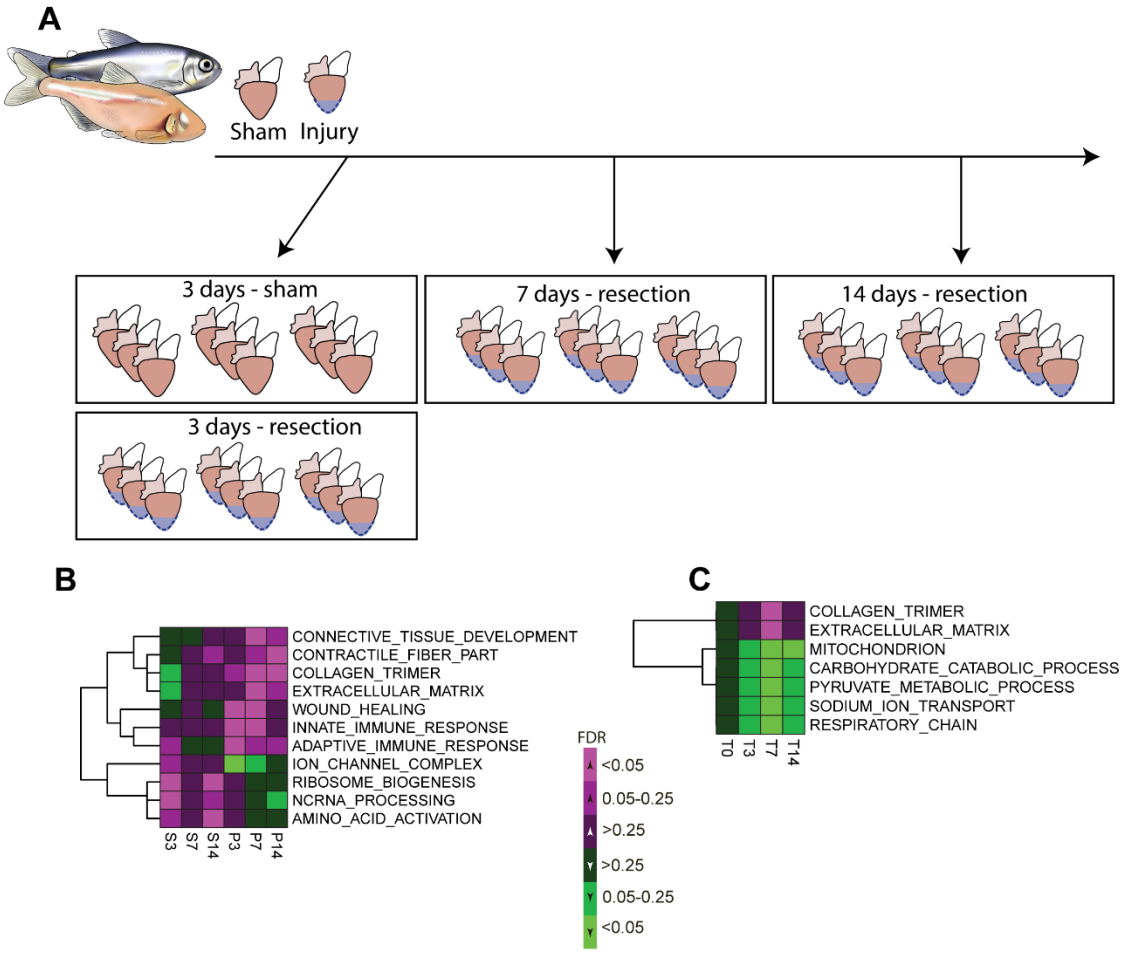


Figure 3.1 Transcriptomic analysis of *Astyanax* hearts after injury.
(A) *Schematic of experimental design. RNAseq analysis performed on Pachón and surface fish ventricles at sham, 3dpi, 7dpi, 14dpi. Three ventricles pooled per sample, three samples per time point.* ***(B)*** *Heatmap for selected Gene Ontology (GO) terms significantly different between sham and at least at one time point per fish. (gene set enrichment analysis; GSEA; FDR < 0.05).* ***(C)*** *Heatmap of FDR values for selected GO terms significantly different between Pachón and surface fish per time point. Selected terms are significantly different at one time point at least (pre-ranked GSEA FDR < 0.05). Figure adapted from (Stockdale et al, 2018)*

3.1.1 Background to candidate genes *fmoda*, *tmem198a*, *gpc5b*, and *lrrc10*

The *tmem198* (Transmembrane Protein 198) gene encodes a seven-transmembrane protein that has been reported to specifically activate Lrp6 (Low-density lipoprotein receptor protein 6) and in turn transduce Wnt/β-catenin signalling during development in the xenopus embryo (*175*). GPC5 (Glypican 5, Gpc5b) is a cell surface heparin sulfate proteoglycan and a member

of the glypican family, which typically regulate morphogens/growth factors, including Wnts and Hedgehogs (*176-178*). Specifically, GPC5 has mostly been reported in the context of cancer. It acts as a tumour suppressor by suppressing Wnt/β-catenin signalling, while on the other hand stimulates Hedgehog signalling, resulting in cell proliferation (*179-181*). Both hedgehog and Wnt signalling are major signalling pathways, which regulate a dizzying array of cellular processes, including processes during heart development and regeneration (*47, 106, 109, 182, 183*). As such, the association of *gpc5b* and *tmem198a* with these pathways make them interesting genes to study. Whilst, not much is known about these genes in the context of the heart regeneration or even in heart function, this unexplored aspect of these genes is part of the draw to explore their role in regeneration.

FMOD (Fibromodulin, Fmoda) is a small leucine-rich proteoglycan that plays a role in the extracellular matrix by binding to collagen, regulating collagen fibrillogenesis and influencing collagen cross-linking (*184, 185*). Its expression is increased in inflammatory, fibrotic and wound healing processes in organs outside the heart (*186-188*). FMOD particularly regulates fibrotic responses through interaction with TGF β (transforming growth factor β) in skin wounding (*186*). Lastly FMOD is expressed within the heart and is upregulated in heart failure patients and mice (*189*). This role in the ECM, a major factor in the regenerative response, and involvement in wound healing/fibrotic responses makes *fmoda* an interesting candidate.

Lrrc10 is a highly conserved heart muscle-specific gene, associated with dilated cardiomyopathy in mouse and human (*190-194*). LRRC10 localises to the dyad region of adult cardiomyocytes and interacts with actin and α-actinin in the heart, implicating a role in the cytoskeleton (*191, 194*). It has also been suggested to bind to L-type Ca2+ channels and regulate channel function (*195*). The fact that the gene is uniquely expressed in the heart but

still has a largely unknown function, particularly in regeneration, makes it an interesting candidate gene to regulate heart regeneration.

3.1.2 Aim

This chapter aims to select candidate genes with potentially a novel and unexplored role in cardiac regeneration from this 141 gene cohort, and assess their importance in the regeneration process. Thereby also validating the ability of the *Astyanax,* as a model, to determine novel factors in heart regeneration. The work utilises a CRISPR-cas9 mediated knockout strategy of selected genes in the regenerating zebrafish to achieve this.

3.2 Results

3.2.1 Analysis of the differential expression kinetics in response to wounding in the *Astyanax*

Hypothesis & expected findings

It was expected that differential expression kinetics across time points after injury within the RNAseq would unbiasedly detect injury responsive genes that are differentially regulated between morphotypes. In combination with qPCR validation this would provide a selection of genes that play a role in cardiac regeneration and ultimately provide a number of novel candidates for further analysis.

Hypothesis: Analysis of the differential expression kinetics alongside qPCR will highlight genes that are important to regeneration or permanent scarring.

Results

The first chapter demonstrates the initial exploration in this 141 gene cohort and the subsequent validation of a number of representative genes.

As part of the analysis into this 141 cohort, genes were clustered together into profiles with similar kinetics (only profiles containing at least 4 genes are displayed) (Fig 3.2 A). Overall, the majority of these genes are upregulated in the Pachón, with the surface fish response to injury being more dampened in the context of this list. Some of these genes in this list have already been linked to regeneration, but a large number have an unexplored role in regeneration to date.

Validation by qPCR of a number of genes at 7dpa from different clusters followed the initial analysis of the dataset (Fig 3.2B-L). The qPCR was performed on RNA from a single ventricle per sample, 3 samples per group/fish. In general, the expression differences in the qPCR data at 7dpa supported the differential expression between Pachón and surface fish seen in the RNAseq. A number of genes from the qPCR analysis were found to be significantly different between the fish whilst others did not reach significance. Nonetheless the difference suggested in these non-significant genes generally supported the difference observed in the RNAseq.

Genes significantly upregulated in Pachón from the qPCR include *snai1b, ckba, sfrp2* and *xpo1a* (Fig 3.2B-E). While genes that were upregulated in Pachón, but not significantly, included *fbp2, itgam, ncam1a, bcat1, loxl2b, pitx2* (Fig 3.2F-K). *snai1b* (*snail family zinc finger 1b*) is important for EMT (*196*) and its upregulation in Pachón with the gene *loxl2b* (*lysyl oxidase-like 2b*), another factor in EMT (*197*), suggests increased EMT in the Pachón heart at 7dpa. The genes *bcat1, ckba and fbp2* are metabolic genes that key to amino acid metabolism, the phosphagen metabolic process and gluconeogenesis respectively (*198-200*). Their upregulation in Pachón suggests upregulation of these pathways relative to surface fish and highlights differences relating to metabolism that have already been previously suggested (*129*). *Itgam* (*Integrin subunit alpha M*) or more commonly known as *cd11b*, is expressed in a variety of leukocytes and is used as marker of these cells (*201*). Again, its upregulation in Pachón suggests an increased leukocyte response in the Pachón at 7dpa.

In contrast to the Pachón heart, surface fish significantly upregulate *cav1* (*caveolin-1*) and *lrrc10* (Fig 3.2L, M). *cav1* has previously been linked to regeneration in the regenerating zebrafish (*202*). It is upregulated in epicardial cells colonizing the injury site and its knockout

in zebrafish impairs heart regeneration. The upregulation of *cav1* in surface fish matches the upregulation seen in zebrafish epicardium after injury, helping to support the RNAseq data.

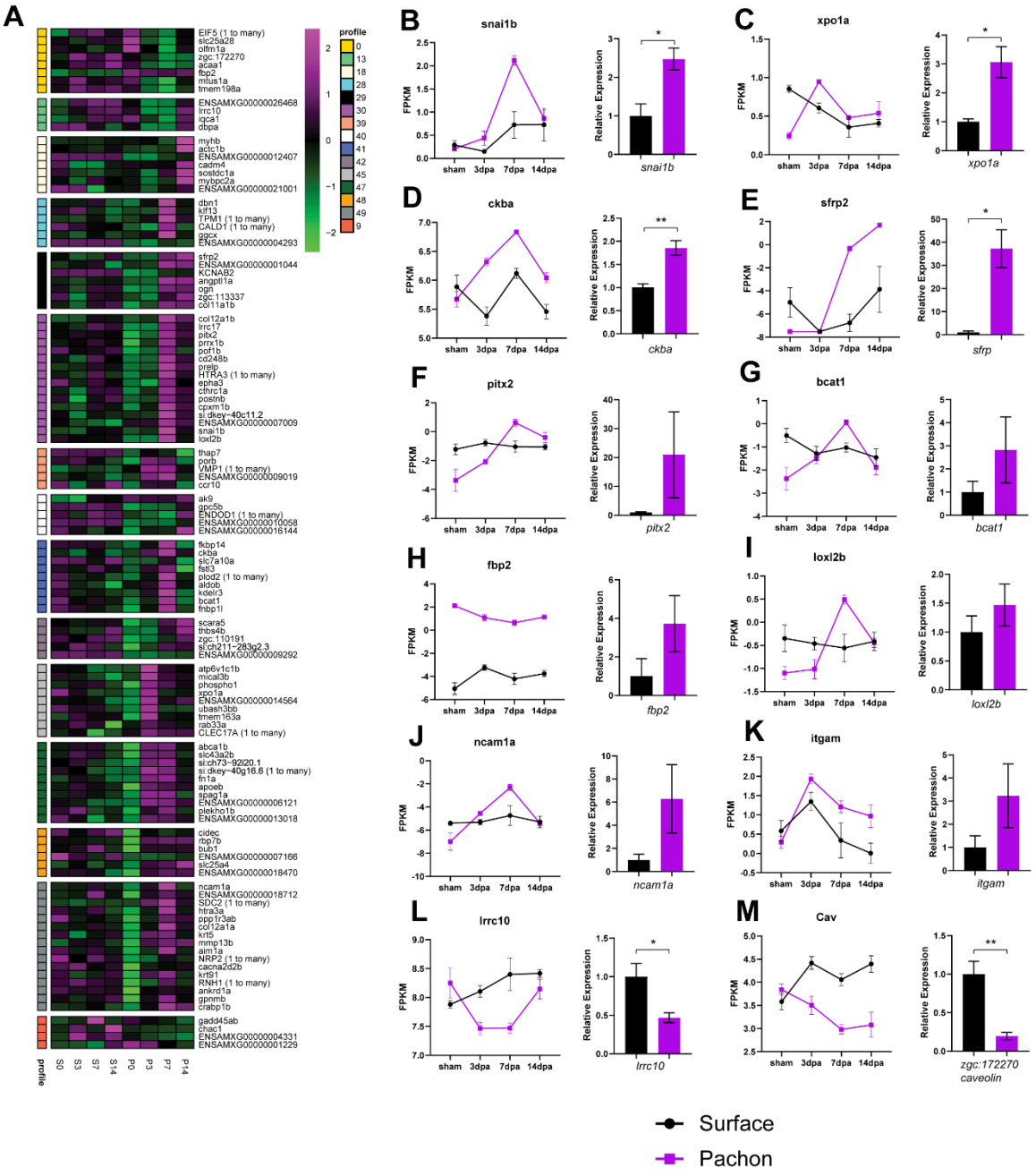


Figure 3.2 141 genes with differential kinetics after injury in the *Astyanax* – identifying *lrrc10*.

(A) *Heatmap of genes with differential kinetics over multiple timepoints. P0/S0 (sham), P3/S3 (3dpa), P7/P7 (7dpa), P14/S14 (14dpa). Each gene expression is row-normalized and genes are clustered into profiles based on similar kinetics.* ***(B-M)*** *RNAseq expression (FPKM) of representative genes over multiple timepoints after injury with qPCR validation of the respective gene at 7dpa. Surface fish in black, Pachón in magenta. RNAseq: two-way ANOVA with Sidak multiple comparisons test. qPCR:*

Unpaired, two-tailed, equal-variance T-test. Both RNAseq and qPCR: n=3. All data shown as mean +/- SEM. p<0.05 (*), p<0.01 (**), p<0.001 (***).

As *cav1* has already been linked to heart regeneration in zebrafish, we selected a number of genes that were upregulated in the regenerating surface fish, but with unknown function during heart regeneration, for further characterisation: *tmem198a*, *gpc5b*, *fmoda* and *lrrc10*.

3.2.2 *tmem198a*, *gpc5b* and *fmoda* knockout has no effect on regeneration capacity in zebrafish

Hypothesis & expected findings

Since *tmem198a*, *gpc5b* and *fmoda* were all upregulated in the regenerating surface fish compared to Pachón after injury, it was expected that CRISPR knockout of these genes in the similarly regenerating zebrafish would impair regeneration – become more Pachón-like. Therefore, this would confirm these genes as having an important role during regeneration.

Hypothesis: Genetic knockout of *tmem198a*, *gpc5b* and *fmoda* in zebrafish will result in increased scar size versus wild type controls, thus suggesting impaired regeneration.

Results

Whilst *lrrc10* is the gene largely focused on in the chapter, initially four genes were selected as candidates to explore their role in regeneration. These also included *fmoda*, *tmem198a* and *gpc5b*, which were selected based on their differential expression in the RNAseq, their function and largely their novelty in regeneration.

All four genes are significantly upregulated at different time points after injury in the surface fish versus Pachón in the RNAseq (Fig 3.3A-B). *tmem198a* expression is similar between fish

at sham but decreases in the Pachón after injury before starting to increase at 14dpa (Fig 3.3A). *gpc5b* expression levels are significantly increased in surface fish versus Pachón across sham, 3dpa and 7dpa. However, expression steadily increases over the time points in Pachón until reaching a similar level to surface fish at 14dpa (Fig 3.3B). *fmoda* expression is again similar between fish at sham but dramatically increases at 3dpa in surface fish, with the significant difference being at this timepoint (Fig 3.3C).

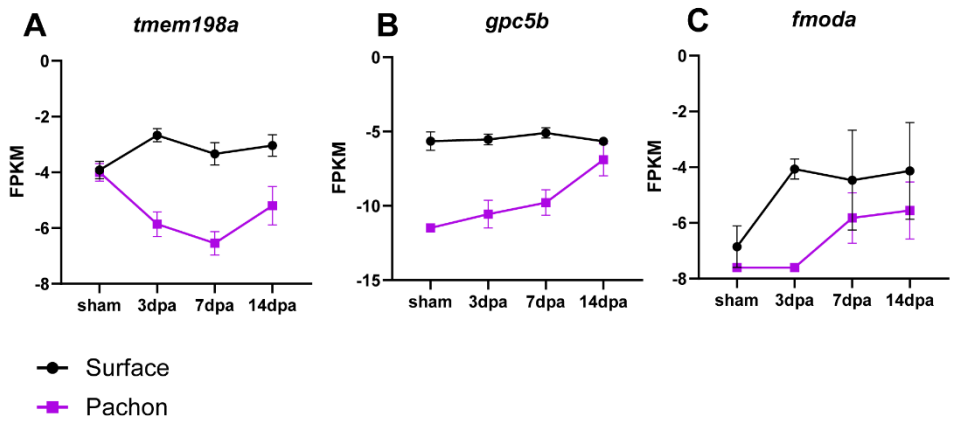


Figure 3.3 Differential expression of candidate genes, *tmem19a*, *gpc5b* and *fmoda*.
*RNAseq expression (FPKM) of **(A)** tmem19a **(B)** gpc5b **(C)** fmoda. Two-way ANOVA with Sidak multiple comparisons test. Surface fish (n=3) in black, Pachón (n=3) in magenta. All data shown as mean +/- SEM.*

To investigate the role of these genes in heart regeneration, the genes were knocked out in the regenerating zebrafish using a CRISPR-cas9 approach (Fig 3.4A, B). The knockouts were performed in zebrafish due to the long-time scale for sexual maturity in the *Astyanax* (~1 year). The general knockout strategy utilised two sgRNAs targeting an exon encoding a functional domain of the respective protein and excised a large region of the exon. A ssODN (single stranded oligonucleotide) with homologous arms complementary to the sequence either side of the cut site was utilised to patch the strands together and insert additional bases

to create a stop codon (Fig 3.4A) (*155*). CRISPR-cas9 components were microinjected into zebrafish embryos, generating F0 offspring, which were grown to adulthood before outcrossing to screen for founders with a desired mutation in the germ line. Founders with the desired mutation were outcrossed generating a heterozygous F1 generation, which were then incrossed to generate a putative homozygote knockout F2 generation. These F2 mutants were used to investigate the role of the gene in regeneration (Fig 3.4B).

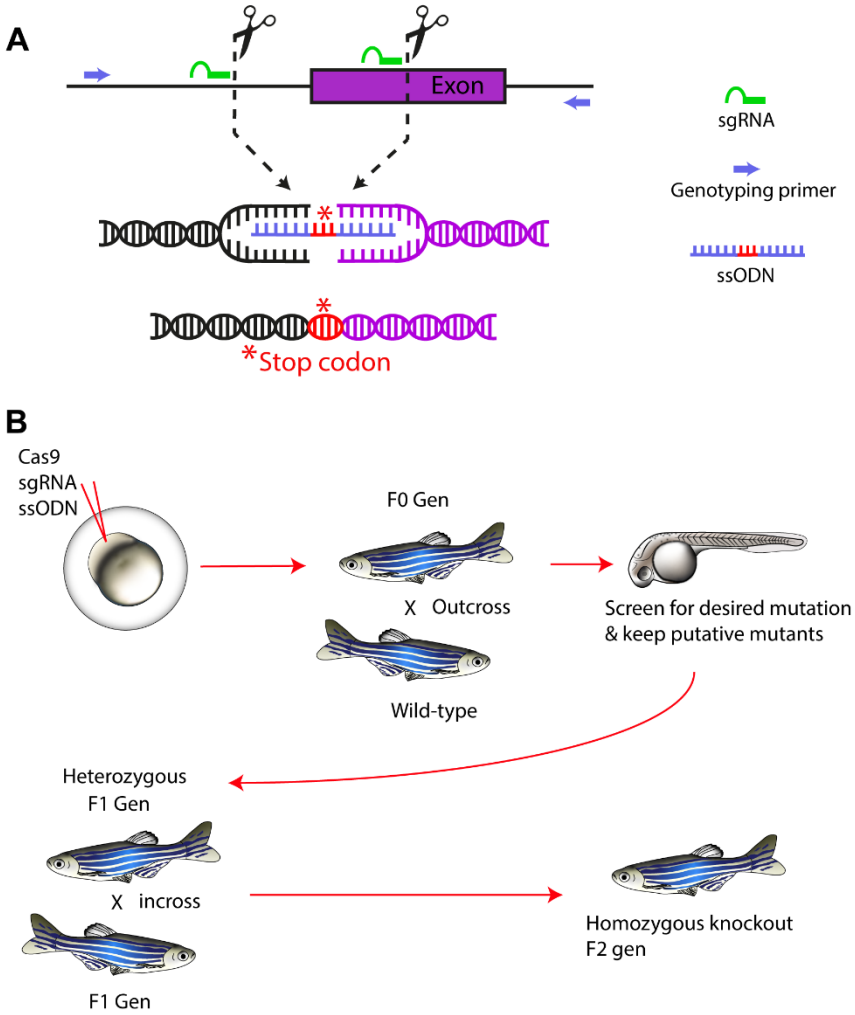


Figure 3.4 CRISPR-cas9 knockout strategy in zebrafish for candidate genes, *tmem19a*, *gpc5b*, *fmoda* and *lrrc10*.

(*A) Schematic of knockout strategy. Two sgRNAs are used to excise a region of the gene, typically targeting a major exon coding for a functional domain. Simultaneously, a ssODN (single stranded oligonucleotide) with homologous arms complementary to the sequence either side of the cut site was utilised to patch the strands together and insert a premature stop codon. Genotyping primers are designed either side of cut sites, generating a truncated PCR product versus wild type.* ***(B)*** *Pipeline for*

generating knockouts. Cas9 protein, sgRNA and ssODN injected in the cell of the embryo, which are raised to create an F0 generation. F0 fish are outcrossed to generate heterozygous F1 offspring, which are screened for the desired mutation. F1 fish with a putative mutation are raised and incrossed, generating a homozygous knockout F2 generation to investigate the role of the gene in heart regeneration.

In the *tmem198a*-/- fish, a large region of exon 3 was removed including the splicing junction resulting in a 472bp deletion and a 7bp insertion, which included a premature stop codon (Fig 3.5 A, B). The entirety of exon 3 was excised from *gpc5b*-/- fish, resulting in a 779bp deletion and just a 1bp insertion (Fig 3.6 A, B). Lastly, in *fmoda*-/- fish a region was excised from exon 2, resulting in a 125bp deletion and a 5bp insertion including a premature stop codon (Fig 3.7 A, B).

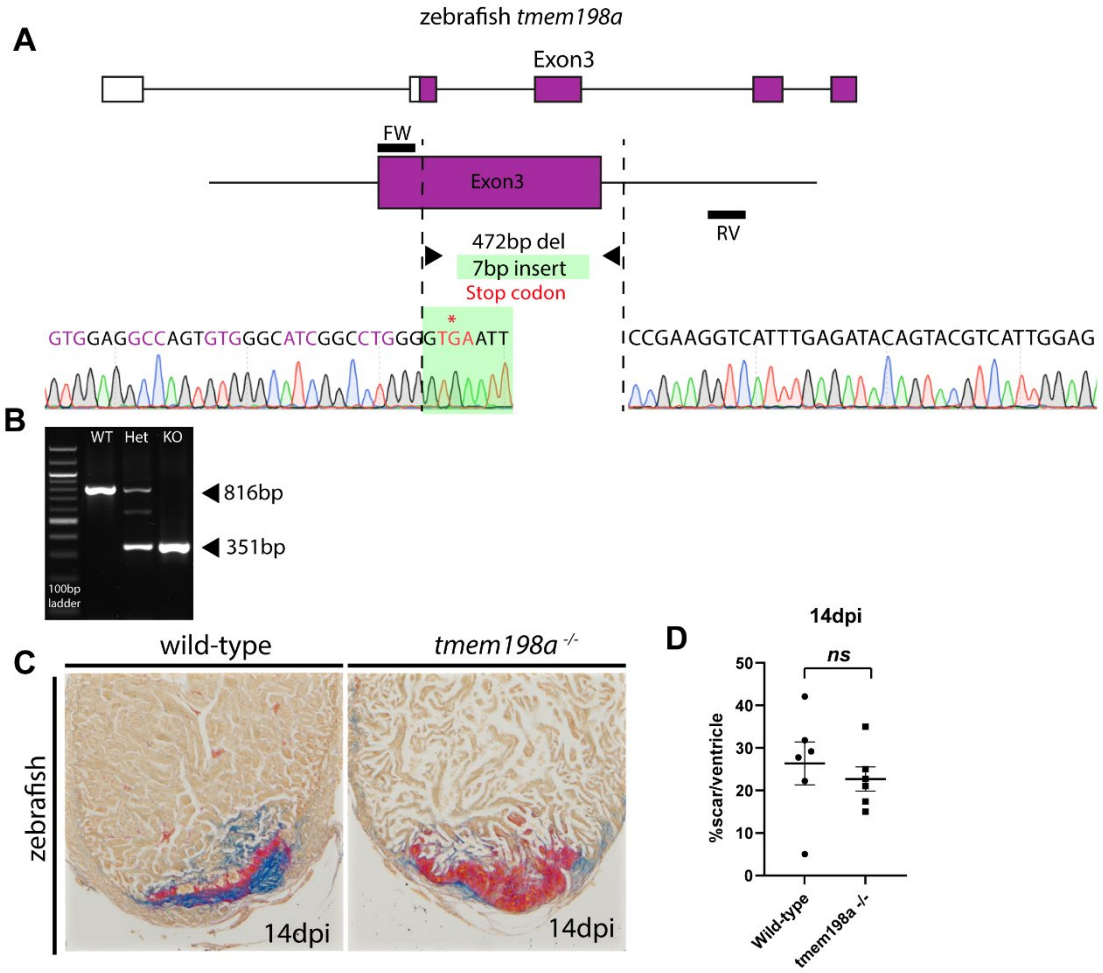


Figure 3.5 Normal regeneration in *tmem19a-/-* zebrafish.

(A) *Schematic of tmem198a mutation. Tmem198a-/- has a 472bp deletion, which includes large region of exon3 and a 7bp insertion, which includes the addition of a premature stop codon.* ***(B)*** *Genotyping with primers just outside the deleted region generates an 816bp product in wild-types and a 232bp in mutants.* ***(C)*** *AFOG staining displaying scar in wild type versus tmem198a-/- hearts after cryoinjury, 14dpi. Blue = collagen, red/orange = fibrin, brown = normal myocardium.* ***(D)*** *Quantification of the scar area normalized to the ventricular area (%) in wild type hearts (n=6) versus mutant hearts. n=6). All data shown as mean +/- SEM. Unpaired, two-tailed, equal-variance T-test.*

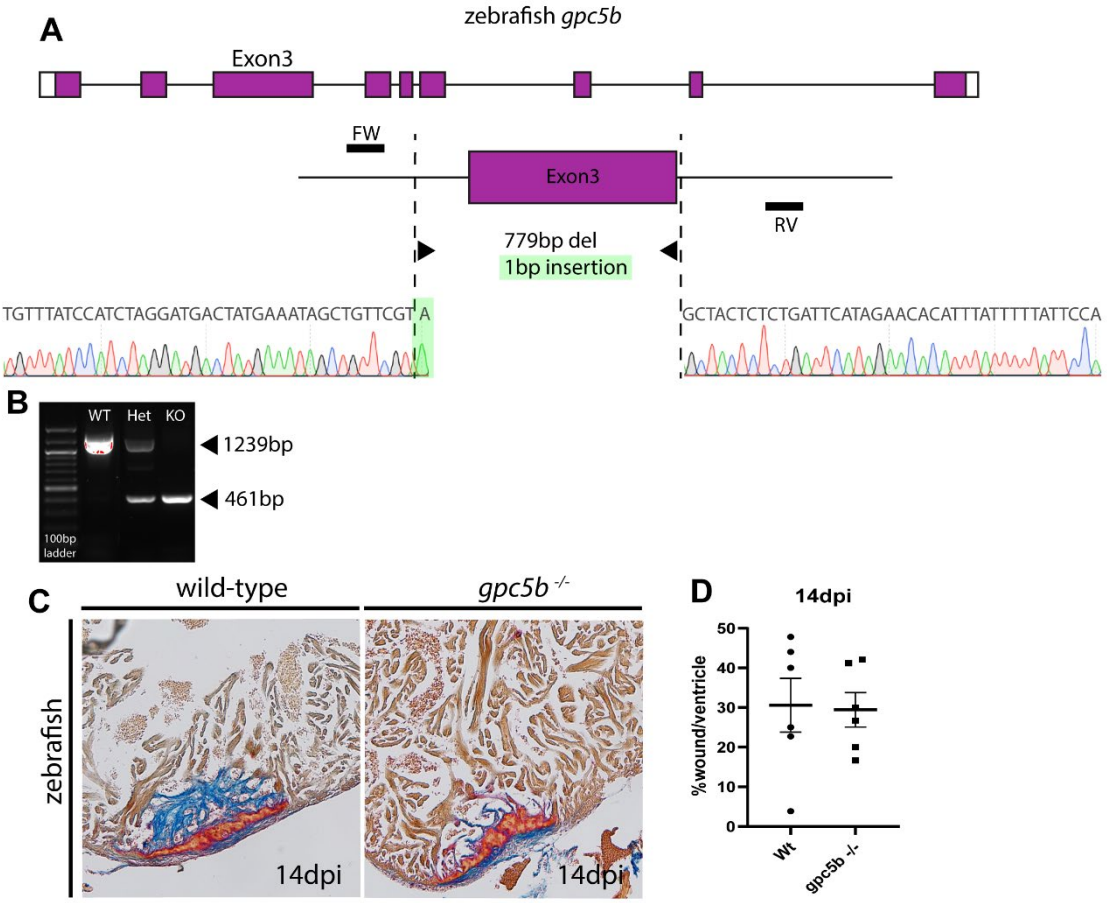


Figure 3.6 Normal regeneration in *gpc5b-/-* zebrafish.

(A) *Schematic of gpc5b mutation. gpc5b-/- has a 779bp deletion, which deletes the entirety of exon3 and a 1bp insertion.* ***(B)*** *Genotyping with primers just outside the deleted region generates an 1239bp product in wild-types and a 461bp in mutants.* ***(C)*** *AFOG staining displaying scar in wild type versus gpc5b -/- hearts after cryoinjury, 14dpi. Blue = collagen, red/orange = fibrin, brown = normal myocardium.* ***(D)*** *Quantification of the scar area normalized to the ventricular area (%) in wild type hearts (n=6) versus mutant hearts (n=6). All data shown as mean +/- SEM. Unpaired, two-tailed, equal-variance T-test.*

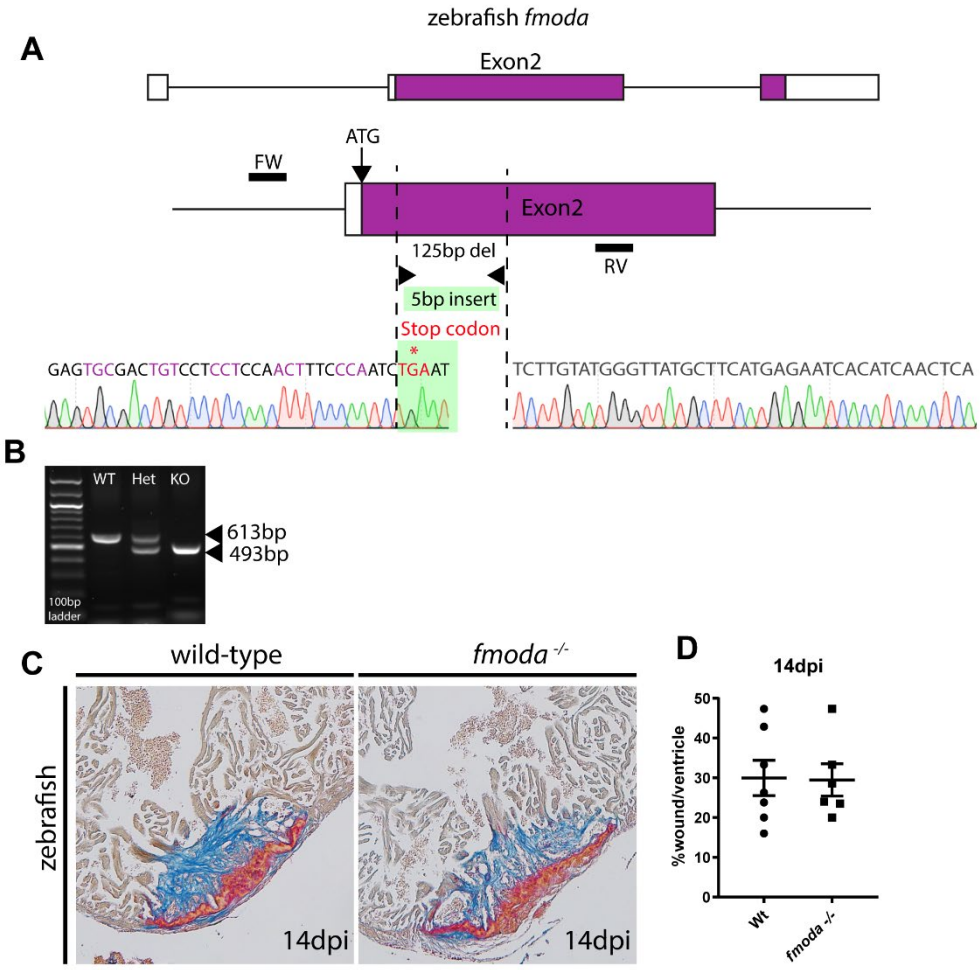


Figure 3.7 Normal regeneration in *fmoda-/-* zebrafish.

(A) *Schematic of fmoda mutation. fmoda-/- has a 125bp deletion, which includes large region of exon2 and a 5bp insertion, which includes the addition of a premature stop codon.* ***(B)*** *Genotyping with primers just outside the deleted region generates an 613bp product in wild-types and a 493bp in mutants.* ***(C)*** *AFOG staining displaying scar in wild type versus fmoda -/- hearts after cryoinjury, 14dpi. Blue = collagen, red/orange = fibrin, brown = normal myocardium.* ***(D)*** *Quantification of the scar area normalized to the ventricular area (%) in wild type hearts (n=7) versus mutant hearts (n=6). All data shown as mean +/- SEM. Unpaired, two-tailed, equal-variance T-test.*

To assess a role in regeneration, knockout mutants were injured using the cryoinjury model to induce collagen scar formation - similar to the *Astyanax* heart after resection. AFOG, a histological stain, was used to observe and measure the scar. Following cryoinjury, all knock out mutants had a similar scar size compared to their respective wild type controls at 14dpi suggesting that these genes do not have a significant role in regeneration (Fig 3.5C, D)(Fig 3.6C, D)(Fig 3.7C, D).

3.2.3 lrrc10 Is required for heart regeneration in zebrafish

Hypothesis & expected findings

Since *lrrc10* is upregulated in the surface fish but downregulated in the Pachón after injury, and previous literature suggesting it as a cardiomyocyte specific gene, it was expected the increased expression of *lrrc10* to localise to the myocardial wound border in surface fish but absent in Pachón. Due to upregulation of *lrrc10* in the regenerating surface fish, it was expected that *lrrc10* knockout in zebrafish would impair regeneration and display a Pachón-like phenotype.

Hypothesis: Genetic knockout of *lrrc10* in zebrafish will result in increased scar size versus wild type controls, thus suggesting impaired regeneration.

Results

As shown above, both RNAseq and qPCR showed that *lrrc10* was significantly upregulated in surface fish versus Pachón. From the RNAseq *lrrc10* expression is at similar levels in sham control hearts in both fish. However, after injury expression moderately increases in the surface fish while dropping extensively in the Pachón, before returning to relatively normal

levels at 14dpa (Fig 3.2L). Similar to the genes above, *lrrc10* was selected based on its differential expression, novelty and specificity to the heart/cardiomyocytes (*192-194*).

To explore the expression pattern of *lrrc10* in the *Astyanax*, RNAscope - an *in-situ* hybridisation technique - was performed on *Astyanax* hearts at 7dpa (Fig 3.8). In confirmation of what has been previously reported in the literature (*192-194*), *lrrc10* expression was specific to the myocardium in both surface fish and Pachón (Fig 3.8A). In the surface fish, expression was increased close to the wound border particularly in the compact wall when compared with the rest of the ventricle (Fig 3.8A, B). This increased expression localised to the wound border corresponds with the area associated with high myocardial proliferation previously reported. However, this increase in expression of *lrrc10* in the border zone was not visible in Pachón (Fig 3.8A, B). *Lrrc10* expression was also explored in the zebrafish heart at 7dpi (cryoinjury) using RNAscope. *Lrrc10* expression in the zebrafish was comparable with that in surface fish, with upregulation in the compact wall close to the wound (Fig 3.8A, B). This suggests a conserved response for *lrrc10* in zebrafish after injury. Again, cryoinjury was used in zebrafish to mimic the *Astyanax* scarring response.

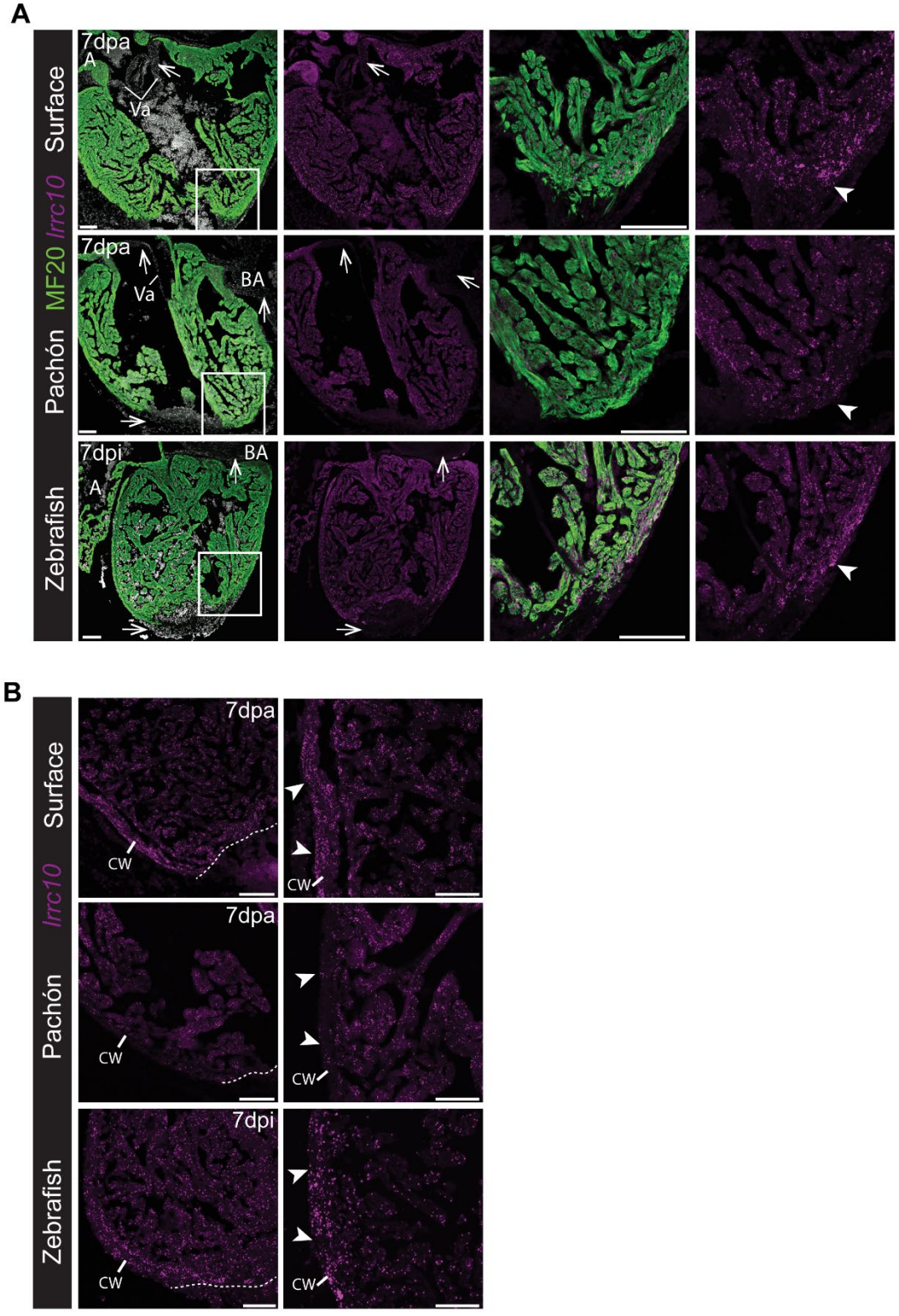


Figure 3.8 Increased *lrrc10* expression at myocardial border zone in surface fish and zebrafish but not in Pachón.

(A) *RNAscope shows lrrc10 is expressed specifically in the myocardium (MF20+) in both surface fish and Pachón at 7dpa as well as zebrafish at 7dpi. Arrows point to negative expression in non-myocardial*

cells/tissues, such as the wound, valves, and bulbus arteriosus. Expression around the wound is higher in surface fish and zebrafish compared with Pachón (arrowheads). n=3. MF20 = green, lrrc10 = magenta. ***(B)*** *lrrc10 expression is particularly higher in the compact wall myocardium (arrowheads), particularly at the wound border (dashed line) at 7dpa/7dpi in surface fish and zebrafish. This localisation is absent in Pachón. n=3. lrrc10 = magenta. All scale bars, 100 µm. BA, bulbus arteriosus; CW, compact wall; Lu, lumen; Va, valves.*

To determine if *lrrc10* has a significant role in natural regeneration, *lrrc10*-/- zebrafish mutants were generated using a CRISPR-cas9 strategy identical to the knockout mutants described above (Fig 3.4). In the *lrrc10* -/- fish, a large region of exon 2 was excised including the splicing junction and the ATG start site, resulting in a 601nt deletion (Fig 3.9A). Traditional whole mount *in situ* hybridisation was used to confirm knockout of *lrrc10* (Fig 3.9C). Wild type 3dpf zebrafish showed signal consistent with *lrrc10* expression specific to the heart, while *lrrc10*-/- 3dpf zebrafish showed no signal, suggesting absence of expression and confirming effective knockout of *lrrc10*. The signal specific to the heart in wild type zebrafish adds another level of confirmation that *lrrc10* is expressed specifically within the heart.

After cryoinjury, *lrrc10*-/- zebrafish had significantly increased scar size compared to wild type controls at 60dpi (Fig 3.9D, E). This reveals impaired heart regeneration in *lrrc10*-/- zebrafish and implicates a role for *lrrc10* during heart regeneration. Interestingly, despite this difference in regeneration, there was no significant difference in cardiomyocyte proliferation near the wound border at 7dpi between the wild-type fish and the *lrrc10* mutants (Fig 3.9F, G). Therefore, similar to the Pachón cavefish, *lrrc10* mutants are able to initiate myocardial proliferation but not effectively repair their heart – displaying a Pachón-like phenotype after injury. While myocardial proliferation was equivalent between *lrrc10*-/- and wild type zebrafish in the wound border zone, myocardial proliferation throughout the ventricle (remote zone) was significantly increased in the *lrrc10*-/- fish at 7dpi (Fig 3.9H, I). This suggests

loss of *lrrc10* has a global impact on cardiomyocyte biology/function, resulting in a greater capacity to initiate proliferation in cardiomyocytes generally.

Ultimately this mutant confirms *lrrc10* as a significant factor required for heart regeneration and the cavefish-like phenotype it displays helps to validate the *Astyanax* as a model, that is capable of detecting novel genes required for natural heart regeneration.

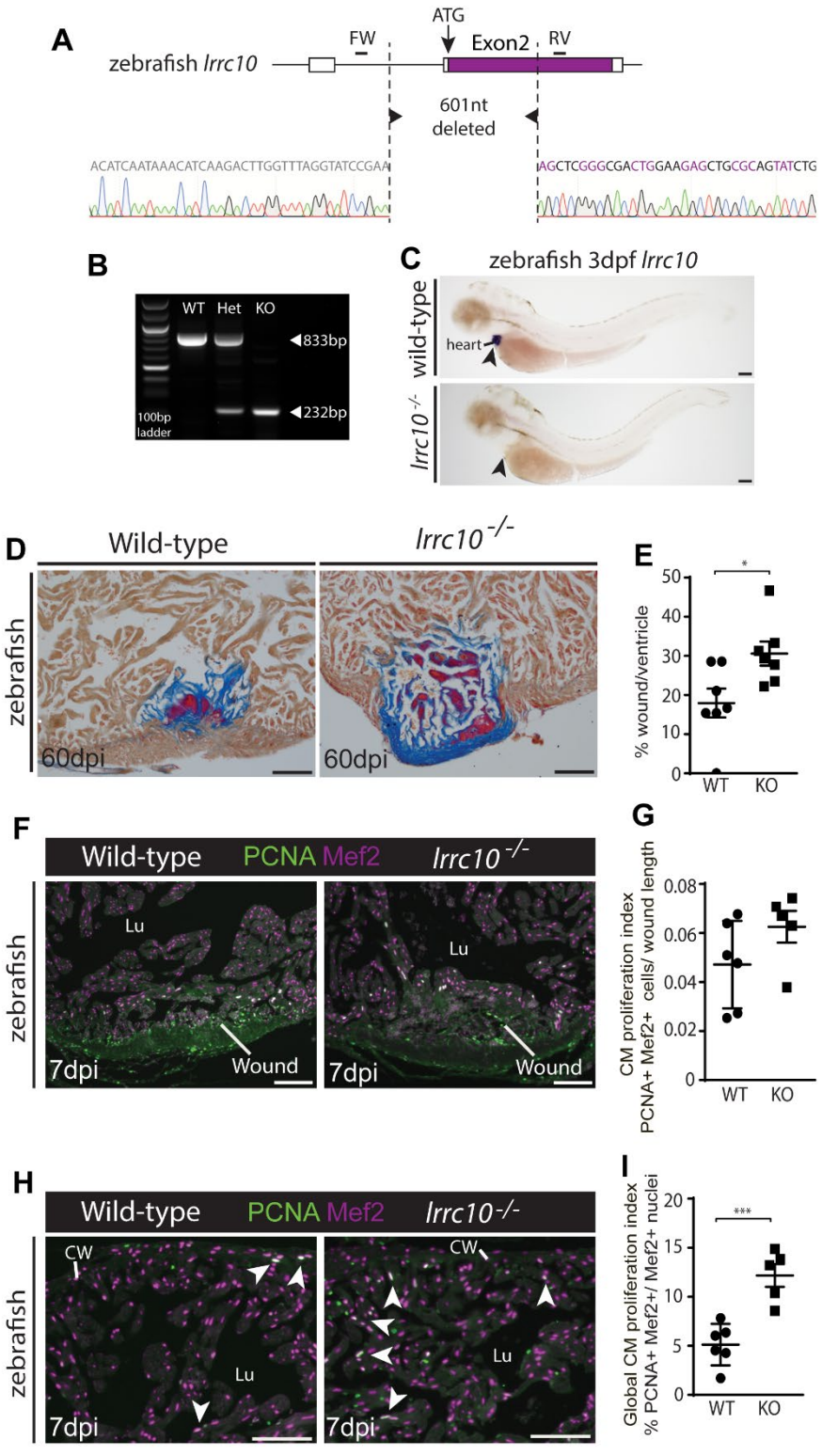


Figure 3.9 *lrrc10* is required for heart regeneration in the regenerating zebrafish.
(A) *Schematic of lrrc10 mutation. Zebrafish lrrc10 -/- has a 601bp deletion, which includes a large region of exon 2 and the ATG start site.* ***(B)*** *Genotyping with primers just outside the deleted region generates an 833bp product in wild-types and a 232bp in mutants.* ***(C)*** *Wholemount in situ*

hybridisation using lrrc10 antisense probe on wildtype (n=25) and lrrc10 -/- (n=12) 3dpf (days post fertilization) embryos. Signal present solely in the heart in wild type embryos (arrow) while no signal present in lrrc10 -/- embryos, consistent with knockout of lrrc10. ***(D)*** *AFOG staining displaying larger scar in lrrc10 -/- hearts versus wild type hearts after cryoinjury, 60dpi. Blue = collagen, red/orange = fibrin, brown = normal myocardium.* ***(E)*** *Quantification of the scar area normalized to the ventricular area (%) in wild type hearts (n=7) versus mutant hearts (n=7) at 60dpi. lrrc10 -/- have significantly increased scar size versus wild type controls. All data shown as mean +/- SEM. Unpaired, two-tailed, equal-variance T-test. p<0.05 (*).* ***(F)*** *PCNA/Mef2 immunohistochemistry at the wound border in zebrafish lrrc10-/- and wildtype controls after cryoinjury, 7dpi. Double positive, mef2 and PCNA cells are proliferating cardiomyocytes. PCNA = green, mef2c = magenta.* ***(G)*** *No significant difference in the number of PCNA/Mef2 double positive cells surrounding the wound in lrrc10-/- (n = 5) compared with wild-type hearts (n = 6) at 7 dpi. Unpaired two-tailed t-test, equal variance. p<0.05 (*).* ***(H)*** *PCNA/Mef2 immunohistochemistry at the base of the ventricle (remote region) in zebrafish lrrc10-/- and wildtype controls after cryoinjury, 7dpi. Double positive, mef2 and PCNA cells are proliferating cardiomyocytes. PCNA = green, mef2c = magenta.* ***(I)*** *Significantly increased number of PCNA/Mef2 double positive cells in the remote region in lrrc10-/- (n = 5) compared with wild-type hearts (n = 6) at 7 dpi. Unpaired two-tailed t test, equal variance. p<0.001 (***).*

3.3 Discussion

The main aim of this chapter was twofold; which was one of determining novel genes in heart regeneration and thereby validating the *Astyanax* model. Overall this was achieved with the identification and validation of *lrrc10* expression and the subsequent phenotype observed in the zebrafish knockout mutant.

3.3.1 Differential kinetics in a wide range of genes and the identification *lrrc10*

The data here displays the 141 gene cohort and the validation of the expression of a number of representative genes. As described, the qPCR data generally supports and validates the expression differences in the RNAseq at 7dpa with significance reached in a number of genes. Genes that were not significant still tended to support the differences observed in the RNAseq. The lack of significance in some of these genes is likely due to the low sample number (n=3) and the variability across the samples that arises from differences in injury size. In this sense, the RNAseq is largely more robust in that each sample is the averaged expression from 3 pooled ventricles, which likely mitigates variation in injury size. While the qPCR is simply a single ventricle per sample.

From the representative genes explored, it is interesting to note a potential upregulation of Epithelial- or Endothelial- to mesenchymal transition (EMT/EndMT) in Pachón hearts via the upregulation of *snai1b* and *loxl2b* – key factors in the activation of EMT/EndMT (*196, 197*). Significantly, EMT or EndMT processes have both been implicated in cardiac fibrosis after injury (*203*). Both the epicardial and endocardial cells via EMT or EndMT respectively, contribute to the generation of myofibroblasts after MI - the major producers of the ECM in the scar (*203, 204*). Additionally, some evidence suggests reducing endothelial-to-mesenchymal transition EndMT can reduce fibrosis and attenuate post-MI cardiac

dysfunction in mice (*204*). Furthermore, LOX isoforms including LOXL2*,* are also direct mediators of fibrosis, and have been associated with cross-linking and stabilisation of collagen fibrils during scar formation (*205*). This activity of LOX family members contributes to the detrimental effects of cardiac remodelling and inhibition of this activity after MI can reduce collagen accumulation and maturation while improving cardiac function (*205*). As such, increased expression of *snai1b* and *loxl2b* in Pachón could be a sign of increased scar deposition, and scar characteristics associated with increased stiffness and adverse remodelling, ultimately being detrimental to regeneration in Pachón. Notably, this is matched from the previous observation that Pachón have increased expression of genes associated with the extracellular matrix compared to surface fish. However, it's important to note, EMT/EMT-like processes have also been reported as a positive factor in regeneration particularly in the context of the epicardium and myocardium (*78, 103, 206, 207*).

It is surprising to find *pitx2* (*paired like homeodomain 2*) upregulated in the non-regenerating Pachón heart, as to date, it has been reported to have largely a positive role in regeneration. In particular, *Pitx2* gain of function enhances cardiomyocyte proliferation and regeneration in the adult mouse, while in the neonatal mouse its conditional knockout impairs cardiomyocyte proliferation and regeneration (*55, 208*). This positive role of *Pitx2* in cardiomyocyte proliferation has been associated with its ability to mediate the antioxidant response and reduce oxidative stress (*55*). Due to this role in cardiomyocyte proliferation, upregulation of *pitx2* in Pachón compared to surface fish could be a factor in Pachón's surprising ability to initiate cardiomyocyte proliferation, despite the absence of cardiomyocyte expansion and regeneration.

The Wnt inhibitor, Sfrp2 (Secreted frizzled related protein 2), is a key modulator of Wnt signalling and has been found to be upregulated with a number of other Wnt antagonists after injury in zebrafish (*182*). The upregulation of these Wnt antagonists, including Sfrp2, are localised to both the border zone myocardium and the epicardium, suggesting reduced Wnt signalling during regeneration (*182*). In support of this, inhibition of Wnt signalling via *dkk1* overexpression enhances cardiomyocyte proliferation and heart regeneration in zebrafish (*182*). As such, *sfrp2* upregulation in the non-regenerating Pachón is surprising, as its increased levels in Pachón would suggest reduced Wnt signalling, which based on above is beneficial for regeneration. Similar to *pitx2*, upregulation of *sfrp2* in Pachón could be a factor in enabling initiation of proliferation in Pachón cardiomyocytes.

NCAM1 (neural cell adhesion molecule 1) is a cell to cell adhesion protein that plays a role in neurogenesis and neurite outgrowth (*209, 210*), is expressed within natural killer cells (*211*) and the myocardial region adjacent to the wound after MI (*212*). Whilst *NCAM1* has not been directly reported in regeneration, it is interesting to note its reported location after MI, which possibly suggests it has a role in cardiomyocyte proliferation. As such, increased *ncam1a* expression in Pachón could be a factor in the reduced cardiomyocyte expansion observed in the Pachón border zone.

Xpo1 (Exportin-1) is a gene that mediates nuclear export and largely has an undefined role in regeneration. However, increases in its gene expression have correlated with left ventricular (LV) dysfunction in patients with ischemic cardiomyopathy and some evidence suggests silencing of the gene attenuates cardiac dysfunction after MI in rats (*213, 214*).

ITGAM is typically used as an immune cell marker which is expressed in a variety of leukocytes, including monocytes, neutrophils, natural killer cells, and particularly macrophages (*201*). As

such, upregulation of *itgam* in Pachón seems to suggest a greater and prolonged inflammatory response after injury in the Pachón versus the surface fish. This could contribute to the contrasting regenerative capacities in the *Astyanax,* as differences in leukocyte dynamics between regenerative and non-regenerative species have been correlated with regeneration (*110*). However, further investigation of *itgam* and characterisation of the innate immune response in the *Astyanax* is needed.

Differences in metabolism, specifically the capacity for anaerobic glycolysis has been proposed to correlate with myocardial proliferation (*63, 65*). As such it was interesting to find the metabolic genes *bcat1*, *ckba* and *fbp2* upregulated in Pachón. However, none of these genes or their respective metabolic pathways have been reported in regeneration to date. Metabolism is explored more in later chapters.

Cav1 (*Caveolin-1*) encodes the main structural protein of caveolae, which participate in multiple cellular processes including, vascular transport, signal transduction and membrane trafficking events. As previously described, in zebrafish it is upregulated in the epicardial cells colonising the wound after resection and its knockout impairs repair and myocardial proliferation – linking it to regeneration (*202*). Additionally, loss of *Cav1* in mice is associated with enhanced collagen deposition via TGF-β1 signalling, increased macrophage infiltration, as well as reduced survival and cardiac function after MI (*215-217*). However, there is some contradictory evidence that suggests that Cav1 is not essential to regeneration after cryoinjury (*218*). Nonetheless, the upregulation of *cav1* in the regenerating surface fish fits with the bulk of the literature. This hints that *cav1* expression after injury is conserved across species, and helps to support the RNAseq/qPCR as well as the *Astyanax* model to detect genes

involved in regeneration. However, further investigation is needed to confirm the importance of Cav1 in regeneration and the mechanism behind its role in regeneration.

As discussed above, the upregulation of a number of these genes in Pachón is in contrast to their previously reported pro-regenerative functions. This could suggest Pachón has some level of regenerative response whilst other factors are ultimately behind the difference in regeneration. Moreover, this could be an indication of the *Astyanax* model to determine factors that are key to regeneration from factors that are possibly less important. On the other hand, these genes could have a more complex role and be cell type specific in the regenerative process. Overall, it is difficult to infer the role of these singular genes during regeneration in any great detail based solely on their expression levels from RNAseq and qPCR alone. Expression experiments, such as these, on entire complex tissues are limited to a degree as they provide no spatial or cell type context and cannot account for cellular heterogeneity. Ultimately, further investigation is required to explore the role of the above genes in regeneration – as was done with *tmem198a*, *gpc5b*, *fmoda* and *lrrc10*.

3.3.2 Normal regeneration in *Tmem198a*, *gpc5b*, *fmoda* knockouts

The mutations generated to knockout *tmem198a*, *gpc5b* and *fmoda* in zebrafish were generally what was planned. However, there was some variation to the predicted mutation in the case of *gpc5b*, where a stop codon was not inserted and the entire exon 3 deleted. Due to the entire deletion of exon3, the largest exon, and no other preferential mutation appearing in the F0 generation, this mutation was picked as the most likely to create a functional knockout.

Due to their upregulation in surface fish and their suspected function it was hypothesised that knockout of the 3 genes would result in increased scar size and therefore impaired regeneration. However, the absence of any phenotype in the knockouts at 14dpi seems to suggest regeneration was normal in the knockouts. The most immediate reasons for this are either that the genes do not have a significant role in their respective mechanisms and thereby regeneration, or their loss is somewhat compensated through the actions of other mechanisms. There is also a case that these genes and their role during regeneration may not be conserved between surface fish and zebrafish. Since the onset of generating these mutants, work has shown mutant mRNA causing nonsense mediated decay can result in genetic compensation by upregulating the expression of similar coding genes (*219*). Therefore, since these mutants likely create mutant RNA that undergoes nonsense mediated decay, it cannot be ruled out that genetic compensation is occurring. Future strategies for genetic knockouts should aim to remove the promotor region of the gene.

However, it is important to note that regenerative capacity was measured at only a single timepoint, 14dpi. It is possible that the difference could emerge at a later timepoint, when the function of the gene is at its most important. Also, there is a question over whether the genes have been knocked out, as reduced mRNA expression was not confirmed in these mutants. qPCR or ISH is needed to confirm reduced mRNA levels and knockout of these genes. As such, this was improved for the *lrrc10* zebrafish mutants, where regeneration capacity was explored at a later timepoint and knockout validated. Ultimately, further timepoints after injury and confirmation of knockout was not performed in *tmem198a*, *gpc5b* and *fmoda* knockouts, largely for the prioritisation of the *lrrc10* work below.

3.3.3 Pachón-like phenotype in zebrafish *lrrc10* mutants

As *lrrc10* was significantly upregulated in the regenerating surface fish from the qPCR and RNAseq, it was chosen as a candidate for further study, with its upregulation pointing to a positive role in regeneration. Previous work had reported *lrrc10* as a gene specific to the heart and expressed solely within the myocardium, which was supported by the expression data reported here, confirming its specificity in both the *Astyanax* and zebrafish (*192-194*). Interestingly, its expression in surface fish and zebrafish seemed to localise to the wound border, particularly the compact wall, whilst being lowly expressed in the Pachón. This potentially points to a role that could underlie contrasting cardiomyocyte proliferation profile seen in the *Astyanax*.

Prior to this work, *lrrc10* had no known role in regeneration, but the observed impaired regeneration seen in the zebrafish knockout ultimately confirmed a role for it in heart regeneration. The impaired regeneration in *lrrc10* zebrafish knockouts was accompanied with similar levels of cardiomyocyte proliferation in the border zone compared to wild type fish, which interestingly mimics the surface fish and Pachón situation. Moreover, both Pachón and *lrrc10*-mutant zebrafish display high global myocardial proliferation, albeit at 30dpa in Pachón compared with 7dpi in *lrrc10* mutants, drawing further similarities between the *lrrc10* zebrafish mutants and the Pachón. An increase in global proliferation seems to suggest cardiomyocytes deficient in *lrrc10* have a greater capacity to initiate proliferation. If the similarities between Pachón and the *lrrc10* mutants remain true, it would also seem to suggest *lrrc10* mutant cardiomyocytes would also not complete the cell cycle as in the cavefish. However, further work is needed to fully confirm an identical proliferation profile between *lrrc10* mutant and Pachón hearts, namely a BrdU pulse chase experiment.

The expression profile and altered global cardiomyocyte proliferation in the mutants indicates that *lrrc10* has a role in cardiomyocyte function and proliferation. What is the potential mechanism that could be behind this cardiomyocyte proliferation but impaired regeneration?

LRRC10 localizes to the dyad region and has been suggested to associate with L-type Ca2+ channels, regulating channel function and potentially calcium signalling (*195*). LRRC10 may also interact with α-actinin and α-sarcomeric actin at the Z-disc in cardiomyocytes (*194*). Indeed, *Lrrc10*-/- mice develop DCM and exhibit changes in the voltage-dependent gating of the channels, potentially causing Ca2+ overload as a potential link to DCM (*191, 195*). *Lrrc10*-/- mice also upregulated multiple myocardial contractile genes and activation of Akt signalling pathway in their development into DCM (*191*). It is possible the Akt pathway could be responsible for the greater capacity to proliferate in the zebrafish mutants as activation of the Akt pathway has been reported to induce cardiomyocyte proliferation (*45, 52, 220, 221*). Additionally, it's interesting to note that while cardiomyocyte numbers in the zebrafish after injury are replaced by 30 days, a small scar persists, which has an adjacent small subset of cardiomyocytes failing to fully mature (*222*). These lacked differentiated sarcomeric structures and displayed defective calcium signalling, both factors changed in *Lrrc10*-/- mice (*222*). Could *lrrc10*-/- cardiomyocytes in zebrafish more readily enter the cell cycle due to activation of the Akt pathway but never fully mature leading to the increased scar size observed?

Lastly, the identical expression profile between the regenerating surface fish and zebrafish, with the zebrafish knockout phenotype, suggests a conserved function for *lrrc10* between the species. It also highlights the potential to utilise the *Astyanax* model to determine novel mechanisms/genes and use the zebrafish to functionally investigate their role in

regeneration. This conservation between species is not completely surprising as both the *Astyanax* and zebrafish are teleost fish, and relatively closely related.

3.3.4 Limitations

Due to the long-time scale for *Astyanax* to reach sexual maturity, it was decided to investigate candidate genes via CRISPR knockout in the regenerating zebrafish, which has a much shorter generation time scale. As a result of this decision, is was also decided to focus on genes that were upregulated in the surface fish compared to the Pachón for the CRISPR knockouts. It was reasoned these genes were more likely to generate a phenotype upon knockout in the zebrafish due to the similar regeneration capacities between surface fish and zebrafish, and thus likely to hold significant similarities in their regenerative mechanisms. However, as a limitation this meant that genes upregulated in Pachón were largely ignored and not explored. These genes upregulated in Pachón are of still significant interest and their upregulation could be key to the Pachóns inability to regenerate its heart. Genes upregulated in the Pachón from this cohort should be considered in future studies.

This chapter also possessed several methodological and experimental-design limitations. Namely, *fmoda*, *gpc5b*, and *tmem198a* expression was not investigated prior to mutant generation in either the *Astyanax* or zebrafish in terms of cell type or localisation after injury – as was done with *lrrc10*. Investigating the expression of these genes using RNAscope would enable insight into the possible role these genes have on regeneration, as well as confirming a conserved role between surface fish and zebrafish. Performing this would provide more confidence in the importance of the gene during regeneration prior to creating the mutant. Ultimately, the expression localisation was not completed for prioritisation for the *lrrc10* work. In addition, regeneration capacity was only investigated at a single timepoint (14dpi) in

fmoda, *gpc5b*, and *tmem198a* knockouts. The main role of these genes on regeneration could be either earlier or later in the regeneration/injury response, and as such this may be responsible for the lack of phenotype observed at 14dpi. Ultimately, this was rectified in the *lrrc10* mutant.

Lastly, the apical resection injury model was used on the *Astyanax* within this chapter. Whilst the apical resection model is the original injury model to investigate heart regeneration, the more commonly used cryoinjury model is considered to be more similar to the MI injury response. In contrast to the resection model, the cryoinjury model generates an injury that involves necrosis and cell apoptosis, which are features that occur in the human heart after MI. As such, work in the following chapters utilised the cryoinjury model over resection.

3.3.5 Conclusions

This chapter highlights a variety of genes that are differentially expressed in the *Astyanax* after injury, of which a number have no known previous role in regeneration and were highlighted for investigation. Knockout of several candidates, *fmoda*, *gpc5b* and *tmem198a* showed no obvious role in regeneration. While knockout of *lrrc10* implicated a significant role in regeneration.

Overall *lrrc10* mutants display a very Pachón-like phenotype in response to injury, displaying impaired regeneration with cardiomyocyte proliferation. This not only shows *lrrc10*s importance in regeneration but also validates the *Astyanax* as a significant model for the study of heart regeneration.

Chapter 4
Single-cell transcriptomics to explore the molecular mechanisms underlying the cardiomyocyte profile after injury

4.1 Introduction

Animal models of heart regeneration are capable of inducing significant proliferation of pre-existing cardiomyocytes, which has been established as one of the key drivers behind natural heart regeneration (*11, 25, 33, 34*). Myocardial proliferation in response to injury mostly occurs in a time dependant manner and in the region adjacent to the wound, also termed as the border zone (*14-16, 25, 33, 34, 223*). In the border zone, cardiomyocytes initially dedifferentiate before proliferating and subsequently migrating into the injury area (*33, 34, 38, 39, 43, 224, 225*). This temporal and spatial activation of cardiomyocyte proliferation is also matched with spatiotemporal changes in gene expression that control this complex process, which has been particularly illustrated in zebrafish by tomo-RNAseq and more recently by single cell RNAseq (scRNAseq) (*37, 63*).

To enable replacement of the lost cardiomyocytes via dedifferentiation and proliferation, border zone cardiomyocytes re-express embryonic cardiac genes and pathways, such as embryonic myosins, the transcription factors *nkx2.5* and *tbx20*, genes in the BMP signalling pathway, as well as activating *gata4* enhancer elements (*34, 36, 37, 78*). All adding to the notion of a developmental gene program and that border zone cardiomyocytes become more

immature in phenotype. In addition, border zone cardiomyocytes express genes that control the cell cycle and undergo metabolic reprogramming by upregulating genes of the developmentally active glycolysis pathway, while also downregulating mitochondrial genes (*63*).

4.1.1 Myocardial proliferation in the *Astyanax*

In the *Astyanax*, two different cardiomyocyte proliferation profiles underlie the contrasting regeneration capacities between surface fish and Pachón. Similar to regenerative models, both the Pachón and surface fish initiate myocardial proliferation in a time and spatial dependant manner (*129*). Proliferation largely occurs in the border zone region and peaks at 7 days after injury, as evidenced by the S phase markers, PCNA and BrdU incorporation. However, the contrasting profiles come to light when tracking the cell cycle over time and determining the degree of cardiomyocyte expansion by using a BrdU pulse chase experiment (*129*). In this pulse chase experiment, BrdU is incorporated and embedded into the cardiomyocytes entering the S phase at 7dpa. Under normal circumstances, BrdU embedded in the DNA is passed to the two daughter cells as they complete nuclear/cellular division. This results in an increased number of BrdU positive cardiomyocytes by 14dpa – indicating cardiomyocyte expansion. Therefore, increased labelling of BrdU at 14dpa compared to 7dpa in surface fish is consistent with cell cycle completion and cardiomyocyte number expansion. However, the number of BrdU positive cardiomyocytes after the pulse chase in the Pachón was significantly lower and equivalent to its 7dpa timepoint, suggesting limited cardiomyocyte expansion despite initiating proliferation and entering the S phase (*129*).

Analysis of apoptosis, via staining for cleaved caspase 3 expression, revealed no clear increase in myocardial apoptosis that could account for the reduced labelling in the Pachón (*129*). (Fig

4.1A). Therefore, it appears Pachón cardiomyocytes have retained the ability to initiate proliferation and enter the S phase (similar levels of PCNA and BrdU) but are unable to complete the cell cycle (no increase in BrdU positive cardiomyocytes in the pulse trace experiment). This leaves the question as to what is happening to these cardiomyocytes. As such, one of the main aims of this chapter is characterise the fate of the cycling cardiomyocytes in Pachón.

To address this question, this chapter focuses on two possibilities that could underlie the lack cardiomyocyte expansion. Firstly, is the proposition of Pachón cycling cardiomyocytes still undergoing apoptosis but through a cleaved caspase independent pathway (Fig 4.1B, C). Second is the potential hypothesis that proliferating cardiomyocytes in the Pachón have impaired cytokinesis and are becoming polyploid – similar to adult mammalian cardiomyocytes (*69, 226*) (Fig 4.1B, C). In this scenario, BrdU would be embedded into the DNA of S phase Pachón cardiomyocytes, but due to neither nuclear division or cytokinesis, no BrdU positive daughter cells are produced. Thus, resulting in undivided cardiomyocytes with double the amount of DNA (tetraploid) and reduced labelling in the pulse chase experiment.

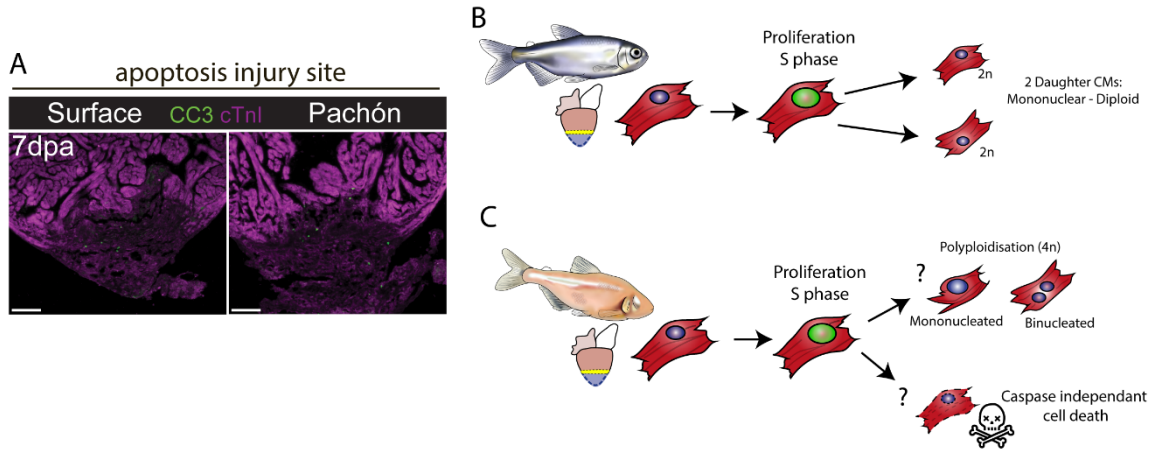


Figure 4.1 No difference in myocardial apoptosis in either Pachón or surface fish.

(A) *Low levels of CC3 positive cells in both Pachón and surface with no noticeable difference between the fish at 7dpa. cTnI, cardiac troponin I. CC3, cleaved caspase3 (apoptosis marker) (129). Figure adapted from (Stockdale et al., 2018)* ***(B)*** *Schematic of proliferation in surface fish. Surface fish cardiomyocytes in the border zone enter the S phase and complete the cell cycle resulting in 2 daughter cells that are mononuclear diploid.* ***(C)*** *Schematic of possible scenarios in Pachón proliferating cardiomyocytes. Pachón enter the S phase but rather than completing the cell cycle, undergo cell cycle arrest forming either binucleated cardiomyocytes or tetraploid (2n) mononucleated cardiomyocytes. Alternatively, Pachón cardiomyocytes die via a caspase independent pathway.*

As mentioned above, cardiomyocyte proliferation is tightly controlled by gene expression that is both temporally and spatially activated (*37, 63*). As such, differences in gene expression dynamics within this specific border zone region likely underlies the contrasting proliferation profiles between surface fish and Pachón. Indeed, this is particularly illustrated in the previous chapter by the expression pattern of *lrrc10* after injury and the Pachón-like phenotype of *lrrc10* knockout zebrafish. This highlights the need to specifically analyse the spatiotemporal dynamics of the cardiomyocyte gene expression to accurately determine the pathways and mechanisms that influence the contrasting proliferation profiles. As such, this forms the second major aim of this chapter; to deduce the gene expression and pathways that could account for the contrasting cardiomyocyte proliferation profiles in the *Astyanax*.

To help characterise both the fate of the proliferating cardiomyocytes in Pachón, and determine the intrinsic pathways that underlie this fate, this chapter employs powerful single cell transcriptomics on *Astyanax* hearts.

4.1.2 Single cell RNAseq

scRNAseq enables the capacity to perform transcriptional profiling in thousands of individual cells. This has provided the ability to understand the behaviour of individual cell types and subtypes during complex biological processes such as heart regeneration.

Both targeted scRNAseq and the related single-nucleus RNAseq technology have been successfully used to explore cardiomyocyte proliferation during zebrafish and neonatal mouse regeneration respectively (*63, 68*). Single cell RNA sequencing of zebrafish cardiomyocytes after injury revealed border zone cardiomyocytes form a transcriptionally distinct population from remote cardiomyocytes (*63*). Comparison of border zone cardiomyocytes with remote cardiomyocytes revealed changes in gene expression consistent with dedifferentiation, the cell cycle and most significantly metabolism. Specifically, border zone cardiomyocytes underwent a metabolic reprogramming, upregulating genes in glycolysis whilst downregulating genes in mitochondrial-based metabolism (*63*). From this, upregulation of glycolysis was later confirmed as an essential component in myocardial proliferation during regeneration. Single-nucleus RNA sequencing performs transcriptional profiling on individual nuclei rather than whole cells and was used to compare regenerative and non-regenerative cardiomyocytes in the mouse heart (*68*). This analysis revealed a unique immature cardiomyocyte population to the regenerating neonatal mouse, which enter the cell cycle upon injury via the activity of NFYa (Nuclear transcription factor Y subunit alpha) and NFE2L1 (Nuclear factor erythroid 2-like 1) transcription factors (*68*). Both these studies demonstrate how using single cell/nucleus technology can enhance our understanding of cardiomyocyte proliferation during regeneration.

Due to its ability to perform transcriptional profiling on individual cells, scRNAseq analysis of both Pachón and surface fish hearts at different timepoints after injury will enable investigation of cell type and cell subtype specific transcriptional changes that occur after injury whilst comparing between morphotypes. This will particularly provide the opportunity to specifically explore the dynamic transcriptional response to injury in the cardiomyocyte

subpopulations, including detecting and targeting the border zone cardiomyocytes that form after injury. Comparison of the temporal gene expression in the border zone between surface fish and Pachón will help to characterise the fate of Pachón proliferating cardiomyocytes and determine the gene expression that results in successful proliferation in surface fish, while causing defective proliferation in Pachón.

4.1.3 Aim

This chapter aims to use comparative single cell transcriptomics to specifically target border zone cardiomyocytes to gain insights into the fate of proliferating cardiomyocytes in Pachón. It also seeks to use the single cell transcriptomics to determine the molecular pathways that underpin this contrasting cardiomyocyte proliferation profile in the *Astyanax*. Deciphering the pathways, will help to enhance our understanding of the factors necessary for complete and efficient myocardial proliferation.

4.2 Results

Hypothesis & expected findings

scRNAseq analysis of the cardiomyocytes after injury was expected to show *Astyanax* cardiomyocytes forming transcriptionally distinct clusters consistent with the different myocardial regions of the fish heart (trabecular, cortical and primordial) and the wound border zone – observing significant myocardial heterogeneity. Specifically, it was predicted that primordial cardiomyocytes would be more immature alongside border zone cardiomyocytes, which would display previously reported characteristics of the zebrafish border zone.

Most importantly, with the identification of the border zone cardiomyocytes, it was expected that comparison of surface fish and Pachón cardiomyocytes would give insight into the fate of Pachón cycling cardiomyocytes and the mechanisms underlying the lack of cardiomyocyte expansion.

Hypothesis: Comparison of Pachón and surface fish border zone cardiomyocytes will determine whether Pachón border zone cardiomyocytes are undergoing apoptosis or cell cycle arrest with polyploidy and the possible mechanisms behind this phenotype.

4.2.1 Identification of trabecular, cortical, primordial and border zone cardiomyocytes

To gain insight into the intrinsic mechanisms that underlie the lack of cardiomyocyte expansion in the Pachón compared to their surface fish counter parts, whole ventricles were single cell sequenced using the 10x chromium platform. Pachón and surface fish underwent either sham-surgery or cryoinjury, and hearts were isolated across different timepoints after

injury, which included 1, 3, 7 and 14 days after injury with sham (isolated at 3dpi) and uninjured controls. Three ventricles from each group were pooled during their dissociation into single cell suspensions (Fig 4.2A).

As part of the pre-processing of this experiment, each sample (e.g. Pachón uninjured) underwent cell quality control and was normalised to account for sequencing depth variations, using Seurat's global-scaling normalization method (*161*). Each sample was then integrated to remove batch effects and group similar cell types together for comparative analysis. Cells were then clustered and annotated to their predicted cell types based on expression of cell type marker genes. For targeted analysis of the cardiomyocytes, *Astyanax* cardiomyocytes from uninjured, 3dpi, 7dpi, 14dpi groups were separated based on expression of known cardiomyocyte markers. The predicted cardiomyocytes from these sample were then pre-processed again and reintegrated to gain a better resolution of the heterogeneity and dynamics in response to cardiac injury (Fig 4.2A).

The cardiomyocytes from the Pachón and surface fish integrated successfully and their transcriptomic profiles were visualised using the dimensionality reduction technique, UMAP (Uniform Manifold Approximation and Projection) (Fig 4.2B, C). The integrated cardiomyocytes were clustered based on significant principal components and at a resolution that formed 8 transcriptionally distinct cardiomyocyte clusters (Fig 4.2F). Each of these clusters contained cells of similar identities and expressed cardiomyocyte markers such as the major marker, *myl7* (Fig 4.2B, D, E).

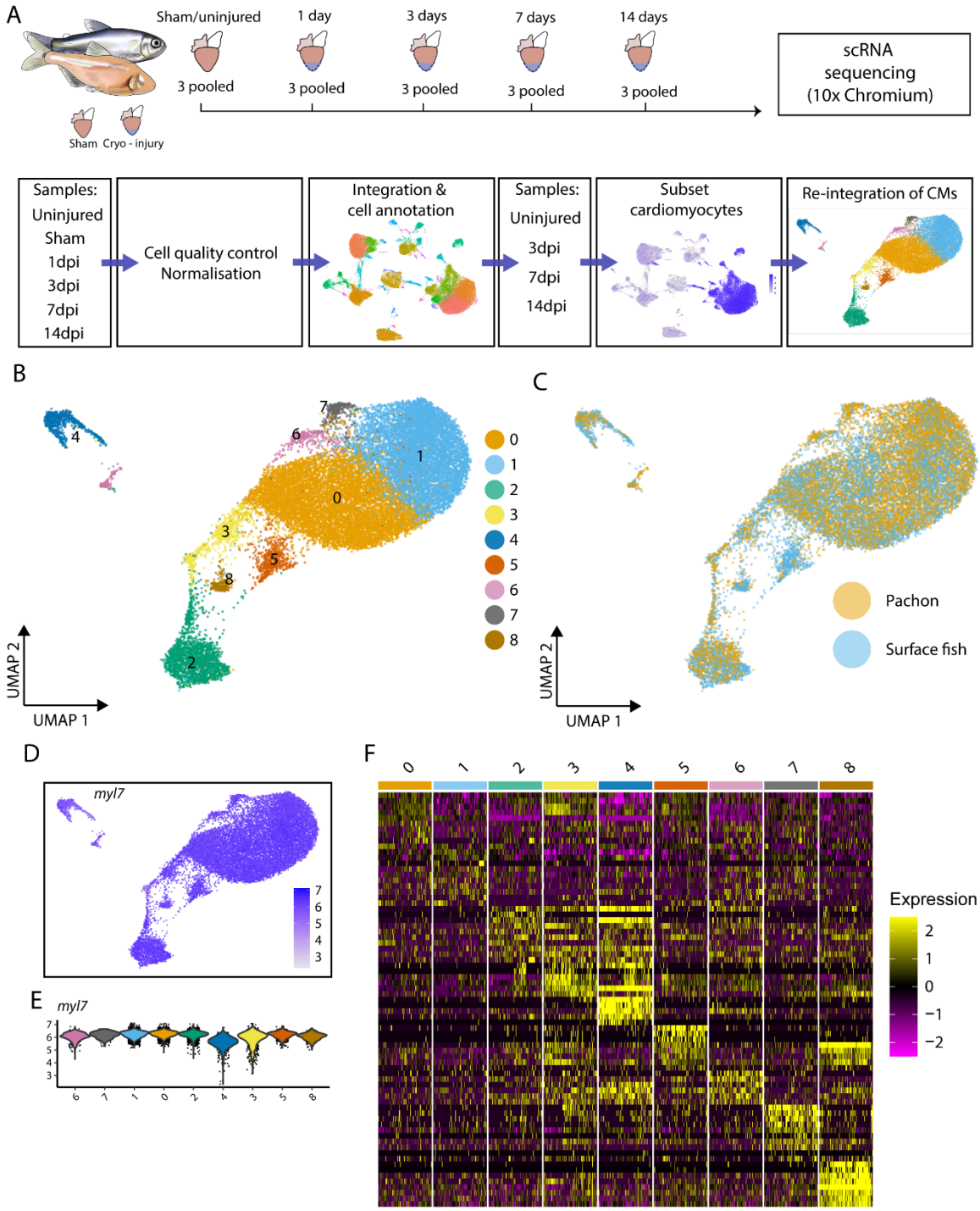


Figure 4.2 scRNAseq analysis on *Astyanax* cardiomyocytes before and after injury.
(A) *Schematic of experimental design and workflow for the single cell analysis of Astyanax cardiomyocytes at 3, 7 and 14 days after injury, with uninjured control.* ***(B)*** *UMAP projection of integrated Astyanax cardiomyocytes coloured by cluster identities. Clusters represent cardiomyocytes of similar identities.* ***(C)*** *UMAP projection of integrated Astyanax cardiomyocytes coloured by fish population – demonstrating successful integration of surface fish and Pachón cardiomyocytes.* ***(D)*** *Feature plot showing expression of the cardiomyocyte marker, myl7.* ***(E)*** *Violin plot of myl7 expression across Astyanax cardiomyocyte clusters.* ***(F)*** *Heatmap of the top 20 differentially expressed genes for*

each cardiomyocyte cluster. Demonstrates significant transcriptional differences between cardiomyocyte clusters. MAST differential expression test used.

In general, each cluster was transcriptionally distinct representing cardiomyocyte heterogeneity, and the clusters were overall classified into 4 types of cardiomyocyte, which included trabecular, cortical, primordial and wound border zone cardiomyocytes (Fig 4.3A, B). A combination of unbiased differential expression analysis and exploration of genes known to be expressed in these cardiomyocyte subtypes was used to annotate these clusters to the above cardiomyocyte types. Specifically, the differential analysis compared each cluster with all other remaining clusters to identify significant markers.

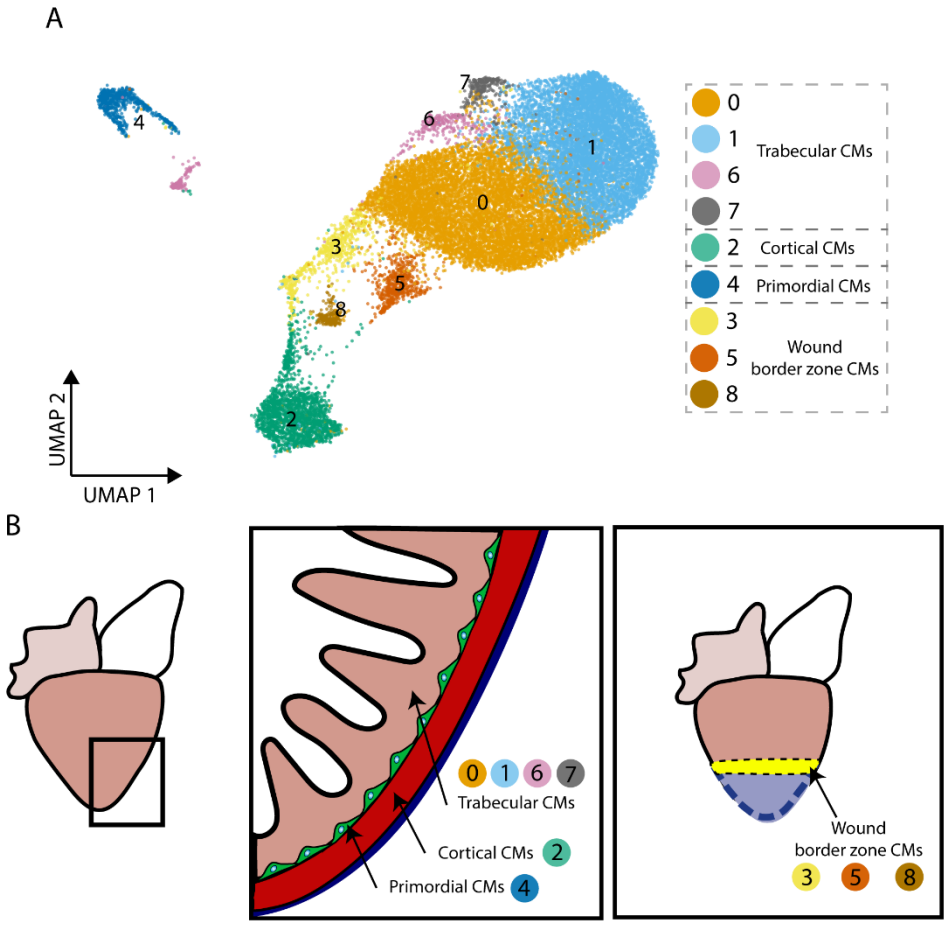


Figure 4.3 *Astyanax* cardiomyocyte subtype annotation.
(A) *Annotation of the cardiomyocyte clusters* ***(B)*** *Diagram of the different cardiomyocyte subtypes in the fish heart and the corresponding cardiomyocyte clusters in the scRNAseq. CM, cardiomyocytes.*

The expression of *nppa*, *nppal* and *tbx5a*, have been previously used to discriminate trabecular myocardium from cortical myocardium in the uninjured adult zebrafish heart (*227, 228*). Both *nppa* and *nppal* are two of the top markers for clusters 0 and 1. tbx5a is expressed throughout most clusters but is highest in clusters 0, 1 and 8. *tbx5a* expression is also noticeably reduced/negligible in clusters 2 and 4 (Fig 4.4A, B). In light of this, clusters 0 and 1 are indicated as trabecular cardiomyocytes.

In addition to their expression in the uninjured trabecular myocardium, *nppa* and *nppal* are also upregulated in the zebrafish myocardial border zone after injury, along with the paralog *nppb (37, 63)*. Each of these genes are noticeably upregulated in cluster 3 suggesting this cluster is formed of border zone cardiomyocytes (Fig 4.4A, B). In addition, *ckmb* and *ckmt2b* are both genes considered to be expressed in adult mature cardiomyocytes in zebrafish[251]. Both these genes are expressed at high levels throughout most clusters but are noticeably lower in cluster 3, indicating an immature-like aspect, a common feature of border zone cardiomyocytes (*33, 34, 36, 37, 63, 78*) (Fig 4.4A, B). Clusters 5 and 8 are implicated as additional border zone clusters by the expression of cell cycle related genes and other known border zone marking genes. Expression of genes related to cell proliferation/DNA synthesis specifically mark cluster 5, which includes *pcna*, *mcm3* and *mcm6* (Fig 4.4A, B). While cluster 8 expresses the cell cycle gene, *cdkn3,* and a previously reported border zone gene, *crip2* (Fig 4.4A, B) (*37*).

The mature cardiomyocyte genes, *ckmb* and *ckmt2b* are also reduced in cluster 4, indicating these are immature cardiomyocytes (Fig 4.4A, B). In combination with low levels of mature cardiomyocyte genes, cluster 4 is marked by expression of genes related to Notch signalling, such as *hey2* and *notch3* (Fig 4.4A, B) (*229*). Low levels of mature cardiomyocyte genes and

high levels of Notch signalling genes are markers of primordial cardiomyocytes in the adult zebrafish heart (*229*).

Cluster 2 is best described by the absence of *tbx5a* expression, which is consistent with cortical cardiomyocytes, while still expressing high levels of mature cardiomyocyte genes, *ckmb* and *ckmt2b* (Fig 4.4A, B) (*227*). Lastly, the nature of clusters 6 and 7 are not completely clear. However, due to the relatively high *nppa* expression in clusters 6 and 7, and combined with their proximity to clusters 0 and 1, clusters 6 and 7 are suggested as additional trabecular cardiomyocytes (Fig 4.4A, B).

Overall, these transcriptional markers suggest clusters 0, 1, 6 and 7 are trabecular cardiomyocytes and clusters 2 and 4 are cortical and primordial cardiomyocytes respectively. Certain cell cycle genes and known wound border zone genes also suggest clusters 3, 5 and 8 are border zone clusters.

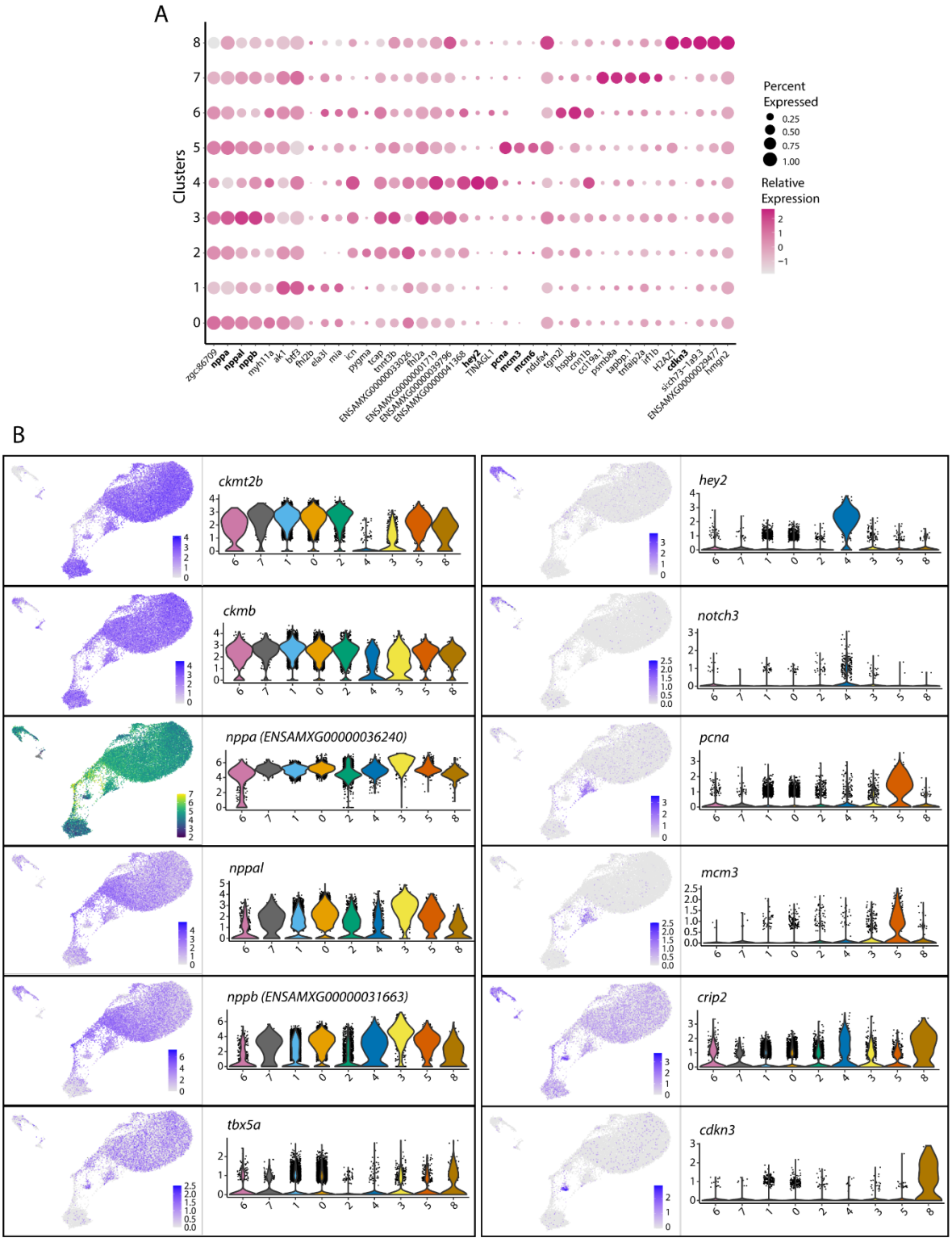


Figure 4.4 Markers of trabecular, cortical, primordial and border zone cardiomyocytes. ***(A)*** *Dot plot illustrating the top 5 marker genes of each cardiomyocyte cluster. Notable marker genes in bold. Dot size represents the percentage of cells in the clusters expressing the marker and the colour intensity represents the average expression of the marker in that cluster.* ***(B)*** *Violin plots and respective feature plots illustrating the expression of selected marker genes across the Astyanax cardiomyocyte clusters. MAST differential expression test used.*

This section confirms the *Astyanax* possess cardiomyocyte subtypes as those previously reported in fish before and after injury, and that these subtypes are generally consistent between Pachón and surface fish. In addition, formation of distinct clusters consistent with these cardiomyocyte subtypes confirms that these that these myocardial layers and the border zone have their own distinct transcriptional profile linked to their function – supporting the notion of cardiomyocyte heterogeneity.

4.2.2 Primordial and border zone cardiomyocytes have reduced maturity

After injury, border zone cardiomyocytes take on immature characteristics in order to proliferate, while primordial cardiomyocytes are considered an immature population within the adult heart (*63, 229*). To support the identification of border zone and primordial cardiomyocytes highlighted in the previous section, two methods were used to predict cardiomyocyte maturity. This included calculating cardiomyocyte entropy and utilising the Cytotrace package (*165, 166*) (Fig 4.5A, B).

Both techniques work in a similar fashion, utilising transcriptional diversity in order to predict differentiation states of cells within scRNAseq datasets. Using transcriptional diversity to predict differentiation potential is a based on the observation that less differentiated cells (immature) typically have a diverse gene expression profile – high transcriptomic entropy (*230-232*). While cells that differentiate have a more specialised function and narrow the variability in their gene expression profile, lowering their transcriptomic entropy. Ultimately, Cytotrace orders cells in each sample according to their predicted developmental potential,

while the entropy-based metric provides an entropy score of each cell, where a higher entropy score suggests a more immature cell and vice versa (*165, 166*).

Running Cytotrace on the cardiomyocyte clusters predicted the potential border zone clusters, 3, 5 and 8, as well as the suggested primordial cardiomyocyte cluster, cluster 4, as the least differentiated (Fig 4.5A). This is supported by the entropy-based metric, which calculated high entropy scores for these clusters but with more moderate differences between clusters (Fig 4.5B). Entropy scores were highest in cluster 4, while scores were raised in clusters 3, 5 and 8 relative to the main trabecular clusters (Fig 4.5B). Surprising, trabecular cardiomyocytes clusters 6 and 7, have raised entropy scores versus the other trabecular clusters but these are not reproduced in Cytotrace ordering (Fig 4.5A, B).

Overall, these two maturity methods confirmed that clusters 3, 5 and 8 are border zone cardiomyocytes and that cluster 4 are primordial cardiomyocytes.

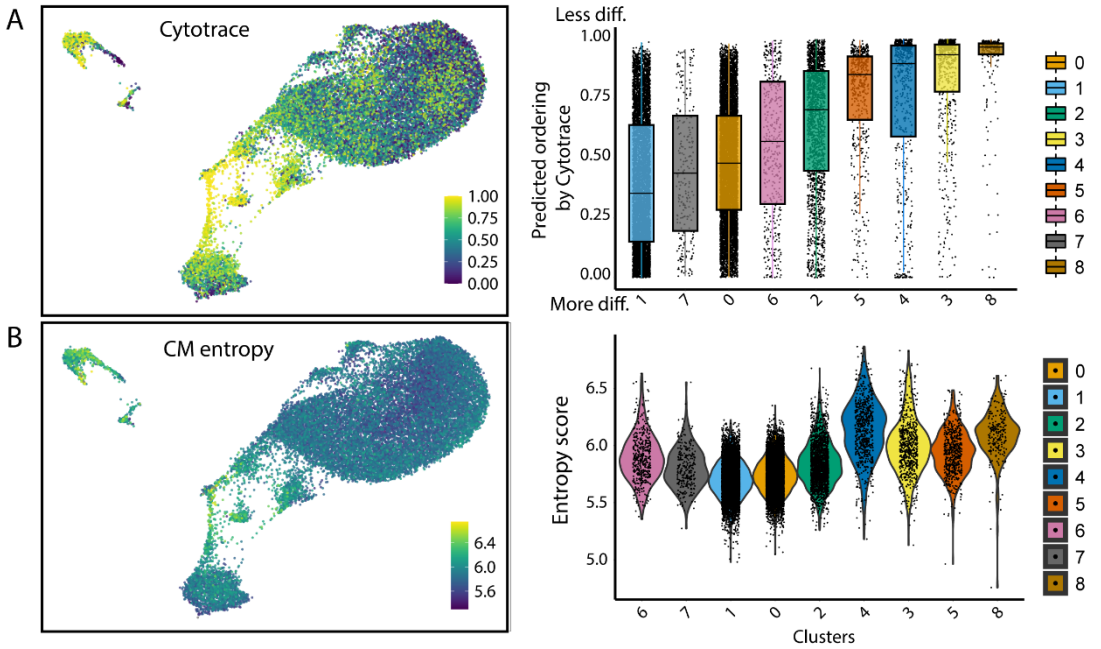


Figure 4.5 *Astyanax* cardiomyocyte maturation estimation by Cytotrace and cellular entropy.

(*A) Feature plot and box plot displaying the Cytotrace ordering of Astyanax cardiomyocytes across the clusters. High Cytotrace scores indicate less differentiated/more immature cells, while low scores indicate more differentiated/more mature. In box plot, clusters are ordered on average Cytotrace scores.* ***(B)*** *Feature plot and violin plot displaying the entropy scores of each cell across the cardiomyocyte clusters. High entropy scores indicate less differentiated/more immature cells, while low scores indicate more differentiated/more mature.*

4.2.3 Cardiomyocyte border zone clusters display characteristics consistent with dedifferentiation/migration and phases of the cell cycle

The presence of 3 individual clusters forming the border zone suggests a variety of transcriptional states in the regenerating cardiomyocytes. To characterise these border zone clusters, positive/upregulated and negative/downregulated marker genes for each of these clusters were utilised in Metascape to identify statistically enriched ontology clusters (Fig 4.6A-D) (*164*). This was performed to determine active or inactive cellular processes and molecular pathways that may describe the function of these clusters.

Cluster 3 upregulated genes falling under notable terms such as focal adhesion and actin filament-based process. This suggests this cell cluster has features consistent with cytoskeleton remodelling and varying adhesion dynamics between cells, leading detachment of cardiomyocytes from each other – potentially for migration (Fig 4.6A). In addition, downregulated genes in cluster 3 also resulted in enrichment of terms relating to heart contraction, suggesting downregulation of sarcomeric genes (Fig 4.6A). As cardiomyocyte dedifferentiation during zebrafish regeneration is characterised by sarcomere disassembly and cardiomyocyte detachment (*33, 224, 225*), the enrichment of these perhaps defines this cluster as border zone cardiomyocytes undergoing dedifferentiation/redifferentiation and possibly migration. To further support this, upregulated genes in cluster 3 also resulted in the significant parent ontology terms, locomotion, biological adhesion and growth (Fig 4.6B).

Both cluster 5 and cluster 8, have upregulated genes leading to enrichment of ontology terms related to the cell cycle (Fig 4.6C, D). Specifically, cluster 5 has significantly upregulated terms such as DNA strand elongation, DNA replication, chromosome organisation and DNA biosynthetic process (Fig 4.6C). These terms related to nucleotide synthesis and replication suggest this cluster consists of cardiomyocytes within the S phase of the cell cycle. Analysis of the upregulated genes in cluster 8 identify ontology terms related to mitosis and cytokinesis, amongst a number of terms related to protein processing (Fig 4.6D). Mitosis and cytokinesis related terms include cytoskeleton-dependent, mitotic sister chromatid segregation and chromosome organisation, which suggests cluster 8 is formed of cells undergoing mitosis/cytokinesis (Fig 4.6D). Similar to cluster 3, both these clusters also downregulate genes related to heart contraction, suggesting downregulation of sarcomeric genes (Fig 4.6C, D). This also indicates that these clusters and their respective phases of the cell cycle also maintain a dedifferentiation state.

Clusters 3 and 8 both notably upregulate genes related to the proteasome as indicated by enrichment of the proteasome GO term (Fig 4.6A, D). As zebrafish sarcomere disassembly during dedifferentiation is regulated in a proteasome dependant process (*224*), this suggests increased proteasome activity in these clusters is regulating the dedifferentiation state described above.

Across all three border zone clusters, the downregulated genes resulted in significant ontology clusters associated with multiple metabolic pathways. Notably, this included ontology terms referring to fatty acid metabolism, oxidative phosphorylation and the TCA cycle, indicating these metabolic pathways are downregulated in border zone cardiomyocytes (Fig 4.6A-D).

To support the notion that clusters 5 and 8 were cardiomyocytes within the S phase and undergoing mitosis/cytokinesis respectively, Seurat's cell cycle scoring feature was utilised (*161*). This function uses the expression of a previously published set of genes to calculate a S phase score and a G2M phase score of each cell (*233*). Based on this scoring feature, cells can also be assigned to a phase; either G1, G2M or S phase. The S phase score was highest in cluster 5, while the G2M was highest in cluster 8, which supported the above annotations (Fig 4.6E, F).

Proportions of the assigned cell cycle phases, showed a noticeably higher percentage of S phase predicted cardiomyocytes within cluster 5, while cluster 8 has higher percentage of cardiomyocytes assigned to the G2M phase of the cell cycle (Fig 4.6 G, H). However, its import to note the assigning of cell cycle phase by this tool is inaccurate on a cell by cell basis as shown by the high base level of cells assigned to the S phase across all clusters. Nonetheless, this tool adds confidence to the notion that cluster 5 is cardiomyocytes in the S phase and cluster 8 is formed of G2M cells.

To conclude, cluster 3 displays the highest dedifferentiation profile, indicating these are cardiomyocytes disassembling sarcomeres and detaching from adjacent cardiomyocytes for potential migration. While cluster 5 and 8 are cardiomyocytes that are actively cycling and within the S and G2M phases of the cell cycle respectively. These cycling cardiomyocytes also retain dedifferentiation characteristics. The dedifferentiation characteristics are possibly under regulation of proteasome activity and each of these border zone clusters are underpinned by changes in metabolism. Overall, each of these characteristics are features of the zebrafish border zone, as such, *Astyanax* border zone cardiomyocytes in general possess similar characteristics to the zebrafish myocardial border zone.

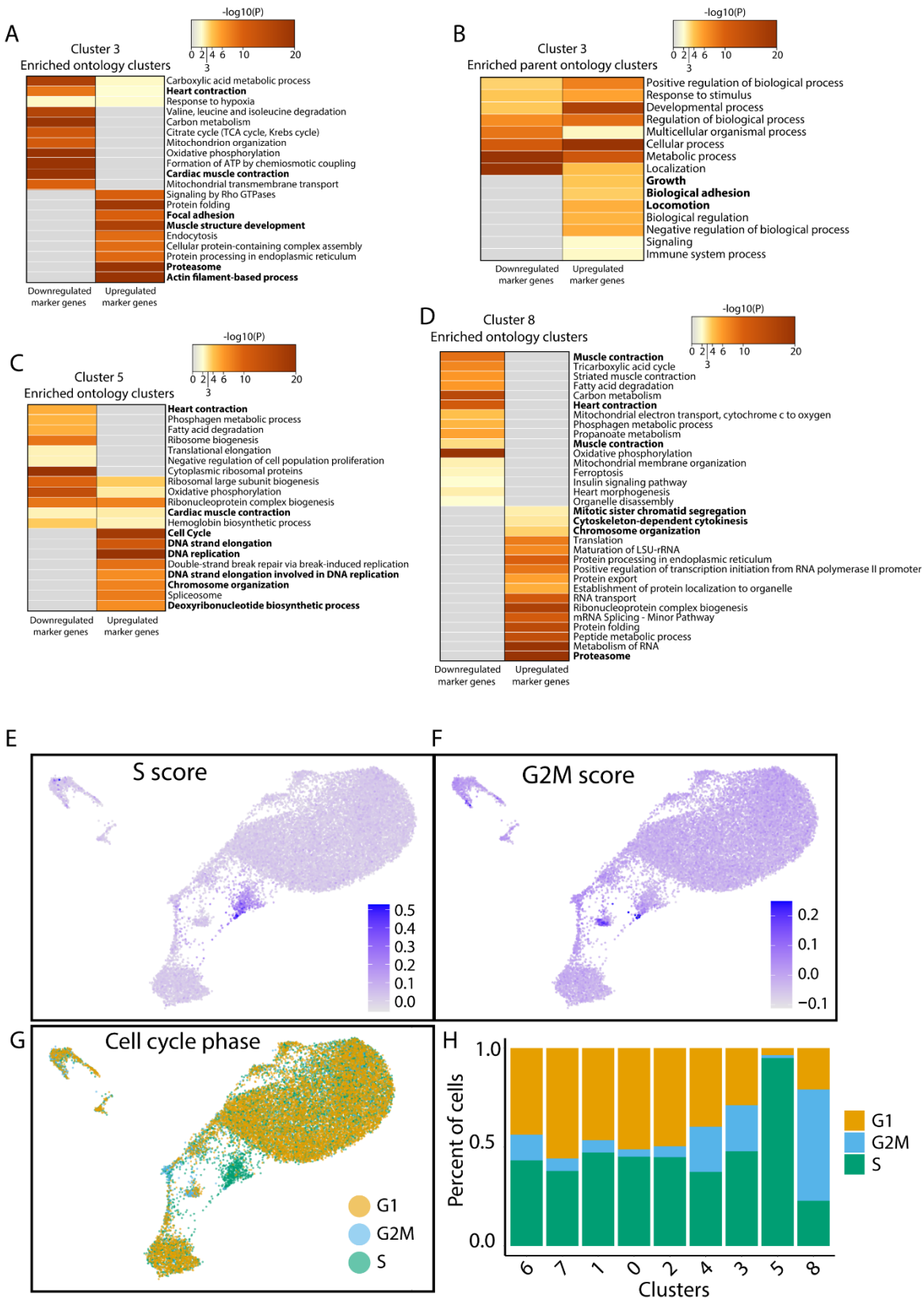


Figure 4.6 Specific border zone clusters display dedifferentiating/migration characteristics and features of the cell cycle.

(A-D) *Metascape analysis - Enriched gene ontology terms based on top differentially expressed markers in the border zone clusters - cluster 3* ***(A&B)****, cluster 5* ***(C)*** *and cluster 8* ***(D)****. Heatmaps display enriched terms based on downregulated marker genes (negative fold change) and enriched terms*

based on upregulated marker genes (positive fold change). ***(E&F)*** *Feature plot of S phase and G2M scores calculated by the cell cycle scoring metric.* ***(G)*** *UMAP projection coloured by the cell cycle phase, assigned by the cell cycle scoring metric.* ***(H)*** *Cell cycle phase composition of each cardiomyocyte cluster.*

4.2.4 Cardiomyocyte subtype composition after injury

So far, the samples have been analysed all together, but the predicted border zone clusters have notable proportional dynamics across the injury timepoints as well as proportional differences between Pachón and surface fish (Fig 4.7A-D).

In both Pachón and surface fish uninjured hearts, each border zone cluster is proportionally low compared to injured hearts (Fig 4.7C, D). However, Pachón have a slight increased proportion of cardiomyocytes in the S phase and G2M clusters compared to surface fish, which possibly suggests a higher basal level of proliferation in the Pachón heart (Fig 4.7B, D).

Upon injury, the cluster 3 proportion increased substantially in both Pachón and surface fish and formed the largest border zone cluster at 3dpi (Fig 4.7B-D). Cluster 3 peaked in proportion at 3dpi before dropping across 7dpi and 14dpi in both Pachón and surface fish (Fig 4.7C, D). This suggests cluster 3 is the first cluster formed in the *Astyanax* border zone. As cluster 3 generally has the largest dedifferentiation profile in terms of gene expression (section 4.2.3, Fig 4.6A, B), and formed first out of the other border zone clusters, this helps to support the indication that this cluster is mainly dedifferentiating cardiomyocytes, which occurs prior to cell cycle entry.

While proportional dynamics of cluster 3 are generally similar between Pachón and surface fish, there are substantial proportional differences between cluster 5 – the S phase cluster, and cluster 8 – the G2M cluster (Fig 4.7C, D). In surface fish, cluster 5 is substantially formed

after injury at 3dpi, while cluster 8 forms later at 7dpi. The initial onset of cluster 5 (S phase cluster), later followed by cluster 8 (G2M cluster) matches the sequence of phases in the cell cycle. In addition, both cluster 5 and 8 proportions peaked at 7dpi in surface fish (Fig 4.7C, D). As cluster 5 and 8 are actively cycling cardiomyocytes, its notable that their peak in proportions coincided with the peak in border zone cardiomyocyte proliferation. Moreover, the peak in PCNA antibody labelling in the border zone at 7dpi matches the proportional peak of cluster 5 - the *pcna* high cluster.

In contrast to surface fish, both cluster 5 and 8 are substantially lower in Pachón across 3, 7 and 14dpi (Fig 4.7C, D). In Pachón, cluster 5 remains low in cell number and does not increase in relation to the uninjured sample. While cluster 8 appears to decline in proportion after injury, remaining low in cell number before returning to similar uninjured levels at 14dpi (Fig 4.7C, D). These lower proportions of cluster 5 and 8 indicate an overall lower S phase and G2M profile in Pachón compared to surface fish. The low number of cardiomyocytes with transcriptional profiles equivalent to these phases of the cell cycle is possibly indicative of the reduced cardiomyocyte expansion in the Pachón border zone.

In addition, Pachón appears to possess a slight but notable higher proportion of cluster 5 (S phase) cardiomyocytes in uninjured hearts compared to surface fish. This possibly suggests a proportion of basal level cardiomyocyte proliferation within the uninjured Pachón heart.

Overall, both surface fish and Pachón seem to be forming a notable dedifferentiation profile prior actively initiating proliferation. However, while surface fish increase number of cells within the S and G2M phase in line with the previous reported peak in proliferation, Pachón maintain an overall lower S phase and G2M profile.

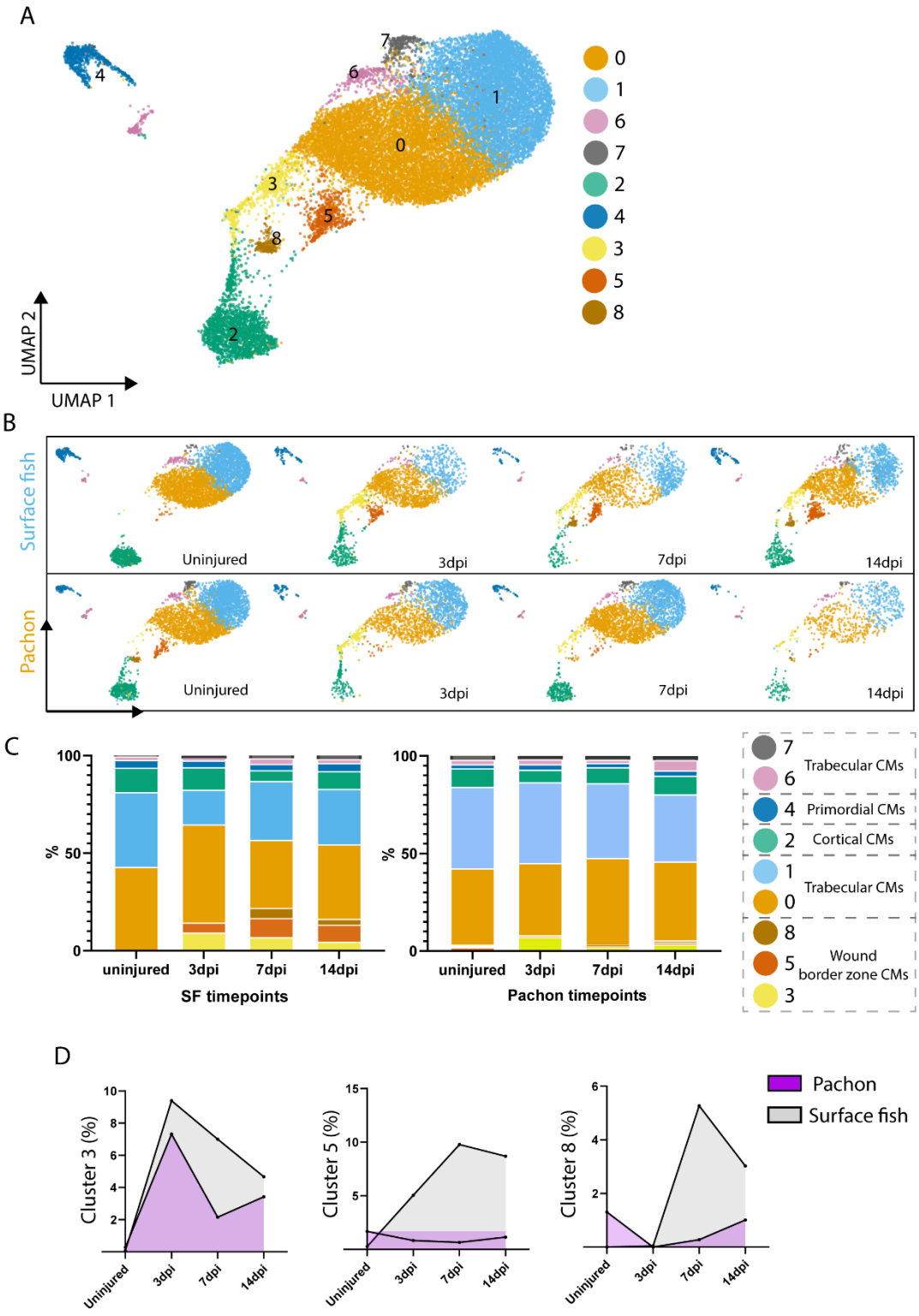


Figure 4.7 Cardiomyocyte cluster composition after injury.

(A) *UMAP projection of integrated Astyanax cardiomyocytes coloured by cluster identities.* ***(B)*** *UMAP projection, coloured by cluster identities and split by both timepoint after injury and fish type. Surface fish above, Pachón below.* ***(C)*** *Cardiomyocyte cluster proportions in Pachón and surface fish across each timepoint after injury.* ***(D)*** *Comparison of border zone cluster proportions between surface fish and Pachón over time. Surface fish, grey. Pachón, magenta.*

4.2.5 No increased apoptotic signature between Pachón and Surface fish cardiomyocytes

One of the main aims of this chapter was to utilise the scRNAseq to gain insight into the fate of the proliferating cardiomyocytes in Pachón. Previous work had shown no increase in myocardial apoptosis via cleaved caspase 3 signalling that could account for the absence of cardiomyocyte expansion. However, it is still possible that Pachón cardiomyocytes are dying through a cleaved caspase independent pathway.

UCell, a single-cell gene signature scoring method was employed to determine any sign of increased apoptosis in Pachón cardiomyocytes (Fig 4.8A-E). UCell generates a score for each cell based on a set of input genes that are related to a specific function/cell type (*167*). In this case, genes from the programmed cell death (GO:0012501) GO term were used as input to generate a gene signature consistent with apoptosis for each cell. In addition, this GO term is recommended when referring to instances of caspase-independent cell death mechanisms, which made it highly relevant to this situation.

When the UCell scoring was applied with the programmed cell death (GO:0012501) GO term, no significant changes in apoptotic gene signature were observed across either Pachón or surface fish cardiomyocyte clusters (Fig 4.8A, E). In addition, comparison between fish showed no significant differences in apoptotic gene signature between Pachón and surface fish in any of the border zone clusters (clusters 3, 5 and 8) or at any time point (Fig 4.8C-E). This suggests that in addition to the absence of cleaved caspase 3 dependent apoptosis, there are also no caspase-independent cell death mechanisms in either surface fish or Pachón border zone cardiomyocytes.

In conclusion, no increase in apoptotic signature was observed in Pachón border zone cardiomyocytes that could account for the reduced cardiomyocyte expansion.

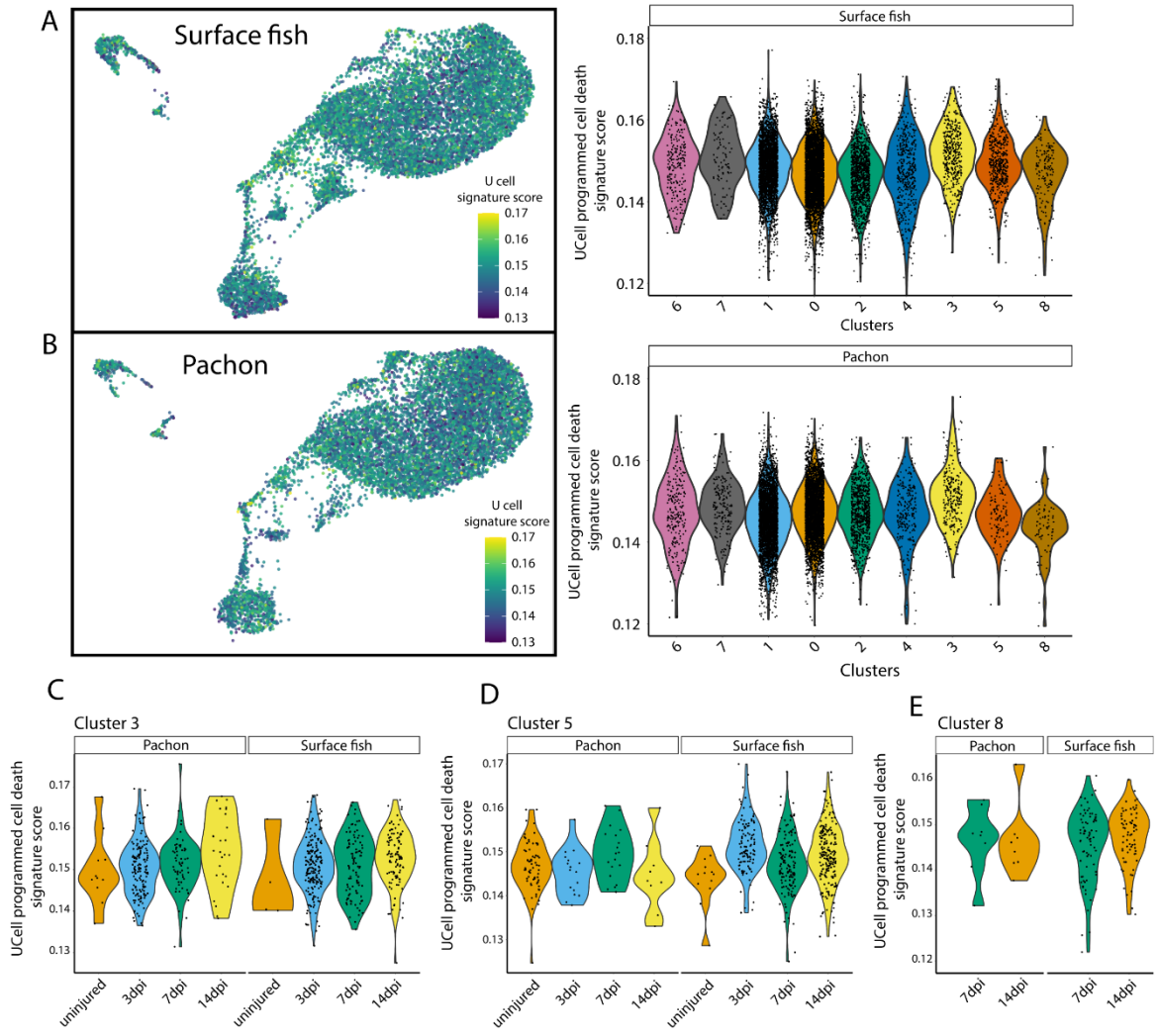


Figure 4.8 Similar apoptotic gene signature between Pachón and surface fish cardiomyocytes after injury.

(A-E) *Feature plot and violin plots displaying gene signature scores based on genes from the programmed cell death GO term (GO:0012501).* ***(A)*** *Programmed cell death gene signature score across surface fish clusters.* ***(B)*** *Programmed cell death gene signature score across Pachón clusters.* ***(C)*** *Violin plots comparing gene signature scores between surface fish and Pachón cardiomyocytes across timepoints after injury in border zone* ***(C)*** *cluster 3,* ***(D)*** *cluster 5 and* ***(E)*** *cluster 8. Very low number of cluster 8 cells in uninjured and 3dpi samples. Therefore cluster 8 gene signature scores not shown in these samples.*

4.2.6 Cell cycle transcriptional differences at 7dpi between Pachón and Surface fish

One of the main aims of this chapter was to utilise the scRNAseq to gain insight into the fate of the proliferating cardiomyocytes in Pachón and determine the possible mechanisms that underlie the contrasting cardiomyocyte profiles between fish.

One of the possibilities proposed for the lack of cardiomyocyte expansion in Pachón, was that Pachón cardiomyocytes are initiating proliferation but exiting the cell cycle at a premature stage and becoming polyploid. In light of this, it was notable that differential expression analysis revealed transcriptional differences between Pachón and surface fish relating to the regulation of the cell cycle (Fig 4.9A-C).

The differential expression analysis was performed on border zone clusters 3 and 5, comparing surface fish and Pachón border zone cardiomyocytes at 7dpi – the peak in proliferation. Differentially expressed genes between the two fish were processed through Metascape to identify enriched gene ontology clusters (*164*) (Fig 4.9A). This analysis was only performed on clusters 3 and 5, as the limited number of cells in Pachón cluster 8 at 7dpi prevented comparison between the fish in this cluster.

Comparison of cluster 5, the S phase cluster, revealed notable expression differences related to the cell cycle (Fig 4.9A-C). Specifically, surface fish had increased expression of genes governing DNA replication and initiation of the S phase. This was represented by enriched ontology terms such as G1 to S cell cycle control, DNA replication and pre-replicative complex assembly (Fig 4.9A). In support of this, expression of the S phase genes utilised in the cell cycle scoring metric, were generally higher throughout all timepoints after injury in surface fish (Fig 4.9C). Together, these suggest a higher S phase transcriptomic profile in proliferating cardiomyocytes compared to Pachón.

In contrast, Pachón had increased expression of genes involved in the negative regulation of the cell cycle. This was evidenced by enrichment of the gene ontology terms: negative regulation of mitotic cell cycle, negative regulation of mitotic cell cycle transition phase and mitotic cell cycle checkpoint signalling (Fig 4.9A). These terms were largely driven by the upregulation of 9 genes (Fig 4.9B). Genes of note included *btg1* and *btg2* – both genes with antiproliferative properties, timp2a – a metallopeptidase inhibitor, the cyclin - *ccng1*, *syf2*, *ZFP36L2* and lastly, *ctnnb2* (beta catenin) – the major component of the canonical Wnt signalling pathway (Fig 4.9B). The upregulation of these genes suggests Pachón proliferating cardiomyocytes are negatively regulating further cell cycle progression, particularly the transition into mitosis. No transition into mitosis would be an indication of an early cell cycle exit/arrest, which could be resulting in polyploid cardiomyocytes. Indeed, a similar process occurs in the adult mammalian heart after MI and during the postnatal period, where diploid cardiomyocytes exit the cell cycle forming polyploid cardiomyocytes – coinciding with the loss of regeneration (*41, 69, 151, 226*).

Prior to these transcriptional differences at 7dpi, there is a notable increase in entropy score at 3dpi in surface fish cluster 5, which does not occur Pachón (Fig 4.9D-G). This suggests that prior to the peak in proliferation, surface fish cardiomyocytes are establishing a more immature phenotype, while Pachón proliferating cardiomyocytes are remaining more mature relative to surface fish. In addition, this possibly suggests that Pachón do not take on the required immature characteristics, such as dedifferentiation, necessary for complete and effective proliferation. In conclusion, increased transcriptional expression of negative regulators of the cell cycle and increased maturity, suggests absence of immature characteristics alongside cell cycle arrest/exit with polyploidisation in Pachón.

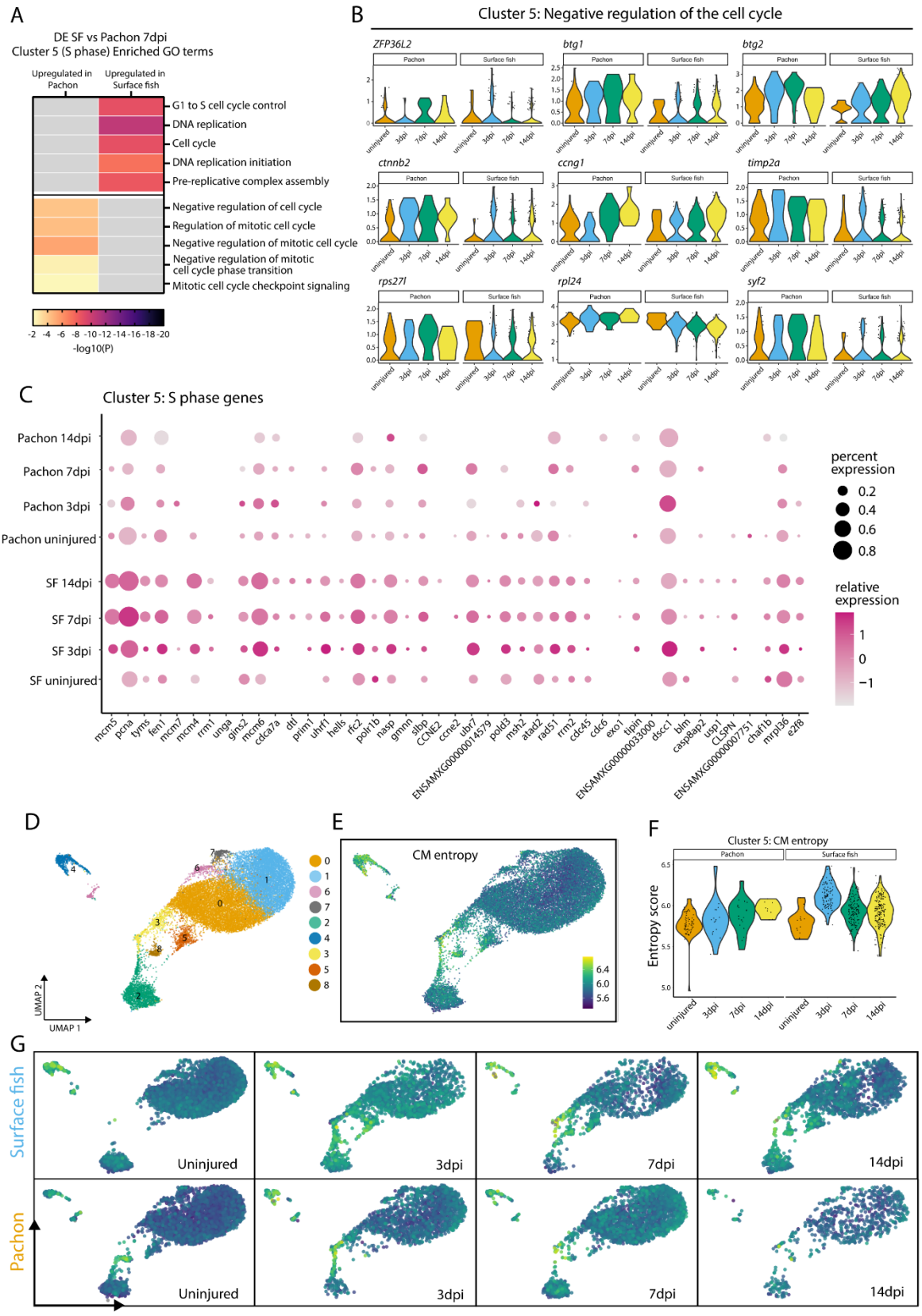


Figure 4.9 Differential expression of cell cycle genes between Pachón and Surface fish in the proliferating cluster - cluster 5

(A) *Metascape analysis on differentially expressed genes between surface fish and Pachón cluster 5 cardiomyocytes at 7dpi. Heatmap displays selected enriched GO terms. Genes upregulated in surface*

fish resulted in enrichment of terms relating to the S phase, while genes upregulated in Pachón resulted in enrichment of terms associated with negative regulation of the cell cycle. Grey cells indicate no enrichment. ***(B)*** *Violin plots displaying expression of selected genes in cluster 5 over time that are involved in the negative regulation of the cell cycle. Genes are upregulated in Pachón particularly at 7dpi.* ***(C)*** *Dotplot illustrating the increased expression of S phase genes in surface fish cluster 5, across injury timepoints. Selected S phase genes from those utilised in cell cycle scoring metric. Dot size represents the percentage of cells in the clusters expressing the marker and the colour intensity represents the average expression of the marker in that cluster.* ***(D)*** *UMAP projection of integrated Astyanax cardiomyocytes coloured by cluster identities.* ***(E)*** *UMAP projection coloured by entropy score.* ***(F)*** *Violin plot illustrating entropy scores in surface fish and Pachón over time after injury in cluster 5. Raised entropy score in surface fish 3 dpi.* ***(G)*** *UMAP projection, coloured by entropy score and split by both timepoint after injury and fish type. Surface fish above, Pachón below.*

4.2.7 Ploidy analysis of *Astyanax* cycling cardiomyocytes after injury

Hypothesis & expected findings

With scRNAseq suggesting cell cycle arrest and polyploidisation in Pachón border zone cardiomyocytes, a ploidy/cell cycle analysis was performed to confirm this. In this analysis, it was expected that Pachón cardiomyocytes in the border zone after a BrdU pulse chase (MF20+/BrdU+) would observe increased DAPI intensity – a readout of increased DNA content. Specifically, it is expected Pachón border zone cardiomyocytes have a DNA content level consistent with the G2M phase, while surface fish contain a DNA content consistent with the G0/G1 phase.

Hypothesis: Ploidy analysis combined with BrdU pulse chase will demonstrate that Pachón border zone cardiomyocytes are becoming polyploid, accounting for the lack of cardiomyocyte expansion.

Results

The low proportions of the G2M cluster combined with the increased expression of negative regulators of the cell cycle and reduced expression of S phase genes in Pachón, are an

indication of early cell cycle arrest. In the absence of any apoptotic signature, this sign of cell cycle arrest could be leading to polyploid cardiomyocytes – similar to the adult mammalian heart.

To functionally validate polyploidisation in Pachón border zone cardiomyocytes, an imaging cell cycle analysis based on a previously published method was combined with a BrdU pulse chase (*71*). This functional cell cycle analysis measures DAPI fluorescence intensity in dissociated cardiomyocytes to estimate DNA content and in turn polyploidy. The combination with a BrdU pulse experiment aimed to specifically target the border zone cardiomyocytes and measure DNA content in cardiomyocytes that had previously entered the cell cycle (Fig 4.10A).

Cryoinjured surface fish and Pachón cavefish were exposed to BrdU at 7dpi for 24hrs, and then isolated at 14dpi. Ventricles were dissociated and dried on slides for staining with DAPI, BrdU and MF20 (cardiomyocyte marker) (Fig 4.10A). Cardiomyocytes were imaged and processed using Cell Profiler to measure DAPI intensity in MF20 positive cells. DAPI intensity measurements were then analysed in a frequency histogram (Fig 4.10A). Typically, a histogram peak with a lower DAPI intensity is produced, which is indicative of diploid cells (2n) that are in the G0/G1 phase. In cycling cells, a second peak at a higher DAPI intensity is consistent with tetraploid cells (4n) or cells within the G2/mitosis phase of the cell cycle. While, cells between these peaks are classed as within the S phase (Fig 4.10A). Following generation of the frequency histogram, the experiment originally aimed to measure DAPI intensity in BrdU and MF20 double positive cells (border zone cardiomyocytes that had entered the S phase at 7dpi) and relate this to the distribution in the histogram, ultimately

estimating the DNA content. For polyploidy (tetraploid) to occur in Pachón, BrdU positive cardiomyocytes should have DAPI intensity/DNA content equivalent to 4n.

Unfortunately, the experiment was unable to detect BrdU positive cardiomyocytes (MF20+/BrdU+ double positive) and specifically analyse the cardiomyocyte population of interest. Alternatively, the overall proportions of cardiomyocytes in G0/G1 (2n), S phase, and G2/M (4n) were compared between surface fish and Pachón (Fig 4.10B-D).

Based on the histogram peaks produced in surface fish, the cut offs for the relevant cell cycle phases or degree of ploidy (diploid/tetraploid) was estimated and the percentage of cardiomyocytes in each phase determined (Fig 4.10B-D). Whilst not significant, based on overall cardiomyocyte percentages, Pachón had an increased proportion of cardiomyocytes within the S phase compared to the surface fish at 14 dpi (Fig 4.10D). Since proliferation is very low at 14dpi, this seems to suggest Pachón cardiomyocytes are arresting in the S phase.

Arresting in the S phase is unique and in contrast to the adult mammalian heart, which exits the cell cycle upon finishing DNA synthesis or nuclear division forming tetraploid cardiomyocytes. This abnormal DNA content in Pachón is suggestive of aneuploidy, a characteristic that occurs in other cell types, such as hepatocytes (*234*), but not yet reported in cardiomyocytes.

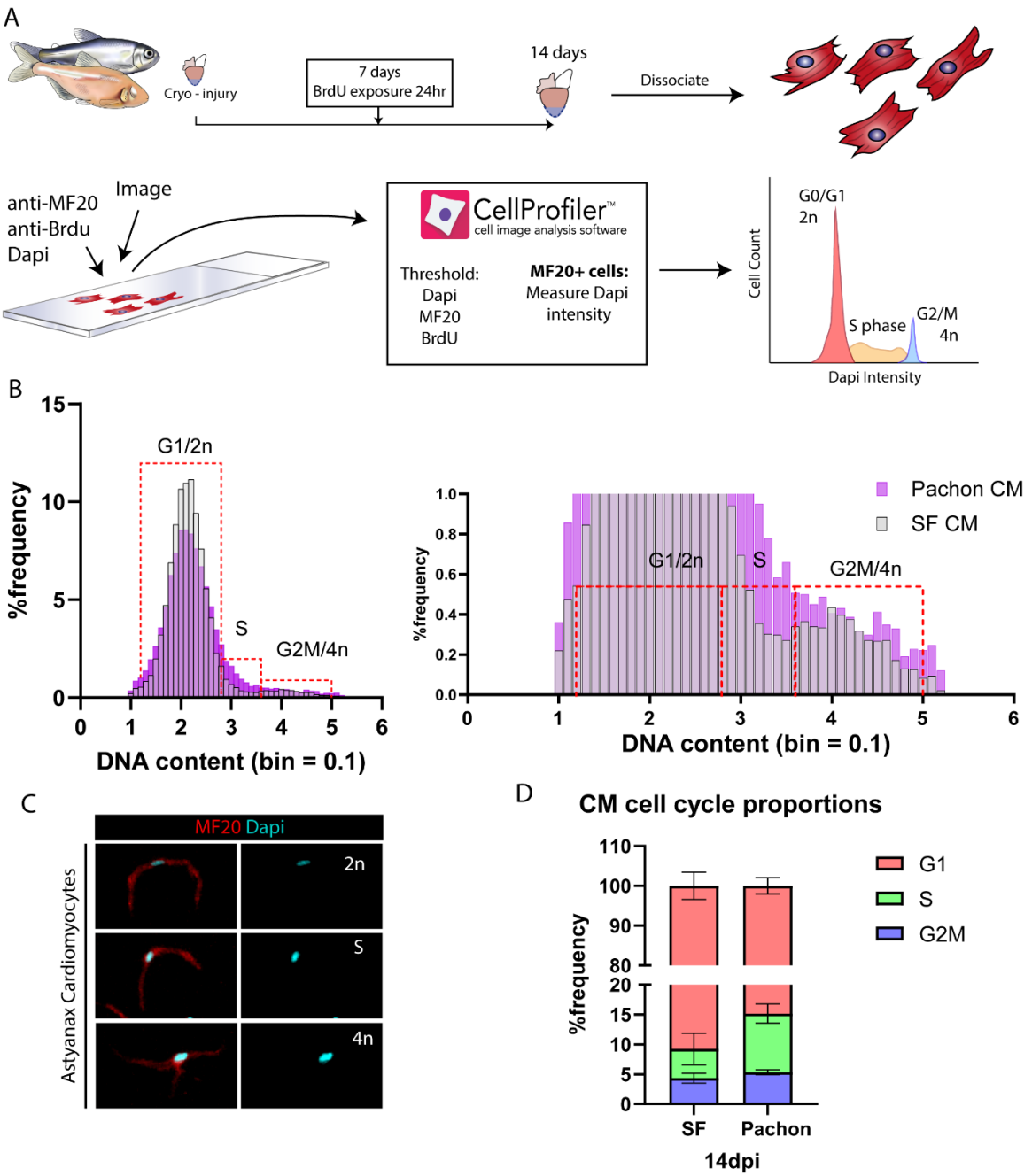


Figure 4.10 Potential arrest of Pachón cycling cardiomyocytes in the S phase.

(*A) Schematic of experimental design. Injured surface fish and Pachón were BrdU pulse chased (24 hr BrdU exposure at 7 dpi with isolation at 14 dpi). Hearts were then dissociated and cells dried on a slide before staining with DAPI, anti-MF20 and anti-BrdU. Cells were then imaged and processed using cell profiler to measure DAPI intensity of MF20 positive cells. The DAPI intensity across cells was analysed in a histogram. Example histogram: Cells in the red peak are diploid(2n) or G0/G1 phase. Cell in orange area are considered S phase. Cells in blue peak are tetraploid (4n) or in G2/M phase.* ***(B)*** *Distributions of Pachón (magenta) and surface fish (grey) cardiomyocyte DNA content at 14dpi. Red demarcated line represents cut offs for cell cycle phase/ploidy. n=4 (>3000 cells measured per heart).* ***(C)*** *Representative images of Astyanax cardiomyocytes with 2n (diploid) DNA content, within the S phase and with 4n (tetraploid) DNA content.* ***(D)*** *Proportion of cardiomyocytes in each indicated*

phase/population in both surface fish and Pachón at 14dpi. Two-way ANOVA with Tukey's multiple comparisons test. All data shown as mean +/- SEM.

4.2.8 Differences in metabolic gene expression between Pachón and Surface fish border zone cardiomyocytes

In addition to the above cell cycle transcriptional differences, many of the gene ontology clusters enriched between Pachón and surface fish were related to metabolic pathways, which were typically consistent across clusters 3 and 5 (Fig 4.11A, B). This is significant as the activity of several metabolic pathways have been linked to cell cycle arrest/polyploidisation and cardiomyocyte proliferation during regeneration (*63-65, 235*).

Both cluster 3 and cluster 5 had genes involved in glucose metabolism upregulated in surface fish compared to Pachón. This is evidenced by the enriched glycolysis and gluconeogenesis gene ontology cluster in surface fish (Fig 4.11A, B).

In addition to glucose metabolism, surface fish had increased expression of genes involved in the TCA (citric acid) cycle in both clusters versus Pachón, which was indicated by enrichment of the relevant GO term (Fig 4.11A, B). An enrichment of the TCA cycle in surface fish also coincided with enrichment of a series of GO terms related to mitochondrial organisation and components of the respiratory chain across both clusters (Fig 4.11A, B). This is matched with increased expression of genes related to oxidative phosphorylation in surface fish cardiomyocytes of cluster 5 (Fig 4.11B). However, the oxidative phosphorylation GO term was similarly enriched in both fish within cluster 3 (Fig 4.11A). Nonetheless, in evidence of increased oxidative metabolism in surface fish across both clusters, genes involved in the response to oxidative stress were upregulated in surface fish (Fig 4.11A, B). Overall, the

enrichment of these GO terms suggests increased mitochondrial based metabolism in surface fish border zone cardiomyocytes compared to Pachón.

In contrast, Pachón had increased expression of genes involved in fatty acid and amino acid metabolism compared to surface fish as indicated by enrichment of relevant GO terms (Fig 4.11A, B). The increased fatty acid metabolism genes are supported by the enrichment of the GO term, fatty acid degradation across both clusters, as well as the very slight enrichment of the GO term fatty acid beta oxidation over surface fish in cluster 5. It is worth noting the degree of enrichment of these terms is low, suggesting only a moderate increase in fatty acid oxidation/degradation in Pachón. In addition to fatty acid degradation/oxidation, fatty acid biosynthesis is also suggested to be increased in cluster 3, as per enrichment of its GO term in Pachón (Fig 4.11A, B). Together, these terms suggest an increase in fatty acid utilisation in Pachón border cluster compared to surface fish.

Outside of metabolism, several notable signalling pathways and cellular processes were suggested to be enriched between surface fish and Pachón (Fig 4.11A, B). This included adrenergic signalling and the Pi3K-Akt signalling pathway, which were enriched in surface fish cluster 5. Also included was the enrichment of TNF-alpha NF-kB signalling in surface fish across both border zone clusters. On the other hand, the cellular process macro-autophagy was enriched in the Pachón cluster 5, suggesting an increase in autophagy within Pachón proliferating cardiomyocytes (Fig 4.11A, B).

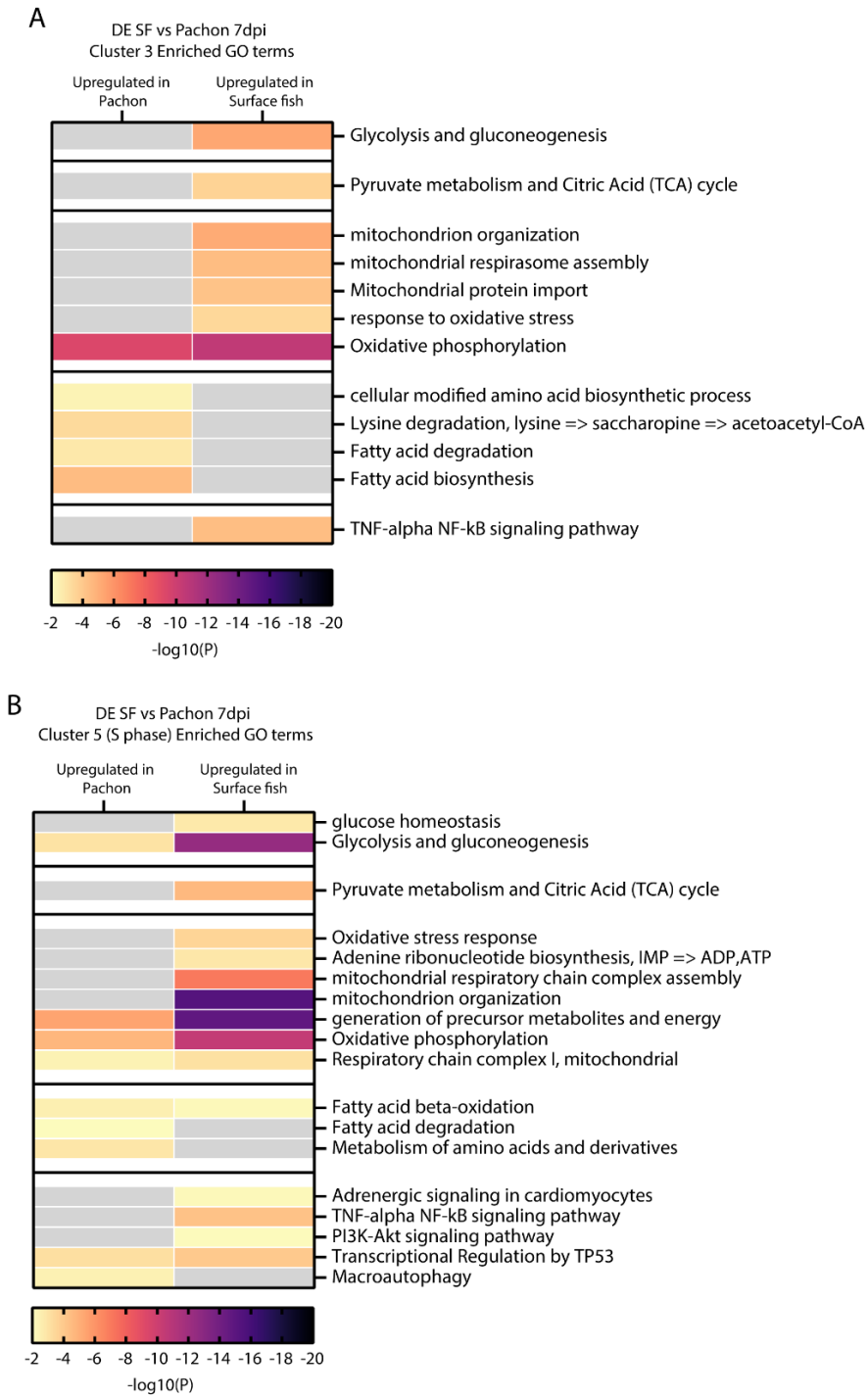


Figure 4.11 Transcriptional differences of metabolic genes between surface fish and Pachón border zone cardiomyocytes.

Differential expression analysis between surface fish and Pachón at 7dpi in clusters 3 ***(A)*** *and 5* ***(B). (A)*** *Heatmap of selected enriched ontology terms from differentially expressed genes between surface fish and Pachón cluster 3 cardiomyocytes at 7dpi. Heatmap includes enriched terms based on genes upregulated in surface fish (right side) and genes upregulated in Pachón (left side). Grey cells indicate no enrichment.* ***(B)*** *Heatmap of selected enriched ontology terms from differentially expressed genes between surface fish and Pachón cluster 5 cardiomyocytes at 7dpi. Heatmap includes enriched terms based on genes upregulated in surface fish (right side) and genes upregulated in Pachón (left side). Grey cells indicate no enrichment.*

4.3 Discussion

The aim of this chapter was to utilise scRNAseq analysis to determine the fate of the proliferating cardiomyocytes in Pachón. In addition, the chapter also sought to determine potential molecular pathways that underlie reduced cardiomyocyte expansion in Pachón and successful proliferation in surface fish.

In summary, targeted analysis revealed expression consistent with trabecular, cortical and primordial cardiomyocytes, indicating cardiomyocyte heterogeneity in both fish. In addition, a transcriptionally distinct border zone was established after injury, which generally possessed similar characteristics as those described in zebrafish. In the absence of any apoptotic signature, increased maturity and raised expression of negative regulators of the cell cycle suggested cell cycle arrest in Pachón proliferating cardiomyocytes. Additional comparison, showed a number of metabolic differences between surface fish and Pachón border zone cardiomyocytes that are possibly key factors in this notion of cell cycle arrest.

4.3.1 Cardiomyocyte heterogeneity in the *Astyanax* heart

Ventricular cardiomyocytes within the zebrafish heart have been shown to form 3 main layers: the innermost trabecular layer, the outermost cortical layer and the thin immature primordial layer that exists between the trabecular and cortical myocardium (*236*). A number of studies have suggested that cardiomyocytes from each of these 3 layers have specific differences in gene expression, indicating a level of cardiomyocyte heterogeneity within the adult fish heart (*227, 229*). In particular, studies by Sanchez-Iranzo *et al*. and more recently Tsedeke *et al.*, have attempted to establish the transcriptional differences that mark the cortical and primordial layers respectively (*227, 229*).

Tsedeke *et al.* reported primordial cardiomyocytes have high levels of notch signalling, as well as displaying immature characteristics (*229*). This is consistent with cluster 4, which displays increased expression of *notch3* and *hey2*, as well as increased immaturity as predicted by the maturation tools. Thus, leading to the annotation of these cells as primordial cardiomyocytes and supporting the previously reported characteristics of primordial cardiomyocytes.

In terms of cortical cardiomyocytes, Sanchez-Iranzo *et al.* found expression of *tbx5a* restricted to the trabecular layer and noticeably absent from the cortical layer (*227*). Utilising this expression pattern the authors attempted to find transcriptional differences between the two layers. However, upon review of Tsedeke *et al*. and Sanchez-Iranzo *et al.*, many of the top marker genes for cortical and primordial cardiomyocytes are similar. Indeed, most of the top genes reported in Sanchez-Iranzo *et al*. are highly expressed in the previously annotated primordial cluster (*227, 229*). As such, the cortical cardiomyocytes were best described by the absence of *tbx5a* expression with expression of genes consistent with mature cardiomyocytes. Nonetheless, the formation of a separate cluster of cortical cardiomyocytes, shows that cortical cells are transcriptionally distinct from other cardiomyocyte subtypes in the *Astyanax* heart. The top markers of cortical cardiomyocytes in this single cell data set appears to be the glycogenolysis enzyme, *pygma* and *limp-2* (*Lysosome membrane protein 2-like/ ENSAMXG00000033026*).

Overall, the identification of distinct clusters displaying gene expression consistent with these individual layers of cardiomyocytes, indicates, as expected, that *Astyanax mexicanus* possess these cardiomyocyte subtypes. The identification of transcriptionally distinct clusters also supported the previously reported evidence that cardiomyocytes of these individual layers have their own transcriptional program (*227, 229*) Thus, supporting the notion of

cardiomyocyte heterogeneity within the fish heart. Future comparison of these cardiomyocyte subtypes between Pachón and surface fish, will help to elucidate functional differences between fish in these cardiomyocyte layers, which may underlie overall differences in *Astyanax* cardiac physiology.

4.3.2 *Astyanax* border zone cardiomyocytes have similar characteristics with the zebrafish border zone

Border zone cardiomyocytes were immediately evident by the generation of three transcriptionally distinct clusters that are only prominent after injury. The formation of these clusters occurred alongside the loss of maturity in the form of increased transcriptional diversity, as well as, upregulation of cell cycle markers and previously established markers of the border zone. A transcriptionally distinct border zone observing increased expression of cell cycle genes with reduced maturity is consistent with zebrafish border zone cardiomyocytes. Notable, immature characteristics in the zebrafish border zone include: reactivating early developmental programs (*34, 37, 63, 78*), disassembly of sarcomere structures (*33, 34, 224, 225*) and reduced mitochondrial activity with increased reliance on glycolysis (*63, 64*).

The reduced mitochondrial activity in the zebrafish border zone was first observed by Honkoop *et al.*, which used single cell transcriptional profiling on zebrafish cardiomyocytes to compare border zone cardiomyocytes with remote cardiomyocytes. The authors found border zone cardiomyocytes had reduced expression of mitochondrial genes, immature mitochondrial morphology and reduced activity of succinate dehydrogenase (SDH - TCA cycle enzyme) (*63*). This suggested maintaining a low oxidative state is important for cardiomyocyte dedifferentiation and proliferation. Significantly, all 3 border zone clusters in the *Astyanax*

exhibited downregulated expression of genes in the TCA cycle and oxidative phosphorylation, matching the zebrafish border zone. This indicates proliferating *Astyanax* cardiomyocytes also generally attempt to maintain a low oxidative environment. The negative influence of mitochondrial oxidative metabolism on cardiomyocyte proliferation has also been highlighted in the neonatal mouse and adult mouse (*65*). During the postnatal period, a switch from glycolysis to mitochondrial oxidative phosphorylation causes increased ROS generation, which has been attributed to increased oxidative stress and cardiomyocyte cell-cycle arrest. Reducing mitochondrial-dependent oxidative metabolism or stress via hypoxemia or ROS scavenging was capable of preventing cardiomyocyte cell cycle arrest - extending the postnatal proliferative window (*65*). As such, a general lowering of oxidative metabolism in the *Astyanax* border zone is possibly reducing oxidative stress for initiation of cardiomyocyte dedifferentiation and proliferation. It is also a possible reason why both surface fish and Pachón are capable of initiating cardiomyocyte proliferation.

Zebrafish border zone cardiomyocytes disassemble sarcomeres as part of their dedifferentiation process before proliferating and migrating into the wound (*33, 34, 224, 225*). Recent work has shown that sarcomeres in these cardiomyocytes remain disassembled both throughout and hours after cell division (*224*). Each of the three *Astyanax* border zone clusters show downregulation of genes involved heart contraction, which is a possible indication of dedifferentiation and sarcomere disassembly. The fact that heart contraction genes are downregulated in both the cycling border zone clusters (cluster 5 and 8), seems to support the finding that loss of sarcomere structures remain throughout the whole cell cycle process and beyond (*224*). This same study also found that zebrafish cardiomyocyte sarcomere disassembly occurred in a proteasome-dependent manner in order to progress

through nuclear division and cytokinesis (*224*). Notably, this is consistent with the observation that proteasomal genes are upregulated in *Astyanax* border zone clusters, suggesting that the dedifferentiation transcriptional profile observed in the border zone clusters is regulated by proteasomal activity.

Overall, it appears the general border zone characteristics in the *Astyanax* are consistent with the reported features of the zebrafish border zone, which is perhaps an indication of why Pachón are still capable of initiating proliferation in response to injury.

4.3.3 Potential cell cycle arrest in Pachón cycling cardiomyocytes – ploidy

One of the major aims of this chapter was to determine the fate of the proliferating cardiomyocytes in Pachón. To decipher this fate, this chapter utilised scRNAseq to address two possible hypothesises. The first of hypothesis proposed cell death through a cleaved caspase independent pathway as a possible explanation for reduced cardiomyocyte expansion in Pachón. However, scRNAseq analysis indicated no increased apoptotic signature within the Pachón border zone cardiomyocytes that could account for reduced cardiomyocyte expansion.

The second proposed mechanism for reduced Pachón cardiomyocyte expansion was cell cycle arrest and polyploidisation of Pachón proliferating cardiomyocytes. Therefore, it was notable that differential expression analysis between surface fish and Pachón cluster 5 (S Phase) cardiomyocytes revealed increased expression of genes associated with negative regulation of the cell cycle in Pachón. The enrichment of these genes within the S phase cluster suggested no continuation into the other phases of the cell cycle and possibly cell cycle arrest. The notion of early cell cycle arrest is complemented by Pachón cardiomyocytes in cluster 5

having reduced expression of S phase/DNA replication genes. Since functional analysis has confirmed Pachón cardiomyocytes undergo DNA synthesis (enter S phase), it is a strong possibility that this cell cycle arrest is resulting in polyploid cardiomyocytes in Pachón.

Several of the genes that are negative regulators of the cell cycle observed here have been previously implicated in cardiomyocyte proliferation and polyploidy. This includes, *btg2 (BTG anti-proliferation factor 2)*, a cell cycle inhibitory transcription co-factor whose expression is repressed by the transcription factor, TBX20 (*57*). Over the post-natal period, *Tbx20* expression reduces and as a result *Btg2* expression increases - all corresponding with postnatal cardiomyocyte cell cycle exit. Significantly, repression of *Btg2* by *Tbx20* overexpression is capable of inducing cardiomyocyte proliferation in adult mouse border zone cardiomyocytes and improving heart function after MI (*57*). This not only supports the possible negative role of *btg2* in Pachón border zone cardiomyocyte cell cycle progression but also raises a possible functional role of *tbx20*. Indeed, *tbx20* is also upregulated in the regenerating zebrafish border zone and is required for cardiomyocyte proliferation in this region (*237*).

The increased expression of *ccng1* (*cyclinG1*) in Pachón cluster 5 cardiomyocytes compared to surface fish is also notable. Previous work has shown that overexpression of *Ccng1* in rat cardiomyocytes promotes DNA synthesis, but inhibits cytokinesis leading to polyploidy and multinucleation (*238*). Based on this phenotype, increased expression of *ccng1* in Pachón is possibly helping to promote the S phase entry as observed by PCNA and BrdU labelling in Pachón, but ultimately inhibiting cytokinesis and leading to polyploidy. Therefore, raised expression of *ccng1* supports the notion of polyploidisation in Pachón border zone cardiomyocytes.

Inferences made on cell compositional differences between fish are limited due to the absence of biological replicates and potential variations in wound size. Despite this, there are notable proportional differences in the border zone clusters. As a potential consequence of the transcriptional differences in the preceding S phase cluster, the proportion of Pachón cardiomyocytes in the G2M cluster is noticeably reduced to the presence of just several cells. The reduced number of cells in the G2M cluster suggests absence of a significant G2M phase in the cycling Pachón cardiomyocytes, and as such absence of either nuclear or cellular division. Therefore, supporting the notion of polyploid in Pachón border zone cardiomyocytes.

The suggestion of cell cycle arrest and ploidy of Pachón proliferating cardiomyocytes is significant, as cardiomyocyte polyploidy has been linked to myocardial regeneration potential (*70, 71*). Over the postnatal period, mammalian cardiomyocytes undergo cell cycle arrest and polyploidisation with increased maturation, which coincides with the loss of cardiomyocyte proliferation and regeneration potential (*69, 226*). Moreover, the very limited cardiomyocyte turnover in the adult mammalian heart after injury typically results in polyploid cells rather than new mononuclear diploid cardiomyocytes (*40, 41, 151*). This is in contrast to the adult heart of the regenerating zebrafish, which possesses mostly diploid cardiomyocytes and retains the ability to proliferate fully, forming new mononuclear diploid cardiomyocytes rather than polyploidy after injury (*71*). Collectively, this has led to the correlation of cardiomyocyte polyploidy and heart capacity. This is supported by impaired regeneration and reduced cardiomyocyte proliferation in zebrafish with genetically induced polyploidy (*71*). Significantly, the mammalian cardiomyocyte polyploidisation during the postnatal period and after MI matches the proposed cardiomyocyte polyploidisation in Pachón after injury.

Ultimately, polyploidy of Pachón proliferating cardiomyocytes could be a key determinant in the contrasting regenerative capacities between surface fish and Pachón.

To functionally validate the possibility of cell cycle arrest and polyploidy in Pachón border cardiomyocytes, a previously reported imaging cell cycle analysis on dissociated cardiomyocytes was performed (*71*). This method measured DAPI intensity to determine the amount of DNA in each cardiomyocyte and hence predict cell cycle stage/polyploidy. The original aim was to combine this analysis with a BrdU pulse chase experiment to specifically target the cardiomyocyte population of interest – measuring DNA content in the border zone cardiomyocytes that had initiated proliferation. Unfortunately, BrdU labelling of cardiomyocytes was unsuccessful and as such, the experiment was unable to specifically analyse the cardiomyocyte population of interest.

As an alternative approach, the ploidy/cell cycle phase was measured across all cardiomyocytes and general proportions of G0/G1 (2n), S phase, and G2/M (4n) were compared between surface fish and Pachón. The analysis indicated a raised percentage of cardiomyocytes predicted within the S phase in the Pachón compared to surface fish at 14dpi, indicating that Pachón cardiomyocytes are arresting within the S phase of the cell cycle and ending with an abnormal DNA content rather than forming tetraploid cardiomyocytes (4n) as in adult mammalian cardiomyocytes. This abnormal DNA content between diploid (2n) and tetraploid (4n) is a possible sign of aneuploidy or copy number variations (CNVs), which has been typically reported to occur in liver hepatocytes but to date has not been reported in cardiomyocytes (*234*).

In conclusion, the differential expression across the S phase cluster and the reduced proportions of G2M cardiomyocytes strongly supports the notion of cell cycle arrest in the

Pachón cycling cardiomyocytes and polyploidisation. However, improvement of the experimental strategy is required to equivocally deduce polyploidisation or aneuploidy in Pachón cardiomyocytes after injury.

4.3.4 Metabolic differences between surface fish and Pachón underlie the contrasting proliferation profiles in the order zone

Work within the field has correlated cardiomyocyte proliferation, cell cycle arrest and polyploidy with variations in metabolism (*63-65, 235*), which interestingly is one of the main transcriptional differences observed between Pachón and surface fish border zone cardiomyocytes. The increased expression of glycolysis genes in surface fish versus Pachón suggests a positive influence on cardiomyocyte proliferation, which significantly, matches the previously reported requirement for increased glycolysis in cardiomyocyte proliferation in both mouse and zebrafish (*63-65*). On the other hand, increased expression of fatty acid metabolism related genes in Pachón suggests a negative aspect on proliferation. Again, this matches work in the mouse, where fatty acid utilisation is considered detrimental to mammalian cardiomyocyte proliferation, causing cell cycle arrest/polyploidisation and promoting maturation with hypertrophic growth (*235, 239, 240*). Indeed, the Pachón proliferating cardiomyocytes also display increased maturity in terms of low transcriptional diversity compared to surface fish, raising the possibility that increased fatty utilisation in the Pachón is promoting maturation rather than cell cycle progression.

Despite the general downregulation of oxidative metabolism in *Astyanax* border zone cardiomyocytes, surface fish exhibit raised levels of gene expression relating to mitochondrial based metabolism compared to Pachón. Particularly in expression related to the assembly of the respiratory complex and oxidative phosphorylation. This is somewhat surprising as

lowering oxidative metabolism to reduce oxidative stress has been reported to be a prerequisite for cardiomyocyte proliferation after injury (*65, 68*). The lack of mitochondrial organisation or respiratory chain assembly may be consequence of macro autophagy, which is moderately enriched in Pachón border zone cardiomyocytes. Autophagy is a process required for the bulk degradation and recycling of cellular components, such as organelles and cytoplasmic proteins (*241*). As such, increased autophagy in the Pachón could be degrading and recycling mitochondria, leading the suggestion of reduced mitochondrial oxidative metabolism in Pachón border zone cardiomyocytes.

In light of the metabolic association with cardiomyocyte proliferation, these metabolic differences in border zone *Astyanax* cardiomyocytes could be key factors in the contrasting cardiomyocyte proliferation profile. As such, metabolic differences in the border zone cardiomyocytes were further characterised and are discussed in the following chapter.

4.3.5 Limitations

Currently, analysis has focused on the transcriptional differences between fish in border zone cardiomyocytes at 7dpi. However, no analysis has been performed with regards to the expression differences between fish that exist at baseline (uninjured cardiomyocytes). Differential expression of baseline cardiomyocytes will enable insights into the fundamental physiological differences between surface fish and Pachón hearts, which could be partly responsible for the contrasting cardiomyocyte proliferation profiles. In addition, the transcriptional dynamics that occur from baseline/uninjured cardiomyocytes to the resulting border zone cardiomyocytes currently remain unexplored. Investigation of the transcriptional dynamics that results in wound border zone cardiomyocytes from baseline cardiomyocytes

would enable identification of the injury dependant transcriptional changes within cardiomyocytes that are different between the morphotypes.

Single cell RNAseq analysis within this chapter suggested that rather than dying, Pachón cardiomyocytes are undergoing cell cycle arrest and possibly becoming polyploid. To confirm this, the chapter aimed to use a cell cycle/ploidy analysis in combination with a BrdU pulse chase to specifically target the cycling cardiomyocytes at 7dpi. However, the analysis was unable to detect BrdU positive cardiomyocytes (BrdU+/MF20+ double positive cells) despite a very small number of non-cardiomyocyte nuclei positive for BrdU. Previous BrdU experiments had employed Mef2c as the cardiomyocyte marker, while this experiment relied on MF20 as a cardiomyocyte marker with the aim of also measuring binucleated numbers. Whilst unlikely, one possible explanation is that the BrdU positive cardiomyocytes after pulse chase in Pachón are no longer expressing MF20, thus resulting in no detected BrdU+/MF20+ double positive cells. Alternatively, the cycling cardiomyocytes within the border zone is a relatively small population, particularly if the injury is small. As such, BrdU positive cardiomyocytes may form a rare population and remain undetected in this analysis. Subsequent experiments to confirm ploidy should rely on the previous validated Mef2c as a marker of cardiomyocytes and utilise tissue sections rather than cell suspensions for finding border zone cardiomyocytes.

Lastly, this scRNAseq analysis specifically targeted the cardiomyocytes and thus, only investigated transcriptional changes intrinsic to cardiomyocytes. As such, the actions of many other cell types on cardiomyocyte proliferation currently remain unexplored. Additional cell types such as fibroblasts, macrophages and others are likely to be different between fish, and thus impacting on the cardiomyocyte profile through intercellular communication. Additional

analysis of the scRNAseq should put the cardiomyocytes in context with the other cell types captured in the single cell.

4.3.6 Conclusion

Single cell transcriptomics of the *Astyanax* heart before and after injury supported the notion of cardiomyocyte heterogeneity as well as revealing similar wound border qualities as those described in the regenerating zebrafish. The *Astyanax* border zone cardiomyocytes show dedifferentiation characteristics, which are consistent across the different phases of the cell cycle and are possibly regulated by an increase in proteasome activity. In addition, the *Astyanax* border zone also observed expression consistent with decreasing mitochondrial oxidative metabolism.

Significantly, cell cycle transcriptional differences and changes in cell cycle phase composition in border zone cardiomyocytes indicates cell cycle arrest of Pachón cycling cardiomyocytes and potentially polyploidy. This interestingly coincides with significant transcriptional differences in several metabolic pathways. These metabolic differences could potentially underlie the lack of cardiomyocyte expansion in the Pachón and therefore are explored further in the next chapter.

Chapter 5
Metabolic differences between Pachón and surface fish cardiomyocytes after injury

5.1 Introduction

To date, little is known of the cardiac metabolism in the *Astyanax*. However, metabolic differences between cavefish and surface fish after injury have now been observed from both comparative bulk and single cell transcriptomics in previous chapters, particularly in the predicted border zone cardiomyocytes. Specifically, genes relating to glycolysis/gluconeogenesis and fatty acid metabolism are differentially regulated, indicating a potential role in the cardiomyocyte proliferation profile in the *Astyanax*. As such, exploring the metabolic response after injury is the focus of this chapter.

5.1.1 Metabolism in the *Astyanax*

In light of these metabolic differences, it is interesting to note that *Astyanax* cavefish have evolved numerous adaptations in their general metabolism in response to cave life, which is characterised by low nutrient levels (*144, 145, 242-244*). Due to the absence of light, cave environments do not possess photosynthesis-driven primary producers for energy input into the cave food chain (*244*). Instead, cave food chains are dependent on energy input from external secondary sources, which are typically inconsistent (*244*). As such, cavefish have to potentially withstand long periods of nutrient deprivation, and to this end, have evolved many different metabolic features to thrive in these unpredictable conditions.

Many of the metabolic adaptions in the cavefish revolve around the ability maximise energy uptake versus energy conservation. These adaptations include lower metabolic rate, reduced metabolic circadian rhythm, increased appetite, and starvation resistance (*145, 146, 245*). Cavefish also have increased body fat and fat storage as well as possessing a fatty liver, which collectively suggests a preference for fatty acid metabolism (*145, 243*). Alongside these fat-based adaptions, cavefish also display hyperglycaemia and insulin resistance – all phenotypes associated with human obesity and diabetes mellitus (*144*). Indeed, cavefish possess a mutation in the insulin receptor (SNP P211L) that has been associated with Rabson-Mendenhall syndrome, a condition of severe insulin resistance (*246*). Despite these extreme metabolic phenotypes, cavefish do not appear to display features of pathologies typically associated with obesity and diabetes such as accumulation of advanced glycation end products (AGEs), chronic tissue inflammation, impaired growth due to insulin dysregulation, and low survivability due to arterial disease (*144, 242*). Ultimately the cavefish have developed a metabolic resilience to their extreme metabolic phenotypes, which have occurred in adaption to their cave environment (*242*). However, could these metabolic adaptions during the course of their evolution be detrimental to cardiomyocyte proliferation during regeneration?

5.1.2 Metabolism during myocardial regeneration

Importantly, it has been proposed within the field that differences in metabolism across the animal kingdom correspond with cardiomyocyte proliferation potential and heart regeneration capacity (*65, 247*). Specifically, the capacity to perform anaerobic glycolysis and maintaining a low oxidative state is vital for cardiomyocyte proliferation in the regenerating neonatal mouse and zebrafish (*63-65*). In zebrafish, the proliferating myocardial border zone

undergoes a metabolic reprogramming by upregulating glycolysis activity and lactate fermentation (anaerobic glycolysis), while downregulating mitochondrial oxidative metabolism (*63, 64*). This switch from oxidative metabolism to anaerobic glycolysis despite the presence of significant oxygen levels, is also termed aerobic glycolysis and referred to as the Warburg effect (*248, 249*). Importantly, this upregulation of glycolysis activity is key to zebrafish cardiomyocyte proliferation during regeneration, and several specific components of the glycolysis pathway have been found to be essential for dedifferentiation and proliferation during regeneration (*63, 64*). This includes the activity of the glycolytic enzyme, pyruvate kinase M2 isoform, and activity of the PDK-PDC axis – both of which are key components of promoting glucose metabolism toward lactate production and anaerobic glycolysis (*64*).

On the other hand, the lowering of mitochondrial oxidative metabolism in zebrafish border zone cardiomyocytes, suggests a low oxidative state is a factor in cardiomyocyte proliferation during regeneration (*63*). This is supported in the neonatal mouse heart after injury, where a population of immature cardiomyocytes, which contribute to the bulk of cardiomyocyte proliferation during regeneration, decrease transcriptional expression consistent with reduced oxidative metabolism (*68*). However, the role of oxidative metabolism on cardiomyocyte proliferation is best illustrated during the mammalian postnatal period and the loss of regeneration (*65*). During the postnatal period the heart undergoes a temporal shift from glucose utilisation and anaerobic glycolysis to mitochondrial oxidative phosphorylation, particularly via increased fatty-acid utilization (*250, 251*). This metabolic shift coincides with cardiomyocyte cell-cycle arrest and loss of regenerative capacity (*25, 65, 235*). Despite the energy advantage of increased fatty utilisation and mitochondrial oxidative

phosphorylation, the oxidative process produces elevated levels of ROS, which causes cardiomyocyte oxidative stress. Through activation of DNA-damage response (DDR) pathway, this raised oxidative stress has been shown to be a factor in cardiomyocyte cell-cycle arrest and in turn loss of regenerative capacity during the postnatal period (*25*). Ultimately, lowering fatty acid metabolism and by association reducing mitochondrial oxidative phosphorylation is a prerequisite for cardiomyocyte proliferation (*25, 235*).

The metabolic differences highlighted by single cell transcriptomics, with the knowledge that cavefish have significant metabolic adaptations, as well as correlations between metabolism and heart regeneration, suggests metabolic differences could underlie the contrasting cardiomyocyte proliferation profile.

5.1.3 Aim

This chapter aims to build on the transcriptomic data from chapter 4 by characterising and validating the metabolic differences observed between *Astyanax* morphotypes in the border zone cardiomyocytes. The chapter then subsequently aims to explore regulators that could account for this difference in metabolism during proliferation and regeneration, namely the insulin receptor mutation observed in Pachón (SNP P211L). Exploring these metabolic differences will help to establish the ideal metabolic environment required for complete and efficient cardiomyocyte proliferation during natural heart regeneration.

5.2 Results

5.2.1 Glucose uptake and glycolysis are increased in the surface fish border zone versus the Pachón

Hypothesis & expected findings

scRNAseq analysis showed enrichment of glycolysis genes in the surface fish border zone cardiomyocytes over Pachón. Therefore, it was predicted that a combination of scRNAseq and RNAscope will confirm increased expression of genes key to glucose uptake and regulation of glycolysis in surface fish border zone cardiomyocytes compared to Pachón. It is also expected that RNAscope will show a number of these genes localised to the surface fish myocardial border zone. Therefore, suggesting surface fish proliferating cardiomyocytes increase glycolysis to higher levels compared to Pachón.

Hypothesis: Expression of the glucose transporter, *glut1a*, and key regulators of glycolysis pathway activity are increased in surface fish border zone cardiomyocytes compared to Pachón

Results

The single cell transcriptomics highlighted differential expression in the border zone cardiomyocytes between Pachón and surface fish that was associated with the glycolysis pathway. Specifically, glycolysis was enriched in surface fish border zone cardiomyocytes, suggesting increased glycolysis activity compared to Pachón. In light of the current work in the field and the results from the single cell transcriptomics, glucose uptake and glycolysis were further investigated.

From the scRNAseq, comparison of border zone cardiomyocytes between fish revealed significantly increased expression of the glucose transporter, *glut1a* (*slc2a1a*), across all timepoints in surface fish compared to Pachón (Fig 5.1C). This suggested increased glucose uptake in the surface fish proliferating cardiomyocytes compared to Pachón and implicated it as a possible factor in the contrasting cardiomyocyte profiles.

Glucose transport into the cell is facilitated by the action of numerous glucose transporters (GLUTs), with *Glut1* and *Glut4* being the two predominant transporters expressed within the mammalian heart (*252*). The insulin independent GLUT1 transporter is expressed in the developing mammalian heart but is inactivated in the adult heart, switching to the insulin dependent GLUT transporter (*252*). In contrast, *glut1a* is significantly the highest expressed glucose transporter in the adult zebrafish heart, while the zebrafish does not possess a *glut4* transporter (*253-255*). As such, Glut12 has been proposed as the main insulin-regulated glucose transporter in the zebrafish larval heart but is minimally expressed within the adult heart (*253*). However, the annotation of the *Astyanax* genome seems to suggest the *Astyanax* possess a *glut4a (slc2a4a)* and *glut4b (slc2a4b)* transporter, which is consistent with other species of fish (*255*). qPCR analysis on whole ventricles found *glut4a* expression to be very low and at similar levels in surface fish and Pachón hearts, both before and after injury (Fig 5.1B). In contrast, *glut1a* expression was significantly higher than *glut4a* in surface fish hearts at baseline and after injury - suggesting *glut1a* is the predominant glucose transporter in the adult surface fish heart. In addition, *glut1a* expression was significantly increased in surface fish compared to Pachón fish, as it was largely absent in the Pachón heart (Fig 5.1B).

To visualise the spatial context of *glut1a* expression after injury, commercial *in situ* hybridisation method RNAscope was performed at 7dpi. RNAscope confirmed low levels of

glut1a expression in the Pachón heart and validated the differential expression between the two morphotypes (Fig 5.1D). Strikingly, it also showed, strong upregulated *glut1a* expression in the highly proliferative border zone myocardium relative to remote cardiomyocytes in the surface fish (Fig 5.1D). Significantly, this was absent in the Pachón border zone.

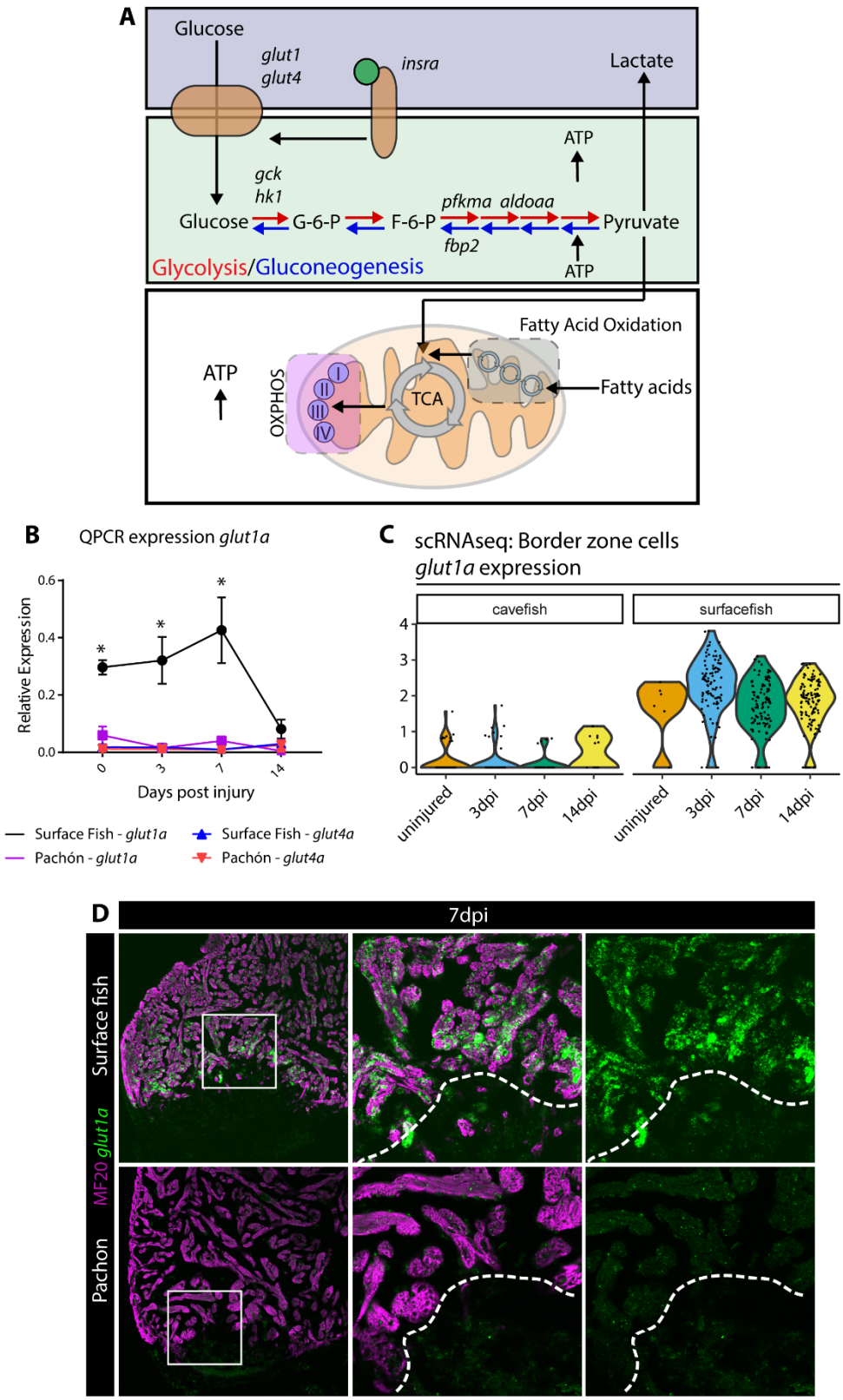


Figure 5.1 Increased *glut1a* expression in surface fish but minimal expression of glucose transporters in Pachón.

(A) *Schematic showing the main metabolic pathways with the genes of interest.* ***(B)*** *Quantitative whole ventricle expression by qPCR of glut1a and glut4a at sham, 3, 7 and 14dpi in surface fish and Pachón. N=3, two-way ANOVA with Sidak multiple comparisons test. Data shown as mean +/- SEM. p<0.05 (*).*

(C) *scRNAseq: Violin plot of glut1a expression in border zone cells (cells from clusters 3, 5 ,8 combined) over time. glut1a significantly differentially expressed between Pachón and surface fish border zone cells in at least one timepoint after injury (adj Pval <0.05). MAST differential expression test.* ***(D)*** *RNAscope in situ hybridisation of glut1a at 7 days after cryoinjury in Pachón and surface fish. MF20(magenta) labels myocardium, glut1a (green). Dashed line indicates wound border.*

Once inside the cell, glucose is metabolised in the glycolysis pathway, producing ATP and pyruvate (Fig 5.1A). Importantly, many of the major genes that function in the glycolysis pathway are significantly upregulated in the regenerating surface fish compared to Pachón border zone cells in the scRNAseq (Fig 5.2A-G). This included *hk1*, a member of the hexokinases that catalyse the first step of glycolysis, and *pfkma* (*ATP-dependent 6-phosphofructokinase*), the rate determining enzyme of glycolysis (Fig 5.2A, B). Moreover, *aldocb* (*aldolase C*) and *pkma (pyruvate kinase M1/2a)*, both enzymes that function further down the pathway, are also significantly upregulated in surface fish border zone cells compared to Pachón (Fig 5.2C, D).

The differential expression of *pfkma* in border zone cells is supported by RNAscope analysis, which indicated upregulated expression of *pfkma* in the myocardial border zone in both surface fish and Pachón hearts at 7dpi, but at an altogether lower level in Pachón (Fig 5.2H). Similar to the *pfkma* expression pattern*, aldoaa (aldolase a)*, a paralog of the previous mentioned *aldocb*, was upregulated in the myocardial border zone in both surface fish and Pachón hearts at 7dpi, but at a lower level in Pachón (Fig 5.2I). Furthermore, *gck*, a hexokinase isoform which also catalyses the first step in glycolysis, is also moderately upregulated in the surface fish myocardial border zone, whilst being mostly absent in Pachón (Fig 5.2J). Collectively, this suggests both surface fish and Pachón, particularly within proliferating

cardiomyocytes, increase glycolysis in response to injury, albeit at a higher level in surface fish.

Notably, the pyruvate dehydrogenase kinases, *pdk2a* and *pdk4*, were also upregulated in surface fish border zone clusters compared to Pachón (Fig 5.2F, G). The pyruvate dehydrogenase kinases drive anaerobic glycolysis via their regulation of pyruvate dehydrogenase (PDH) and their upregulation in surface fish suggests higher levels of anaerobic glycolysis in surface fish border zone cardiomyocytes. In further support of raised anaerobic glycolysis levels, *ldha* (lactate dehydrogenase), which catalyses pyruvate to lactate under anaerobic conditions, is upregulated in surface fish border zone cardiomyocytes (Fig 5.2E).

In conclusion, these results suggest surface fish proliferating cardiomyocytes in the border zone increase glucose uptake, which coincides with increased glycolysis. In contrast, glucose uptake is minimal in Pachón border zone cardiomyocytes, and while glycolysis is also moderately increased in the Pachón border zone, it is to a much lower level compared to surface fish.

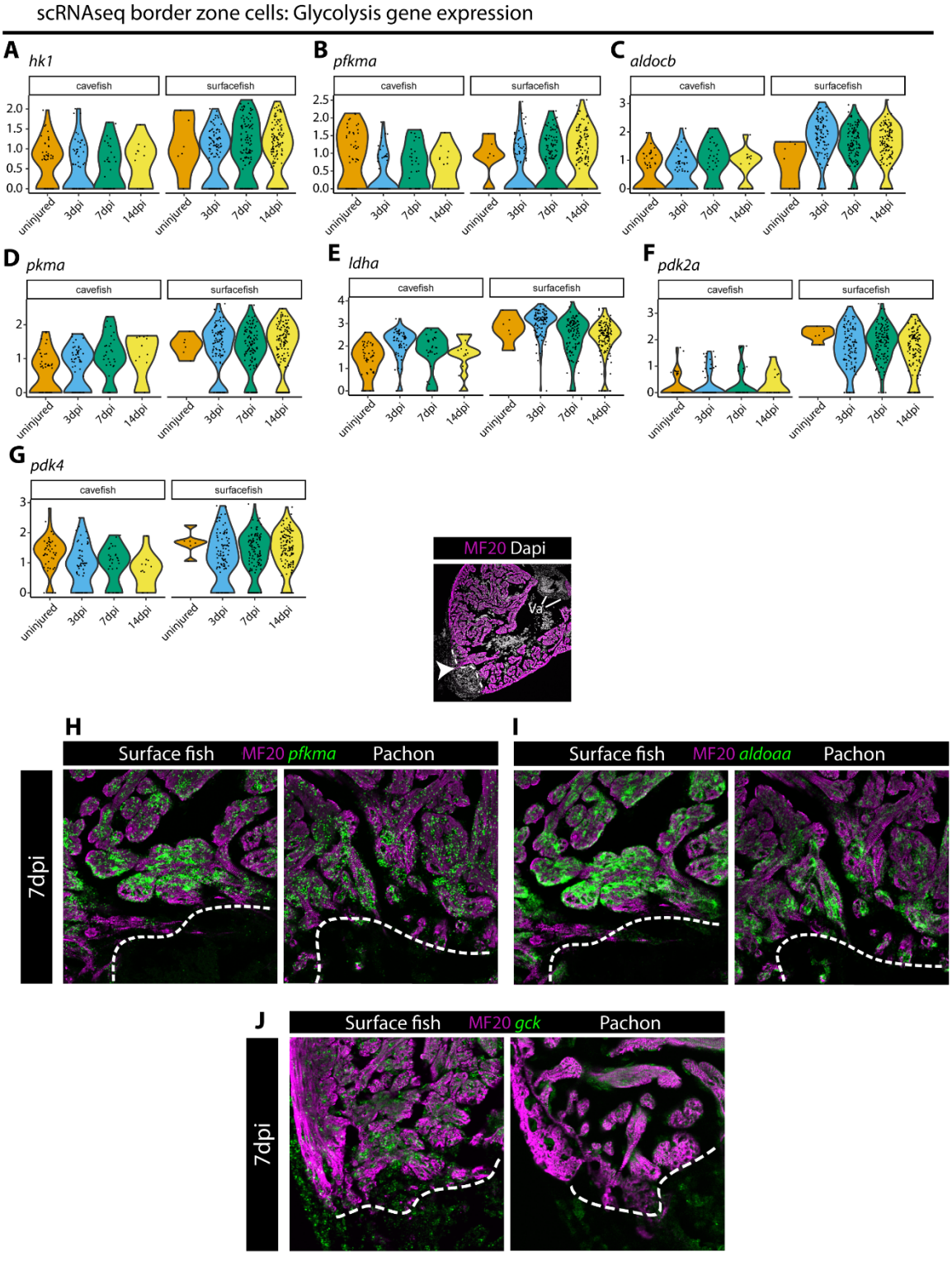


Figure 5.2 Increased expression of glycolysis genes in surface fish versus Pachón cavefish at the wound border.

(A-G) *scRNAseq: Violin plot of selected glycolysis gene expression in border zone cells (cells from clusters 3, 5 ,8 combined) over time. Each gene significantly differentially expressed between Pachón and surface fish border zone cells in at least one timepoint after injury (adj Pval <0.05). MAST differential expression test.* ***(H-I)*** *RNAscope in situ hybridisation of pfkma* ***(H)****, aldoaa* ***(I)*** *and gck* ***(J)*** *at 7dpi in Pachón and surface fish, showing higher expression in the wound border myocardium in both*

fish. MF20 (magenta) labels myocardium, pfkma, aldoaa and gck (green). Dashed line indicates wound border.

5.2.2 Increased gluconeogenesis in Pachón

Hypothesis & expected findings

scRNAseq analysis showed enrichment of gluconeogenesis in the Pachón border zone cardiomyocytes over surface fish. Therefore, it was predicted that a combination of scRNAseq and RNAscope will show increased expression of the rate limiting enzyme of gluconeogenesis, *fbp2,* in Pachón compared to surface fish. RNAscope is also predicted to establish *fbp2* localisation in the myocardium after injury.

Hypothesis: Expression of the rate limiting enzyme of gluconeogenesis, *fbp2*, is increased in Pachón myocardium compared to surface fish.

Results

Gluconeogenesis is closely linked to glycolysis but in an opposing fashion, generating glucose through the breakdown of lactate, glucogenic amino acids and odd-chain fatty acids (*256*). Comparison of cardiomyocytes in the scRNAseq highlighted gluconeogenesis as a differentially regulated pathway in the *Astyanax*, with gluconeogenesis suggested to be upregulated in the Pachón heart versus the surface fish. This is mainly observed through the differential expression of *fbp2* (fructose-1, 6-bisphosphatase 2), the rate limiting enzyme of gluconeogenesis, which is increased in the Pachón heart (Fig 5.3A). RNAscope showed strong *fbp2* expression throughout the Pachón myocardium at 7dpi, while *fbp2* was only lowly expressed throughout the ventricle in the surface fish at this stage, which confirmed the differential expression between the fish (Fig 5.3B). However, *fbp2* expression appeared to be

reduced in the proliferating border zone myocardium in the Pachón, suggesting a reduction of gluconeogenesis in Pachón proliferating cardiomyocytes (Fig 5.3B').

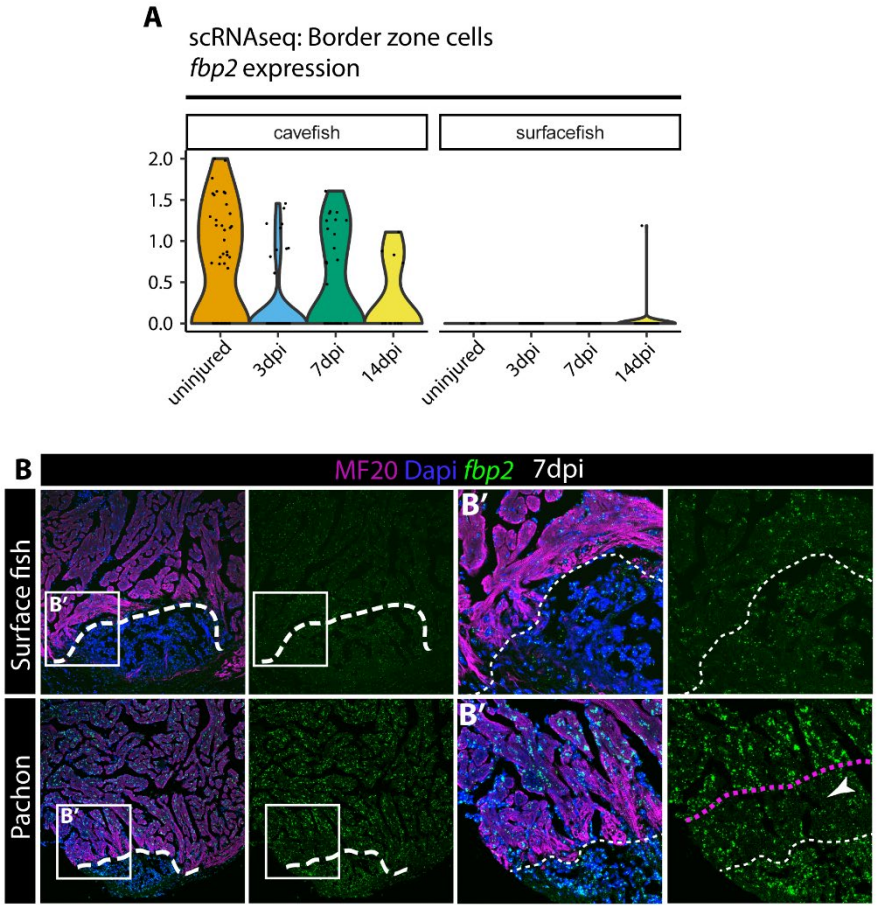


Figure 5.3 Pachón cavefish have increased expression of *fbp2*, a key enzyme in gluconeogenesis.

(A) *scRNAseq: Violin plot of fbp2 expression in border zone cells (cells from clusters 3, 5 ,8 combined) over time. fbp2 significantly differentially expressed between Pachón and surface fish border zone cells in at least one timepoint after injury (adj Pval <0.05). MAST differential expression test.* ***(B)*** *RNAscope in situ hybridisation of fbp2 at 7 days after injury in Pachón and surface fish, showing much higher expression throughout the ventricle in Pachón compared to surface fish.* ***B')*** *Higher magnification of* ***B****, showing reduced expression of fbp2 in the wound border myocardium in Pachón compared to the rest of the ventricle. MF20 (magenta) labels myocardium, fbp2 (green). Dashed line indicates wound border.*

5.2.3 Key fatty acid transporter, *cd36*, localises to proliferating cardiomyocytes in Pachón

Hypothesis & expected findings

scRNAseq analysis showed a moderate enrichment of genes involved in fatty acid metabolism in the Pachón border zone cardiomyocytes compared to surface fish. Therefore, it was expected that a combination of scRNAseq and RNAscope will confirm increased expression of the fatty acid metabolism genes in Pachón border zone cardiomyocytes. In particular, it was predicted that the key fatty acid transporter, *cd36*, would be increased in Pachón border zone cardiomyocytes compared to the surface fish, and would localise to the myocardial border zone. Therefore, suggesting increased fatty acid utilisation in Pachón border zone cardiomyocytes compared to surface fish.

Hypothesis: Expression of the fatty acid transporter, *cd36*, and enzymes of fatty acid metabolism are increased Pachón border zone cardiomyocytes compared to surface fish.

Results

The absence or minimal expression of glucose transporters in Pachón, particularly in the border zone, suggested little glucose uptake occurs in Pachón cardiomyocytes. This raised the question as to what these cells use as an energy source. Cavefish possess a fatty liver and increased fat storage, which suggests a preference for fatty acid in cavefish metabolism. As such, cavefish physiology and the scRNAseq to a moderate extent, suggest a preference for fatty acid utilisation in Pachón compared to the surface fish. Specifically, *decr* – an accessory enzyme in beta-oxidation and *gcdhb* – a member of the acyl-CoA dehydrogenase family, are upregulated in Pachón compared to surface fish in both border zone clusters (cluster 3 and cluster 5) (Fig 5.4A, B). Additionally, both *acadm* (*acyl-CoA dehydrogenase medium chain*) and

acads (*acyl-CoA dehydrogenase short chain*) are upregulated in cluster 3 and cluster 5 respectively (Fig 5.4A, B). These genes importantly catalyse the first step of mitochondrial fatty acid beta-oxidation and members of the acyl-CoA dehydrogenase family.

In support of increased fatty acid utilisation in Pachón, *cd36*, a gene key to fatty acid transport into the cell, was sharply upregulated 7 days after injury in the Pachón heart (Fig 5.4C). RNAscope revealed *cd36* expression in the Pachón localised to the wound border at 7dpi, while largely absent in the surface fish (Fig 5.4C). Strikingly, the expression of *cd36* solely localised to the proliferating cardiomyocytes (Mef2+/PCNA+ cells) at the very edge of the wound border in Pachón fish at 7dpi, suggesting proliferating cardiomyocytes in Pachón have greater fatty acid uptake (Fig 5.4D).

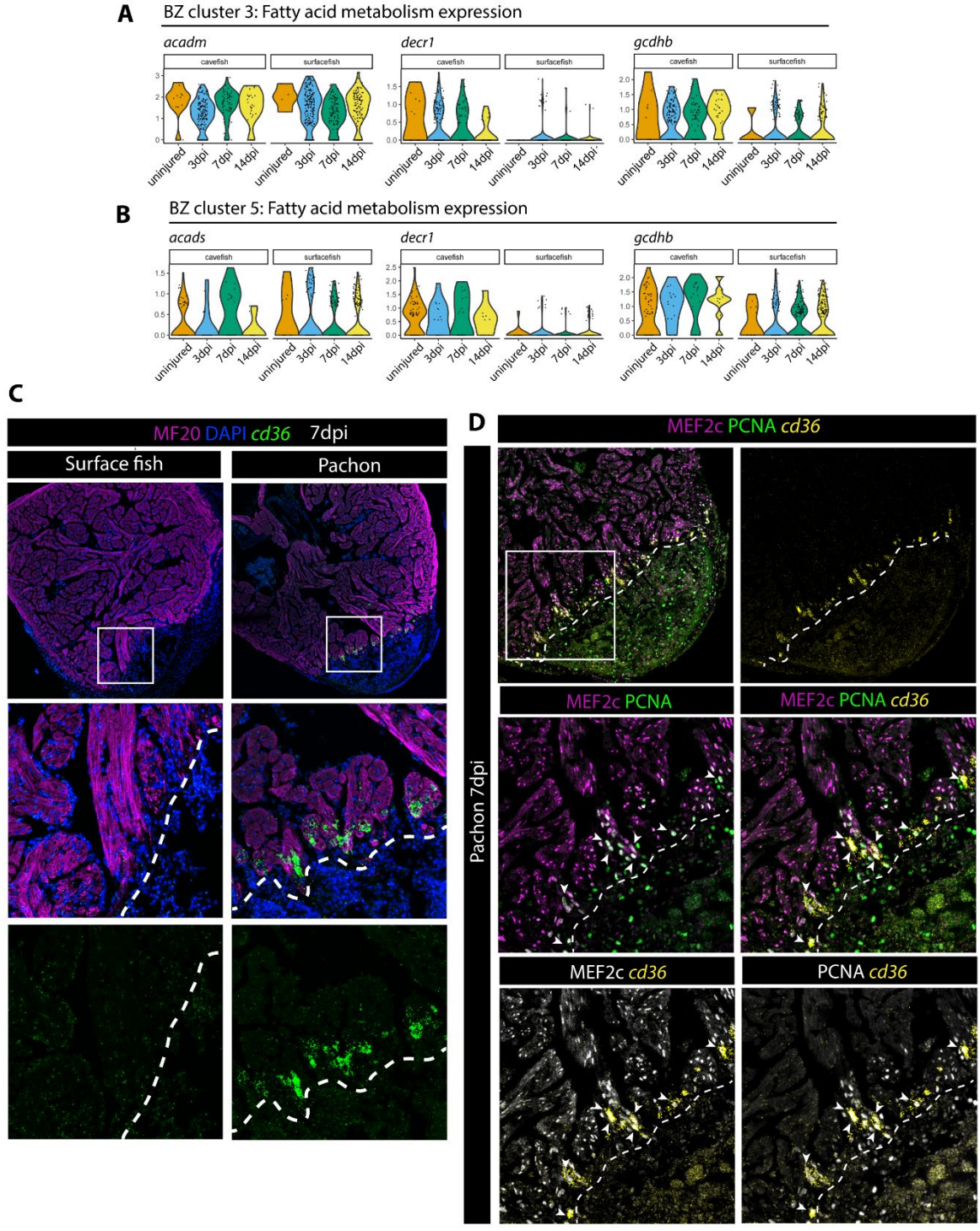


Figure 5.4 Upregulation of *cd36*, a fatty acid transporter, in the proliferating cardiomyocytes in Pachón.

(A-B) *scRNAseq: Violin plot illustrating expression of selected genes associated with fatty acid metabolism in border zone cells over time, cluster 3* ***(A)****, cluster 5* ***(B)****. Each gene is significantly differentially expressed between Pachón and surface fish border zone cardiomyocytes in at least one timepoint after injury (adj Pval <0.05). MAST differential expression test.* ***(C)*** *Strongly increased expression of cd36 around the wound border in Pachón at 7 days after injury. Little to no expression in surface fish. MF20 (magenta) labels myocardium, cd36 (green). Dashed line indicates wound border.*

(D) *Increased expression of cd36 localises to the proliferating cardiomyocytes (mef2+/PCNA+ cells) at the wound border (arrows). MF20 (magenta) labels myocardium, cd36 (yellow). Dashed line indicates wound border.*

5.2.4 Metabolomics indicates metabolic inflexibility in the Pachón heart after injury

Hypothesis & expected findings

Analysis of RNA expression has suggested a metabolic reprogramming in *Astyanax* border zone cardiomyocytes, alongside the suggestion of differential activity of several metabolic pathways between surface fish and Pachón border zone cardiomyocytes. To confirm and validate if these transcriptional differences led to altered metabolic pathway activity between fish, metabolomics was performed. It was expected that surface fish would have raised levels of glycolysis metabolites after injury, which would also be increased in comparison with Pachón. It was also expected metabolomics to show fatty acid metabolism metabolites raised in Pachón compared to surface fish ventricles, thus validating the increased fatty acid utilisation in Pachón. Overall, it was predicted the metabolomics would determine the metabolic fingerprint underlying the difference in regeneration between fish.

Hypothesis: Metabolomics will validate the metabolic transcriptional differences that are observed after injury, and between fish. It will also provide insights into the metabolic fingerprint required for myocardial regeneration.

Results

In order to confirm these differences in metabolic gene expression and to identify the overall metabolic fingerprint underlying the difference in regeneration between fish, metabolomics analysis was performed on uninjured and 7dpi ventricles (Fig 5.5A). Interestingly, uninjured

and injured Pachón ventricles clustered closely in the principal component analysis (PCA), indicating the Pachón do not change their metabolism to a high degree in response to injury (Fig 5.5B). In confirmation of this, only two metabolites were found to be significantly changing between the injured and uninjured setting in the Pachón (Fig 5.5D). These two metabolites were an unannotated metabolite and acetyl carnitine. This lack of significantly changing metabolites suggests a metabolic inflexibility in the Pachón heart after injury. In contrast, surface fish uninjured and injured ventricles clustered separately in the PCA plot with multiple metabolites significantly changed, suggesting the surface fish change their metabolism in response to injury (Fig 5.5C). Furthermore, significant differences in metabolism were observed between surface fish and Pachón fish with multiple metabolites significantly changed at both uninjured and 7dpi settings (Fig 5.5E, F).

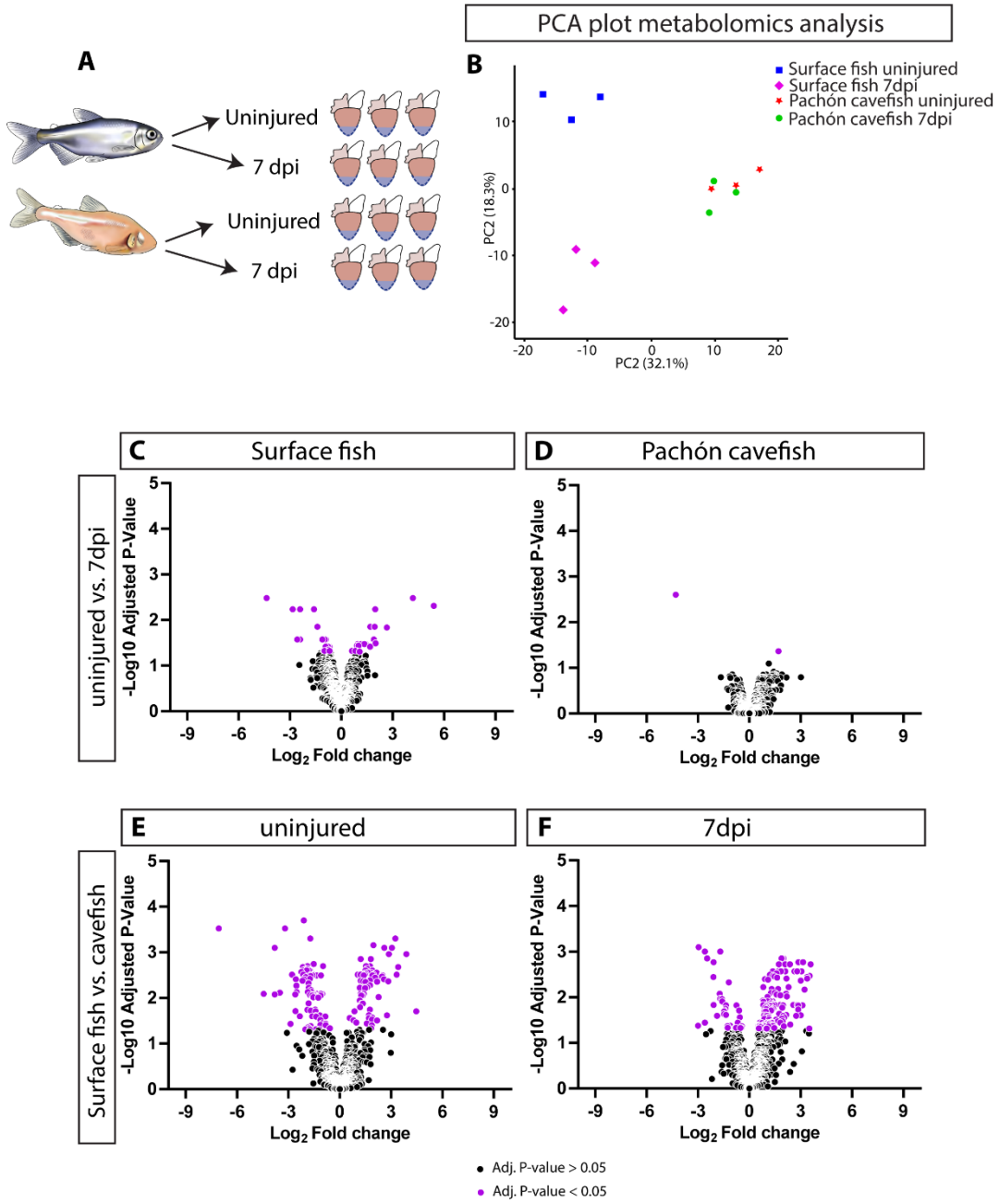


Figure 5.5 Metabolomics reveals a metabolic inflexibility in Pachón hearts after injury.
(A) *Schematic of experimental set up – 3 individual ventricles per fish per time point.* ***(B)*** *PCA plot of surface fish and Pachón uninjured and 7dpi samples. PCA shows that surface fish samples are different from Pachón samples both before and after injury. In contrast, there is not much difference between Pachón uninjured and 7dpi samples.* ***(C&D)*** *Volcano plot comparing metabolite levels between uninjured and 7dpi per fish. Significantly different metabolites are shown in magenta, with only 2 metabolites significantly different in Pachón. N=3, unpaired T-test* ***(E&F)*** *These Volcano plots directly compare surface fish with Pachón at the different time points. Many metabolites are differentially present between the two fish, both in uninjured hearts and at 7dpi n=3, unpaired t-test with Benjimini Hochberg correction.*

Notably, metabolites from the TCA cycle had an overall increased fold change in surface fish compared to Pachón (Fig 5.6A). TCA metabolites, citrate, cis-aconitate and malate, were all significantly higher in the uninjured surface fish hearts versus Pachón uninjured hearts, while isocitrate and 2-oxoglutarate were significantly higher in the 7dpi surface fish hearts versus Pachón 7dpi hearts (Fig 5.6B). Interestingly, the fold change between fish is highest in uninjured hearts, with the difference between morphotypes decreasing after injury (Fig 5.6A).

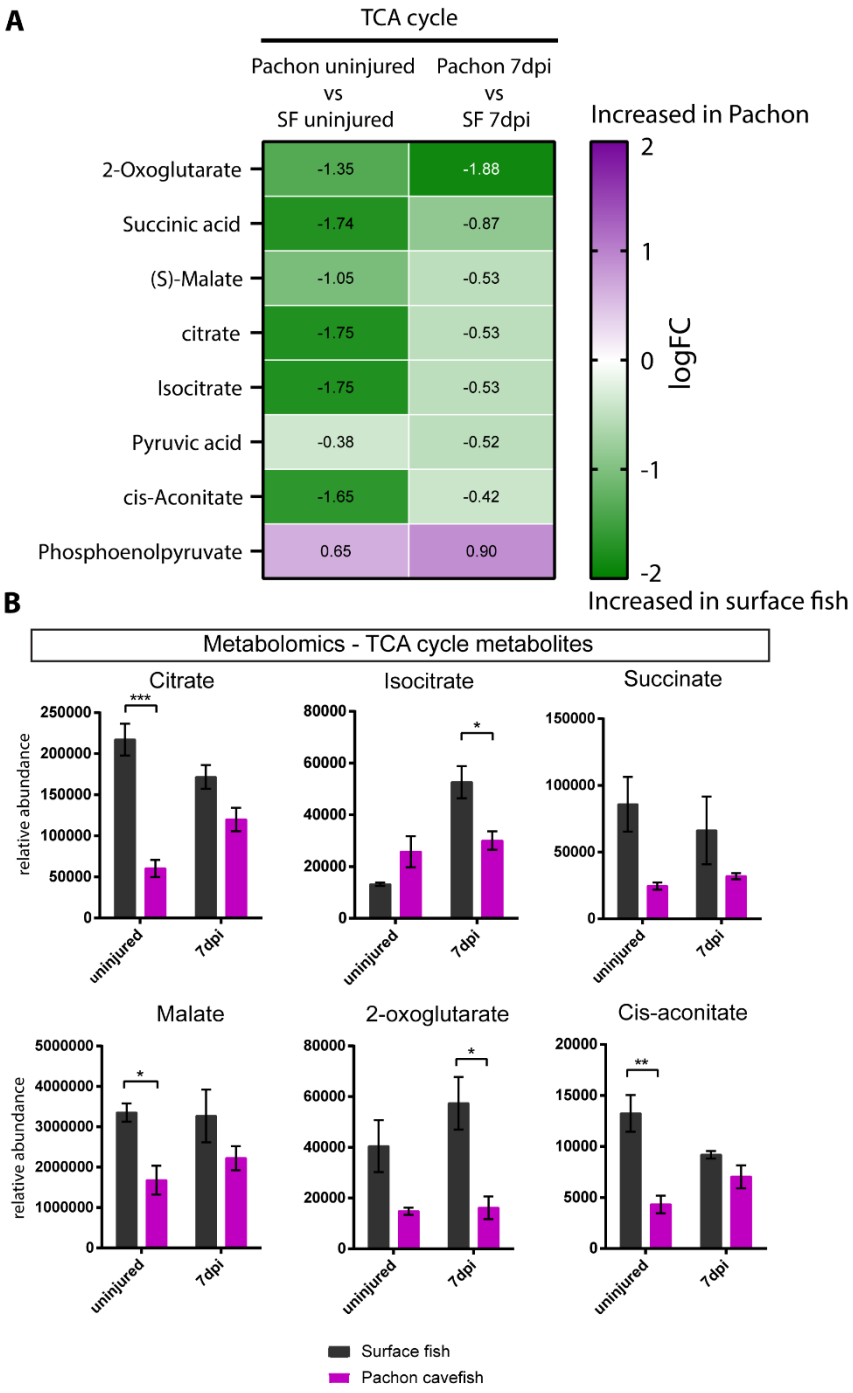


Figure 5.6 Metabolomics analysis shows increased abundance of TCA cycle metabolites in surface fish.

(A) *Heatmap illustrating the log fold changes of TCA metabolites between surface fish and Pachón in uninjured and 7dpi hearts. Positive fold change indicates increased in Pachón. Negative fold change indicates increased in surface fish. logFC value in each cell.* ***(B)*** *Relative abundance of TCA cycle metabolites in surface fish compared to Pachón. Surface fish, black. Pachón, magenta. n=3, unpaired t-test with Benjimini Hochberg correction. All data shown as mean +/- SEM. adj p<0.05 (*), adj p<0.01 (**), adj p<0.001 (***).*

In addition, metabolites of lipid metabolism were more abundant in Pachón hearts compared to their surface fish counterparts at 7dpi (Fig 5.7A). This is shown by the top 15 detected lipid metabolites based on their fold change being more abundant in Pachón compared to surface fish at 7dpi (Fig 5.7A). Notably, this included oleic acid, one of the two main fatty acid substrates used in fatty acid metabolism (Fig 5.7B) (*257*). Whilst the difference is not significant, likely due to the small sample size, oleic acid abundance increases after injury in the Pachón, while no change in surface fish.

Many of the lipid metabolites that are different between fish at 7dpi are from α-linolenic acid metabolism (omega-3) (Fig 5.7A, C). This is illustrated by the pathway activity level score (PALS) indicting α-linolenic acid metabolism as one of the top5 pathways significantly different between surface fish and Pachón at 7dpi (Fig 5.7C). These metabolites were typically reduced in surface fish after injury but remained higher in Pachón (Fig 5.7D).

Overall, these differences in lipid metabolites add to the idea that Pachón fish preferentially utilise fatty acid metabolism.

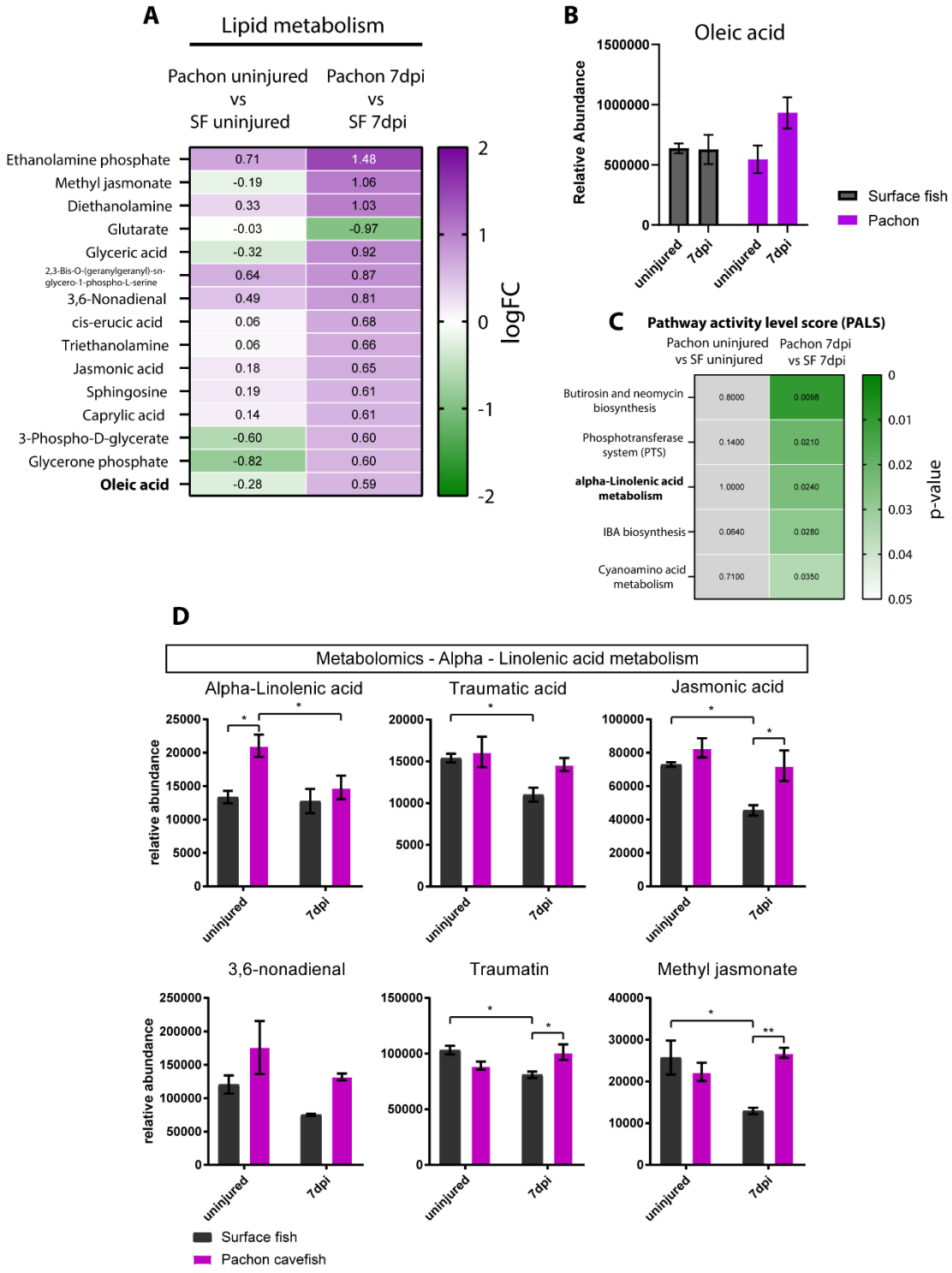


Figure 5.7 Metabolomics analysis shows increased abundance of lipid metabolites in Pachón versus surface fish.

(A) *Heatmap illustrating the log fold changes between fish of the top15 detected lipid metabolites with the highest fold changes (both positive and negative) between fish at 7dpi. Positive fold change (magenta) indicates increased in Pachón. Negative fold change (green) indicates increased in surface fish. logFC value in each cell.* ***(B)*** *Relative abundance of Oleic acid in surface fish and Pachón. Surface fish, black. Pachón, magenta. n=3. Data shown as mean +/- SEM.* ***(C)*** *Top5 significantly different metabolic pathways between surface fish and Pachón at 7dpi as calculated by the Pathway activity*

level score (PALS). Heatmap coloured by p-value, indicating degree of significance. P-value displayed in each cell. ***(D)*** *Relative abundance of alpha linolenic acid metabolites in surface fish compared to Pachón. Surface fish, black. Pachón, magenta. n=3, unpaired t-test with Benjimini Hochberg correction. All data shown as mean +/- SEM. Adj p<0.05 (*), p<0.01 (**).*

5.2.5 Pachón insulin receptor mutation does not negatively impact on regeneration in zebrafish

Hypothesis & expected findings

The *Astyanax* cavefish possess a mutation in their insulin receptor, which confers a level of insulin resistance. Therefore, due to the nature of the *insra* mutation, the P211L mutant zebrafish were expected to display a more Pachón-like phenotype after cardiac injury with increased scar size and impaired cardiomyocyte proliferation.

Hypothesis: Cavefish insulin receptor mutation in the regenerating zebrafish impairs cardiomyocyte proliferation and cardiac regeneration.

Results

Insulin signalling is a major pathway critical for controlling energy function, such as glucose and lipid metabolism (*258*). Interestingly, Riddle *et al.* have shown the Pachón cavefish are hyperglycaemic compared to surface fish, which is owed in part to a mutation in the insulin receptor, which confers a level of insulin resistance in Pachón (*144*). As part of this work the cavefish mutation (P211L) was recreated in the regenerating zebrafish. The insulin receptor mutation is a potential upstream factor of the glucose and fatty acid metabolic differences that occur during cardiomyocyte proliferation in the *Astyanax*. As such, its role in cardiomyocyte proliferation and heart regeneration was investigated by utilising the P211L mutant zebrafish.

In surface fish and Pachón the *insra* gene is expressed at similar levels before and after injury, while RNAscope also showed no wound border localisation at 7dpi and expression was more specific to areas associated with the endocardium, as well as being expressed in cells of the wound (Fig 5.8A). Surprisingly, the P211L mutant zebrafish had enhanced regeneration as shown by reduced scar size versus wild type fish by 15dpi (Fig 5.8B, C). Furthermore, the P211L mutants had no difference in myocardial proliferation compared to wild type controls at 7dpi that could account for this difference, suggesting the enhanced regeneration occurs through another cell type (Fig 5.8D, E). Ultimately, this phenotype suggests that the cavefish *insra* mutation is not a key factor in the contrasting regenerative capacities between surface fish and Pachón.

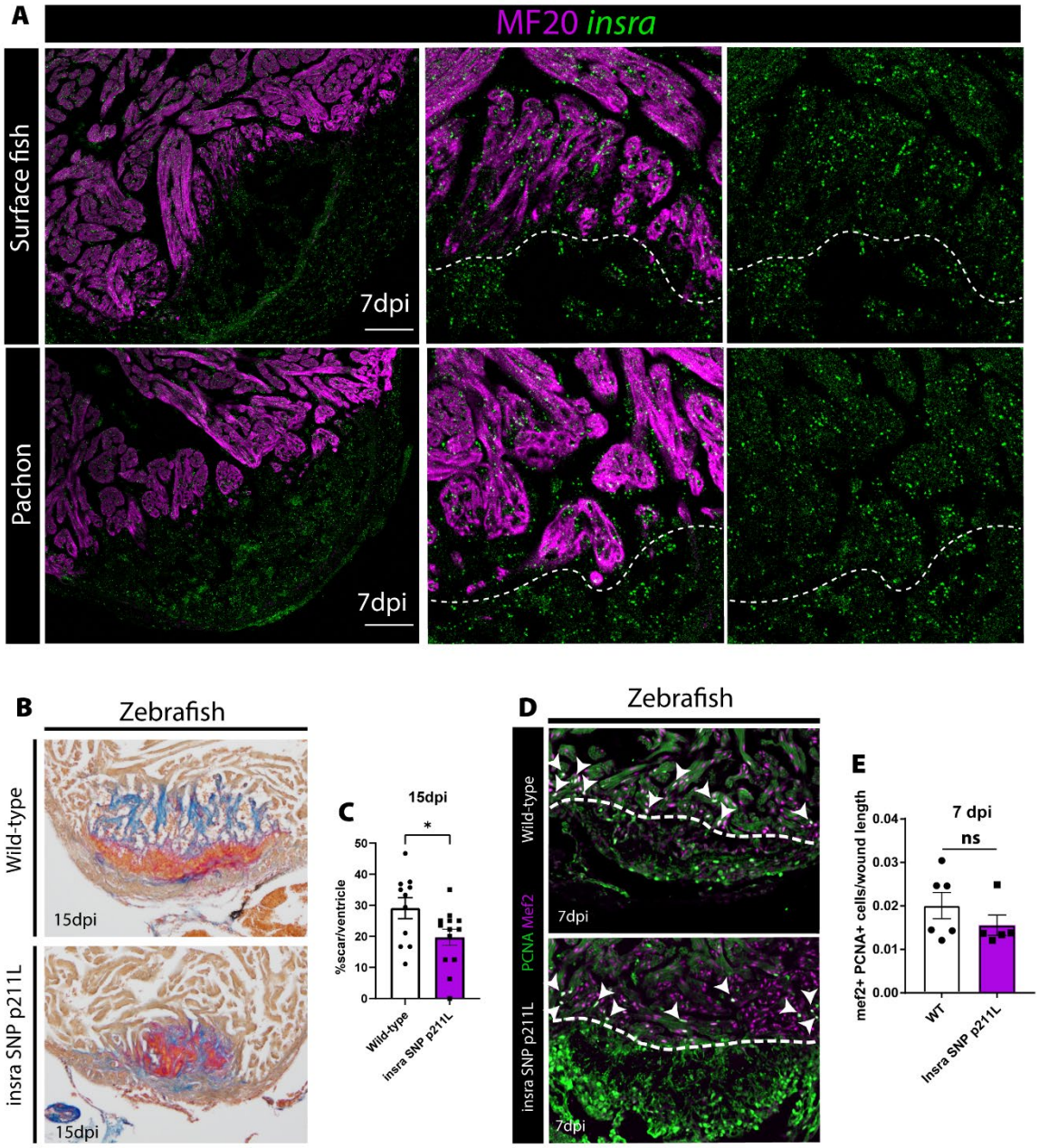


Figure 5.8 Zebrafish with the Pachón insulin receptor mutation have enhanced regeneration.

(A) *RNAscope in situ hybridisation of insra at 7 days after cryoinjury in Pachón and surface fish. MF20 (magenta) labels myocardium, insra (green). Dashed line indicates wound border.* ***(B)*** *AFOG staining of wild-type and insra P211L mutant zebrafish ventricles at 15 days after cryoinjury.* ***(C)*** *Graph showing reduced scar size in insra SNP P211L fish compared to wild-type fish.* ***(D)*** *IHC showing myocardial proliferation at the wound border in WT and insra mutant fish at 7dpi. PCNA, proliferation marker (green). Mef2, nuclear cardiomyocyte marker (magenta).* ***(E)*** *No difference in the number of mef2+/PCNA positive cells around the wound between WT and insra P211L fish. Dashed line indicates wound border. CM proliferation index: mef2+/PCNA positive cells normalised by wound length. n= ≥5. Unpaired t-test.*

5.3 Discussion

This chapter aimed to build on the work in the previous chapters, by investigating the metabolic response after injury in the *Astyanax*. The work sought to identify the overall metabolic fingerprint in border zone cardiomyocytes in both Pachón and surface fish, as well as validate the specific metabolic differences that may contribute to the contrasting cardiomyocyte proliferation profiles.

Based on mRNA expression, the surface fish proliferating myocardial border zone upregulated glucose uptake and anaerobic glycolysis. While in Pachón, glucose uptake is limited and the raised glycolysis in the Pachón border zone in response to injury is notably reduced compared to surface fish. In contrast, gene expression and metabolomics revealed metabolic inflexibility in the Pachón heart after injury, and a potential preference for fatty acid metabolism with increased fatty acid uptake, particularly in the border zone cardiomyocytes. These are characteristics of the diabetic heart. However, the cavefish insulin receptor mutation (P211L) does not negatively impact on zebrafish heart regeneration and surprisingly enhances regeneration. Lastly, TCA metabolite levels were raised in the surface fish heart compared to Pachón, suggesting increased TCA cycle activity in the surface fish heart. These differences in metabolic characteristics are potential determinants in the contrasting cardiomyocyte proliferation profiles and regeneration capacities.

5.3.1 Differences in glycolysis, particularly *glut1a*, could underlie cardiomyocytes proliferation profile in Pachón

The expression data throughout this chapter indicates border zone cardiomyocytes in surface fish upregulate expression of genes related to glucose uptake and glycolysis - coinciding with

the peak in proliferation. This suggests proliferating cardiomyocytes during regeneration in surface fish undergo a metabolic shift to glycolysis. While in Pachón, a similar glycolytic shift in border zone cardiomyocytes is also observed in terms of gene expression, but altogether at a lower level with some fundamental differences in key genes of glucose metabolism. Such a metabolic shift to anaerobic glycolysis has also been described in the zebrafish border zone cardiomyocytes and is necessary for the initiation of proliferation to the point that inhibition of glycolysis impairs proliferation (*63, 64*). As inhibition of glycolysis impairs proliferation during regeneration in the zebrafish, the low level of glycolytic reprogramming in the Pachón could be causative of the reduced cardiomyocyte expansion (*63, 64*).

Several notable differences of key genes in glucose uptake/glycolysis were observed between Pachón and surface fish. This included the striking differential expression of the glucose transporter, *glut1a*, in the border zone between Pachón and surface fish, suggesting increased glucose uptake in the surface fish. The absence of *glut1a* expression in the border zone could possibly indicate Pachón proliferating cardiomyocytes are not taking up the necessary glucose required for the glycolytic reprogramming that is important to during proliferation. Interestingly, overexpression of Glut1 in the neonatal mouse increases mitotic activity in a subset of cardiomyocytes, leading to enhanced cardiomyocyte proliferation and regeneration - highlighting it as having a role in cardiomyocyte proliferation (*259*).

In addition to *glut1a*, the differential expression relating to the *pdk2a* and *pdk4* genes is of particular importance as these genes are key to diverting pyruvate away from the TCA cycle and promoting anaerobic glycolysis rather than glucose oxidation (*260-262*). Therefore, the expression of these genes is fundamental for maintaining the low oxidative state that has been proposed for cardiomyocyte proliferation (*64*). Importantly, inhibition of Pdk activity in

zebrafish leads to a decrease in cardiomyocyte proliferation in the border zone following injury (*64*). As such, the upregulation in surface fish versus the Pachón suggests an increased level of anaerobic glycolysis in surface fish, which could be factor in the contrasting proliferation profiles.

Gluconeogenesis mainly generates glucose through the breakdown of lactate, glucogenic amino acids and odd-chain fatty acids. Therefore, the suggestion of increased gluconeogenesis via the raised expression of *fbp2* in Pachón is possibly to compensate for the reduced glucose uptake caused by the absence or low expression of glucose transporters and its insulin resistance phenotype. Alternatively, the increased gluconeogenesis could be generating metabolites required for glycogen storage in Pachón. However, the proliferating myocardial border zone in Pachón expressed less *fbp2* compared to the rest of the heart, which suggests that Pachón border zone cardiomyocytes reduced gluconeogenesis and glucose synthesis. Therefore, alongside the reduced glucose uptake, reduced gluconeogenesis in the border zone potentially supports the suggestion of insufficient levels of cellular glucose in Pachón proliferating cardiomyocytes.

5.3.2 Increased Fatty acid metabolism but reduced TCA cycle in the Pachón heart

Increased expression of genes related to fatty acid oxidation in Pachón versus the surface fish, in combination with the impressive upregulation and localisation of the fatty acid transporter, *cd36*, points to increased fatty acid metabolism in Pachón. This is further supported by the metabolomics, which suggests a general higher abundance of lipid metabolites in Pachón, specifically the major fatty acid substrate, oleic acid, and metabolites in α-linolenic acid metabolism. This matches the cavefish physiology, which displays increased fat storage and body fat, alongside a fatty liver, which suggests a preference for fatty acids in metabolism

(*145, 243*). Collectively, it appears the Pachón has a higher preference for fatty acids, perhaps as an alternative for the reduced glucose metabolism.

The preference for fatty acid metabolism in the Pachón draws similarities with the adult mammalian heart, which uses fatty acid-oxidative phosphorylation as its main source of energy (*251*). The utilisation of fatty acids is closely linked to cardiomyocyte proliferation and heart regeneration, with the mammalian postnatal metabolic shift from glucose to fatty acids coinciding with cell cycle arrest of cardiomyocytes and loss of regeneration (*25, 65, 235, 251*). Specifically, the increasing fatty acid metabolism that occurs in the postnatal period drives cell cycle arrest and polyploidisation alongside maturation and hypertrophic growth of cardiomyocytes (*235, 239*). In further support of this, fatty acid supplement drives maturation and hypertrophic growth of human pluripotent stem cell-derived cardiomyocytes (hPSC-CMs) (*240*). Notably, *cd36* expression can be used to selectively identify matured hPSC-CMs, which perhaps suggest the cd36 positive proliferating cardiomyocytes in Pachón are more mature cardiomyocytes (*263*). Ultimately, reducing fatty acid utilisation in cardiomyocytes by altering diet or genetic modification is capable of promoting cardiomyocyte proliferation after injury in mice (*235*). As such, the possible higher fatty acid utilisation in Pachón could be driving cardiomyocyte cell cycle arrest alongside maturation and hypertrophic growth, and thus, be a causative factor in the limited cardiomyocyte expansion.

The negative role of fatty acid utilisation on cardiomyocyte proliferation and its ability to promote cell cycle arrest with polyploidy during the postnatal period has been attributed to increased levels of mitochondrial oxidative phosphorylation that occurs with the increased fatty-acid beta-oxidation (*65, 235*). It's been proposed that the raised levels of mitochondrial oxidative phosphorylation cause oxidative stress via increased ROS production, which induces

cell cycle arrest through oxidative DNA damage and the DDR pathway (*65*). As such, maintaining a low oxidative environment is believed to be important to proliferation, which is achieved in zebrafish as part of their metabolic reprogramming where they reduce expression of mitochondrial genes (*63*). However, despite the apparent increase in fatty acid utilisation in Pachón, there is no evidence of an associated increase in oxidative metabolism within the scRNAseq analysis. In fact, a general increase in TCA metabolite abundance in surface fish suggests oxidative metabolism is actually reduced in the Pachón compared to surface fish.

This suggestion of reduced oxidative metabolism despite a potential increase in fatty acid uptake combined with lower levels of glucose metabolism, raises the question whether this is an energy saving feature that is common in cavefish physiology. Could a lack of energy supply in the form of ATP be responsible the defective proliferation? Further exploration of mitochondrial oxidative phosphorylation and mitochondrial biology is needed.

5.3.3 Is the lack of cardiomyocyte expansion in the Pachón a consequence of its diabetic phenotype?

Metabolomics revealed minimal differences between uninjured and 7dpi hearts in the Pachón, suggesting a metabolic inflexibility, which is interestingly a feature of the diabetic heart (*264, 265*). The suggestion of a diabetic-like phenotype in the cavefish heart is becoming a recurring theme of their overall physiology, with various studies observing a number of diabetic-like phenotypes (*144*). The suggestion that Pachón preferentially utilise fatty acids, is consistent with the mammalian diabetic heart, which undergoes a metabolic remodelling, namely upregulating fatty acid metabolism (*266-268*). Chronically increased fatty acid metabolism is thought to contribute to ventricular dysfunction in the diabetic heart by

increased oxidative stress from increased activity of oxidative pathways, or through the toxic effects caused by accumulated lipid species – lipotoxic cardiomyopathy (*269-272*). Interestingly, CD36 is a necessary factor for the development of lipotoxic cardiomyopathy in a mouse model of the diabetic heart, and notably, deficiency of CD36 can reduce myocyte lipid accumulation and cardiac dysfunction (*273*). As such, the increased expression of *cd36* in Pachón proliferating cardiomyocytes in the border zone, could be leading to lipotoxicity from increased lipid accumulation, which is ultimately impairing complete cardiomyocyte proliferation. This metabolic remodelling in the diabetic heart has also been associated with impaired cardiac function post-ischemia and poorer long-term prognosis following MI (*274-276*). In light of this, could the metabolic differences that underlie defective proliferation and the lack of regeneration in Pachón be a consequence of the diabetic phenotype?

The idea that cavefish are diabetic is mostly driven by the observation that cavefish are hyperglycaemic and display a level of insulin resistance compared to their surface fish counterparts (*144*). These observations are closely associated with a mutation in the insulin receptor, which due to the critical role of insulin signalling in regulating glucose and lipid metabolism, is a potential upstream determinant of the cardiac metabolic differences between fish (*144, 258*). To this end, the effect of the P211L *insra* mutation on proliferation and regeneration was investigated in the zebrafish.

Due to the nature of the *insra* mutation, the P211L mutant zebrafish were expected to display a more Pachón-like phenotype after injury with increased scar size. Surprisingly, the mutation had the opposite effect in the context of the zebrafish, resulting in enhanced regeneration. As this is a mutation that causes a single amino acid change that confers only a reduction in insulin binding it seems to suggest that some level of insulin insensitivity in the zebrafish is

beneficial for cardiac regeneration. Due to the similar levels of cardiomyocyte proliferation it is likely this moderate level of enhanced regeneration occurs through the function of another cell type. Expression of the *insra* receptor appears to be localised in the endocardial area and within the wound in the *Astyanax*, therefore the mutation could potentially be impacting on the function of these cells during regeneration.

Ultimately, this phenotype in the mutant zebrafish suggests the P211L mutation in the cavefish is not a factor in the proliferation profile of Pachón cardiomyocytes or their inability to regenerate. However, it's important not to rule out the diabetic-like phenotype as causative factor in Pachóns proliferation profile as the hyperglycaemia seen in the cavefish is not a monogenic feature, with other factors and pathways likely contributing to this diabetic-like aspect of the cavefish (*144*).

5.3.4 Limitations

A combination of scRNAseq and RNAscope has confirmed large transcriptional differences relating to several metabolic pathways in border zone cardiomyocytes, but questions remain to what degree RNA levels are indictive of protein levels or even metabolic pathway activity. In particular, the inference that glucose uptake and glycolysis is increased in surface fish compared to Pachón is made solely on mRNA levels. Additional experiments utilising antibodies to explore protein localisation or specifically measuring metabolic pathway activity will provide more confidence that the differentially expressed metabolic pathways are functionally different between fish.

In an attempt to determine metabolic pathway activity and confirm transcriptional differences, metabolomics was performed. Whilst metabolomics was able to suggest several

metabolic pathway differences, many of the differences were small and showed no support of the previous transcriptional evidence suggesting increased glycolysis in surface fish border zone cardiomyocytes. This is likely due to use of whole ventricles for the metabolomics and the border zone cardiomyocytes only representing a very small percentage of cells within the injured heart. Therefore, any metabolic pathway alterations in border zone cardiomyocytes may be become "diluted" amongst all the other cells, resulting in only very small or completely masked changes in metabolite abundance. In addition, metabolomics only provides a "snapshot" of metabolite abundance at a single point in time. Therefore, when metabolic pathways are interconnected and share metabolites, such as glycolysis and gluconeogenesis, inference of metabolic pathway activity is difficult. In this case, measurement of metabolic pathway flux would be a more accurate measure of pathway activity.

Lastly, much of the metabolic data within this chapter is correlative - mostly correlates metabolic differences with the lack of cardiomyocyte expansion in Pachón. Functional analysis, such as genetic knockouts or gain of function, is required to confirm the impact of these metabolic differences on *Astyanax* myocardial regeneration.

5.3.5 Conclusion

This chapter shows a number of metabolic differences between Pachón cavefish and surface fish that both temporally and spatially coincide with the contrasting cardiomyocyte proliferation profiles. In general, genes in glycolysis, glucose uptake and pyruvate metabolism are upregulated in surface fish border zone cardiomyocytes compared to Pachón. While gene expression and metabolomics suggests a preference for fatty acid metabolism in Pachón but surprisingly no associated increase in oxidative phosphorylation.

A potential upstream controller of these differences in metabolism, a mutation in the cavefish insulin receptor, has no obvious role cardiomyocyte proliferation and regeneration in the context of the zebrafish heart.

Overall, these metabolic differences coincide with the contrasting proliferation profiles in the *Astyanax* and could be key determinants in achieving complete cardiomyocyte expansion and regeneration.

Chapter 6
General Discussion

6.1 Main findings

The contrasting regenerative capacities of the Pachón cavefish and surface fish morphotypes within the *Astyanax mexicanus* species make it a unique model to investigate heart regeneration. The model sets itself apart from other comparative strategies by enabling the ability to compare adult fish-like regeneration with human-like scarring all within the same species. Importantly, it forgoes certain limitations seen in other comparative models such as circumventing background variations, which include interspecies and developmental differences. Altogether, the *Astyanax* model offers a unique opportunity to decipher new mechanisms/genes behind natural heart regeneration.

One of the defining features between the contrasting regenerative capacities is lack of cardiomyocyte expansion in the Pachón heart after injury. Specifically, the Pachón is capable of initiating proliferation but does not complete the cell cycle, resulting in no discernible cardiomyocyte expansion, which is a likely driver behind the contrasting regenerative capacities.

Aims:

- This work first set out to use the advantages of the *Astyanax* with comparative bulk transcriptomics to unbiasedly detect novel genes that are generally key to cardiac

regeneration and to functionally investigate their role in regeneration. Therefore, validating the ability of the *Astyanax* as a model to enhance our understanding of natural regeneration.

- The second aim of the work was more targeted and specifically focused on cardiomyocyte proliferation. Here, the work aimed to investigate the fate of the impaired proliferating cardiomyocytes seen in the Pachón heart and determine the mechanisms that underlie this profile using singe cell transcriptomics.

Main findings:

- Comparison of *Astyanax* morphotypes after injury identified *lrrc10*, which was established as a gene required for cardiac regeneration.
- *Astyanax* heart possesses myocardial heterogeneity and after injury, a myocardial border zone that displays characteristics consistent with reduced maturity, dedifferentiation, cell proliferation and metabolic reprogramming.
- Single cell transcriptional profiling suggests cell cycle arrest and polyploidisation of Pachón proliferating cardiomyocytes are responsible for the reduced cardiomyocyte expansion.
- Increased glucose uptake and glycolytic reprogramming in the surface fish myocardial border zone compared to Pachón.
- Increased fatty acid uptake and utilisation but reduced oxidative metabolism in Pachón border zone cardiomyocytes versus surface fish.
- Diabetic characteristics in the Pachón heart, but the *insra* P211L mutation, responsible for insulin resistance in Pachón, does not have a negative impact cardiac regeneration.

6.1.1 Lrrc10 is required for heart regeneration

The bulk RNAseq analysis highlighted many differences between Pachón and surface fish hearts after injury. Particularly notable was a cohort of genes with significant differential kinetics over time after injury. Many of these genes had no known role in heart regeneration and as such, were potential candidates with a novel role in heart regeneration. Selection and investigation of candidate genes led to the identification one gene, *lrrc10*, with a significant role in heart regeneration.

CRISPR-mediated knockout of *lrrc10* in the regenerating zebrafish resulted in impaired regeneration but with normal levels of cardiomyocyte proliferation, ultimately displaying a Pachón-like phenotype after injury. Due to the specificity of *lrrc10* to the myocardium and its localisation in the border zone after injury, it is likely that reduction in regeneration is caused by impaired cardiomyocyte function, particularly in terms of the proliferating cardiomyocytes. However, further work is needed to determine how much the cardiomyocyte proliferation defect seen in the lrrc10 mutant matches the Pachón cardiomyocyte profile and the mechanism by which lrrc10 loss impairs normal cardiomyocyte function/proliferation.

Previous studies have shown localization of LRRC10 to the dyad region of adult cardiomyocytes and association with L-type Ca2+ channels (*195*). Thus, putting it at the hub of calcium cycling, excitation-contraction coupling and mechanosensing. Moreover, knockout of *Lrrc10* in mice effects voltage-dependent gating of Ca2+ channels as well as resulting in transcriptional changes relating to the actin cytoskeleton, focal adhesion and causing contractile dysfunction (*191, 193, 195*). Significantly, mechanosensing of changing mechanical forces can result in cardiomyocyte cellular responses such as differentiation or maturation (*277*). Actin cytoskeleton organisation is linked to the differentiation status of cardiomyocytes

and its reorganisation occurs during the dedifferentiation/re-differentiation process during proliferation (*33, 34, 38, 43, 224, 225*). As such, one possible suggestion is that *lrrc10* loss in zebrafish is altering cardiomyocyte maturation and interfering with the dedifferentiation, migration and re-differentiation/reintegration sequence of events necessary for regeneration.

As *lrrc10* expression is reduced in Pachón, adverse maturation could in part be responsible for the lack of cardiomyocyte expansion in the Pachón. Perhaps in support of this, Pachón border zone cardiomyocytes, particularly from the scRNAseq analysis have increased maturity in terms of low transcriptional diversity relative to surface fish. This raises the possibility that the dedifferentiation/re-differentiation or mitotic process in Pachón proliferating cardiomyocytes is impaired and caused in part by downregulation of *lrrc10*.

Overall, the work in chapter 3 demonstrates the identification of *lrrc10* using the *Astyanax* model and the requirement of its function for normal regeneration. Importantly, this work was also significant for validating the ability of *Astyanax* to detect novel genes or mechanisms and thus, introducing the *Astyanax* as a model capable of enhancing our understanding of regeneration.

6.1.2 *Astyanax* myocardial border zone displays characteristics consistent with reduced maturity, dedifferentiation, cell proliferation and metabolic reprogramming

Whilst the bulk RNAseq experiment on whole ventricles was capable of detecting differences that are key to regeneration, it was somewhat limited in that it is unable to provide cell type or cell subtype context to the transcriptional differences observed. In addition, due to the

complex cellular composition of the heart after injury, transcriptional differences within small but significant cell populations can be masked. This is potentially the case with the cycling cardiomyocytes in the border zone, which are a relatively small subset within the fish heart. To this end, single cell transcriptomics was utilised for a targeted analysis of the cells of interest – the cycling cardiomyocytes in the border zone. Specifically, this analysis aimed to begin piecing together the fate of the Pachón cycling cardiomyocytes and the potential pathways that underpin the opposing cardiomyocyte proliferation profiles.

Through analysis of the cardiomyocytes in the scRNAseq dataset, 8 transcriptionally distinct cardiomyocyte clusters were formed in both morphotypes. These clusters were transcriptionally consistent with cardiomyocyte subtypes previously reported in the zebrafish heart, leading to the annotation of clusters corresponding with trabecular, cortical and primordial layers. The presence of transcriptionally distinct clusters of these individual layers, supports the notion of cardiomyocyte heterogeneity within the fish heart.

Three of these cardiomyocyte clusters also included the predicted border zone cardiomyocytes, which differentially regulated genes that have been previously reported as upregulated or downregulated in the border zone in either mouse or zebrafish. These 3 clusters, were separated by gene expression correlating to phases of the cell cycle, as well as expression of genes related to the cytoskeleton and focal adhesion. Ultimately, the *Astyanax* border zone transcriptional profile was consistent with dedifferentiation, proliferation, migration and reintegration sequence of events that are necessary for regeneration (*33, 34, 38, 224, 225*). This occurred with the simultaneous reduction in maturity, as well as downregulation of mitochondrial based metabolism, which included downregulation of the TCA cycle, oxidative phosphorylation and fatty acid degradation. Taking on a less mature

phenotype as well as undergoing a metabolic reprogramming, particularly reducing oxidative metabolism are all necessary features of the zebrafish border zone (*33, 34, 37, 63, 78*). Altogether the *Astyanax* myocardial border zone in general matches the characteristics of the zebrafish border zone - perhaps an indication of why Pachón are capable of initiating proliferation despite ultimately lacking successful cardiomyocyte expansion.

6.1.3 Evidence of cell cycle arrest and polyploidisation of Pachón proliferating cardiomyocytes

While there are some general trends occurring in both surface fish and Pachón border zone cardiomyocytes, there are also significant differences, particularly relating to the cell cycle that may explain the fate of the cycling Pachón cardiomyocytes. Pachón border zone cardiomyocytes displayed enrichment of genes involved in the negative regulation of the cell cycle, while expressing low levels of S phase genes relative to surface fish. Despite these transcriptional differences in the cell cycle, the predicted border cardiomyocytes in Pachón still cluster together with the surface fish S phase cardiomyocytes, also indicating a large degree of similarity. These transcriptional differences in combination with the limited number of G2M cardiomyocytes in the Pachón border zone suggest potential cell cycle arrest in Pachón cardiomyocytes.

Interestingly, Pachón contained a notable proportion of S phase cluster (cluster 5) cardiomyocytes in the uninjured samples. Since no wound border is formed in uninjured hearts, this seemed to suggest that Pachón hearts at baseline contain a notable basal level of cardiomyocyte proliferation, which could be a feature of the Pachón heart to meet unique aspects of its physiology. It may also indicate a naturally higher capacity for cardiomyocytes to proliferate/enter S phase in the Pachón. A higher capacity for Pachón cardiomyocytes to

undergo proliferation could be partly responsible for their ability to initiate significant proliferation upon injury, despite their inability to regenerate their heart. Surprisingly, the proportion of S phase cardiomyocytes in Pachón did not increase after injury, which is in contrast with the initial staining for proliferation markers, PCNA and BrdU. It is not clear why this discrepancy, but one possible suggestion is that the S phase transcriptional profile in Pachón border zone cardiomyocytes is only very transient. Therefore, Pachón border zone cardiomyocytes transition rapidly from the S phase cluster to a cluster other than cluster 8 (G2M cluster). This leads to the low proportion and possibly contributes to the idea of cell cycle arrest. Alternatively, it is possible that Pachón border zone cardiomyocytes do not possess a transcriptional profile that is typically consistent with the S phase of the cell cycle, despite entering the S phase.

Ultimately, in the absence of cell death and evidence of a gene/cellular signature consistent with cell cycle arrest, it was hypothesised that Pachón cardiomyocytes are becoming polyploid. In support of this, a similar process happens in the non-regenerative adult mammalian heart, where the low level of cardiomyocyte turnover that is induced after MI mostly results in polyploid cardiomyocytes and hypertrophic growth (*40, 41, 151*). This polyploidisation is also in evidence during the post-natal period where mammalian cardiomyocytes undergo cell cycle arrest forming polyploid cardiomyocytes (*69, 226, 278, 279*). This is accompanied by hypertrophic growth and maturation but with loss of proliferation and regeneration potential (*9, 25, 28, 277*). The maturation is also potentially matched in Pachón border zone cardiomyocytes, which display increased maturation relative to surface fish in terms of transcriptional diversity. Could the Pachón border zone cardiomyocytes becoming polyploid after injury?

To confirm polyploidisation, a targeted functional cell cycle analysis was attempted. Whilst significant technical limitations of this experiment remain, it seemed to suggest a greater proportion of S phase cardiomyocytes in terms of DNA content at 14dpi. This supports cell cycle arrest but not the typical polypoid (tetraploid - 4n) formation seen in adult cardiomyocytes – aneuploidy or copy number variations (CNVs). The concept of CNVs in Pachón cycling cardiomyocytes is interesting, but to date, it has not been reported in polyploid cardiomyocytes. However, CNVs occurs in alternative polyploid cell types, such as polyploid hepatocytes, which has been hypothesized to generate genetic diversity for adaptation of hepatocytes to adverse conditions (*234, 280*). While unlikely, it's interesting to consider a similar possibility in the Pachón border zone cardiomyocytes.

The possibility of increased DNA content in Pachón cardiomyocytes is significant, as polyploidy has been linked to reduced cardiomyocyte proliferation capacity and reduced heart regeneration potential across the animal kingdom (*70, 71, 247*). This view is supported by a study that reported the natural variation in heart regeneration across inbred mouse lines is in part dependant on the frequency of mononuclear diploid cardiomyocytes (*70*). This is further supported by impaired proliferation and regeneration in zebrafish with genetically induced cardiomyocyte polyploidisation (*71*).

The physiological and functional benefit of cardiomyocyte polyploidisation is not completely understood. However, it's been speculated that polyploid cardiomyocytes have increased resistance to stress, and undergo polyploidisation with hypertrophic growth during the postnatal period due to the increased demands of the heart. In the healthy heart, this is potentially to cope with the large cardiac output, as well as, the increased blood pressure, ventricular pressure and cardiac wall stress that occurs with physiological heart growth, whilst

maintaining proper contractile function (*69, 281*). In addition, the onset of polyploidisation within the mammalian heart also occurs in tandem with changes in energy metabolism. This change in metabolism comes with an increase in oxidative stress and in turn genotoxic stress. As such, it's been speculated that the extra copy of chromosomes in polyploid is to mitigate for mutations (*69*). Therefore, the differences in metabolism observed between fish in this work are notable and discussed further below. This suggested enhanced resistance to stress raises the notion of polyploidisation in Pachón border zone cardiomyocytes as a mechanism to cope with the stress of cardiac injury and a way to maintain proper contractile function.

Ultimately, cell cycle arrest and polyploidisation of Pachón cardiomyocytes would account for the absence of cardiomyocyte expansion after injury, which could make the *Astyanax* a novel model in studying cardiomyocyte polyploidisation.

6.1.4 Increased fatty acid uptake and utilisation but reduced oxidative metabolism in Pachón border zone

One the major factors that has been associated with mammalian cardiomyocyte cell cycle arrest and polyploidisation has been changes in metabolism, namely the switch from anaerobic glycolysis to fatty acid-based oxidative metabolism that occurs concurrently with polyploidisation (*65, 69, 226, 235, 250, 251*). This is particularly significant as one of the major components in cavefish evolution is adaption of their metabolism to cave life (*144-146, 242, 243, 245*). This is made further significant by the differences in cardiac metabolism between surface fish and Pachón, that are observed within the bulk RNAseq and scRNAseq data sets, particularly in border zone cardiomyocytes.

Highly proliferative cardiomyocytes in the neonatal heart mainly use glucose via glycolysis as a source of energy (*251, 282*). However, in response to increased energy demands during the post-natal period, the heart switches to fatty acid beta-oxidation (*250, 251*). The switch to fatty acid utilisation promotes polyploidisation, maturation and hypertrophic growth (*235, 239, 240*). This matches the situation in Pachón border zone cardiomyocytes, where the cell cycle arrest, raised maturation and increased growth indicated by the scRNAseq coincides with increased fatty acid uptake and utilisation relative to surface fish, as well as raised levels of lipid metabolites.

This not only helps to support the notion of Pachón polyploidisation, but perhaps is an indication that increased fatty acid metabolism in Pachón cardiomyocytes is a determinant of the suggested polyploidisation. Furthermore, inhibition of fatty acid utilisation is capable of promoting cardiomyocyte proliferation in mice after injury (*235*). Drawing upon this, the reduced level of fatty acid utilisation in surface fish is a possible determinant of the successful cardiomyocyte proliferation seen over the Pachón.

The cell cycle arrest and polyploidisation caused by fatty acid metabolism within the mammalian heart has been attributed to mitochondrial oxidative phosphorylation, which is raised as a result of increased fatty acid substrate utilisation (*65, 235*). Despite the energy advantage, oxidative phosphorylation from fatty acid utilisation within the cardiomyocyte mitochondria produces elevated rates of ROS and in turn oxidative stress. This is thought to cause cell cycle arrest through activation of DNA-damage response pathway (*65, 235*). The need to maintain a low oxidative cellular environment during proliferation is also in evidence in the zebrafish border zone cardiomyocytes which lowers mitochondrial based metabolism, particularly oxidative phosphorylation (*63*). However, this is where the surface fish and

Pachón comparison sits in contrast. Despite an increase in fatty acid metabolism in Pachón, both TCA cycle activity and oxidative phosphorylation gene expression are increased in surface fish versus the Pachón. As such, it appears oxidative stress is not the mechanism that is causing possible cell cycle arrest in Pachón border zone cardiomyocytes.

As an alternative to catabolic functions, the reduced TCA cycle activity and metabolites in Pachón, could be suggestive of insufficient metabolic intermediates for anabolic processes that are necessary for sustaining proliferation. Additionally, TCA metabolites have been reported to have key roles as signal transducers in cardiomyocytes, and as such, Pachón could lack for key signalling metabolites needed to promote complete proliferation.

Overall, the suggestion of increased fatty acid utilisation in Pachón border zone cardiomyocytes is a potential factor driving the notion of cell cycle arrest, polyploidisation and maturation. However, this does not appear to be caused by raised oxidative stress from increased fatty acid dependant oxidative metabolism as this is noticeably lower in Pachón. Currently, further work is needed to determine whether increased fatty acid uptake and reduced mitochondrial based metabolism are key factors in the reduced cardiomyocyte expansion seen in Pachón.

6.2.5 Increased glucose uptake and glycolytic reprogramming in the surface fish myocardial border zone

As alluded to above, the increasing fatty acid utilisation and oxidative metabolism during the postnatal period, also occurs with decreasing levels of anaerobic glycolysis (*250, 251*). This coincides with cell cycle arrest and polyploidisation, indicating a role of glycolysis in maintaining cardiomyocyte proliferation (*25, 65, 235*). The significance of glycolysis in

proliferating cardiomyocytes is also indicated in the regenerating zebrafish, where the border zone cardiomyocytes upregulate anaerobic glycolysis alongside downregulation of oxidative phosphorylation (*63, 64*). Significantly, pharmacological inhibition of glycolysis in zebrafish impairs cardiomyocyte proliferation during regeneration – confirming glycolysis as a key component in cardiomyocyte proliferation (*63, 64*).

The importance of glycolysis is highlighted in the *Astyanax*, where genes in glucose uptake and glycolysis are upregulated in the myocardial border zone to a greater extent in the surface fish compared to Pachón. In light of the importance of glycolysis on proliferation, this difference is a possible determinant in the Pachóns ability to complete proliferation. However, Pachón border zone cardiomyocytes do appear to increase glycolysis, perhaps to a sufficient level to initiate proliferation but not complete it. Several notable components of glucose uptake and glycolysis were significantly different between the Pachón and surface fish border zone cardiomyocytes. These included, *glut1a* - the glucose transporter, *pkma* – catalyses the last step of glycolysis, as well as, *pdk2a* and *pdk4a* - key regulators of anaerobic glycolysis. The activity of these components of glucose metabolism have significant or essential roles in cardiomyocyte proliferation during either neonatal mouse or zebrafish regeneration (*64, 259*). As such, each of these are potential candidates for the lack of cardiomyocyte expansion in Pachón.

In addition to cardiomyocytes, glycolysis has also been reported to play an important role in proliferation of a range of cell types, but was first described in tumour cells by Otto Warburg (*248, 283-285*). Similar to zebrafish proliferating border zone cardiomyocytes, proliferating tumour cells undergo a metabolic shift from mitochondrial oxidative phosphorylation to anaerobic glycolysis despite the presence of oxygen – known as the Warburg effect (*248, 285*).

In addition to cancer cells, progenitor cells of the developing embryo and induced pluripotent stem cells rely on glycolysis for proliferation and maintaining their potency (*284*). This is in part why glycolysis is considered a more developmental feature of cells, adding to the notion that proliferating cardiomyocytes during regeneration resemble embryonic cardiomyocytes.

The mechanism by which glycolysis promotes cellular proliferation remains elusive. However, it is thought that the mechanism lies beyond its catabolic function, particularly as glycolysis is less efficient, generating much less ATP compared to fatty acid oxidation (*249, 251*). Indeed, within tumour cells it's thought that glycolysis and connected pathways, such as the pentose phosphate pathway, produce essential metabolite intermediates that create the biomass need to sustain proliferation (*249*). In addition, certain glycolytic enzymes can also directly influence regulators of the cell cycle to promote proliferation cancer cells, such as PKM2, which is noticeably raised in surface fish border zone cardiomyocytes versus Pachón (*286*).

Due to the preference of the energy inefficient glycolytic pathway in proliferating cells, ATP levels are only considered a defining factor in proliferation when resources are scarce (*249*). However, the reduction of genes involved in both glycolysis and mitochondrial oxidative phosphorylation in Pachón border zone cardiomyocytes compared to surface fish, raises the notion of whether insufficient ATP is causing cell cycle arrest. Indeed, chemical inhibition of mitochondrial respiration reduced the proliferative capacity of early cardiomyocytes *in vitro (287)*. Moreover, normal proliferating cultured cells (non-cardiomyocytes) undergo cell cycle arrest and reactivate catabolic (energy-producing) metabolism through autophagy when their ability to produce ATP from glucose is compromised (*288*). Notably, autophagy is moderately enriched in Pachón border zone cardiomyocytes versus surface fish, suggesting that Pachón have increased autophagy to produce the required ATP in response to their reduced glucose

metabolism. Interestingly, mitophagy, a form of autophagy that degrades mitochondria, is enhanced in hypoxia induced cardiomyocyte polyploidisation, drawing correlations between autophagic processes and polyploidy (*289*). Overall, comprised/reduced energy metabolism in Pachón could be resulting in cell cycle arrest and activation of autophagic processes to mitigate reduced ATP output.

Ultimately, glucose metabolism and specifically anaerobic glycolysis is crucial to cardiomyocyte proliferation. As such, the reduced glucose uptake and glycolytic reprogramming in Pachón border zone cardiomyocytes could be a key determinant in possible cell cycle arrest. However, further investigation is needed to confirm this.

6.1.5 Diabetic characteristics in the Pachón heart, but cavefish *insra* P211L mutation, does not have a negative impact cardiac regeneration.

One of the notable physiological differences between surface fish and Pachón was the suggestion of a diabetic phenotype in the Pachón as indicted by hyperglycaemia and a mutation in the insulin receptor, which confers a level of insulin resistance (*144*). This diabetic aspect seems to extend to the heart after injury, as evidenced by the metabolic inflexibility indicated in the metabolomics, which is a feature of the diabetic heart (*264, 265*). Diabetes impacts on both wound healing and cardiac function post-ischemia with poorer long-term prognosis following MI (*274-276, 290*). One of the factors implicated in this, is the metabolic reprogramming further towards fatty acid metabolism within the diabetic heart, which can be detrimental to active signalling pathways after ischemia, such as HIF signalling (*274*). This greater dependence on fatty acid metabolism in the diabetic heart is consistent with the Pachón, which appears to have a greater capacity for fatty acid utilisation compared to surface fish. Evidence of a diabetic phenotype in the heart after injury, raises the possibility

that these changes in metabolism alongside loss of cardiomyocyte expansion and regeneration in Pachón are a pathological consequence of the diabetic physiology of the cavefish.

Insulin signalling is a major regulator of metabolic homoeostasis with central roles in growth control, aging and wound healing. Reduction in the insulin signalling can extend lifespan and have a positive role in ageing-related diseases (*291, 292*). On the other hand, reduction of this network can impair other aspects of health, such as wound healing (*293*). This could be a potential reason why impaired wound healing is a common complication of diabetes. In terms of cardiac regeneration, IGF2-INSR signalling is an important factor in proliferation of mononuclear diploid cardiomyocytes during early neonatal mouse heart regeneration (*294*). As such, it was hypothesised the insulin resistance from the Pachón *insra* mutation as an upstream factor governing these metabolic differences in the border zone, and ultimately the lack of cardiomyocyte expansion in the Pachón. However, investigation of the P211L mutation on zebrafish cardiomyocyte proliferation and regeneration, seemed to suggest that this mutation, on its own, is not a significant factor in the reduced cardiomyocyte expansion and absent regeneration in the Pachón. Surprisingly, in the context of the zebrafish, this mutation seems to enhance regeneration, likely through the functions of a non-cardiomyocyte cell type.

Whilst the *insra* mutation in cavefish does not have a significant role in its cardiomyocyte proliferation profile or regeneration capacity on its own, other identified cavefish mutations in upstream pathways may contribute the metabolic differences and proliferation profile. In particular, the mc4r (melanocortin 4 receptor) is mutated in the cavefish resulting in an increased appetite (*145*). Significantly, mc4r and its signalling pathway is crucial for energy

homeostasis during xenopus limb regeneration (*295*). Thus, making the mc4r signalling and the mutation in cavefish an upstream candidate influencing the metabolic differences that underpin the contrasting cardiomyocyte proliferation profiles.

A further possible upstream pathway influencing the metabolic differences and proliferation profile in the *Astyanax*, is the TNF-alpha/ NF-κB signalling pathway, which is enriched in surface fish border zone cardiomyocytes compared to Pachón. NF-κB signalling is upregulated in the zebrafish border zone and has been shown to be a key component in cardiomyocyte proliferation during zebrafish regeneration (*296*). Additionally, NF-κB signalling has also been shown to increase glucose uptake and glycolysis flux in cultured cancer cells, suggesting NF-κB signalling has a direct role in regulating glucose metabolism and promoting the Warburg effect (*297, 298*). Therefore, increased NF-κB signalling in surface fish border zone cardiomyocytes is a possible upstream determinant of the increased glucose uptake/glycolysis and successful proliferation.

6.2 Study translational prospective

As previously described, the human heart after MI is only capable of limited cardiomyocyte turnover, which mostly results in additional polyploid cardiomyocytes. This is ultimately responsible for the permanent loss of functional myocardium and the deleterious consequences of MI. As such, the concept of cardiac regenerative therapies has focused on the idea of replacing the lost cardiomyocytes, with new fully functioning myocardium. One of the main regenerative strategies has been cell-replacement therapies, which involves transplanting stem cells or iPSC-derived cardiomyocytes into the injured heart to replace the lost cardiomyocytes (*299*). Whilst these cell-based strategies have shown initial promise in numerous pre-clinical settings they observe a number of limitations, such as low engraftment rates and poor cell survival alongside the risk of arrhythmias and tachycardia (*299*). Moreover, preclinical outcomes of cell-based therapies have not translated effectively to clinical trials (*299*). A possible alternative strategy is to promote endogenous cardiomyocyte proliferation within the human heart and thus mimic what occurs in fish and neonatal mammals after cardiac damage. Therefore, it is logical to turn to model systems of regeneration to determine the mechanisms that induce endogenous cardiomyocyte proliferation, such as the zebrafish and neonatal mouse, or as this study demonstrates, the *Astyanax*.

In the first instance, this study compared *Astyanax* morphotypes and identified *lrrc10* as a gene with a key role in cardiomyocyte function during natural fish regeneration. In the context of humans, genetic variants in the *LRRC10* gene have been linked to DCM in the human heart, which has been supported by *lrrc10* mutant mouse models (*190, 191, 195*). This link with human DCM in combination with lrrc10s specificity to the myocardium suggests an important role in human cardiomyocyte function and subsequently a potential translational perspective

of *lrrc10* within myocardial regeneration. Additional investigation of *lrrc10s* role in myocardial regeneration within mammalian models of regeneration, such as neonatal mouse, alongside studies utilising human cardiomyocyte cell lines will enable further insight in the translational potential of *lrrc10*.

This study also showed that while surface fish are capable of inducing complete cardiomyocyte renewal after injury, Pachón cavefish exhibit impaired cardiomyocyte turnover, with the possibility of cell cycle arrest and polyploidisation. As alluded to above, the possibility of polyploidisation of Pachón cardiomyocytes is similar to the human heart after birth, and after MI (*40, 41, 151, 279*). Therefore, the promise of ploidy in Pachón could present the *Astyanax* as a unique model to study myocardial regeneration and specifically cardiomyocyte polyploidisation, thus providing insight into the possible factors/mechanisms that lead to human cardiomyocyte ploidy after injury. Establishing these mechanisms will enable the possibility of modulating them to induce complete cardiomyocyte proliferation in the human heart after MI.

Indeed, one such mechanism/factor that this study identified that could be responsible for the contrasting cardiomyocyte proliferation profiles was differences in metabolism, namely increased fatty acid utilisation and reduced glucose metabolism in the Pachón compared to the surface fish. Whilst these metabolic differences need to be functionally investigated as having an impact on *Astyanax* cardiomyocyte renewal, comparison of the metabolic response between fish in the border zone cardiomyocytes could provide insights into the ideal metabolic state critical for successful cardiomyocyte renewal. Understanding the ideal metabolic state for cardiomyocyte proliferation could contribute to the notion of modulating

human myocardial metabolism as a strategy to promote endogenous cardiomyocyte renewal in the human heart after MI.

Overall, comparison of regenerative capacities in *Astyanax* will help to discover new basic mechanisms controlling myocardial regeneration. Finding these mechanisms involved in myocardial regeneration in fish will contribute to finding novel strategies to restore the functional myocardium in human hearts after MI.

6.3 Future work

One of the main goals of this work was to determine the fate of the proliferating cardiomyocytes in Pachón during regeneration. To decipher more precisely how surface fish and Pachón cycling cardiomyocytes differ, trajectory analysis can be employed on the *Astyanax* border zone cardiomyocytes. This analysis enables the ability to order cells across dynamic cellular processes/transitions and explore the temporal expression that occurs along these processes. As such, trajectory analysis will enable investigation of the temporal gene expression across the dedifferentiation, migration and re-differentiation/reintegration sequence of events, as well as the phases of the cell cycle in both Pachón and surface fish. Comparison of the dynamic gene expression that occurs across the trajectory between fish will possibly help to determine the point at which Pachón proliferating cardiomyocytes deviate from surface fish proliferating cardiomyocytes.

The scRNAseq analysis in chapter 4 suggested the possibility of early cell cycle arrest in Pachón proliferating cardiomyocytes without cell death, which led to the hypothesis of polyploidisation. Functional ploidy analysis by measuring the DNA content of dissociated cardiomyocytes at 14dpi seemed to support this notion, but suggested cell cycle arrest in the S phase – forming aneuploid cardiomyocytes. However, due to the inability to detect BrdU/MF20 positive cells, the experiment was unable to specifically target and measure DNA content in the border zone proliferating cardiomyocytes. Therefore, an alternative strategy is needed to fully confirm cell cycle arrest and polyploidisation in Pachón cardiomyocytes. One possible alternative strategy is an in-situ ploidy analysis on 3D reconstructed confocal Z-stacks of tissue sections (*300*). This would use the main basic principle of measuring DNA content through DAPI fluorescence intensity to determine ploidy. When combined with BrdU/EdU

pulse chase this will enable targeted analysis of the cycling cardiomyocytes, as well as a spatial context.

The scRNAseq analysis revealed differential expression of genes related to a number of metabolic pathways, some of which were supported by RNAscope analysis and metabolomics in chapter 5. This included the surprising enrichment of oxidative phosphorylation, mitochondrial organisation and respiratory complex assembly in surface fish compared to Pachón, which hints at increased mitochondrial biogenesis and mitochondrial based metabolism in surface fish. However, these mitochondrial differences remain unexplored outside the scRNAseq and therefore require validation. This can be done collectively through RNAscope analysis of relevant genes from these enriched GO terms in combination with transmission electron microscopy (TEM) of border zone cardiomyocytes to analyse mitochondria number, the mitochondrial morphology and cristae density. Both mitochondrial morphology and cristae density have been linked to mitochondrial function (*301, 302*) and as such, analysis of mitochondria via TEM will help functionally validate increased mitochondrial based metabolism in surface fish.

In addition, TEM analysis will also enable investigation of sarcomere structure and morphology, which can give an indication of the differentiation/maturation state of the border zone cardiomyocytes in Pachón and surface fish. Mature cardiomyocytes possess a highly organised sarcomere structure, which is dissembled during dedifferentiation. Therefore, increased maturity or defective dedifferentiation in Pachón cardiomyocytes would show more highly organised sarcomeres. Ultimately, this will possibly confirm an altered maturation in the Pachón border zone, which was hinted at with lower transcriptional entropy scores.

Many of the differences in metabolic pathway activity between the *Astyanax* morphotypes and after injury are inferred through RNA expression. However, questions remain how much RNA expression is indicative of pathway activity, particularly as much of metabolism is regulated at the protein level. To a degree, the metabolomics gives an indication of pathway activity and supports a number of the metabolic differences highlighted through transcriptional expression, such as fatty acid metabolism and the TCA cycle. Despite this, the metabolomics was unable to a support metabolic activity of all pathways highlighted by transcriptomic expression, such as the increased expression of genes related to glucose uptake and glycolysis in surface fish. This is likely due to the upregulation of gluconeogenesis in Pachón, which shares many of the same metabolite intermediates as glycolysis. A more precise measurement of metabolic pathway activity is likely to measure the flux through the candidate pathway. There are several possible methodologies for potentially measuring metabolic pathway flux, but the most robust is the use of isotope tracers for steady-state labelling combined with metabolomics. This has been successfully used to measure metabolic flux in the context of the liver and melanoma in zebrafish (*303*). Alternatively, metabolic flux in tissues can be measured using the Seahorse system.

Whilst characterisation of the metabolism in the *Astyanax* after injury can be enhanced, notable metabolic candidates have been observed that could be determinants in the contrasting cardiomyocyte proliferation profiles. This includes the increased glycolytic reprogramming in the surface fish border zone compared to Pachón, and the possible preference for fatty acid metabolism in Pachón. These metabolic differences are exemplified by the upregulation of the glucose transporter, *glut1a*, in the surface fish border zone, and the upregulation of *cd36* in the Pachón border zone – both specific candidates. However,

whether these metabolic differences impact on the cardiomyocyte proliferation profile needs to be functionally determined. This can be performed through pharmacological inhibition of *Astyanax* hearts or genetic loss and gain of function mutants in zebrafish. Inhibitors currently exist for both glycolysis (2-Deoxy-D-Glucose) and fatty acid oxidation (Etomoxir), as well as specific inhibitors for GLUT1 (BAY-876) and CD36 (Sulfosuccinimidyl Oleate). These can be applied to surface fish and Pachón after injury followed by investigation of their effect on cardiomyocyte proliferation/expansion and regeneration.

Similar to what was achieved with *lrrc10*, the role of both *glut1a* and *cd36* in cardiomyocyte proliferation can also be investigated by CRISPR-mediated knockout of *glut1a* or genetic overexpression of *cd36* in the regenerating zebrafish. In particular, *cd36* can be overexpressed at the wound border by utilising the 103runx1ENfos:EGFP construct, which is activated around the wound border in multiple cell types including proliferating cardiomyocytes at 7dpi (*304*). Therefore, this enables targeting *cd36* overexpression to the proliferating cardiomyocytes in the border zone. Following their generation, both these genetically modified zebrafish lines can be investigated for cardiomyocyte proliferation/expansion potential and heart regeneration capacity.

Ultimately, these pharmacological inhibition experiments and the genetic gain/loss of function in zebrafish lines or Pachón will determine the metabolic pathways that are causative of reduced myocardial regeneration in Pachón and the possibility of rescuing the Pachón phenotype.

6.4 Concluding remarks

The opposing regenerative capacities in the *Astyanax* model enable the ability to compare natural heart regeneration with permanent scarring in a single species. Through the identification and confirmation of *lrrc10* as a gene required for the regeneration, this work demonstrated the *Astyanax* as a model capable of enhancing our understanding heart regeneration.

This work also provides insights into the cardiomyocyte proliferation differences that underpin the *Astyanax* opposing regenerative capacities, with evidence suggesting polyploidisation of Pachón proliferating cardiomyocytes at the expense of meaningful cardiomyocyte expansion. In addition, this suggestion of polyploidisation was underlined by profound metabolic differences in the myocardial border zone. Identification of these metabolic differences provides the initial strides into establishing the metabolic fingerprint required for successful cardiomyocyte proliferation during cardiac regeneration.

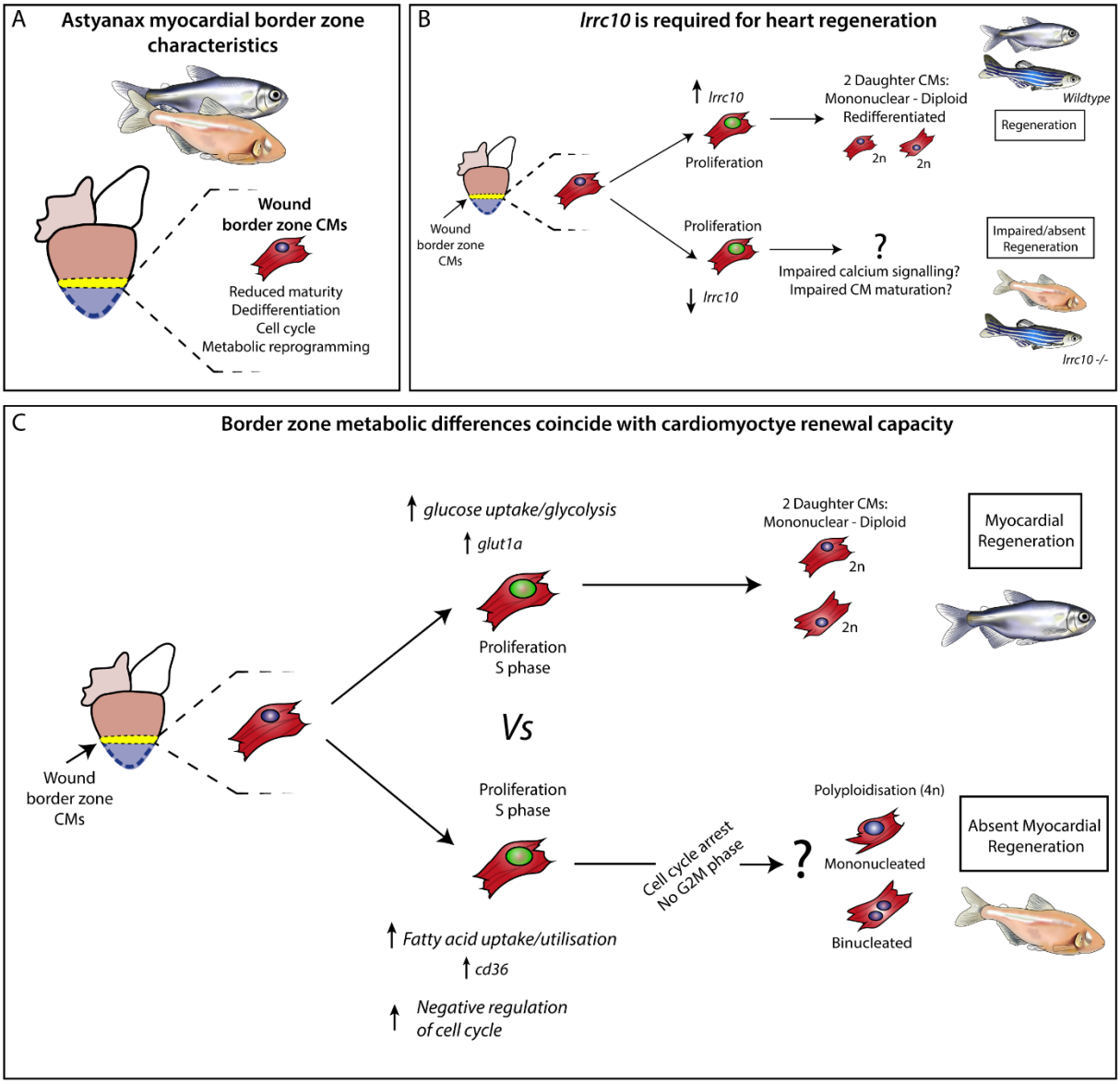


Figure 6.1 Summary of main findings and possible mechanisms highlighted in the study

(A) *Astyanax myocardial border zone display characteristics consistent with reduced maturity, dedifferentiation, cell proliferation and metabolic reprogramming.* ***(B)*** *After injury, both the regenerating zebrafish and surface upregulate lrrc10 expression in border zone cardiomyocytes. In the Pachon and lrrc10-/- zebrafish, lrrc10 expression is reduced/absent, which impairs cardiac regeneration. Reduction/loss of lrrc10 likely impairs regeneration by causing defective calcium signalling, altering cardiomyocyte maturation and interfering with the dedifferentiation, migration and re-differentiation/reintegration sequence of events.* ***(C)*** *Proliferating cardiomyocytes in the surface fish border zone upregulate glucose uptake/ glycolysis, which results in two daughter diploid cardiomyocytes and significant cardiomyocyte expansion. In contrast, Pachon proliferating cardiomyocytes in the border zone have increased fatty acid uptake/utilisation, alongside enrichment of genes involved in negative regulation of the cell cycle over surface fish. As a result, this possibly causes cell cycle arrest with polyploidisation and thus, no observable cardiomyocyte expansion.*

Appendix

Contributions

All experiments and (bioinformatic) analysis were carried out exclusively by me, except the following:

- Prof Mathilda Mommersteeg aided with sample preparation for bulk RNAseq analysis (RNA extraction and RNA sequencing preparation).
- Dr Madeleine Lemieux completed the bioinformatic analysis of the bulk RNAseq. Dr Madeleine Lemieux also completed the genome alignment through the cell ranger pipeline for the scRNAseq experiment.
- Helen Potts completed the dissociation of hearts into a single cell suspension for scRNAseq. Submission of samples for 10x Genomics and sequencing was completed by Helen Potts in collaboration with Neil Ashley of the MRC WIMM Single Cell Facility.
- Metabolomics was performed in collaboration with Glasgow Polyomics (as a service). Erin Manson performed submission of samples to the LC-MS and Dr Gavin Backburn completed subsequent data analysis.

Publications

Helen G. Potts*, **William T. Stockdale*** & Mathilda T. M. Mommersteeg. “Unlocking the secrets of the regenerating fish heart: Comparing regenerative models to shed light on successful regeneration”. *Journal of Cardiovascular Development and Disease* vol. 8 1–18 (2021).

Jana Koth*, Xiaonan Wang*, Abigail C. Killen*, **William T. Stockdale**, Helen G. Potts, Andrew Jefferson, Florian Bonkhofer, Paul R. Riley, Roger K. Patient, Berthold Göttgens, Mathilda T.

M. Mommersteeg. “Runx1 promotes scar deposition and inhibits myocardial proliferation and survival during zebrafish heart regeneration”. *Development* (Cambridge). 147, (2020).

William T. Stockdale*, Madeleine E. Lemieux, Abigail C. Killen, Juanjuan Zhao, Zhilian Hu, Noemie Hamilton, Tetsuhiro Kudoh, Paul R. Riley, Ronny van Aerle, Yoshiyuki Yamamoto, Mathilda T. M. Mommersteeg. “Heart regeneration in the Mexican cavefish” *Cell Rep*. 25, 1997–2007.e7 (2018).

Jocelyn L.Y*. Tang, Yu Guo, **William T. Stockdale**, Kerisha Rana, Mathilda T.M. Mommersteeg, Yoshiyuki Yamamoto. “The Developmental Origin of Heart Size and Shape Differences in *Astyanax mexicanus*” *Dev. Biol*. 441, (2018).

References

1. G. A. Roth *et al.*, Global, regional, and national age-sex-specific mortality for 282 causes of death in 195 countries and territories, 1980–2017: a systematic analysis for the Global Burden of Disease Study 2017. *The Lancet* **392**, 1736-1788 (2018).

2. G. A. Roth *et al.*, Global Burden of Cardiovascular Diseases and Risk Factors, 1990–2019. *Journal of the American College of Cardiology* **76**, 2982-3021 (2020).

3. P. Scarborough, K. Wickramasinghe, P. Bhatnagar, M. Rayner, Trends in coronary heart disease, 1961-2011. (2011).

4. R. S. Velagaleti *et al.*, Long-Term Trends in the Incidence of Heart Failure After Myocardial Infarction. *Circulation* **118**, 2057-2062 (2008).

5. J. A. Ezekowitz *et al.*, Declining In-Hospital Mortality and Increasing Heart Failure Incidence in Elderly Patients With First Myocardial Infarction. *Journal of the American College of Cardiology* **53**, 13-20 (2009).

6. M. A. Pfeffer, E. Braunwald, Ventricular remodeling after myocardial infarction. Experimental observations and clinical implications. *Circulation* **81**, 1161-1172 (1990).

7. P. S. Jhund, J. J. V. McMurray, The neprilysin pathway in heart failure: a review and guide on the use of sacubitril/valsartan. *Heart* **102**, 1342-1347 (2016).

8. A. M. Katz, The “Modern” View of Heart Failure. *Circulation: Heart Failure* **1**, 63-71 (2008).

9. C. J. Vivien, J. E. Hudson, E. R. Porrello, Evolution, comparative biology and ontogeny of vertebrate heart regeneration. *npj Regenerative Medicine* **1**, 16012 (2016).

10. J. O. Oberpriller, J. C. Oberpriller, Response of the adult newt ventricle to injury. *Journal of Experimental Zoology* **187**, 249-259 (1974).

11. K. D. Poss, L. G. Wilson, M. T. Keating, Heart regeneration in zebrafish. *Science* **298**, 2188-2190 (2002).

12. J. Wang *et al.*, The regenerative capacity of zebrafish reverses cardiac failure caused by genetic cardiomyocyte depletion. *Development* **138**, 3421-3430 (2011).

13. V. Parente *et al.*, Hypoxia/Reoxygenation Cardiac Injury and Regeneration in Zebrafish Adult Heart. *PLoS ONE* **8**, e53748 (2013).

14. F. Chablais, J. Veit, G. Rainer, A. Jaźwińska, The zebrafish heart regenerates after cryoinjury-induced myocardial infarction. *BMC Developmental Biology* **11**, 21 (2011).

15. J. M. González-Rosa, V. Martín, M. Peralta, M. Torres, N. Mercader, Extensive scar formation and regression during heart regeneration after cryoinjury in zebrafish. *Development* **138**, 1663-1674 (2011).

16. K. Schnabel, C.-C. Wu, T. Kurth, G. Weidinger, Regeneration of Cryoinjury Induced Necrotic Heart Lesions in Zebrafish Is Associated with Epicardial Activation and Cardiomyocyte Proliferation. *PLoS ONE* **6**, e18503 (2011).

17. K. D. Poss, M. T. Keating, A. Nechiporuk, Tales of regeneration in zebrafish. *Developmental Dynamics* **226**, 202-210 (2003).

18. G. F. B. Hanna, N. N. Nawar, S. C. Sharma, Regeneration of ascending spinal axons in goldfish. *Brain Research* **791**, 235-245 (1998).

19. T. S. Vihtelic, J. E. Soverly, S. C. Kassen, D. R. Hyde, Retinal regional differences in photoreceptor cell death and regeneration in light-lesioned albino zebrafish. *Experimental Eye Research* **82**, 558-575 (2006).

20. C. Q. Diep *et al.*, Identification of adult nephron progenitors capable of kidney regeneration in zebrafish. *Nature* **470**, 95-100 (2011).

21. P. J. Lafontant *et al.*, The Giant Danio (D. Aequipinnatus) as A Model of Cardiac Remodeling and Regeneration. *The Anatomical Record: Advances in Integrative Anatomy and Evolutionary Biology* **295**, 234-248 (2012).

22. J. Grivas *et al.*, Cardiac repair and regenerative potential in the goldfish (Carassius auratus) heart. *Comparative Biochemistry and Physiology Part C: Toxicology & Pharmacology* **163**, 14-23 (2014).

23. W. Wang *et al.*, Changes in regeneration-responsive enhancers shape regenerative capacities in vertebrates. *Science* **369**, (2020).

24. K. Ito *et al.*, Differential reparative phenotypes between zebrafish and medaka after cardiac injury. *Developmental Dynamics* **243**, 1106-1115 (2014).

25. E. R. Porrello *et al.*, Transient Regenerative Potential of the Neonatal Mouse Heart. *Science* **331**, 1078-1080 (2011).

26. A. Darehzereshki *et al.*, Differential regenerative capacity of neonatal mouse hearts after cryoinjury. *Developmental Biology* **399**, 91-99 (2015).

27. E. R. Porrello *et al.*, Regulation of neonatal and adult mammalian heart regeneration by the miR-15 family. *Proceedings of the National Academy of Sciences* **110**, 187-192 (2013).

28. L. Ye *et al.*, Early Regenerative Capacity in the Porcine Heart. *Circulation* **138**, 2798-2808 (2018).

29. A. C. Sturzu *et al.*, Fetal Mammalian Heart Generates a Robust Compensatory Response to Cell Loss. *Circulation* **132**, 109-121 (2015).

30. B. J. Haubner *et al.*, Functional Recovery of a Human Neonatal Heart After Severe Myocardial Infarction. *Circulation Research* **118**, 216-221 (2016).

31. S. Fratz *et al.*, Long-Term Myocardial Scarring After Operation for Anomalous Left Coronary Artery From the Pulmonary Artery. *The Annals of Thoracic Surgery* **92**, 1761-1765 (2011).

32. E. L. Price, J. M. Vieira, P. R. Riley, Model organisms at the heart of regeneration. *Disease Models & Mechanisms* **12**, dmm040691 (2019).

33. C. Jopling *et al.*, Zebrafish heart regeneration occurs by cardiomyocyte dedifferentiation and proliferation. *Nature* **464**, 606-609 (2010).

34. K. Kikuchi *et al.*, Primary contribution to zebrafish heart regeneration by gata4+ cardiomyocytes. *Nature* **464**, 601-605 (2010).

35. C. E. Murry *et al.*, Haematopoietic stem cells do not transdifferentiate into cardiac myocytes in myocardial infarcts. *Nature* **428**, 664-668 (2004).

36. P. Sallin, A.-S. De Preux Charles, V. Duruz, C. Pfefferli, A. Jaźwińska, A dual epimorphic and compensatory mode of heart regeneration in zebrafish. *Developmental Biology* **399**, 27-40 (2015).

37. C.-C. Wu *et al.*, Spatially Resolved Genome-wide Transcriptional Profiling Identifies BMP Signaling as Essential Regulator of Zebrafish Cardiomyocyte Regeneration. *Developmental Cell* **36**, 36-49 (2016).

38. J. Itou *et al.*, Migration of cardiomyocytes is essential for heart regeneration in zebrafish. *Development* **139**, 4133-4142 (2012).

39. R. Marín-Juez *et al.*, Coronary Revascularization During Heart Regeneration Is Regulated by Epicardial and Endocardial Cues and Forms a Scaffold for Cardiomyocyte Repopulation. *Developmental Cell* **51**, 503-515.e504 (2019).

40. O. Bergmann *et al.*, Evidence for Cardiomyocyte Renewal in Humans. *Science* **324**, 98-102 (2009).

41. S. E. Senyo *et al.*, Mammalian heart renewal by pre-existing cardiomyocytes. *Nature* **493**, 433-436 (2013).

42. X. Liu *et al.*, Cell proliferation fate mapping reveals regional cardiomyocyte cell-cycle activity in subendocardial muscle of left ventricle. *Nature Communications* **12**, (2021).

43. G. D'Uva *et al.*, ERBB2 triggers mammalian heart regeneration by promoting cardiomyocyte dedifferentiation and proliferation. *Nature Cell Biology* **17**, 627-638 (2015).

44. M. Gemberling, R. Karra, A. L. Dickson, K. D. Poss, Nrg1 is an injury-induced cardiomyocyte mitogen for the endogenous heart regeneration program in zebrafish. *eLife* **4**, (2015).

45. Z. Lin *et al.*, Pi3kcbLinks Hippo-YAP and PI3K-AKT Signaling Pathways to Promote Cardiomyocyte Proliferation and Survival. *Circulation Research* **116**, 35-45 (2015).

46. M. Xin *et al.*, Hippo pathway effector Yap promotes cardiac regeneration. *Proceedings of the National Academy of Sciences* **110**, 13839-13844 (2013).

47. B. N. Singh *et al.*, A conserved HH-Gli1-Mycn network regulates heart regeneration from newt to human. *Nature Communications* **9**, (2018).

48. W.-Y. Choi *et al.*, In vivo monitoring of cardiomyocyte proliferation to identify chemical modifiers of heart regeneration. *Development* **140**, 660-666 (2013).

49. C.-L. Lien, M. Schebesta, S. Makino, G. J. Weber, M. T. Keating, Gene Expression Analysis of Zebrafish Heart Regeneration. *PLoS Biology* **4**, e260 (2006).

50. Y. Huang *et al.*, Igf Signaling is Required for Cardiomyocyte Proliferation during Zebrafish Heart Development and Regeneration. *PLoS ONE* **8**, e67266 (2013).

51. W. Yu *et al.*, GATA4 regulates Fgf16 to promote heart repair after injury. *Development* **143**, 936-949 (2016).

52. N. Tahara *et al.*, The FGF-AKT pathway is necessary for cardiomyocyte survival for heart regeneration in zebrafish. *Developmental Biology* **472**, 30-37 (2021).

53. M. A. Missinato *et al.*, Dusp6 attenuates Ras/MAPK signaling to limit zebrafish heart regeneration. *Development* **145**, dev157206 (2018).

54. J. Kim *et al.*, PDGF signaling is required for epicardial function and blood vessel formation in regenerating zebrafish hearts. *Proceedings of the National Academy of Sciences* **107**, 17206-17210 (2010).

55. G. Tao *et al.*, Pitx2 promotes heart repair by activating the antioxidant response after cardiac injury. *Nature* **534**, 119-123 (2016).

56. Y. L. Schindler *et al.*, Hand2 elevates cardiomyocyte production during zebrafish heart development and regeneration. *Development* **141**, 3112-3122 (2014).

57. F.-L. Xiang, M. Guo, K. E. Yutzey, Overexpression of Tbx20 in Adult Cardiomyocytes Promotes Proliferation and Improves Cardiac Function After Myocardial Infarction. *Circulation* **133**, 1081-1092 (2016).

58. J. Koth *et al.*, Runx1 promotes scar deposition and inhibits myocardial proliferation and survival during zebrafish heart regeneration. *Development* **147**, dev186569 (2020).

59. A. I. Mahmoud *et al.*, Meis1 regulates postnatal cardiomyocyte cell cycle arrest. *Nature* **497**, 249-253 (2013).

60. S. Crippa *et al.*, Comparative transcriptome profiling of the injured zebrafish and mouse hearts identifies miRNA-dependent repair pathways. *Cardiovascular Research* **110**, 73-84 (2016).

61. V. P. Yin, A. Lepilina, A. Smith, K. D. Poss, Regulation of zebrafish heart regeneration by miR-133. *Developmental Biology* **365**, 319-327 (2012).

62. A. Eulalio *et al.*, Functional screening identifies miRNAs inducing cardiac regeneration. *Nature* **492**, 376-381 (2012).

63. H. Honkoop *et al.*, Single-cell analysis uncovers that metabolic reprogramming by ErbB2 signaling is essential for cardiomyocyte proliferation in the regenerating heart. *eLife* **8**, (2019).

64. R. Fukuda *et al.*, Stimulation of glycolysis promotes cardiomyocyte proliferation after injury in adult zebrafish. *EMBO reports* **21**, (2020).

65. Bao *et al.*, The Oxygen-Rich Postnatal Environment Induces Cardiomyocyte Cell-Cycle Arrest through DNA Damage Response. *Cell* **157**, 565-579 (2014).

66. Y. Nakada *et al.*, Hypoxia induces heart regeneration in adult mice. *Nature* **541**, 222-227 (2017).

67. C. Jopling, G. Suñé, A. Faucherre, C. Fabregat, J. C. Izpisua Belmonte, Hypoxia Induces Myocardial Regeneration in Zebrafish. *Circulation* **126**, 3017-3027 (2012).

68. M. Cui *et al.*, Dynamic Transcriptional Responses to Injury of Regenerative and Non-regenerative Cardiomyocytes Revealed by Single-Nucleus RNA Sequencing. *Developmental Cell* **53**, 102-116.e108 (2020).

69. W. Derks, O. Bergmann, Polyploidy in Cardiomyocytes. *Circulation Research* **126**, 552-565 (2020).

70. M. Patterson *et al.*, Frequency of mononuclear diploid cardiomyocytes underlies natural variation in heart regeneration. *Nature Genetics* **49**, 1346-1353 (2017).

71. J. M. González-Rosa *et al.*, Myocardial Polyploidization Creates a Barrier to Heart Regeneration in Zebrafish. *Developmental Cell* **44**, 433-446.e437 (2018).

72. R. Marín-Juez *et al.*, Fast revascularization of the injured area is essential to support zebrafish heart regeneration. *Proceedings of the National Academy of Sciences* **113**, 11237-11242 (2016).

73. S. Kapuria, T. Yoshida, C.-L. Lien, Coronary Vasculature in Cardiac Development and Regeneration. *Journal of Cardiovascular Development and Disease* **5**, 59 (2018).

74. V. Lowe, L. Wisniewski, C. Pellet-Many, The Zebrafish Cardiac Endothelial Cell—Roles in Development and Regeneration. *Journal of Cardiovascular Development and Disease* **8**, 49 (2021).

75. L. He *et al.*, Genetic lineage tracing discloses arteriogenesis as the main mechanism for collateral growth in the mouse heart. *Cardiovascular Research* **109**, 419-430 (2016).

76. S. Das *et al.*, A Unique Collateral Artery Development Program Promotes Neonatal Heart Regeneration. *Cell* **176**, 1128-1142.e1118 (2019).

77. W.-C. Huang *et al.*, Treatment of Glucocorticoids Inhibited Early Immune Responses and Impaired Cardiac Repair in Adult Zebrafish. *PLoS ONE* **8**, e66613 (2013).

78. A. Lepilina *et al.*, A Dynamic Epicardial Injury Response Supports Progenitor Cell Activity during Zebrafish Heart Regeneration. *Cell* **127**, 607-619 (2006).

79. Michael *et al.*, Chemokine-Guided Angiogenesis Directs Coronary Vasculature Formation in Zebrafish. *Developmental Cell* **33**, 442-454 (2015).

80. A. M. Segura, O. H. Frazier, L. M. Buja, Fibrosis and heart failure. *Heart Failure Reviews* **19**, 173-185 (2014).

81. A. C. Silva, C. Pereira, A. Fonseca, O. P. Pinto-do, D. S. Nascimento, Bearing My Heart: The Role of Extracellular Matrix on Cardiac Development, Homeostasis, and Injury Response. *Front Cell Dev Biol* **8**, 621644 (2020).

82. O. Kanisicak *et al.*, Genetic lineage tracing defines myofibroblast origin and function in the injured heart. *Nature Communications* **7**, 12260 (2016).

83. K. Kikuchi *et al.*, tcf21+ epicardial cells adopt non-myocardial fates during zebrafish heart development and regeneration. *Development* **138**, 2895-2902 (2011).

84. J. M. González-Rosa, M. Peralta, N. Mercader, Pan-epicardial lineage tracing reveals that epicardium derived cells give rise to myofibroblasts and perivascular cells during zebrafish heart regeneration. *Developmental Biology* **370**, 173-186 (2012).

85. J. Wang, R. Karra, A. L. Dickson, K. D. Poss, Fibronectin is deposited by injury-activated epicardial cells and is necessary for zebrafish heart regeneration. *Developmental Biology* **382**, 427-435 (2013).

86. F. C. Simões *et al.*, Macrophages directly contribute collagen to scar formation during zebrafish heart regeneration and mouse heart repair. *Nature Communications* **11**, (2020).

87. H. Sánchez-Iranzo *et al.*, Transient fibrosis resolves via fibroblast inactivation in the regenerating zebrafish heart. *Proceedings of the National Academy of Sciences* **115**, 4188-4193 (2018).

88. J. Duan *et al.*, Wnt1/βcatenin injury response activates the epicardium and cardiac fibroblasts to promote cardiac repair. *The EMBO Journal* **31**, 429-442 (2012).

89. C. Bonnans, J. Chou, Z. Werb, Remodelling the extracellular matrix in development and disease. *Nature Reviews Molecular Cell Biology* **15**, 786-801 (2014).

90. W. C. W. Chen *et al.*, Decellularized zebrafish cardiac extracellular matrix induces mammalian heart regeneration. *Science Advances* **2**, e1600844 (2016).

91. E. Bassat *et al.*, The extracellular matrix protein agrin promotes heart regeneration in mice. *Nature* **547**, 179-184 (2017).

92. Z. Chen *et al.*, Ablation of periostin inhibits post-infarction myocardial regeneration in neonatal mice mediated by the phosphatidylinositol 3 kinase/glycogen synthase kinase 3β/cyclin D1 signalling pathway. *Cardiovascular Research* **113**, 620-632 (2017).

93. D. Ladage *et al.*, Stimulating Myocardial Regeneration with Periostin Peptide in Large Mammals Improves Function Post-Myocardial Infarction but Increases Myocardial Fibrosis. *PLoS ONE* **8**, e59656 (2013).

94. D. Mukherjee *et al.*, Ccn2a/Ctgfa is an injury-induced matricellular factor that promotes cardiac regeneration in zebrafish. *Development* **148**, dev193219 (2020).

95. F. Chablais, A. Jaźwińska, The regenerative capacity of the zebrafish heart is dependent on TGFβ signaling. *Development* **139**, 1921-1930 (2012).

96. S. E. Mercer, S. J. Odelberg, H.-G. Simon, A dynamic spatiotemporal extracellular matrix facilitates epicardial-mediated vertebrate heart regeneration. *Developmental Biology* **382**, 457-469 (2013).

97. L. Gamba, A. Amin-Javaheri, J. Kim, D. Warburton, C.-L. Lien, Collagenolytic Activity Is Associated with Scar Resolution in Zebrafish Hearts after Cryoinjury. *Journal of Cardiovascular Development and Disease* **4**, 2 (2017).

98. C. Patra *et al.*, The zebrafish ventricle: A hub of cardiac endothelial cells for in vitro cell behavior studies. *Scientific Reports* **7**, (2017).

99. F. C. Simões, P. R. Riley, The ontogeny, activation and function of the epicardium during heart development and regeneration. *Development* **145**, dev155994 (2018).

100. K. Kikuchi *et al.*, Retinoic Acid Production by Endocardium and Epicardium Is an Injury Response Essential for Zebrafish Heart Regeneration. *Developmental Cell* **20**, 397-404 (2011).

101. A. A. Wills, J. E. Holdway, R. J. Major, K. D. Poss, Regulated addition of new myocardial and epicardial cells fosters homeostatic cardiac growth and maintenance in adult zebrafish. *Development* **135**, 183-192 (2008).

102. J. Cao, K. D. Poss, The epicardium as a hub for heart regeneration. *Nature Reviews Cardiology* **15**, 631-647 (2018).

103. M. A. Missinato, K. Tobita, N. Romano, J. A. Carroll, M. Tsang, Extracellular component hyaluronic acid and its receptor Hmmr are required for epicardial EMT during heart regeneration. *Cardiovascular Research* **107**, 487-498 (2015).

104. K. Sugimoto, S. P. Hui, D. Z. Sheng, K. Kikuchi, Dissection of zebrafish shha function using site-specific targeting with a Cre-dependent genetic switch. *eLife* **6**, (2017).

105. J. Marro, C. Pfefferli, A.-S. De Preux Charles, T. Bise, A. Jaźwińska, Collagen XII Contributes to Epicardial and Connective Tissues in the Zebrafish Heart during Ontogenesis and Regeneration. *PLOS ONE* **11**, e0165497 (2016).

106. J. Wang, J. Cao, A. L. Dickson, K. D. Poss, Epicardial regeneration is guided by cardiac outflow tract and Hedgehog signalling. *Nature* **522**, 226-230 (2015).

107. J. Münch, D. Grivas, Á. González-Rajal, R. Torregrosa-Carrión, J. L. De La Pompa, Notch signalling restricts inflammation and serpine1 in the dynamic endocardium of the regenerating zebrafish heart. *Development* **144**, 1425-1440 (2017).

108. L. Zhao *et al.*, Notch signaling regulates cardiomyocyte proliferation during zebrafish heart regeneration. *Proceedings of the National Academy of Sciences* **111**, 1403-1408 (2014).

109. L. Zhao, R. Ben-Yair, C. E. Burns, C. G. Burns, Endocardial Notch Signaling Promotes Cardiomyocyte Proliferation in the Regenerating Zebrafish Heart through Wnt Pathway Antagonism. *Cell Reports* **26**, 546-554.e545 (2019).

110. S.-L. Lai, R. Marín-Juez, D. Y. R. Stainier, Immune responses in cardiac repair and regeneration: a comparative point of view. *Cellular and Molecular Life Sciences* **76**, 1365-1380 (2019).

111. L. Farache Trajano, N. Smart, Immunomodulation for optimal cardiac regeneration: insights from comparative analyses. *npj Regenerative Medicine* **6**, (2021).

112. A.-S. De Preux Charles, T. Bise, F. Baier, P. Sallin, A. Jaźwińska, Preconditioning boosts regenerative programmes in the adult zebrafish heart. *Open Biology* **6**, 160101 (2016).

113. C. Han *et al.*, Acute inflammation stimulates a regenerative response in the neonatal mouse heart. *Cell Research* **25**, 1137-1151 (2015).

114. N. Natarajan *et al.*, Complement Receptor C5aR1 Plays an Evolutionarily Conserved Role in Successful Cardiac Regeneration. *Circulation* **137**, 2152-2165 (2018).

115. S.-L. Lai *et al.*, Reciprocal analyses in zebrafish and medaka reveal that harnessing the immune response promotes cardiac regeneration. *eLife* **6**, (2017).

116. H. Lörchner *et al.*, Myocardial healing requires Reg3β-dependent accumulation of macrophages in the ischemic heart. *Nature Medicine* **21**, 353-362 (2015).

117. M. Nahrendorf *et al.*, The healing myocardium sequentially mobilizes two monocyte subsets with divergent and complementary functions. *Journal of Experimental Medicine* **204**, 3037-3047 (2007).

118. M. Shiraishi *et al.*, Alternatively activated macrophages determine repair of the infarcted adult murine heart. *Journal of Clinical Investigation* **126**, 2151-2166 (2016).

119. X. Yan *et al.*, Temporal dynamics of cardiac immune cell accumulation following acute myocardial infarction. *Journal of Molecular and Cellular Cardiology* **62**, 24-35 (2013).

120. A. B. Aurora *et al.*, Macrophages are required for neonatal heart regeneration. *Journal of Clinical Investigation* **124**, 1382-1392 (2014).

121. A. Sanz-Morejón *et al.*, Wilms Tumor 1b Expression Defines a Pro-regenerative Macrophage Subtype and Is Required for Organ Regeneration in the Zebrafish. *Cell Reports* **28**, 1296-1306.e1296 (2019).

122. K. Kaikita *et al.*, Targeted Deletion of CC Chemokine Receptor 2 Attenuates Left Ventricular Remodeling after Experimental Myocardial Infarction. *The American Journal of Pathology* **165**, 439-447 (2004).

123. K. J. Lavine *et al.*, Distinct macrophage lineages contribute to disparate patterns of cardiac recovery and remodeling in the neonatal and adult heart. *Proceedings of the National Academy of Sciences* **111**, 16029-16034 (2014).

124. L. Bevan *et al.*, Specific macrophage populations promote both cardiac scar deposition and subsequent resolution in adult zebrafish. *Cardiovascular Research* **116**, 1357-1371 (2020).

125. L. Timmers *et al.*, Toll-Like Receptor 4 Mediates Maladaptive Left Ventricular Remodeling and Impairs Cardiac Function After Myocardial Infarction. *Circulation Research* **102**, 257-264 (2008).

126. J.-I. Oyama *et al.*, Reduced Myocardial Ischemia-Reperfusion Injury in Toll-Like Receptor 4-Deficient Mice. *Circulation* **109**, 784-789 (2004).

127. F. Arslan *et al.*, Myocardial Ischemia/Reperfusion Injury Is Mediated by Leukocytic Toll-Like Receptor-2 and Reduced by Systemic Administration of a Novel Anti–Toll-Like Receptor-2 Antibody. *Circulation* **121**, 80-90 (2010).

128. H. G. Potts, W. T. Stockdale, M. T. M. Mommersteeg, Unlocking the Secrets of the Regenerating Fish Heart: Comparing Regenerative Models to Shed Light on Successful Regeneration. *Journal of Cardiovascular Development and Disease* **8**, 4 (2021).

129. W. T. Stockdale *et al.*, Heart Regeneration in the Mexican Cavefish. *Cell Reports* **25**, 1997-2007.e1997 (2018).

130. J. B. Gross, B. Meyer, M. Perkins, The rise of Astyanax cavefish. *Developmental Dynamics* **244**, 1031-1038 (2015).

131. J. B. Gross, The complex origin of Astyanax cavefish. *BMC Evolutionary Biology* **12**, 105 (2012).

132. J. Fumey *et al.*, Evidence for late Pleistocene origin of Astyanax mexicanus cavefish. *BMC Evolutionary Biology* **18**, (2018).

133. Y. Yamamoto, D. W. Stock, W. R. Jeffery, Hedgehog signalling controls eye degeneration in blind cavefish. *Nature* **431**, 844-847 (2004).

134. J. Krishnan, N. Rohner, Cavefish and the basis for eye loss. *Philosophical Transactions of the Royal Society B: Biological Sciences* **372**, 20150487 (2017).

135. B. A. Stahl, J. B. Gross, Alterations in Mc1r gene expression are associated with regressive pigmentation in Astyanax cavefish. *Development Genes and Evolution* **225**, 367-375 (2015).

136. M. E. Protas *et al.*, Genetic analysis of cavefish reveals molecular convergence in the evolution of albinism. *Nature Genetics* **38**, 107-111 (2006).

137. M. Yoshizawa, W. Jeffery, S. Van Netten, M. McHenry, The sensitivity of lateral line receptors and their role in the behavior of Mexican blind cavefish (Astyanax mexicanus). *Journal of Experimental Biology* **217**, 886-895 (2013).

138. E. Lloyd *et al.*, Evolutionary shift towards lateral line dependent prey capture behavior in the blind Mexican cavefish. *Developmental Biology* **441**, 328-337 (2018).

139. M. Blin *et al.*, Developmental evolution and developmental plasticity of the olfactory epithelium and olfactory skills in Mexican cavefish. *Developmental Biology* **441**, 242-251 (2018).

140. Y. Yamamoto, M. S. Byerly, W. R. Jackman, W. R. Jeffery, Pleiotropic functions of embryonic sonic hedgehog expression link jaw and taste bud amplification with eye loss during cavefish evolution. *Developmental Biology* **330**, 200-211 (2009).

141. A. Beale *et al.*, Circadian rhythms in Mexican blind cavefish Astyanax mexicanus in the lab and in the field. *Nature Communications* **4**, (2013).

142. K. L. Mack *et al.*, Repeated evolution of circadian clock dysregulation in cavefish populations. *PLOS Genetics* **17**, e1009642 (2021).

143. Erik, Alex, Richard, Evolutionary Convergence on Sleep Loss in Cavefish Populations. *Current Biology* **21**, 671-676 (2011).

144. M. R. Riddle *et al.*, Insulin resistance in cavefish as an adaptation to a nutrient-limited environment. *Nature* **555**, 647-651 (2018).

145. A. C. Aspiras, N. Rohner, B. Martineau, R. L. Borowsky, C. J. Tabin, Melanocortin 4 receptor mutations contribute to the adaptation of cavefish to nutrient-poor conditions. *Proceedings of the National Academy of Sciences* **112**, 9668-9673 (2015).

146. D. Moran, R. Softley, E. J. Warrant, Eyeless Mexican Cavefish Save Energy by Eliminating the Circadian Rhythm in Metabolism. *PLoS ONE* **9**, e107877 (2014).

147. M. Yoshizawa, Š. Gorički, D. Soares, W. R. Jeffery, Evolution of a Behavioral Shift Mediated by Superficial Neuromasts Helps Cavefish Find Food in Darkness. *Current Biology* **20**, 1631-1636 (2010).

148. Y. Elipot, H. Hinaux, J. Callebert, S. Rétaux, Evolutionary Shift from Fighting to Foraging in Blind Cavefish through Changes in the Serotonin Network. *Current Biology* **23**, 1-10 (2013).

149. J. E. Kowalko *et al.*, Convergence in feeding posture occurs through different genetic loci in independently evolved cave populations of Astyanax mexicanus. *Proceedings of the National Academy of Sciences* **110**, 16933-16938 (2013).

150. K. E. O'Quin, M. Yoshizawa, P. Doshi, W. R. Jeffery, Quantitative Genetic Analysis of Retinal Degeneration in the Blind Cavefish Astyanax mexicanus. *PLoS ONE* **8**, e57281 (2013).

151. P. Meckert *et al.*, Endomitosis and polyploidization of myocardial cells in the periphery of human acute myocardial infarction. *Cardiovascular Research* **67**, 116-123 (2005).

152. K. J. Livak, T. D. Schmittgen, Analysis of Relative Gene Expression Data Using Real-Time Quantitative PCR and the 2−ΔΔCT Method. *Methods* **25**, 402-408 (2001).

153. M. Stemmer, T. Thumberger, M. Del Sol Keyer, J. Wittbrodt, J. L. Mateo, CCTop: An Intuitive, Flexible and Reliable CRISPR/Cas9 Target Prediction Tool. *PLOS ONE* **10**, e0124633 (2015).

154. J.-P. Concordet, M. Haeussler, CRISPOR: intuitive guide selection for CRISPR/Cas9 genome editing experiments and screens. *Nucleic Acids Research* **46**, W242-W245 (2018).

155. J. A. Gagnon *et al.*, Efficient Mutagenesis by Cas9 Protein-Mediated Oligonucleotide Insertion and Large-Scale Assessment of Single-Guide RNAs. *PLoS ONE* **9**, e98186 (2014).

156. R. N. Wilkinson, S. Elworthy, P. W. Ingham, F. J. M. Van Eeden, A method for high-throughput PCR-based genotyping of larval zebrafish tail biopsies. *BioTechniques* **55**, 314-316 (2013).

157. A. Dobin *et al.*, STAR: ultrafast universal RNA-seq aligner. *Bioinformatics* **29**, 15-21 (2013).

158. H. Li, R. Durbin, Fast and accurate short read alignment with Burrows-Wheeler transform. *Bioinformatics* **25**, 1754-1760 (2009).

159. M. D. Robinson, D. J. McCarthy, G. K. Smyth, edgeR: a Bioconductor package for differential expression analysis of digital gene expression data. *Bioinformatics* **26**, 139-140 (2010).

160. M. I. Love, W. Huber, S. Anders, Moderated estimation of fold change and dispersion for RNA-seq data with DESeq2. *Genome Biology* **15**, (2014).

161. Y. Hao *et al.*, Integrated analysis of multimodal single-cell data. *Cell* **184**, 3573-3587.e3529 (2021).

162. D. J. McCarthy, K. R. Campbell, A. T. L. Lun, Q. F. Wills, Scater: pre-processing, quality control, normalization and visualization of single-cell RNA-seq data in R. *Bioinformatics*, btw777 (2017).

163. G. Finak *et al.*, MAST: a flexible statistical framework for assessing transcriptional changes and characterizing heterogeneity in single-cell RNA sequencing data. *Genome Biology* **16**, (2015).

164. Y. Zhou *et al.*, Metascape provides a biologist-oriented resource for the analysis of systems-level datasets. *Nature Communications* **10**, (2019).

165. G. S. Gulati *et al.*, Single-cell transcriptional diversity is a hallmark of developmental potential. *Science* **367**, 405-411 (2020).

166. S. Kannan, M. Farid, B. L. Lin, M. Miyamoto, C. Kwon, Transcriptomic entropy benchmarks stem cell-derived cardiomyocyte maturation against endogenous tissue at single cell level. *PLOS Computational Biology* **17**, e1009305 (2021).

167. M. Andreatta, S. J. Carmona, UCell: Robust and scalable single-cell gene signature scoring. *Computational and Structural Biotechnology Journal* **19**, 3796-3798 (2021).

168. D. G. Bunis, J. Andrews, G. K. Fragiadakis, T. D. Burt, M. Sirota, dittoSeq: universal user-friendly single-cell and bulk RNA sequencing visualization toolkit. *Bioinformatics* **36**, 5535-5536 (2021).

169. T. R. Jones *et al.*, CellProfiler Analyst: data exploration and analysis software for complex image-based screens. *BMC Bioinformatics* **9**, 482 (2008).

170. D. J. Creek, A. Jankevics, K. E. V. Burgess, R. Breitling, M. P. Barrett, IDEOM: an Excel interface for analysis of LC–MS-based metabolomics data. *Bioinformatics* **28**, 1048-1049 (2012).

171. A. Chokkathukalam *et al.*, mzMatch–ISO: an R tool for the annotation and relative quantification of isotope-labelled mass spectrometry data. *Bioinformatics* **29**, 281-283 (2013).

172. Y. Gloaguen *et al.*, PiMP my metabolome: an integrated, web-based tool for LC-MS metabolomics data. *Bioinformatics* **33**, 4007-4009 (2017).

173. R. A. Scheltema, A. Jankevics, R. C. Jansen, M. A. Swertz, R. Breitling, PeakML/mzMatch: A File Format, Java Library, R Library, and Tool-Chain for Mass Spectrometry Data Analysis. *Analytical Chemistry* **83**, 2786-2793 (2011).

174. K. McLuskey *et al.*, Ranking Metabolite Sets by Their Activity Levels. *Metabolites* **11**, 103 (2021).

175. J. Liang *et al.*, Transmembrane Protein 198 Promotes LRP6 Phosphorylation and Wnt Signaling Activation. *Molecular and Cellular Biology* **31**, 2577-2590 (2011).

176. B. Ohkawara, T. S. Yamamoto, M. Tada, N. Ueno, Role of glypican 4 in the regulation of convergent extension movements during gastrulation in Xenopus laevis. *Development* **130**, 2129-2138 (2003).

177. H. H. Song, W. Shi, Y.-Y. Xiang, J. Filmus, The Loss of Glypican-3 Induces Alterations in Wnt Signaling. *Journal of Biological Chemistry* **280**, 2116-2125 (2005).

178. C. Han, T. Y. Belenkaya, B. Wang, X. Lin, Drosophila glypicans control the cell-to-cell movement of Hedgehog by a dynamin-independent process. *Development* **131**, 601-611 (2004).

179. X. Hong *et al.*, MicroRNA-301b promotes the proliferation and invasion of glioma cells through enhancing activation of Wnt/β-catenin signaling via targeting Glypican-5. *European Journal of Pharmacology* **854**, 39-47 (2019).

180. S. Yuan *et al.*, GPC5, a novel epigenetically silenced tumor suppressor, inhibits tumor growth by suppressing Wnt/β-catenin signaling in lung adenocarcinoma. *Oncogene* **35**, 6120-6131 (2016).

181. F. Li, W. Shi, M. Capurro, J. Filmus, Glypican-5 stimulates rhabdomyosarcoma cell proliferation by activating Hedgehog signaling. *Journal of Cell Biology* **192**, 691-704 (2011).

182. X. Peng *et al.*, Induction of Wnt signaling antagonists and p21-activated kinase enhances cardiomyocyte proliferation during zebrafish heart regeneration. *Journal of Molecular Cell Biology* **13**, 41-58 (2021).

183. G. Ozhan, G. Weidinger, Wnt/β-catenin signaling in heart regeneration. *Cell Regeneration* **4**, 4:3 (2015).

184. L. Svensson *et al.*, Fibromodulin-null Mice Have Abnormal Collagen Fibrils, Tissue Organization, and Altered Lumican Deposition in Tendon. *Journal of Biological Chemistry* **274**, 9636-9647 (1999).

185. S. Kalamajski, Å. Oldberg, The role of small leucine-rich proteoglycans in collagen fibrillogenesis. *Matrix Biology* **29**, 248-253 (2010).

186. Z. Zheng *et al.*, Fibromodulin-Deficiency Alters Temporospatial Expression Patterns of Transforming Growth Factor-β Ligands and Receptors during Adult Mouse Skin Wound Healing. *PLoS ONE* **9**, e90817 (2014).

187. K. Rydell-Törmänen, K. Andréasson, R. Hesselstrand, G. Westergren-Thorsson, Absence of fibromodulin affects matrix composition, collagen deposition and cell turnover in healthy and fibrotic lung parenchyma. *Scientific Reports* **4**, 6383 (2015).

188. E. Mormone, Y. Lu, X. Ge, M. I. Fiel, N. Nieto, Fibromodulin, an Oxidative Stress-Sensitive Proteoglycan, Regulates the Fibrogenic Response to Liver Injury in Mice. *Gastroenterology* **142**, 612-621.e615 (2012).

189. K. Andenæs *et al.*, The extracellular matrix proteoglycan fibromodulin is upregulated in clinical and experimental heart failure and affects cardiac remodeling. *PLOS ONE* **13**, e0201422 (2018).

190. X.-K. Qu *et al.*, Prevalence and spectrum of LRRC10 mutations associated with idiopathic dilated cardiomyopathy. *Molecular Medicine Reports* **12**, 3718-3724 (2015).

191. M. J. Brody *et al.*, Ablation of the Cardiac-Specific Gene Leucine-Rich Repeat Containing 10 (Lrrc10) Results in Dilated Cardiomyopathy. *PLoS ONE* **7**, e51621 (2012).

192. I. I. Adameyko *et al.*, Expression and regulation of mouse SERDIN1, a highly conserved cardiac-specific leucine-rich repeat protein. *Developmental Dynamics* **233**, 540-552 (2005).

193. K.-H. Kim *et al.*, Lrrc10 is required for early heart development and function in zebrafish. *Developmental Biology* **308**, 494-506 (2007).

194. K.-H. Kim, T.-G. Kim, B. K. Micales, G. E. Lyons, Y. Lee, Dynamic expression patterns of leucine-rich repeat containing protein 10 in the heart. *Developmental Dynamics* **236**, 2225-2234 (2007).

195. M. T. Woon *et al.*, Pediatric Dilated Cardiomyopathy-Associated LRRC10 (Leucine-Rich Repeat–Containing 10) Variant Reveals LRRC10 as an Auxiliary Subunit of Cardiac L-Type Ca 2+ Channels. *Journal of the American Heart Association* **7**, e006428 (2018).

196. A. Barrallo-Gimeno, M. A. Nieto, The Snail genes as inducers of cell movement and survival: implications in development and cancer. *Development* **132**, 3151-3161 (2005).

197. A. Millanes-Romero *et al.*, Regulation of Heterochromatin Transcription by Snail1/LOXL2 during Epithelial-to-Mesenchymal Transition. *Molecular Cell* **52**, 746-757 (2013).

198. J. S. Ingwall, Energy metabolism in heart failure and remodelling. *Cardiovascular Research* **81**, 412-419 (2008).

199. S. Sivanand, M. G. Vander Heiden, Emerging Roles for Branched-Chain Amino Acid Metabolism in Cancer. *Cancer Cell* **37**, 147-156 (2020).

200. H.-J. Park *et al.*, The essential role of fructose-1,6-bisphosphatase 2 enzyme in thermal homeostasis upon cold stress. *Experimental & Molecular Medicine* **52**, 485-496 (2020).

201. D. A. Solovjov, E. Pluskota, E. F. Plow, Distinct Roles for the α and β Subunits in the Functions of Integrin αMβ2. *Journal of Biological Chemistry* **280**, 1336-1345 (2005).

202. J. Cao *et al.*, Single epicardial cell transcriptome sequencing identifies Caveolin-1 as an essential factor in zebrafish heart regeneration. *Development* **143**, 232-243 (2015).

203. J. C. Kovacic, N. Mercader, M. Torres, M. Boehm, V. Fuster, Epithelial-to-Mesenchymal and Endothelial-to-Mesenchymal Transition. *Circulation* **125**, 1795-1808 (2012).

204. L. Alonso-Herranz *et al.*, Macrophages promote endothelial-to-mesenchymal transition via MT1-MMP/TGFβ1 after myocardial infarction. *eLife* **9**, (2020).

205. J. González-Santamaría *et al.*, Matrix cross-linking lysyl oxidases are induced in response to myocardial infarction and promote cardiac dysfunction. *Cardiovascular Research* **109**, 67-78 (2016).

206. A. Aharonov *et al.*, ERBB2 drives YAP activation and EMT-like processes during cardiac regeneration. *Nature Cell Biology* **22**, 1346-1356 (2020).

207. P. Quijada, M. A. Trembley, E. M. Small, The Role of the Epicardium During Heart Development and Repair. *Circulation Research* **126**, 377-394 (2020).

208. L. Li *et al.*, Pitx2 maintains mitochondrial function during regeneration to prevent myocardial fat deposition. *Development* **145**, dev168609 (2018).

209. M. V. Pedersen *et al.*, Neuritogenic and survival-promoting effects of the P2 peptide derived from a homophilic binding site in the neural cell adhesion molecule. *Journal of Neuroscience Research* **75**, 55-65 (2004).

210. D. Kiryushko, V. Berezin, E. Bock, Regulators of Neurite Outgrowth: Role of Cell Adhesion Molecules. *Annals of the New York Academy of Sciences* **1014**, 140-154 (2004).

211. H. H. Van Acker, A. Capsomidis, E. L. Smits, V. F. Van Tendeloo, CD56 in the Immune System: More Than a Marker for Cytotoxicity? *Front Immunol* **8**, 892 (2017).

212. S. Gattenlöhner *et al.*, NCAM(CD56) and RUNX1(AML1) Are Up-Regulated in Human Ischemic Cardiomyopathy and a Rat Model of Chronic Cardiac Ischemia. *The American Journal of Pathology* **163**, 1081-1090 (2003).

213. M. García-Manzanares *et al.*, XPO1 Gene Therapy Attenuates Cardiac Dysfunction in Rats with Chronic Induced Myocardial Infarction. *Journal of Cardiovascular Translational Research* **13**, 593-600 (2020).

214. M. M. Molina-Navarro *et al.*, Heart failure entails significant changes in human nucleocytoplasmic transport gene expression. *Int J Cardiol* **168**, 2837-2843 (2013).

215. J.-F. Jasmin *et al.*, Caveolin-1 deficiency exacerbates cardiac dysfunction and reduces survival in mice with myocardial infarction. *American Journal of Physiology-Heart and Circulatory Physiology* **300**, H1274-H1281 (2011).

216. P. Shivshankar *et al.*, Caveolin-1 deletion exacerbates cardiac interstitial fibrosis by promoting M2 macrophage activation in mice after myocardial infarction. *Journal of Molecular and Cellular Cardiology* **76**, 84-93 (2014).

217. S. K. Miyasato *et al.*, Caveolin-1 modulates TGF-β1 signaling in cardiac remodeling. *Matrix Biology* **30**, 318-329 (2011).

218. D. Grivas, Á. González-Rajal, C. Guerrero Rodríguez, R. Garcia, J. L. De La Pompa, Loss of Caveolin-1 and caveolae leads to increased cardiac cell stiffness and functional decline of the adult zebrafish heart. *Scientific Reports* **10**, (2020).

219. M. A. El-Brolosy *et al.*, Genetic compensation triggered by mutant mRNA degradation. *Nature* **568**, 193-197 (2019).

220. L. Zhen *et al.*, miR-301a-PTEN-AKT Signaling Induces Cardiomyocyte Proliferation and Promotes Cardiac Repair Post-MI. *Molecular Therapy - Nucleic Acids* **22**, 251-262 (2020).

221. F. Xiao, W. Kimura, H. A. Sadek, A Hippo "AKT" Regulates Cardiomyocyte Proliferation. *Circulation Research* **116**, 3-5 (2015).

222. A. Bertozzi *et al.*, Is zebrafish heart regeneration "complete"? Lineage-restricted cardiomyocytes proliferate to pre-injury numbers but some fail to differentiate in fibrotic hearts. *Developmental Biology* **471**, 106-118 (2021).

223. D. Bednarek *et al.*, Telomerase Is Essential for Zebrafish Heart Regeneration. *Cell Reports* **12**, 1691-1703 (2015).

224. H. Honkoop, P. D. Nguyen, V. E. M. Van Der Velden, K. F. Sonnen, J. Bakkers, Live imaging of adult zebrafish cardiomyocyte proliferation ex vivo. *Development* **148**, (2021).

225. A. Beisaw *et al.*, AP-1 Contributes to Chromatin Accessibility to Promote Sarcomere Disassembly and Cardiomyocyte Protrusion During Zebrafish Heart Regeneration. *Circulation Research* **126**, 1760-1778 (2020).

226. M. H. Soonpaa, K. K. Kim, L. Pajak, M. Franklin, L. J. Field, Cardiomyocyte DNA synthesis and binucleation during murine development. *Am J Physiol* **271**, H2183-2189 (1996).

227. H. Sánchez-Iranzo *et al.*, Tbx5a lineage tracing shows cardiomyocyte plasticity during zebrafish heart regeneration. *Nature Communications* **9**, (2018).

228. B. Jensen *et al.*, Identifying the Evolutionary Building Blocks of the Cardiac Conduction System. *PLoS ONE* **7**, e44231 (2012).

229. A. T. Tsedeke *et al.*, Cardiomyocyte heterogeneity during zebrafish development and regeneration. *Developmental Biology* **476**, 259-271 (2021).

230. A. E. Teschendorff, P. Sollich, R. Kuehn, Signalling entropy: A novel network-theoretical framework for systems analysis and interpretation of functional omic data. *Methods* **67**, 282-293 (2014).

231. A. E. Teschendorff, T. Enver, Single-cell entropy for accurate estimation of differentiation potency from a cell's transcriptome. *Nature Communications* **8**, 15599 (2017).

232. D. Grün *et al.*, De Novo Prediction of Stem Cell Identity using Single-Cell Transcriptome Data. *Cell Stem Cell* **19**, 266-277 (2016).

233. I. Tirosh *et al.*, Dissecting the multicellular ecosystem of metastatic melanoma by single-cell RNA-seq. *Science* **352**, 189-196 (2016).

234. A. W. Duncan *et al.*, The ploidy conveyor of mature hepatocytes as a source of genetic variation. *Nature* **467**, 707-710 (2010).

235. A. C. Cardoso *et al.*, Mitochondrial substrate utilization regulates cardiomyocyte cell-cycle progression. *Nature Metabolism* **2**, 167-178 (2020).

236. V. Gupta, K. D. Poss, Clonally dominant cardiomyocytes direct heart morphogenesis. *Nature* **484**, 479-484 (2012).

237. Y. Fang *et al.*, Tbx20 Induction Promotes Zebrafish Heart Regeneration by Inducing Cardiomyocyte Dedifferentiation and Endocardial Expansion. *Front Cell Dev Biol* **8**, 738 (2020).

238. Z. Liu, S. Yue, X. Chen, T. Kubin, T. Braun, Regulation of Cardiomyocyte Polyploidy and Multinucleation by CyclinG1. *Circulation Research* **106**, 1498-1506 (2010).

239. T. Cao *et al.*, Fatty Acid Oxidation Promotes Cardiomyocyte Proliferation Rate but Does Not Change Cardiomyocyte Number in Infant Mice. *Front Cell Dev Biol* **7**, 42 (2019).

240. X. Yang *et al.*, Fatty Acids Enhance the Maturation of Cardiomyocytes Derived from Human Pluripotent Stem Cells. *Stem Cell Reports* **13**, 657-668 (2019).

241. K. Nishida, S. Kyoi, O. Yamaguchi, J. Sadoshima, K. Otsu, The role of autophagy in the heart. *Cell Death & Differentiation* **16**, 31-38 (2009).

242. J. K. Medley *et al.* (Cold Spring Harbor Laboratory, 2020).

243. S. Xiong, J. Krishnan, R. Peuß, N. Rohner, Early adipogenesis contributes to excess fat accumulation in cave populations of Astyanax mexicanus. *Developmental Biology* **441**, 297-304 (2018).

244. H. C. D. C. H. W. F. Wilkens, *Subterranean ecosystems*. (Elsevier, Amsterdam; New York, 2000).

245. K. Hüppop, Oxygen consumption of Astyanax fasciatus (Characidae, Pisces): a comparison of epigean and hypogean populations. *Environmental Biology of Fishes* **17**, 299-308 (1986).

246. N. Longo, Y. Wang, M. Pasquali, Progressive Decline in Insulin Levels in Rabson-Mendenhall Syndrome1. *The Journal of Clinical Endocrinology & Metabolism* **84**, 2623-2629 (1999).

247. K. Hirose *et al.*, Evidence for hormonal control of heart regenerative capacity during endothermy acquisition. *Science* **364**, 184-188 (2019).

248. O. Warburg, F. Wind, E. Negelein, THE METABOLISM OF TUMORS IN THE BODY. *Journal of General Physiology* **8**, 519-530 (1927).

249. M. G. Vander Heiden, L. C. Cantley, C. B. Thompson, Understanding the Warburg Effect: The Metabolic Requirements of Cell Proliferation. *Science* **324**, 1029-1033 (2009).

250. J. J. Lehman, D. P. Kelly, Transcriptional activation of energy metabolic switches in the developing and hypertrophied heart. *Clin Exp Pharmacol Physiol* **29**, 339-345 (2002).

251. G. D. Lopaschuk, R. L. Collins-Nakai, T. Itoi, Developmental changes in energy substrate use by the heart. *Cardiovasc Res* **26**, 1172-1180 (1992).

252. C. Postic *et al.*, Development and regulation of glucose transporter and hexokinase expression in rat. *Am J Physiol* **266**, E548-559 (1994).

253. V. Jiménez-Amilburu, S. Jong-Raadsen, J. Bakkers, H. P. Spaink, R. Marín-Juez, GLUT12 deficiency during early development results in heart failure and a diabetic phenotype in zebrafish. *Journal of Endocrinology* **224**, 1-15 (2015).

254. Y. C. Tseng *et al.*, Specific expression and regulation of glucose transporters in zebrafish ionocytes. *Am J Physiol Regul Integr Comp Physiol* **297**, R275-290 (2009).

255. R. Marín-Juez, E. Capilla, F. Carvalho-Simoes, M. Camps, J. V. Planas. (InTech, 2014), chap. Structural and Functional Evolution of Glucose Transporter 4 (GLUT4): A Look at GLUT4 in Fish.

256. X. Zhang, S. Yang, J. Chen, Z. Su, Unraveling the Regulation of Hepatic Gluconeogenesis. *Frontiers in Endocrinology* **9**, (2019).

257. L. Hagenfeldt, J. Wahren, B. Pernow, L. Räf, Uptake of individual free fatty acids by skeletal muscle and liver in man. *Journal of Clinical Investigation* **51**, 2324-2330 (1972).

258. L. Bertrand, S. Horman, C. Beauloye, J. L. Vanoverschelde, Insulin signalling in the heart. *Cardiovascular Research* **79**, 238-248 (2008).

259. V. M. Fajardo *et al.*, GLUT1 overexpression enhances glucose metabolism and promotes neonatal heart regeneration. *Scientific Reports* **11**, (2021).

260. S. Zhang, M. W. Hulver, R. P. McMillan, M. A. Cline, E. R. Gilbert, The pivotal role of pyruvate dehydrogenase kinases in metabolic flexibility. *Nutrition & Metabolism* **11**, 10 (2014).

261. G. Zhao *et al.*, Overexpression of pyruvate dehydrogenase kinase 4 in heart perturbs metabolism and exacerbates calcineurin-induced cardiomyopathy. *Am J Physiol Heart Circ Physiol* **294**, H936-943 (2008).

262. S. Park *et al.*, Role of the Pyruvate Dehydrogenase Complex in Metabolic Remodeling: Differential Pyruvate Dehydrogenase Complex Functions in Metabolism. *Diabetes & Metabolism Journal* **42**, 270 (2018).

263. E. N.-Y. Poon *et al.*, The cell surface marker CD36 selectively identifies matured, mitochondria-rich hPSC-cardiomyocytes. *Cell Research* **30**, 626-629 (2020).

264. M. Rohm *et al.*, Cardiac Dysfunction and Metabolic Inflexibility in a Mouse Model of Diabetes Without Dyslipidemia. *Diabetes* **67**, 1057-1067 (2018).

265. N. D. Oakes *et al.*, Cardiac metabolism in mice: tracer method developments and in vivo application revealing profound metabolic inflexibility in diabetes. *Am J Physiol Endocrinol Metab* **290**, E870-881 (2006).

266. C.-R. Chong, K. Clarke, E. Levelt, Metabolic remodelling in diabetic cardiomyopathy. *Cardiovascular Research* **113**, 422-430 (2017).

267. J. B. McGill *et al.*, Potentiation of abnormalities in myocardial metabolism with the development of diabetes in women with obesity and insulin resistance. *Journal of Nuclear Cardiology* **18**, 421-429 (2011).

268. L. J. Rijzewijk *et al.*, Myocardial Steatosis Is an Independent Predictor of Diastolic Dysfunction in Type 2 Diabetes Mellitus. *Journal of the American College of Cardiology* **52**, 1793-1799 (2008).

269. Q. Liang *et al.*, Overexpression of Metallothionein Reduces Diabetic Cardiomyopathy. *Diabetes* **51**, 174-181 (2002).

270. H.-C. Chiu *et al.*, A novel mouse model of lipotoxic cardiomyopathy. *Journal of Clinical Investigation* **107**, 813-822 (2001).

271. Y. T. Zhou *et al.*, Lipotoxic heart disease in obese rats: Implications for human obesity. *Proceedings of the National Academy of Sciences* **97**, 1784-1789 (2000).

272. X. Shen, S. Zheng, N. S. Metreveli, P. N. Epstein, Protection of Cardiac Mitochondria by Overexpression of MnSOD Reduces Diabetic Cardiomyopathy. *Diabetes* **55**, 798-805 (2006).

273. J. Yang *et al.*, CD36 Deficiency Rescues Lipotoxic Cardiomyopathy. *Circulation Research* **100**, 1208-1217 (2007).

274. M. S. Dodd *et al.*, Fatty Acids Prevent Hypoxia-Inducible Factor-1α Signaling Through Decreased Succinate in Diabetes. *JACC: Basic to Translational Science* **3**, 485-498 (2018).

275. R. M. Cubbon *et al.*, Diabetes mellitus is associated with adverse prognosis in chronic heart failure of ischaemic and non-ischaemic aetiology. *Diabetes and Vascular Disease Research* **10**, 330-336 (2013).

276. P. H. Stone *et al.*, The effect of diabetes mellitus on prognosis and serial left ventricular function after acute myocardial infarction: Contribution of both coronary disease and diastolic left ventricular dysfunction to the adverse prognosis. *Journal of the American College of Cardiology* **14**, 49-57 (1989).

277. Y. Guo, W. T. Pu, Cardiomyocyte Maturation. *Circulation Research* **126**, 1086-1106 (2020).

278. L. Ye *et al.*, Cardiomyocytes in Young Infants With Congenital Heart Disease: a Three-Month Window of Proliferation. *Scientific Reports* **6**, 23188 (2016).

279. M. Mollova *et al.*, Cardiomyocyte proliferation contributes to heart growth in young humans. *Proceedings of the National Academy of Sciences* **110**, 1446-1451 (2013).

280. A. W. Duncan *et al.*, Frequent Aneuploidy Among Normal Human Hepatocytes. *Gastroenterology* **142**, 25-28 (2012).

281. K. Tiemann *et al.*, Increasing myocardial contraction and blood pressure in C57BL/6 mice during early postnatal development. *Am J Physiol Heart Circ Physiol* **284**, H464-474 (2003).

282. D. J. Fisher, M. A. Heymann, A. M. Rudolph, Myocardial oxygen and carbohydrate consumption in fetal lambs in utero and in adult sheep. *Am J Physiol* **238**, H399-405 (1980).

283. Katrien *et al.*, Role of PFKFB3-Driven Glycolysis in Vessel Sprouting. *Cell* **154**, 651-663 (2013).

284. Clifford *et al.*, Somatic Oxidative Bioenergetics Transitions into Pluripotency-Dependent Glycolysis to Facilitate Nuclear Reprogramming. *Cell Metabolism* **14**, 264-271 (2011).

285. M. V. Liberti, J. W. Locasale, The Warburg Effect: How Does it Benefit Cancer Cells? *Trends in Biochemical Sciences* **41**, 211-218 (2016).

286. W. Yang *et al.*, Nuclear PKM2 regulates β-catenin transactivation upon EGFR activation. *Nature* **480**, 118-122 (2011).

287. A. E. T. S. De Carvalho *et al.*, Early Postnatal Cardiomyocyte Proliferation Requires High Oxidative Energy Metabolism. *Scientific Reports* **7**, (2017).

288. J. J. Lum *et al.*, Growth Factor Regulation of Autophagy and Cell Survival in the Absence of Apoptosis. *Cell* **120**, 237-248 (2005).

289. Y.-H. Jiang *et al.*, Multinucleated polyploid cardiomyocytes undergo an enhanced adaptability to hypoxia via mitophagy. *Journal of Molecular and Cellular Cardiology* **138**, 115-135 (2020).

290. R. Nunan, K. G. Harding, P. Martin, Clinical challenges of chronic wounds: searching for an optimal animal model to recapitulate their complexity. *Disease Models & Mechanisms* **7**, 1205-1213 (2014).

291. C. J. Kenyon, The genetics of ageing. *Nature* **464**, 504-512 (2010).

292. L. Partridge, N. Alic, I. Bjedov, M. D. W. Piper, Ageing in Drosophila: The role of the insulin/Igf and TOR signalling network. *Experimental Gerontology* **46**, 376-381 (2011).

293. P. Kakanj *et al.*, Insulin and TOR signal in parallel through FOXO and S6K to promote epithelial wound healing. *Nature Communications* **7**, 12972 (2016).

294. H. Shen *et al.*, Mononuclear diploid cardiomyocytes support neonatal mouse heart regeneration in response to paracrine IGF2 signaling. *eLife* **9**, (2020).

295. M. Zhang *et al.*, Melanocortin Receptor 4 Signaling Regulates Vertebrate Limb Regeneration. *Developmental Cell* **46**, 397-409.e395 (2018).

296. R. Karra, A. K. Knecht, K. Kikuchi, K. D. Poss, Myocardial NF-κB activation is essential for zebrafish heart regeneration. *Proceedings of the National Academy of Sciences* **112**, 13255-13260 (2015).

297. R. F. Johnson, I.-I. Witzel, N. D. Perkins, p53-Dependent Regulation of Mitochondrial Energy Production by the RelA Subunit of NF-κB. *Cancer Research* **71**, 5588-5597 (2011).

298. K. Kawauchi, K. Araki, K. Tobiume, N. Tanaka, p53 regulates glucose metabolism through an IKK-NF-κB pathway and inhibits cell transformation. *Nature Cell Biology* **10**, 611-618 (2008).

299. H. Hashimoto, E. N. Olson, R. Bassel-Duby, Therapeutic approaches for cardiac regeneration and repair. *Nature Reviews Cardiology* **15**, 585-600 (2018).

300. J. G. Bensley, R. De Matteo, R. Harding, M. J. Black, Three-dimensional direct measurement of cardiomyocyte volume, nuclearity, and ploidy in thick histological sections. *Scientific Reports* **6**, 23756 (2016).

301. M.-F. Giraud *et al.*, Is there a relationship between the supramolecular organization of the mitochondrial ATP synthase and the formation of cristae? *Biochimica et Biophysica Acta (BBA) - Bioenergetics* **1555**, 174-180 (2002).

302. P. Paumard *et al.*, The ATP synthase is involved in generating mitochondrial cristae morphology. *The EMBO Journal* **21**, 221-230 (2002).

303. F. J. Naser *et al.*, Isotope tracing in adult zebrafish reveals alanine cycling between melanoma and liver. *Cell Metabolism* **33**, 1493-1504.e1495 (2021).

304. J. A. Goldman *et al.*, Resolving Heart Regeneration by Replacement Histone Profiling. *Developmental Cell* **40**, 392-404.e395 (2017).